University of Udine

Doctoral Program

Biomedical Sciences and Biotechnology

Cycle XXXIII

Circulating Tumor DNA Monitoring and Pharmacogenetics Patients' Profiling: Pharmacological Implications in Locally Advanced Rectal Cancer and Gastrointestinal Stromal Tumor

Supervisor: Dr. Erika Cecchin

Chiara Dalle Fratte

2021

This doctoral thesis has been carried out at the
Experimental and Clinical Pharmacology Unit
of the National Cancer Institute (IRCCS - Centro di Riferimento Onclogico di Aviano)
directed by Dr. Giuseppe Toffoli

To my family

Table of Contents

Table of Contents …… I
Abbreviations…….. III
Abstract…… VI
Chapter 1. Introduction…… 1
1.1 Personalized Medicine in Oncology…… 1
1.2 Liquid Biopsy for Precision Oncology…… 1
1.2.1 The Biology of Circulating Tumor DNA…… 2
1.2.2 Pre-Analytical and Analytical Variability in cfDNA Processing…… 3
1.2.3 Sequencing Platforms and Analysis of cfDNA…….. 4
1.3 Clinical Application of ctDNA in Gastrointestinal Tumors…… 6
1.3.1 Locally Advanced Rectal Cancer (LARC)……. 9
1.3.1.1 Application of ctDNA Analysis in LARC…….. 10
1.3.2 Gastrointestinal Stromal Tumor (GIST)……. 11
1.3.2.1 Pharmacodynamics of Imatinib…….. 14
1.3.2.2 Pharmacokinetics and Pharmacogenetics of Imatinib…… 17
Chapter 2. Aims…….. 23
Chapter 3. Materials and Methods…….. 25
3.1 Patients' Selection and Inclusion's Criteria……. 25
3.1.1 LARC Patients…… 25
3.1.2 GIST Patients…….. 25
3.1.3 Healthy Subjects…….. 26
3.2 Blood Processing and Plasma Storage……. 26
3.3 cfDNA Extraction, Storage and Characterization…….. 26
3.4 Genomic DNA Extraction and Quantification…… 27
3.5 DNA Extraction from FFPE Tumor Tissue, Quantification and QC…….. 27
3.6 Genes Selection and Customized Panel Design…….. 28
3.7 Next Generation Sequencing…….. 28
3.7.1 Fragmentation of FFPE DNA of LARC Patients…… 28
3.7.2 Libraries Preparation for sWGS…….. 29
3.7.3 Targeted Sequencing of FFPE DNA from LARC Biopsies…… 29
3.7.4 Targeted Sequencing of cfDNA and FFPE DNA from GIST Patients…….. 30
3.7.5 Targeted Sequencing of Genomic DNA from GIST Patients……. 31
3.8 Sequencing Platforms…….. 31
3.9 Bioinformatics Analysis…….. 31
3.10 Variants' Calling and CNAs' Detection…… 32
3.11 Droplet Digital PCR…….. 32
3.12 Computational Prediction of Splicing Defects…….. 33
3.13 GIST Patients Genotyping and Phenotype Assignment…… 33
3.14 Acquisition of Data on Concomitant Administered Drugs…… 35
3.15 Evaluation and Rating of Imatinib Interacting Drugs…… 35
3.16 Calculation of the Drugs' Impact on CYP's and Transporters' Activity…….. 37
3.17 Assessment of the Pathological Response to Treatment…….. 37
3.18 Assessment of Therapeutic Response to Imatinib…… 38
3.19 Immunohistochemical Analysis and Biomarkers' Expression in LARC Biopsies…….. 38
3.20 LC/MS-MS Quantification of Imatinib Plasma Concentrations…….. 39
3.21 Estimation of Imatinib Trough Levels…….. 39
3.22 Statistical Methods……. 40
Chapter 4. Results…… 43
4.1 Locally Advanced rectal Cancer: Patients' Characteristics and Study Design…….. 43

4.2 Molecular Characterization of Plasma cfDNA of LARC Patients……. 45
4.2.1 Plasma cfDNA Levels in LARC Patients: Analysis and Clinical Considerations…….. 45
4.2.2 CNAs Profiling of Plasma cfDNA of LARC Patients…….. 46
4.2.3 Distribution of CNAs in Pre-treatment cfDNA (T_1)…….. 46
4.2.4 Distribution of CNAs in cfDNA during nCRT (T_2)…….. 47
4.2.5 Distribution of CNAs in Post-treatment cfDNA (T_3)…… 48
4.3 Molecular Characterization of Primary tumor tissue of LARC…….. 49
4.3.1 CNAs Profiling of Primary Tumor DNA and Comparison with cfDNA in LARC…… 50
4.3.2 Genetic Variants in Primary Tumor DNA of LARC……... 51
4.3.3 Immunohistochemical Analysis of Pre-treatment Tumor Tissue of LARC…… 55
4.4 Gastrointestinal Stromal Tumor: Patients' Characteristics…….. 58
4.5 Plasma cfDNA Levels in GIST Patients: Analysis and Clinical Considerations…… 59
4.6 Dynamic Monitoring of ctDNA in GIST Patients……... 62
4.6.1 Case Report #16……... 64
4.6.2 Case Report #21……... 66
4.7 Imatinib Pharmacogenetics…….. 70
4.7.1 Genotyping of CYPs and Transporters in GIST Patients…… 70
4.7.2 Assessment of the Metabolic Phenotype of CYPs……. 70
4.7.3 Assessment of the Metabolic Phenotype of Transporters……... 71
4.7.4 Description of Imatinib Interacting Drugs in the Study Population…… 73
4.7.5 Assessment of Imatinib Trough Levels…….. 75
4.7.6 Impact of Pharmacokinetic Variability on the Disease Progression……... 76
4.7.7 Impact of the Metabolic Phenotype of CYPs on Imatinib Pharmacokinetics……. 79
4.7.7.1 The Pharmacogenetics Activity Score (PGx-AS) approach……... 79
4.7.7.2 The Single Gene Approach…… 80
4.7.8 Impact of the Metabolic Phenotype of Transporters on Imatinib Pharmacokinetics….. 82
4.7.9 Concurrent Impact of DDI and Genotype on Imatinib Pharmacokinetics…….. 84
4.7.10 Impact of Carbamazepine on Imatinib Pharmacokinetics: the Role of CYP3A4……. 86
4.7.11 Impact of the Tobacco Smoke on Imatinib Pharmacokinetics: the Role of CYP1A2... 87
Chapter 5. Discussion…….. 89
5.1 ctDNA Monitoring in LARC Patients to Predict nCRT Outcome and Prognosis……... 89
5.2 Clinical Application of ctDNA Monitoring in GIST Patients…… 94
5.3 Pharmacogenetics and DDIs…… 96
5.4 Conclusions and Outlooks……... 100
References…… 103
Appendix…….. 127
Publications…….. 129
Acknowledgments…… 131

Abbreviations

5-FU: 5-fluorouracil
ABCB1: ATP-binding cassette sub-family B member 1
ABCG2: ATP-binding cassette sub-family G member 2
AIFA: Agenzia Italiana del Farmaco
AS: activity score
AUC: area under the curve
BCRP: breast cancer resistance protein
BEAMing: beads emulsion amplification magnetics PCR
BRAF: v-raf murine sarcoma viral oncogene homolog B
c-KIT: V-Kit Hardy-Zuckerman 4 feline xarcoma viral oncogene
CA19-9: carbohydrate antigen 19
CART: classification and regression tree
CDS: coding sequence
CEA: carcinoembryonic antigen
cfDNA: cell-free DNA
CML: chronic myeloid leukemia
CNAs: copy number aberrations
CPIC: Clinical Pharmacogenetic Implementation Consortium
CR: complete response
CRC: colorectal cancer
CRO: Centro di Riferimento Oncologico
CT: computed tomography
CTCAE: common terminology criteria for adverse events
CTCs: circulating tumor Cells
ctDNA: circulating tumor DNA
CYP: cytochrome
DDI: drug-drug interaction
ddPCR: droplet digital PCR
DFS: disease free survival
DIN: DNA integrity index
DIs: drug interacting score
DPWG: Dutch Pharmacogenetic Working Group
DPYD: dihydropyridine dehydrogenase
EGFR: epidermal growth factor receptor

EM: extensive metabolizer

EMA: European Medicine Agency

EVs: extracellular vesicles

FDA: U. S. Food and Drug Administration

FFPE: formalin fixed paraffin embedded

FGF: fibroblast growth factor

GIST: gastrointestinal stromal tumor

IHC: immunohistochemistry

IM: intermediate metabolizer

IQR: interquartile range

IRCCS: Istituto di Ricovero e Cura a Carattere Scientifico

K_2-EDTA: potassium ethylenediaminetetraacetic acid

KRAS: Kirsten rat sarcoma viral oncogene homolog

LARC: locally advanced rectal cancer

LC-MS/MS: liquid chromatography tandem mass spectrometry

MAF: minor allele frequency

MDR1: multidrug resistance protein

miRNA: microRNA

MKI: multi-kinase inhibitor

MRD: minimal residual disease

NCCN: National Comprehensive Cancer Network

nCRT: neoadjuvant chemoradiotherapy

NF1: neurofibromin 1

NGS: next-generation sequencing

NSCLC: non-small cell lung cancer

OR: odds ratio

OS: overall survival

PBMC: peripheral blood mononuclear cell

pCR: pathological complete response

PCR: polymerase chain reaction

PD: progression disease

PDGFRA: platelet derived growth factor receptor

PET: positron emission tomography

PFS: progression free survival

PgP: P-glycoprotein

PGx-AS: pharmacogenetics activity score

PGx: pharmacogenetics

PM: poor metabolizer

PPi: proton-pump inhibitors

PR: partial response

READ: rectum adenocarcinoma

RECIST: Response Evaluation Criteria in Solid Tumors

RFS: relapse-free survival

ROC: receiver operating characteristic

sd: standard deviation

SDH: succinate dehydrogenase

SNP: single nucleotide variant

SNV: single nucleotide variant

sWGS: shallow whole genome sequencing

TCGA: The Cancer Genome Atlas

TFx: tumor fraction

TKI: tyrosine kinase inhibitor

TME: total mesorectal excision

TRG: tumor regression grade

TTP: time to progression

UM: ultrarapid metabolizer

UMI: unique molecular indexes

UTR: untranslated region

VAF: variant allele frequency

VEGFR: vascular endothelial growth factor

WES: whole exome sequencing

Abstract

Background

The standard of care for the management of locally advanced rectal cancer (LARC) relies on neoadjuvant chemoradiotherapy (nCRT), followed by surgery. The achievement of a pathological complete response (pCR) after nCRT is observed in up to 30% of patients and is positively associated with a lower risk of local and distant recurrence. The need to discriminate good from poor responder in the early steps of nCRT is urgently required to optimize the therapeutic strategies and improve prognosis. In gastrointestinal stromal tumor (GIST), the development of resistance to first line imatinib treatment represents the leading cause of disease progression and is determined by pharmacodynamics and pharmacokinetics alterations. The chance of interrogating circulating tumor DNA (ctDNA) represents an appealing tool for the real-time monitoring of treatment response in a low-invasive manner and to sustain the decision making for treatment's personalization in gastrointestinal malignancies.

Aims

The aims can be summarized as follow: i) Assess whether the presence of copy number aberrations (CNAs) in the cell-free DNA (cfDNA) of LARC patients receiving nCRT might represent an early biomarker of treatment efficacy. ii) Test whether the detection of ctDNA in GIST might help in the identification of disease progression. iii) Assess whether the presence of specific pharmacogenetic variants, as well as the administration of imatinib interacting drug, might explain the pharmacokinetics variability of imatinib.

Materials and Methods

84 blood samples were collected from 40 consent LARC patients with available clinical data at the Clinical Pharmacology Unit of IRCCS CRO Aviano (Italy). cfDNA was extracted and the presence of CNAs was assessed by means of shallow whole genome sequencing (sWGS) in a tumor-informed manner. The response to nCRT was assessed using the Mandard's tumor regression grade (TRG) scale. 188 blood samples were collected from 39 consent GIST patients. cfDNA was extracted and the presence of ctDNA was assessed by means of targeted deep sequencing in a panel of GIST relevant genes. Imatinib trough levels were quantified by means of LC-MM/MS validated method and the presence of genetic variants in cytochromes and transporters was assessed on genomic DNA by means of target allele discrimination assays and NGS. Intake of co-administrated drugs was retrieved from clinical records and patients' interview. Response to imatinib was assessed according to RECIST criteria.

Results

For all LARC patients the plasma sample collected at the time of diagnosis (T_1, n = 40) was available. Further longitudinal plasma samples were collected in the course of nCRT (T_2, n = 24) and after nCRT (T_3, n = 15). The presence of CNAs was detected in the cfDNA of 6/40 patients (15.0%) at the T_1, with a median tumor fraction (TFx) of 10.41% (range 5.89–27.34). When comparing the variation of TFx between T_2 and T_1, 6/24 evaluable patients (25.0%) showed an increase of the TFx, which was associated with an increased rate of pCR (RR: 3.75; 95% CI 1.47 – 9.56). For GIST patients, ctDNA was detected in 2/9 (22.2%) patients with progressive disease and was informative on the mechanisms of imatinib resistance. Pharmacogenetic profiling was performed on 33 GIST patients and the genotype of CYP2D6 was shown to influence the imatinib plasma exposure, while the concomitant intake of strong CYP3A4 inducers (carbamazepine) and CYP1A2 inhibitors (smoking) were associated with a faster imatinib clearance and risk of under-dosage.

Conclusions

The identification of CNAs and their quantification by means of TFx estimation is feasible in the cfDNA of LARC patients and preliminary data suggests that an increased TFx in course of nCRT is associated with a higher probability of achieving a pCR. The identification of ctDNA in GIST shows a low sensitivity (22.2%) and a high specificity (100%) in identifying patients with progressive disease and might represent a valuable tool to get information on the mechanisms governing the imatinib resistance. Moreover, the pharmacogenetics coupled with the analysis of drug-drug interactions might represent a valuable strategy to address the issue of imatinib pharmacokinetic variability.

CHAPTER 1. INTRODUCTION

1.1 Personalized Medicine in Oncology

In recent years, healthcare in oncology has been gradually shifting from a "one size fits all" paradigm, which is centered on an average response to therapeutics, to a more precise personalized regimen. Precision oncology may be broadly defined as the tailoring of medical treatment to the individual genetic makeup of patients to optimize the efficacy and safety profile of drugs. The potential to improve patient outcomes through precision medicine has led to much excitement among scientists, clinicians, and patients alike. From the US Food and Drug Administration's (FDA) perspective, precision medicine promises to increase benefit and reduce risk of medical products.[1]

Revolutionary improvements in the analytical tools required for personalized medicine have accompanied the introduction of high-throughput technologies, as well as the terrific development of computational biology for the handling and conceptualization of the amount of huge data provided by massive genetic analyses. Modern medicine urges the clinical implementation of "the right drug, right dose, right time, and right way" approach of treatment in the medical field as there are unknown areas that still need to be researched and validated with backing evidence. Both somatic and germline mutations are utilized to better understand the underlying biology of cancer growth and treatment response.

During the past decade, the use of liquid biopsies, which consist of harvesting cancer biomarkers, such as circulating tumor cells (CTCs), circulating tumor DNA (ctDNA) and extracellular vesicles (EVs) from body fluids, has gained tremendous attention. These biomarkers provide a source of clinically actionable molecular information that can improve the effectiveness of precision medicine. The application of liquid biopsy in clinical oncology is a process that requires a careful validation step to prove the reliability of liquid-based tests. The ultimate goal of personalized medicine is the ability to put together these molecular-based biomarkers with pharmacogenetics, environmental and epidemiological information to corroborate and improve the efficacy of current treatment strategies. As a consequence, the built and the harmonization of multidisciplinary teams formed by clinicians, pharmacologists and biologists represent a mandatory choice to guarantee the translation of actionable knowledge on tumors' and host molecular features into the routine clinical practice.

1.2 Liquid Biopsy for Precision Oncology

The identification of minimally invasive methods to assess cancers has long been a central goal of oncology research. The major advances in analytical techniques to examine tumor-derived material in the circulation and other biofluids, has made possible the isolation and the ultra-highly sensitive detection of poorly represented cancer-specific analytes immersed in a vast excess of analytes derived

from normal cells. The analytes used for liquid biopsy include ctDNA, CTCs, proteins, metabolites, exosomes, mRNA, and miRNAs. Each analyte has its own advantages and disadvantages that must be considered when choosing a marker to answer specific clinical questions. In the present work the application of liquid biopsy by means of ctDNA detection will be examined in the framework of gastrointestinal human malignancies.

1.2.1 The Biology of Circulating Tumor DNA

The presence of circulating nucleic acids in the blood of healthy subjects was reported for the first time in 1948 by Mandel and Metais,[2] but it was only in 1977 that a significant enrichment of circulating cell-free DNA (cfDNA) amount in patients with cancer over healthy individuals was demonstrated.[3] The potential clinical interest around the cfDNA in oncology was then finally postulated in 1994, when the presence of mutated *RAS* fragments in the blood of cancer patients was first detected.[4] cfDNA can be defined as the portion of DNA that is encapsulated within circulating vesicles or that is free (not encapsulated) in the bloodstream as well as in other body fluids (urine, saliva, tears), while the fraction of cfDNA that derives from cancer cells refers to circulating tumor DNA (ctDNA). The precise mechanism by which cfDNA is shed from cancerous and non-cancerous cells into the blood stream remains partially unclear, but the most accredited and sound evidences suggest that the cfDNA release is mostly driven by apoptosis, necrosis and by the active vesicles-mediated secretion (Figure 1).[5]

The most peculiar morphological feature of cfDNA is its fragmentation pattern into molecules showing a median length of 160-200 base pairs (bp), which reflects the length of DNA wrapped around the nucleosome protein. This size distribution sustains that a significant amount of cfDNA originates from apoptotic processes and that the presence of nucleosomes actually protects cfDNA from the nucleases-mediated DNA degradation, which is therefore allowed only in the DNA linker regions.[6] A fraction of high-molecular weight cfDNA, *i.e.* larger than 1000 bp, has also been detected and suggests a minor contribution of necrotic processes and phagocytosis to the cfDNA release.[7]

The evidence that cancer patients present higher cfDNA levels than healthy subjects has gained much attention from the clinical and scientific community. In fact, the concentration of cfDNA in plasma of cancer patients ranges between 5 and >1000 ng/mL, while in healthy subjects it ranges between 0 and 100 ng/mL.[8] However, increased cfDNA levels do not represent a sensitive and specific marker for cancer detection, as the same condition has been reported also in patients with non-malignant diseases, such as inflammation, liver injury and autoimmune disorders, and in transplant-receivers subjects.[9–11] Moreover, the level of ctDNA in the blood stream was proven to be extremely influenced by the tumor burden and localization, as well as by the extent of tumor metabolism and vascularization.[12] In this regard, the majority of patients with metastatic disease of the liver, colon, breast, ovaries, esophagus, stomach, pancreas and bladder presents detectable ctDNA in their blood.[13] On the contrary, patients

with tumors located in the prostate, thyroid or within the central nervous system showed a lower amount of ctDNA in their blood, regardless to the concomitant presence of metastatic sites.

Since ctDNA carries the same genetic and epigenetic alterations that are present in the cancer cells of origin, it represents a highly appealing tumor-specific marker to decipher the tumor's genomic landscape in a low invasive manner, hence the term *liquid biopsy*. Moreover, the rapid turnover of circulating nucleic acids from the blood stream, which is estimated to be around 20 minutes, makes the ctDNA a suitable marker for the real-time characterization of the tumor's genome. The possibility of interrogating ctDNA by means of liquid biopsy also promises to virtually overcome the spatial limitation provided by the traditional tissue biopsies, which are restricted to the area of sampling and risk to underestimate the tumor's genome heterogeneity.

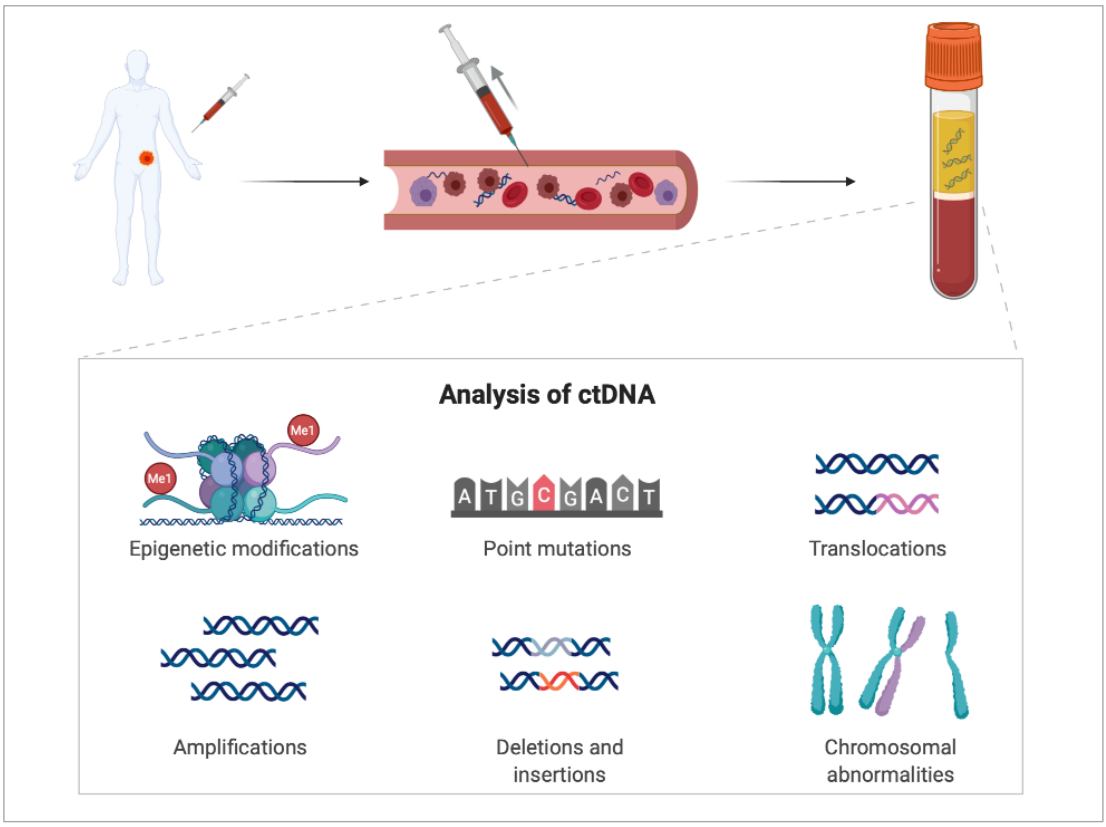

Figure 1. Mechanism of cfDNA collection and isolation from the blood stream. Exemplary analytical approaches for the detection of tumor derived aberrations in the cfDNA are depicted. (created with BioRender.com)

1.2.2 Pre-analytical and Analytical Variability in cfDNA Processing

The clinical translation of liquid biopsy for ctDNA detection is not free of challenges, which are mainly related to the pre-analytical and analytical procedures and whose standardization is necessary to guarantee the obtaining of reproducible results. Plasma was proven to be the most precious source of ctDNA in the vast majority of malignancies when compared with other body fluids as it provides the highest amount of ctDNA.[14] With respect to the pre-analytical variables, it is of crucial importance to

prevent the leukocyte lysis in the blood sample in order to avoid the dilution of ctDNA fragments with massive amounts of genomic DNA. To this end, updated guidelines for optimization of cfDNA recovery suggest that blood should be drawn in K_2EDTA tubes and that the plasma isolation should be performed as soon as possible, with a delay not exceeding the 4 h from blood collection.[12] If longer delayed are forecasted, dedicated tubes containing stabilizers agents should be preferred to ensure the stability of samples up to fifteen days at room temperature.[15] The plasma isolation should be performed by means of two serial centrifugations, the first one for 800 to 1200*g* at 4 °C for 10 min and the second one for 14000 to 16000*g* at 4 °C for 10 min. A careful retrieval of the plasma supernatant after the first centrifugation is necessary to prevent its contamination with leukocyte. The partitioning of the harvested plasma into different vials is encouraged to avoid multiple thaw and refreezing of the samples, which must be stored at -80 °C till cfDNA extraction.

Since ctDNA is present in low amount in a background of genomic DNA, most analytical protocols include an initial PCR-based amplification step, which increases the risk of artifacts introduced by the DNA polymerase and leads to flawed results. To overcome this analytical limitation, the introduction of unique molecular indexes (UMIs), *i.e.* a pool of unique random-generated sequences of 12 nucleotides, has been leveraged to tag every single DNA fragment with a different UMI before their amplification and to allow the downstream accurate discrimination between mutations and PCR-induced artifacts. Beside growing efforts to standardize the pre-analytical and analytical protocols for cfDNA handling, a huge inter- and intra-laboratory variability still remains, resulting in a cross-laboratory error rate that is deeply affected by the cfDNA quantification methods and the different genotyping platforms. These evidences claim for an urgent need for harmonization of procedures and workflows.[16]

1.2.3 Sequencing Platforms and Analysis of cfDNA

The clinical application of liquid biopsy in oncology has remained neglected for a long time, mainly due to the limited analytical sensitivity of techniques used for tumor DNA genotyping in a background of wild-type DNA, which hampered the detection of ctDNA at clinically relevant concentrations. Over the last twenty years, the development of next generation sequencing (NGS)-based technologies has led to the rapid improvement of the analytical approaches for the identification and quantification of low-abundance ctDNA molecules, thus implementing the clinical applicability of ctDNA.The necessity to detect and characterize the ctDNA has entailed the development of many analytical approaches, which can be ascribed to two main categories.

The first analytical strategy relies on targeted approaches, which are aimed at the identification of tumor-specific mutations within selected genomic coordinates. This type of analysis requires highly sensitive techniques, including PCR-based assays such as droplet digital PCR (ddPCR) and beads, emulsion, amplification, magnetics (BEAMing)-PCR, as well as NGS-based methods such as Safe-

SeqS, CAPP-Seq, and TAmSeq.[17] While PCR-based methods interrogate a limited number of known mutations, NGS-based methods allow the parallel sequencing of wider genomic regions comprising up to hundreds of genes. Overall, the candidate-based strategies virtually allow the detection of tumor specific variants at an allele frequency below 0.01% and with a specificity above 80%, depending on genotyping platform used. However, achieving a high sensitivity is deeply affected by the amount of input DNA, so that the cfDNA quantities to be analyzed must be carefully tailored according to the desired level of analytical sensitivity.

The second analytical strategy comprises the untargeted approaches, which are aimed at the characterization of ctDNA at the whole-exome or the whole-genome scale.[18] To these purposes, NGS-based platforms are necessary to screen in parallel wide genomic regions. This kind of analysis is particularly suited when no prior knowledge on tumor's genotype are available and new insights on tumor's genetic aberrations, also in response to administered therapies, are needed. Beside the huge burden of information provided by untargeted sequencing strategies, the sensitivity of the method is lower when compared to targeted approaches (1 – 5%). NGS-based approaches are not free of biases and an error rate of 0.1 – 1% must be considered. To overcome this limitation, the adoption of molecular UMIs together with the application of robust bioinformatic pipelines aimed at reducing the background noise, represent valuable strategies to improve the quality of sequencing results. Moreover, the application of NGS technology requires high purity and quality of starting material to ensure the reliability of results, thus remarking the crucial need for careful cfDNA processing and storage.

A complementary strategy to interrogate genome abnormalities in cancer cells is provided by the characterization of somatic copy number aberrations (CNAs) of tumor DNA at the whole genome scale. To this end, shallow whole genome sequencing (sWGS) has been reported to be a simple, robust, and cost-effective technique optimized for the identification of CNAs in tumor samples. The analytical background for CNAs estimation from sWGS is that the depth of coverage in a genomic region is correlated with the copy number of the region, e.g. a gain of copy number is supposed to have a higher read count than a non-amplified region.[19] For copy number calling, the genome is virtually divided into windows (bins) and reads that are mapped to these genomic regions are counted. After data correction for GC content, the copy number profile is estimated for each bin and specific segmentation algorithms are applied to detect aberrant copy number regions.[20] Although CNAs can be retrieved also from whole exome sequencing (WES) data, this approach introduces more biases and noise than the WGS and that make CNAs detection more challenging (Figure 2).

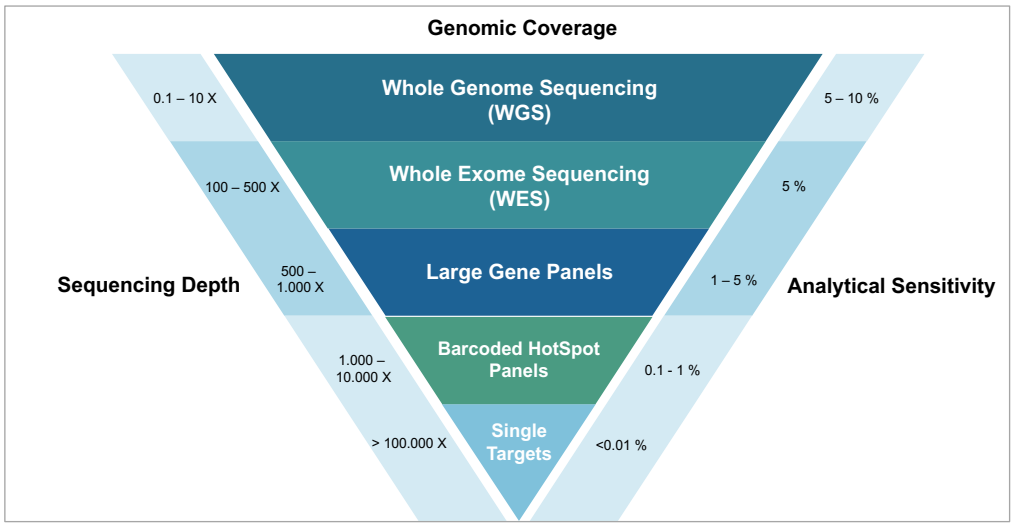

Figure 2. Increasing genomic coverage is accompanied by a decreasing analytical sensitivity.

1.3 Clinical Application of ctDNA in Gastrointestinal Tumors

Gastrointestinal cancers, including esophageal, gastric and colorectal cancer (CRC), have a high incidence and mortality worldwide, with the CRC being the most prevalent with almost 1.4 million new cases diagnosed and over 600 thousand deaths worldwide per year. By contrary, the gastrointestinal stromal tumor (GIST) is a mesenchymal tumor that is not common and represents less than 1% of all gastrointestinal tumors, with a 5-years overall survival (OS) of 50%.[21] Despite tremendous improvements in clinical diagnosis and treatment of gastrointestinal malignancies in last years, the occurrence of progression disease (PD) or metastatic relapse in this field represent the major cause of cancer-related death. The implementation of currently available strategies for the early cancer detection, patient's stratification and for the prompt identification of disease recurrence is urgently needed.

In this context, the possibility of interrogating ctDNA to refine the clinical decision algorithms represent a valuable strategy. In fact, ctDNA analysis has demonstrated excellent specificity and good sensitivity in the detection of somatic tumor derived mutations across many kinds of tumors, with specific regard to the metastatic disease and its clinical utility for detecting EGFR mutations has been approved from regulatory agency, EMA and FDA, in stage IV non-small cell lung cancer (NSCLC) patients, in whom invasive and repeated tumor biopsy might be difficult to obtain due to limited accessibility to tumor site and/or organ disfunction.[22] The NSCLC scenario represents a brilliant example of the clinical utility of ctDNA surveillance, which drives the clinical decision making in downstream personalization of therapeutic options. However, even though this achievement has flattered the clinical and scientific community worldwide, many hurdles remain to be addressed before the ctDNA analysis could find a validated clinical application also in other types of tumors and in different treatment's settings.

The possibility to detect ctDNA in gastrointestinal malignancies embraces a huge variety of applications, spanning from the early cancer detection to the monitoring of metastatic spread disease.[23,24] The clinical advantages arising from ctDNA analysis deeply depend on the clinical needs within

different therapeutic settings and are influenced by the therapeutic options available. Different aspects of ctDNA application in the context of gastrointestinal malignancies are briefly summarized below.

i) *Early cancer detection*: the early cancer diagnosis represents one of the most appealing and challenging application of liquid biopsy in oncology. The fraction of ctDNA in early stage tumors is generally very low (<1%),[25] thus making its detection very difficult, despite the use of high sensitivity techniques. Patients are significantly more likely to be ctDNA positive with multiple organ metastatic disease and increasing number of lymph node metastases.[26,27] Currently, the main methods for early diagnosis of gastrointestinal malignancies are stool occult blood detection, in case of CRC, digital rectal examination, and serum tumor marker (carcinoembryonic antigen (CEA) and carbohydrate antigen 19-9 (CA19-9)) analysis.[28] However, the detection of the serum tumor marker CEA and CA19-9 cannot fully satisfy clinical needs owing to their low sensitivity and specificity. Therefore, the ctDNA detection, specifically when coupled with CEA, CA19-9 and other biomarkers' assessment, virtually represents a great advantage for the early cancer diagnosis. Despite challenging, the application of liquid biopsy to this end might find specific application in the screening of high-risk populations, who present familiar history or a genetic predisposition to cancer. For instance, mutations in genes associated with Lynch syndrome (*MLH1, MSH2, MSH6, PMS2, EPCAM*) represent a genetic hereditary condition that increase the risk to develop CRC, as well as the presence of inflammatory bowel disease, ulcerative colitis and Crohn's disease.[29] The ctDNA application needs further support from prospective clinical trials with large sample sizes, as well as the standardization of detection methods, before it can be used for routine clinical cancer diagnosis.

ii) *Tumor genotyping*: even though the transition from a tumor testing to a blood-based testing requires a multiple steps validation process, the acquisition of information on tumor genotype, with specific regard to the identification of druggable mutations, is gradually taking hold. The shift from a spatially limited tissue sampling to a virtually unbiased blood test is particularly suited when the tumor site is difficult to reach or is spread in different locations.[30] In CRC, the use of targeted panels for the identification in cfDNA of target mutations in the proto-oncogenes (*KRAS*, *BRAF*), which define the sensitivity toward anti-EGFR monoclonal antibodies, has revealed a concordance rate with tumor tissue of 96%,[31] while the validation of cfDNA based screening test for tumor genotyping across multiple cancer types in a study population including 21807 subjects revealed a concordance rate with tumor tissue of 80 – 90%.[32] This modest agreement might be attributable to a limited assay sensitivity in detecting mutant circulating tumors clones as well as to a misrepresentative tissue sampling, in case of ctDNA negativity and tissue test positivity for interrogated mutations. In the context of GIST, the precise characterization of tumor activating mutations in *KIT* and *PDGFRA* genes is of pivotal relevance for the preemptive assessment of tumor's sensitivity toward tyrosine kinase inhibitors (TKIs) and, therefore, to tailor therapeutic strategies accordingly. Today, the exclusive reliance of tumor diagnosis on liquid biopsy requires a careful appraisal and should be integrated with the tissue biopsy.

iii) *Risk-stratification and prognosis*: Recently, the emerging role of ctDNA in early-stage cancers has been achieving increasing attention and pre- and post-operative ctDNA in various cancers has been investigated as a useful prognostic biomarker to indicate risk to recurrence after surgical resection. Several studies have reported the association of pretreatment ctDNA levels with tumor burden and prognosis, highlighting that higher ctDNA levels were observed in patients bearing a wider measurable disease and were commonly associated with a shorter time to progression (TTP).[33,34] This evidence might be attributed to the fact that aggressive tumors are characterized by a high proliferation rate that is associated with high levels of apoptosis, resulting in the shedding of higher quantities of ctDNA. In stage III melanoma patients receiving curative tumor resection, the presence of detectable ctDNA before surgery was associated to a shorted melanoma specific survival, representing a powerful biomarker to refine the stratification of patients for adjuvant treatments.[35] Conversely, ctDNA levels before treatment in locally advanced rectal cancer (LARC) were not prognostic of relapse-free survival.[36] In this framework, the application of liquid biopsy in gastrointestinal malignancies represents a powerful tool to implement the currently available risk-stratification algorithms and to guide the treatments personalization accordingly;

iv) *Detection of minimal residual disease (MRD)*: One of the main challenges in clinical oncology is the early identification of residual tumor cells after surgical removal of tumor. The presence of occult metastatic nieces might not be detectable with traditional imaging techniques and represents a source of tumor cells capable to drive a rapid disease recurrence in absence of any concomitant adjuvant treatment. Therefore, the research of ctDNA after curative tumor resection is a powerful tool to help the detection of MRD. Although the ideal window for detecting MRD is not defined, the majority of published studies examine blood samples approximately 4–12 weeks after treatment.[37,38] Many retrospective studies across different tumor entities have demonstrated the clinical validity of ctDNA in detecting MRD ahead of clinical or radiographic relapse, with lead times varying from about 3 to 11 months, with the notable caveat that in many cases there was no simultaneous surveillance imaging.[39] In LARC the detection of ctDNA after radical surgery successfully identified patients most likely to have a shorter disease-free survival,[40] while ctDNA detection after stage II colon cancer resection provides direct evidence of residual disease and identifies patients at very high risk of recurrence.[38]

v) *Monitoring of treatment response and emergence of secondary resistance*: The logical application of ctDNA monitoring in the metastatic setting is the early identification of tumor progression before metastases become radiographically or clinically detectable. The possibility to tailor therapeutic options according to identified tumor resistant subclones would allow the early intervention and the implementation of the efficacy of therapeutics, avoiding delays in treatment administration. In CRC, the *EGFR* gene is frequently amplified and overexpressed at the protein levels. Therefore, anti EGFR-targeted therapies, mainly represented by the monoclonal antibodies cetuximab and panitumumab, are widely used in metastatic CRC (mCRC) patients overexpressing EGFR.[41] However, these drugs show clinical benefits in only a subset of patients with mCRC owing to molecular alterations in EGFR

pathway effectors. In fact, the presence of activating mutations in *KRAS* gene results in the activation of the downstream RAS-RAF-mitogen-activated protein kinase (RAS-RAF-MAPK) signaling pathway, regardless of EGFR activation or blockade. Therefore, *KRAS* mutations may predict the development of resistance to anti-EGFR antibodies and are consistently correlated with reduced OS and progression-free survival (PFS).[42] The identification of secondary acquired resistance in mCRC patients receiving anti-EGFR targeted agents, has been detected by means of ctDNA analysis in the 38% of patients with baseline wild-type *KRAS*.[43] *KRAS* mutations were shown to emerge in the blood of metastatic CRC patients treated with anti-EGFR monoclonal antibodies up to 10 months before the emergence of radiological disease progression.[44]

The identification of a drug-resistance phenotype is of crucial relevance to drive the clinical decision making in term of treatment selection, as mCRC presenting mutant KRAS are commonly treated with traditional chemotherapy. Apart from *RAS* mutations, also the amplification of the *MET* protooncogene is also associated with acquired resistance in patients treated with anti-EGFR therapy. Amplification of the *MET* locus was detected in ctDNA before clinically diagnosis of relapse, and the prompt administration of MET kinase inhibitors can overcome the acquired resistance.[45] In GIST, the presence of ctDNA bearing *KIT* mutations in exon 13 or 18 have been associated to the acquisition of an imatinib-resistant phenotype, sustaining the application of liquid biopsy as a promising strategy to guide therapeutic decisions in drug-resistant cancers.

In the present work, the application of ctDNA monitoring in the clinical context of LARC and GIST will be analyzed, with specific attention to the monitoring of pharmacological treatments.

1.3.1 Locally Advanced Rectal Cancer (LARC)

CRC is the third most commonly diagnosed cancer type and represents the fourth leading cause of cancer-related death worldwide.[46] Rectal cancer accounts for approximately the 30% of CRC and is characterized by morphological and molecular features that make it a private entity with respect to CRC. The locally advanced rectal cancer (LARC) is defined as stage II/III rectal tumor, with or without lymph nodes involvement and without concomitant presence of metastatic sites. By a molecular point of view, the most frequently mutated genes in LARC are *APC*, *TP53*, *KRAS*, *PIK3CA*, *BRAF* and *NRAS*. As expected, the mutated *KRAS* and *NRAS* genes usually had oncogenic codon 12 ,13 or 61 mutations, whereas the remaining genes had inactivating mutations.[47] The standard of care for the clinical management of LARC relies on neoadjuvant chemoradiotherapy (nCRT) treatment, followed by radical surgery, mainly represented by total mesorectal excision, and optionally followed by an adjuvant chemotherapy. The nCRT was proven to be of crucial importance for the proper management of LARC, as it can improve the rate of curative resection and significantly reduce local recurrence rate.[48,49] Despite these advantages, the recurrence rate of LARC has not decreased significantly and about the 30% of patients treated with a curative surgery will eventually develop distant metastases.[49,50] Administration

of 5-fluorouracil (5-FU)-based adjuvant therapy has been proposed to prevent the development of distant metastases. However, its clinical benefit for LARC patients treated with nCRT and surgery is still controversial as adjuvant treatment was demonstrated to not improve OS, disease-free survival (DFS) or distant recurrence rate.[51,52] The pathological examination of surgical specimen represents nowadays the gold standard for the assessment of response to neoadjuvant treatment. To this end, different scoring systems aimed at assessing the tumor's regression grade (TRG) at the time of surgery are currently used in clinic as they were proven to correlate with survival outcomes. Specifically, the pathological complete response (pCR), which is the absence of visible residual tumor's cells in surgical specimen, is commonly observed in a subset of 15 to 30% of LARC patients,[53,54] and is associated with a longer OS and a lower risk of local and distant recurrence after surgery with respect to patients without pCR.[55] The remaining patients span between a minimal residual disease after nCRT and the total lack of response with possible tumor's progression in course of neoadjuvant treatment, thus making the response to nCRT not only extremely variable in term of prevalence, but also very unpredictable.

The possibility to predict the outcome of nCRT before treatment initiation or during its very early course would be of crucial clinical relevance to select and optimize the following therapeutic options. While intensified nCRT programs could be hypothesized for poor responders,[56] the application of more conservative surgical strategies or watch-and-wait approaches, could be adopted in patients with optimally responding tumors, with a concomitant improvement of the quality of life.[57]

The selection of patients for these personalized treatment strategies is currently based essentially on clinical-pathological criteria, including tumor size, N stage, distance of tumor from the anal verge, and interval from nCRT to surgery. However, additional and more effective stratification criteria are needed to improve the currently available risk stratification algorithms in LARC and to sustain the clinical decision making for treatment optimization. The possibility of interrogating ctDNA as a surrogate of tumor tissue in the context of LARC represents a highly appealing strategy for the close monitoring of nCRT and for the early patient stratification into good and poor responders.[58]

1.3.1.1 Application of ctDNA Analysis in LARC

LARC is characterized by a small panel of well described point mutations in selected genes, *i.e. KRAS*, *TP53*, *BRAF*, *APC*, *PIK3CA*, which are not druggable and of limited prognostic impact. In sharp contrast with the CRC, to date only a few studies have investigated the clinical utility of ctDNA monitoring in the context of LARC, and reported findings exhibited a limited prognostic role of ctDNA in LARC with respect to the early assessment of nCRT outcome. Specifically, the identification of ctDNA after surgery has been associated with a shorter time to progression, suggesting that it might represent a suitable marker for the identification of minimal residual disease and for the selection of candidate patients to adjuvant treatments.[40] However, the detectability of ctDNA at the time of diagnosis showed no significant association with the response to nCRT, thus hampering its application as an early

biomarker of treatment efficacy.[40,59] Investigations carried out till now have been focusing on the identification of selected point mutations in the ctDNA, by scanning genes that are frequently mutated in LARC or by tracking point mutations previously identified in the matched tumor tissue.

Other appealing but poorly investigated markers for ctDNA detection and monitoring relies on the identification of wider genomic aberrations, such as gene amplifications or chromosomal rearrangements. Genomic instability is a hallmark of cancer and approximately the 90% of solid tumors are aneuploid and harbor CNAs. CNAs include loss of chromosomal material (deletions), gain of chromosomal material (duplications). Chromosomal instability and microsatellite instability are well known markers described in CRC, whereas their presence, as well as their prognostic significance in LARC has achieved a lower level of evidence. A recent analysis of 33 treatment naïve LARC biopsies revealed an increased level of genome instability, *i.e.* copy number imbalance, in patients reporting an incomplete pathological response to nCRT, with respect to pCR patients, suggesting that untargeted ctDNA detection strategies might be attempted in LARC.[60]

While targeted approaches have the potential of capturing major known driver mutations at a high resolution, they mostly interrogate only single or small set of genes and are therefore unable to assess the genetic heterogeneity of ctDNA in an unbiased manner. However, given that tumor genomes are constantly changing under the selective pressures of therapies, a comprehensive genome-wide analysis might be advantageous in this setting. In the context of a complex phenotypic trait, such as the response to a chemotherapy combined with a concomitant radiation treatment, the application of unbiased whole-genome approaches. Recent studies evaluated the application of low coverage sWGS of cfDNA as a tool to identify the presence of specific somatic CNAs in cancer that can be used for the treatment monitoring and for the early assessment of disease progression.[61,62] This approach could be of particular relevance especially for the surveillance of cancers that do not harbor specific patterns of actionable point mutations and for which the monitoring of selected mutations is of limited clinical utility.

1.3.2 Gastrointestinal Stromal Tumor (GIST)

By an epidemiological point of view, GIST is a rare disease. However, it represents the most common mesenchymal tumor affecting the gastrointestinal tract.[63] According to epidemiological surveys, most population-based studies report a GIST incidence between 10 and 15 cases per million people, with an increase of incidence over the past twenty years attributable to a misclassification of GIST before the 21st century.[64] GIST has no gender predominance as its distribution is equal between male and female. On the other hand, the age of diagnosis is very wide among the population with a median age of 58 years.

GISTs can arise everywhere through the gastrointestinal tract. However, its most common primary localizations are the stomach (50%) and the small bowel (25%) followed by the rectum (5%) and the esophagus (<5%). The canonical metastatic sites of GIST are the liver and the abdomen, whereas extra-

abdominal colonization is rare and mostly affecting lungs and bones. So far, the identification of intestinal cell of Cajal as a likely precursor of GIST is the most accredited hypothesis upon the origin of the disease, as GIST cells were proved to have common features with them. Intestinal cells of Cajal are innervated cells belonging to the myenteric plexus that have autonomous pacemaker functions and coordinate peristalsis through the gastrointestinal tract.

Morphologically, the vast majority of GIST cells (70%) presents a characteristic spindled shape with eosinophilic cytoplasm and presence of multiple nuclei. GIST cells with epithelioid morphology and poorly eosinophilic cytoplasm accounts for roughly 20% of GISTs, whereas the remaining 10% of GIST cells is represented by a mixture of the two previous types. The immunohistochemistry analysis of GIST cells is an integral part of the GIST diagnosis as GIST cells usually show positivity for CD117 (KIT) and/or DOG1, CD34, ACAT2, S100, DES and keratin. Even thou KIT is the most specific antigen in GISTs, a sub-population of them (5%) result KIT-negative, encouraging the screening for a panel of antigens.

By a molecular point of view, oncogenic *KIT* mutations are found in approximately the 80% of GISTs and represent the predominant mechanism of GIST initiation. Gain-of-function mutations, deletions or indels in *KIT* gene are most commonly located in the intracellular juxtamembrane domain, encoded by exon 11, and account for the 67% of the overall mutations in GIST. Their presence disrupts the normal autoinhibitory state of KIT receptor, resulting in its constitutive ligand-independent activation. The remaining *KIT*-mutant GISTs display activating mutations in the extracellular ligand-binding domain, encoded by exon 9 and found in the 10% of GISTs, and, to a lower extent (<2%) in the kinase domain, encoded by exon 13 and 17.[65] Approximately 15% of GISTs are driven by oncogenic *PDGFRA* activating mutations, which are mainly localized in homologous regions to KIT receptor (exon 12, 14 and 18).[66] Owing to their role as initiating clonal events in GIST's etiology, *KIT* and *PDGFRA* mutations are mutually exclusive. A small proportion of GISTs, representing roughly 5% of the GIST general population, does not harbor *KIT* or *PDGFRA* oncogenic mutations and is universally known as wild-type GISTs (Table 1).

A growing body of evidence sustains the role of RAS/MAPK and PI3K/mTOR as the two main pathways transducing KIT/PDGFRA-mediated oncogenic signaling, while a minor contribution to the oncogenic cascade is supported by pathways involving STAT3, AXL and Src.[67] However, a definitive characterization of players involved in the biochemical signal transduction in GIST is not fully understood yet. Moreover, genomics events leading to MAPK pathway hyperactivation, such as *BRAF* and *RAS* mutations, and *NF1* loss-of-function mutations, are oncogenic drivers in wild type GIST.[68] Consistently, wild type GISTs that are deficient in the succinate dehydrogenase (SDH) harbor a remarkable epigenetic dysregulation that converges in the functional activation of KIT and FGF in the absence of canonical kinases' mutations, thus leading to a highly expressed MAPK signature.[69]

Table 1. Oncogenic initiating mutations in GISTs and their relative frequency within GIST patients.

Genetic Alteration	Frequency (%)
KIT mutations	75-80
Exon 11	67
Exon 9	10
Exon 13	1
Exon 17	<1
PDGFRA mutations	10-15
Exon 18 (D842V)	8
Exon 18 (non-D842V)	3
Exon 12	1
Exon 14	<1
KIT/PDGFRA wild type	5-10
SDH-deficient	8
BRAF mutant	1
RAS mutant	<1
NF1 mutant	<1

KIT mutations alone are insufficient to induce malignant behavior, and additional genetic events are necessary to transform micro-GISTs (<1 cm) into tumors with increasingly malignant potential. Indeed, clinical and biological progression of GIST from micro- localized disease to an aggressive metastasized malignancy is a dynamic process involving the acquisition of additional mutations mainly located in genes such as *MAX*, *CDKN2A* and *DMD* (Figure 3).[70,71]

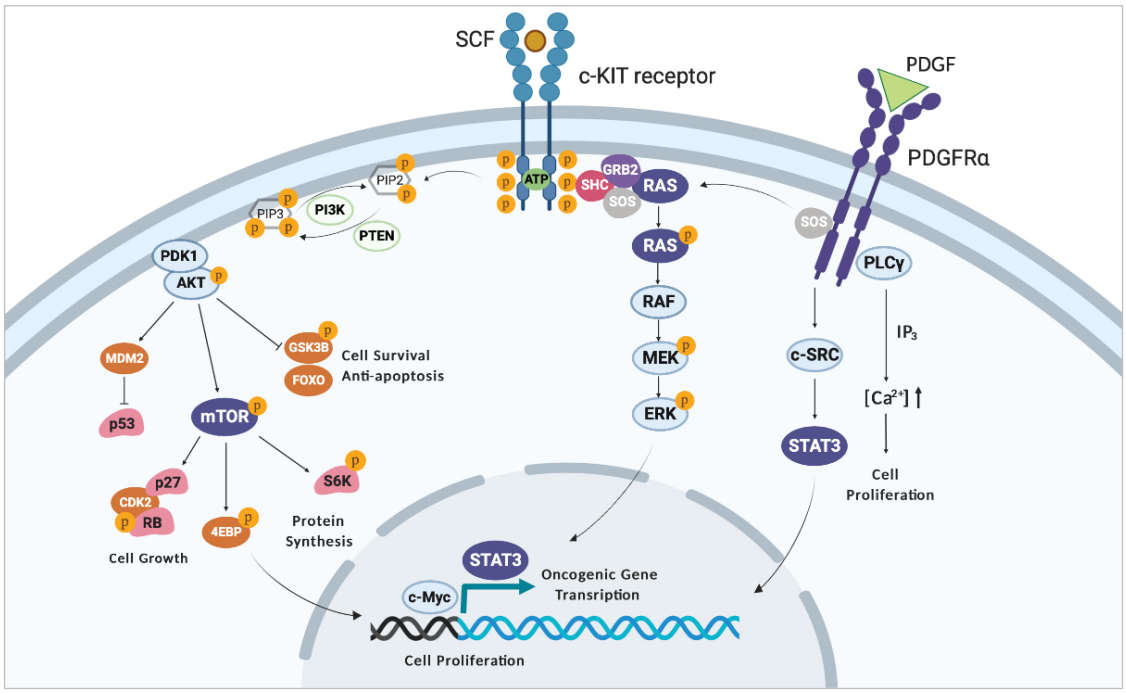

Figure 3. KIT and PDGFRA-mediated signaling pathways that drive the oncogenic signaling in GIST cells (created with BioRender.com)

Since few decades ago, GIST was classified as a general leiomyosarcoma and treated accordingly by means of standard chemo-radiotherapy. However, in contrast with the other kinds of soft tissue sarcomas, the response rate of GIST toward traditional therapies was poor enough to consider GIST a treatment-refractory tumor. Drug development in GIST has successfully exploited the high reliance on KIT/PDGFRA oncogenic signaling as a therapeutic vulnerability, so that GIST has been the first tumor taking advantage from the approval of a molecularly targeted therapy – imatinib – nearly two decades ago. Since then, the management and prognosis of GIST have undergone a terrific improvement in term of acute treatment response and long-term survival, and imatinib still represents the cornerstone of care for the treatment of GIST. GIST was first recognized as a private entity with respect to other mesenchymal tumors in 1998, after the discovery that gain-of-function mutations in KIT or PDGFRA tyrosine-kinase receptors orchestrate GIST growth and survival from tumor initiation to clinically symptomatic disease.[72,73]

1.3.2.1 Pharmacodynamics of Imatinib

Imatinib mesylate is a tyrosine kinase inhibitor (TKI) that selectively binds KIT, PDGFRA tyrosine kinase receptors in GIST and the bcr-abl tyrosine kinase, the chimeric receptor created by the Philadelphia chromosome abnormality in chronic myeloid leukemia (CML). Imatinib binds the TKIs' ATP binding site, locking them in a self-inhibited conformation, therefore inhibiting the enzymatic activity of the receptors and interrupting the downstream signaling pathways.

The regulatory approval of imatinib as a first-line treatment in patients with advanced or metastatic GIST has triggered a new era of targeted therapy. Approximately, two thirds of patients administered with imatinib present objective radiographic response, with a median PFS of 20 months and a median OS of 57 months,[74] in striking contrast to the pre-imatinib era, when the median OS was restricted to 10 – 20 months. These outstanding clinical improvements sustain the central tumor's reliance on KIT/PDGFRA-mediated oncogenic signaling and their crucial involvement as effective actionable targets for therapeutic purposes in GIST. However, despite 7 – 9% of patients exhibits an excellent imatinib sensitivity and experiences a complete clinical response while on treatment, the molecular scenario of different *KIT/PDGFRA* mutations is the main decisive element to predict the clinical sensitivity to imatinib.[75,76] Accordingly, genetic alterations involving *KIT* exon 11 predict for deeper and prolonged tumor response, while patients with *KIT* exon 9 mutations are usually less sensitive to imatinib and benefit from an increased imatinib daily dose (800 mg). Conversely, mutations in *PDGFRA* exon 18 D842V are intrinsically insensitive to imatinib.[77,78] However, even patients who achieve a clinical complete response to imatinib, the disease could not be deemed cured, as the imatinib interruption leads to tumor relapse in almost all patients,[79] and surgery remains the only curative intervention for GIST eradication. This evidence is consistent with the mechanism of action of TKIs, which are cytostatic rather than cytotoxic agent and the imatinib administration was proven to induce

the development of a quiescent phenotype in cancer cells, whose effect is reversible and dependent on the drug's intake.

The selective pressure exerted by imatinib in cancer cells tend to trigger the positive selection and expansion of clones with acquired secondary mutations in *KIT*, which represents the main mechanism of imatinib failure in approximately 90% of relapsed GIST patients.[80] Secondary *KIT* mutations cluster in two regions of the KIT kinase domain, the ATP binding pocket and the activation loop, whereas resistance occurrence in imatinib sensitive PDGFRA-driven GISTs is not well known, although it is conceivable that homologous domains to KIT receptor will be affected. It is also not clear whether resistance mutations are preexistent, emerge through selective pressure, or both mechanisms are involved. Moreover, imatinib failure may not result from biological progression, but from a reduction in drug exposure, specifically after prolonged treatments. After imatinib failure, two main strategies are possible, although never compared formally: doubling imatinib dose (400 mg twice a day) or administering sunitinb as an alternative. The emergence of new metastases, as well as the primary tumors regrowth, most commonly herald the presence of resistance subclones against which imatinib cannot bind the receptor, and therefor starting sunitinib would seem the best choice. Both sunitinib and regorafenib are multi-kinase inhibitors (MKIs) with a broader spectrum of action against KIT, PDGFR-family and VEGFR-family. Several other TKIs have been proposed for the management of advanced GIST, providing a modest improvement of the PFS (up to 6.3 months with ripretinib), regardless to the line of treatment.[81,82]

Among the still unmet clinical needs for the management of advanced GISTs is the huge heterogeneity of *KIT* secondary mutations that leads to mixed responses and modest clinical benefit in patients experiencing imatinib failure.[80,83] For its paradigmatic scenario of *KIT/PDGFRA* secondary mutations that drive the disease progression, GIST represents an excellent model to implement the ctDNA-guided treatment. The National Comprehensive Cancer Network (NCCN) Clinical Practice Guidelines recommend genetic analysis to guide targeted therapy in newly diagnosed GIST patients.[84] However, aside the genetic characterization of driver mutations, which is usually performed on the diagnostic tissue specimen, the dynamic monitoring of mutational pattern under treatment is of pivotal relevance to guarantee the efficacy of administered drugs over time. In this framework, the detection and monitoring of ctDNA represents a safe alternative to the tissue rebiopsy for the genetic analysis of GIST mutational spectrum. In 2013, Demetri and colleagues presented an exploratory analysis to assess GIST genotypes on patients in the GRID study. Mutations in the *KIT* gene were detected in 58% of the blood samples compared with 66% of the tumor tissue samples.[85] A recent study demonstrated the reliability of ctDNA detection by NGS for the assessment of diagnostic genotype in twenty-five localized GIST patients, showing an overall agreement 72.2% between ctDNA and primary tumor DNA of in the 18 *KIT*-mutant GISTs. Conversely, no ctDNA was detected in *KIT/PDGFRA* wild-type GISTs, who remain a still poorly understood category deserving more specifically devoted research efforts.[86]

Beside tumor genotyping, the most promising application of ctDNA detection on GIST is represented by the dynamic monitoring of ctDNA within different therapeutic settings. The identification of ctDNA in patients treated with first line therapy for the management of the metastatic or localized non-operable disease may provide early information upon an ongoing disease progression and upon mechanisms behind it, thus driving the clinical decision making in term of downstream pharmacological intervention. On the other hand, patients administered with imatinib in the adjuvant setting, which is commonly given for three years after radical surgery, might benefit from the ctDNA monitoring aimed at the identification of disease relapse or, more challenging, at the surveillance of minimal residual disease. In the context of neo-adjuvant setting, liquid biopsy in GIST displays a more negligible application, since the tumor's genotype is the major determinant to accurately predict the imatinib sensitivity and the tracking of ctDNA beyond its diagnostic purpose would appear redundant. In 2013, Demetri *et al.* investigated the detectability of secondary *KIT* mutations, which drive resistance to imatinib and sunitinib, in the blood of GIST patients and compared them with the matched tumor tissue. They found mutations in 47% of tested blood samples compared with only 12% of tissue samples. In addition, nearly half of blood samples in which secondary *KIT* mutations were found, harbored multiple secondary mutations. That study pioneered a new era for ctDNA research in GIST, which was proposed as an efficient marker of mutational GIST status and disease itself.[85] Thereafter, few studies tried to validate ddPCR or NGS-based methods for the monitoring of ctDNA in GIST patients showing that i) ctDNA shedding in GIST is usually very low, thus posing a challenge to its clinical routinely application,[87] ii) ctDNA detection is more successful in advanced imatinib-resistant patients[88] and iii) when positive, ctDNA monitoring reflects the course of the disease and the expected sensitivity pattern to TKIs.[89] Beside the great specificity of ctDNA detection, which would seem to recapitulate the mutational background of the tumor tissue, its detection rate seems to represent the main limiting step against its clinical application as a prognostic tool in GIST.

However, even in presence of imatinib-sensitizer mutations, the imatinib efficacy and the disease control cannot be taken for granted and the 10 to 20% of patients will eventually develop disease progression. The exacerbation of an imatinib resistant phenotype is only partially dependent on a deficient pharmacodynamic interaction between the drug and its molecular target. In fact, imatinib represents a paradigmatic case of pharmacokinetic heterogeneity. Imatinib plasma exposure, which can be described by pharmacokinetic parameters such as the area under the curve (AUC) and the trough concentration at the steady state, was reported to vary significantly among the population, thus exposing the patients to the risk of treatment inefficacy or toxicity. The reasons leading to this phenomenon are partially unknown, even though both genetic and environmental factors have been proposed as major determinants on pharmacokinetic variability. Specifically, the contribute of pharmacogenetic variants affecting drug's metabolizing enzymes and transporters and the concomitant administration of potentially interacting drugs is being gradually considered in clinical practice as a complementary tool to improve the treatment efficacy in clinical oncology.

1.3.2.2 Pharmacokinetics and Pharmacogenetics of Imatinib

After oral administration imatinib is rapidly absorbed through the gastrointestinal tract, with a bioavailability of 98%. The drug is extensively bound to plasma proteins (95%), predominantly to albumin and *alpha* glycoprotein.[90] The plasma half-life of imatinib is approximately 18 hours, thus allowing the daily drug administration. Imatinib is mainly metabolized by the liver, and only 13% is being excreted unchanged in urine.[91] Imatinib is absorbed through the intestinal wall and interacts with P-glycoprotein (P-gp, ABCB1) or with ATP-binding cassette sub-family G member 2 (ABCG2) transporters at the membranes of intestinal epithelial cells and is then transported to the intestinal lumen. Imatinib undergoes a first pass effect metabolic step, where a fraction of active drug is metabolized in the liver. Most of imatinib is metabolized by cytochrome P450 isoenzyme CYP3A4 to its main metabolite (N-demethylated piperazine derivate or nor-imatinib), which shows in vitro potency similar to the parent drug. Other enzymatic players, such as CYP3A5, CYP1A2, CYP2D6, CYP2C9, CYP2C8 and CYP2C19, have a minor contribution in imatinib catabolism (Figure 4).

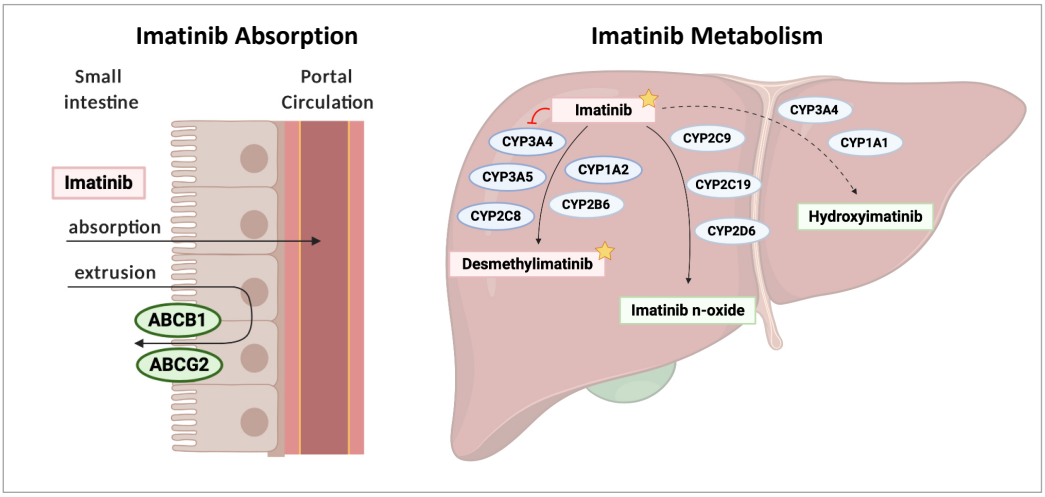

Figure 4. Exemplary representation of the transport and metabolism of imatinib. Imatinib is absorbed through the gastrointestinal lumen and is distributed to tissues after a first-passage step of metabolism. The transporters ABCB1 and ABCG2 play a role in the extrusion of imatinib from the luminal gut cells. In the liver, a complex system of cytochromes catalyzes the imatinib biotransformation into inactive species. One imatinib metabolite, i.e. the desmethylimatinib is biologically active. (created with BioRender.com)

A direct linear proportionality between administered imatinib dose and its plasma exposure has been observed at the steady state. However, a remarkable variability of imatinib plasma AUC has been reported among subjects and was shown to correlate with treatment inefficacy or toxicity.[92,93] The toxicity of Imatinib are usually mild and not life-threatening when compared with conventional chemotherapy. The main toxicities reported are edema (periorbital, face, and limbs), cutaneous rash, asthenia and anemia. The incidence of imatinib adverse events has been associated with a range of clinical factors, showing associations with sex, age and performance status with the incidence of severe imatinib-induced, non-hematological adverse events such as fatigue, nausea, diarrhea and edema.[94]

Although toxicity can be debilitating, non-hematological toxicity can be treated with other drugs and hematological toxicity is often asymptomatic and acceptable considering the need for antitumor therapy. On the counterpart, the risk to develop disease progression or recurrence as a consequence of low imatinib plasma exposure is a clear example of adverse drug reaction showing a severe impact on patients' prognosis.

It has been demonstrated that genetic polymorphisms of main drug-metabolizing enzymes and transporters may significantly influence the inter-individual variations in drug metabolism and disposition.[95] The presence of pharmacogenomic variants in drug metabolizing enzymes and transporters has led different pharmacogenetic working groups, such as the Dutch Pharmacogenetics Working Group (DPWG) and the international Clinical Pharmacogenetics Implementation Consortium (CPIC), to formulate pharmacogenetic guidelines to optimize pharmacotherapy.[96,97] The use of pharmacogenetic (PGx) tests aimed at defining the genotype-driven functional level of drug's metabolizing enzymes and transporters before dugs' administration allow the healthcare providers to treat patients with a more personalized drug therapy, ultimately helping to increase the efficacy and safety of medical treatments. The impact of genotype in defining the activity of codified proteins has been translated into the gene activity scoring system, which allows the quantification of the enzymes' functionality with respect to the wild type allele. The activity score (AS) also represents a strategy to make easier the pharmacogenetic interpretation and to sustains the implementation of PGx recommendation into the clinical practice. The growing body of PGx evidences has also led the regulatory agencies EMA and FDA to include pharmacogenetic information into the summary of product characteristics for those drugs presenting actionable dosing recommendation guidelines according to patients' genotype. One of the best fitting examples of the successful application of PGx information in oncology is the gene-drug pair represented by the dihydropyrimidine dehydrogenase (*DPYD*) gene and the chemotherapeutic agent 5-FU. The *DPYD* gene codifies the homonym enzyme DPD, which catalyzes the conversion of the active form of 5-FU into inactive metabolites.[98] The presence of loss-of-function genetic polymorphisms in the *DPYD* gene is a condition that affects the roughly 10% of Caucasian population and that leads to a reduced DPD activity. The loss of DPD catabolic activity, or its reduced expression, culminates in the accumulation of 5-FU and leads to the onset of severe life-threatening toxicities. To date, four genetic polymorphisms have been straightforwardly associated with different extents of reduced DPD activity, *i.e.* DPYD*2A (c.1905+1G>A), DPYD*13 (c.1679T>G), DPYD c.2846A>T and DPYD c.1236G>A.[99] For these variants, PGx guidelines recommend a starting 5-FU dose reduction, or the switch to another therapy, according to the patient's genotype and the *DPYD* activity score is currently used to optimize the individual's starting dose. The gene activity score ranges from 0 (no DPD activity) to 2 (normal DPD activity).[100,101] The preemptive DPYD genotyping and the according 5-FU dose optimization has been proven not only to reduce the onset of severe toxicity in CRC patients,[102] but also to be cost-effective by reducing the costs related to the toxicities' management and hospitalization.[103,104]

Imatinib is predominantly metabolized by CYP3A4 in the liver, with a minor contribute provided by the CYPs isoforms CYP3A5, CYP1A2, CYP2D6, CYP2C9, CYP2C8 and CYP2C19. Moreover, the drugs' transporters ABCB1 and ABCG2 play a role in imatinib absorption and distribution, as well as in the drug extrusion from cancer cell. These enzymes and transporters are located in highly polymorphic genetic loci and the presence of loss-of-function and gain-of-faction genetic variants playing a role in modulating the enzymes' metabolic activity is well documented. Accordingly, PGx recommendations based on CYPs and transporters genotype have been proposed and are currently used in clinical setting to personalize the pharmacological treatment of many commercially available drugs. However, no PGx recommendations for imatinib have been proposed so far, partially owing to the paucity of studies investigating the gene-drug interaction and to the lack of ground evidences with respect to the impact of genetic polymorphisms on imatinib exposure. The pharmacogenetic of metabolizing enzymes and transporters involved in imatinib disposition have been investigated and the association with clinical variables, such as the time to progression or the imatinib plasma exposure have been explored. However, literature has provided controversial findings, partially owing to different methodological approaches used to evaluate the patients' metabolic phenotype.

The ABCG2 transporter, also known as breast cancer resistance protein (BCRP), is encoded by the *ABCG2* gene and acts as a cellular transmembrane transporter able to excrete xenobiotic molecules.[105] Imatinib is known to be substrate for the ABCG2 transporters, which is highly expressed in the intestinal epithelium and on the membrane of cancer cells.[106] In a study aimed at evaluating the association between 34 SNPs in genes involved in imatinib metabolism in GIST patients and the need for imatinib dose reduction or discontinuation as a consequence of toxicity, Verboom *et al.* observed that the A-allele in rs2231137 in *ABCG2* gene were associated with an increased risk of imatinib dose reduction in comparison with wild-type patients (OR 7.35; $p = 0.0002$).[107] The presence of the A-allele in rs2231137 had been previously associated with better response to imatinib in Korean patients, but the mechanism by which this SNP may lead to higher imatinib plasma levels is uncertain, as an association with imatinib steady state trough levels was not reported in two cohorts of GIST patients from China and Korea.[108–110]

The gene *ABCB1*, also known as multidrug resistance protein 1 (MDR1), encodes for the drug transporter P-gp. ABCB1 is expressed the small and large intestines, adrenal gland, placental trophoblasts, kidney, liver, pancreas (pancreatic ductile cells) and capillary endothelial cells of the brain and testes. Its expression is specifically abundant in the small intestine, up to seven times higher than in the liver.[111] However, a huge variability in the expression level of P-gp in the liver was reported, sustaining the interindividual variability in drug's metabolism.[112] Evidences including findings in knockout mice support that P-gp plays an active role in and excreting substrate drugs through the canalicular membrane of the hepatocytes into the bile, through the brush-border membrane of enterocytes into the gut lumen and through the brush-border membrane of proximal tubules into the urine.[113] P-gp accepts a broad spectrum of structurally and functionally unrelated drugs. Interestingly,

there is a strong overlap in substrate specificity and tissue distribution between P-gp and CYP3A4 and 3A5. Hoffmeyer *et al.* first reported that the presence of a synonymous SNP (3435C>T; rs1045642) in the exon 26 of *ABCB1* gene was associated with significantly reduced intestinal P-gp content in subjects with the T/T genotype in comparison with subjects homozygous for the C allele (genotype C/C), leading to higher steady-state plasma concentrations after the oral administration of digoxin.[114] After this discovery, a considerable number of studies has been conducted on the association between *ABCB1* genotype and drug-related phenotype, sometimes with inconclusive or controversial results. An association with the need for imatinib dose reduction and homozygous carriers of T-allele in rs28656907 in *ABCB1* was found (OR 0.19 p=0.040) but the association lost its significance after multivariate analysis corrected for age, gender and performance status.[107] This SNP has been also shown to increase the ABCB1 expression.[115]

According to imatinib summary product characteristics, the main CYPs involved in imatinib metabolism are CYP3A4 and CYP2C8, whereas other isoforms play a minor role in influencing imatinib plasma concentration.[91] The metabolic activity of CYP3A4 is irreversibly inhibited by imatinib itself, which was proven to lead to a hepatic CYP3A4 inhibition up to 90% under clinically relevant imatinib concentrations *in vitro*.[116] In fact, the concomitant administration of the strong CYP3A4-inhibitor, ketoconazole, was reported to cause an AUC imatinib increase by only 40%,[117] whereas other CYP3A4-inhibitors had little to no effect on imatinib exposure,[118] suggesting that the exacerbation of a comedication-mediated phenotype is dramatically dampen from an already drug-triggered deficit of enzymatic activity. As a consequence of CYP3A4 imatinib-driven modulation, the relative contribution of other CYPs involved in imatinib metabolism was proven to change significantly in course of treatment. In fact, *in vitro* studies reported that at the beginning of imatinib treatment, the fraction of imatinib hepatic catabolism is mediated for the 60% from CYP3A4 and for the remaining 40% from CYP2C8, whereas after long-term imatinib administration the contribution of CYP3A4 drops to the 25-35% as a consequence of a dose- and time-dependent imatinib-mediated auto-inactivation of CYP3A4. Consequently, the contribution of CYP2C8 in imatinib catabolism rose up to 65-75%, thus accounting for the main enzyme involved in imatinib metabolism.[119] Therefore, in course of a long-term imatinib therapy, the concomitant presence of SNPs affecting the activity of CYP2C8 and the concomitant administration of CYP2C8 interacting drugs may largely contribute to the interindividual variability in imatinib exposure. For instance, the gain-of-function CYP2C8*3 allele has been associated with a remarkable increased clearance of several drugs, including rosiglitazone and pioglitazone.[120–122]

The *CYP2D6* gene is highly polymorphic and can therefor give rise to enzymes that range between non-functional (*i.e.* poor metabolizers) and increased functional (*i.e.* ultra-rapid metabolizers). The CYP2D6*3, *4, *5 and *6 alleles are non-functional as a consequence of frameshift variants (*3, *6), splicing defects (*4) or whole-gene deletion (*6). The imatinib clearance after oral administration was reduced in individuals with at least 1 CYP2D6*4 allele (median, 7.78 vs 10.6 L/h; $p < .0695$).[123]

However, data are conflicting as a more recent study showed that the clearance of imatinib was not influenced by the *CYP2D6* genotype.[124]

With respect to the *CYP1A2*, only one study has investigated the relationship between *CYP1A2* genotype and imatinib exposure, evaluated by means of the need for imatinib dose reduction dictated by the reported side effects. The presence of two C-alleles in rs762551 in *CYP1A2* was associated to the need for imatinib dose reduction (OR 7.12; $p = 0.001$) since the C-allele yields a slower metabolic activity of the enzyme resulting in higher imatinib plasma levels.[107]

Beyond the gene-drug interaction, another relevant and frequently neglected issue in clinical pharmacology is the drug-drug interaction (DDI). The multimorbidity and the consequent intake of multiple medicines is a common condition, especially in older population. Together with prescribed drugs, which are given under medical supervision, the availability of self-medicating agents, herbal products and food supplements represent a source of uncontrolled biologically active compounds whose cross-interactions are rarely considered and might expose the patient at an increased risk of adverse events and poor health outcomes. DDIs can be classified as pharmacodynamic or pharmacokinetic. Pharmacokinetic DDIs are defined as drug interactions regarding drug absorption, metabolism, distribution and elimination leading to altered plasma concentrations of a drug and possible unfavorable outcomes (e.g. increased toxicity and reduced treatment efficacy).[125] The mechanism behind the pharmacokinetic DDIs mainly relies on the interaction between two or more drugs and the same metabolizing enzymes or transporters, whose activity might be differentially modulated, *i.e.* inhibited or enhanced, in presence of specific drugs resulting in an unpredicted altered metabolism of the target drug. Pharmacodynamic DDIs can be additive, antagonistic or synergistic.[126] Conversely, a pharmacodynamic interaction is the altered response in terms of toxicity and efficacy when two or more drugs affect similar molecular targets (e.g. membrane receptors).

Therefore, the metabolic activity of a drug metabolizing enzyme or transporter, is modulated not only by the subject's genetic makeup but also by the concomitantly administration of other drugs, which may exhibit an additive, antagonistic or synergistic effect with respect to the genotype-driven metabolic activity. The temporary transition from the genotype-predicted metabolizing phenotype to the phenotype registered in presence of a concomitant interacting non-genetic factor (*e.g.* drugs, smoking) has been named *phenoconversion*.[127] These evidences have led to reconsider the association between genotype and predicted phenotype and have shifted the paradigm of pharmacogenetic from the investigation of the pair gene-drug interactions to the more sophisticated triplet gene-drug-drug interactions.

To date, the literature on gene-drug-drug interactions is limited, with only a few reviews evaluating the impact of *CYP2C9*, *CYPC19*, and *CYP2D6* variants and their interplay with concomitantly administered interacting drugs.[128,129] In the framework of TKIs, one review has summarized the potential clinical impact of DDIs on TKIs plasma exposure and the association with the risk to develop adverse drugs reactions, such as inefficacy or toxicity.[125] With respect to imatinib, the impact of comedications has

been reported to play a minor role in defining its plasmatic levels, suggesting that other factors might significantly contribute to the interindividual variability. As stated above, CYP3A4 is the main enzyme involved in the imatinib metabolism. The concomitant administration of CYP3A4 inhibitors (e.g. ketoconazole) was shown to increase by 40% the imatinib AUC in healthy subjects.[117] However, an imatinib dose reduction in presence of concomitant strong CYP3A4 inducers is not recommended from regulatory agencies, in favor of the close monitoring of toxic effects.[91] Moreover, the concomitant administration of strong CYP3A4 inhibitor compounds is recommended to be as short as possible. Conversely, for CYP3A4 strong inducers (e.g. carbamazepine), a 50% imatinib dose increase should be applied to minimize the risk of imatinib underexposure and inefficacy. Also, the close monitoring of imatinib pharmacotherapy is recommended for concomitant use of CYP3A4, CYP2C9 and CYP2B6 substrates with narrow therapeutic windows, as imatinib itself can modify the bioavailability of other drugs.

Evidences suggesting a mild involvement of DDIs in imatinib pharmacokinetic, leave unmet the need for a better understanding of the interpatient pharmacokinetic heterogeneity in imatinib clinical pharmacology. Moreover, the phenomenon of gene-drug-drug interactions, with specific regard to the mechanism of photoconversion, in imatinib has never been investigated so far.

CHAPTER 2. AIMS

The main aim of the present doctorate thesis is the assessment of the feasibility of circulating tumor DNA (ctDNA) analysis as an integrative tool aimed at the implementation of the pharmacological treatments' monitoring and optimization in the framework of human gastrointestinal malignancies. Specifically, the ctDNA analysis clinical validity has been investigated in the context of locally advanced rectal cancer (LARC) and in localized or metastatic gastrointestinal stromal tumor (GIST). To this end, specific analytical strategies have been chosen to better address the different clinical needs within the two different therapeutic settings.

In the context of LARC, the cell-free DNA (cfDNA) collected at the time of diagnosis, in course of neoadjuvant chemoradiotherapy (nCRT) and after nCRT, has been interrogated in newly diagnosed LARC patients by means of a low-coverage whole genome sequencing approach. The untargeted ctDNA profiling has been selected to get an unbiased portrait of the somatic copy number aberrations (CNAs) of tumor and their dynamics in course of treatment delivery. Specific aims are:

i) the assessment of the feasibility of CNAs detection in the cfDNA of LARC patients treated with nCRT, with specific focus on the analytical specificity;
ii) the evaluation of ctDNA validity as a tool to recapitulate the clinical based risk-stratification algorithms of LARC patients at the time of diagnosis and its utility in refining the current risk-classification;
iii) the evaluation of ctDNA as an early marker to predict the outcome of nCRT in LARC.

In the context of GIST, the cfDNA collected every 3 to 6 months in course of imatinib has been analyzed by means of the targeted deep sequencing of a panel of genes known to play a major role in GIST initiation and progression. The use of a targeted approach has been selected in light of the molecular basis governing the GIST relapse and progression. Specific aims are:

i) the assessment of feasibility of ctDNA detection in GIST patients in the adjuvant and metastatic treatment setting by means of targeted digital approaches;
ii) the assessment of the ctDNA utility as a tool to dynamically monitor the presence of active disease and to early identify the onset of disease progression before imaging-based diagnosis.

Moreover, the interplay between imatinib pharmacodynamics, analyzed through ctDNA monitoring, and pharmacokinetics has been investigated as a complementary determinant of treatment efficacy. In this regard the presence of pharmacogenetic variants in imatinib metabolizing enzymes and transporters as well as the concomitant administration of drugs showing a potential metabolic interaction with imatinib have been analyzed and correlated with the imatinib plasma exposure.

CHAPTER 3. MATERIALS AND METHODS

3.1 Patients' Selection and Inclusion's Criteria

3.1.1 LARC Patients

A retrospective population of 40 LARC patients who were admitted to the Radiotherapy division at IRCCS CRO Aviano (PN) from 2016 and 2019 were selected according to the following criteria:

i) availability of biological material (plasma) stored at the Clinical and Experimental Pharmacology Unit Biobank of IRCCS CRO Aviano (PN), Italy, collected before the first dose administration of nCRT and (optionally) in course of and after nCRT;
ii) histologically confirmation of stage II or III rectal adenocarcinoma with clinical confirmation of the absence of visible metastatic sites;
iii) completion of fluoropyrimidine-based nCRT treatment without interruption or discontinuations;
iv) availability of detailed clinical data, including TNM stage at diagnosis, CEA levels at diagnosis, date of start and end of treatment, date and type of surgery, clinical and pathological assessment of treatment response, TRG score and date of disease progression;
v) age ≥ 18;
vi) presence of signed informed consent for clinical and biological data analysis.

3.1.2 GIST Patients

GIST patients were prospectively enrolled in the framework of a clinical research protocol approved by the local ethical committee and registered in AIFA (N.EudraCT: 2017-002437-36) entitled "Pilot study to evaluate the feasibility of an innovative approach to monitor patients with gastrointestinal stromal tumor treated with imatinib". Patients were enrolled according to the following inclusion criteria:

i) eligibility for treatment with imatinib either in adjuvant or in first-line setting;
ii) performance status of 0 or 1, according to the Eastern Cooperative Oncology Group (ECOG), and adequate liver, renal and bone marrow function;
iii) just for patients already on treatment with imatinib, the therapy must be initiated more than three months prior to the first sample collection for the evaluation of the C_{trough} at the steady state;
iv) age ≥ 18;
v) presence of signed informed consent at the time of enrollment.

For each patient, 15 mL of blood were routinely collected in K_2-EDTA containing tubes at the time of regular medical check-up every 3 to 6 months from enrollment till the time of imatinib discontinuation for any cause. 10 mL of blood were used for the cfDNA extraction and 5 mL were used for imatinib trough levels' quantification.

3.1.3 Healthy Subjects

Healthy subjects were randomly selected among those who volunteer the blood for transfusion and, upon request, for research at the Transfusion division at IRCCS CRO Aviano (PN), Italy. Volunteers have a medical check-up before their blood is taken and they must satisfy the following requirements:

i) blood pressure ranges between 110 and 180 mmHg (systolic) and between 50 and 100 mmHg (diastolic);
ii) age comprised between 18 and 65;
iii) weight of at least 50 kg;
iv) absence of chronic diseases, organs impairments (e.g. liver, heart) or transmissible infectious disease (e.g. AIDS, hepatitis);
v) minimum hemoglobin level for blood donation (12.5 g/dL for females and not less than 13.5 g/dL for males);

A complete list of donor's requirements is reported in the attachment IV of Decree of Italian Ministry of Health, November 2, 2015 reporting "Provisions with regard to quality and safety requirements of bloods and blood components".

3.2 Blood Processing and Plasma Storage

Blood was collected in K_2-EDTA containing tubes and processed within two hours after sampling in a two-centrifugation steps protocol to optimize the recovery of ctDNA while minimizing the contamination with genomic DNA. Briefly, blood was centrifuged at 1600 x g for ten minutes without brake and the supernatant plasma was carefully collected and put into a new tube to avoid contaminations with peripheral blood mononuclear cell (PBMC). The harvested plasma was then centrifuged again at 3400 x g (or maximum speed) for ten minutes without brake to promote cell debris precipitation. The supernatant plasma was then collected and stored at -80 °C until cfDNA extraction. Buffy coat for genomic DNA extraction was taken from the PBMC layer remained after the first centrifugation's passage.

3.3 cfDNA Extraction, Storage and Characterization

cfDNA was extracted starting from a variable amount of plasma (1-5 mL) by using the QIAamp MinElute ccfDNA Mini Kit (Qiagen, Hilden, Germany), with the following protocol adjustments: the final cfDNA elution was performed in a final volume of 120 µL, instead of the 40-70 µL recommended, by a three-steps elution process to optimize the cfDNA recovery. Briefly, 40 µL of nuclease-free water at 56 °C were kept in contact with the column membrane for five minutes, then the cfDNA was eluted in a one-minute centrifugation step at 22000 x g. This passage was repeated for two other times. Eluted cfDNA was fluorometrically quantified by using Quantus Fluorometer (Promega, Madison, WI, U.S.A.) with the QuantiFluor dsDNA Dye (Promega, Madison, WI, U.S.A.). The cfDNA fragment size was

assessed by using the Agilent 4200 TapeStation (Agilent Technologies, Santa Clara, CA, U.S.A.) with the High Sensitivity D1000 ScreenTape and the High Sensitivity D1000 Reagent kit. cfDNA was stored at -20 °C until use.

3.4 Genomic DNA Extraction and Quantification

Genomic DNA was extracted from 200 µL of blood by using the GeneJET Whole Blood Genomic DNA Purification Mini kit (Thermo Fisher Scientific, Wilmington, DE, U.S.A.). To increase the DNA purity, genomic DNA was purified by using the Agencourt AMPure XP Beads (Beckman Coulter, Brea, CA, USA). Purified DNA was quantified by means of NanoDrop (Thermo Fisher Scientific, Wilmington, DE, U.S.A.) and Quantus Fluorometer (Promega, Madison, WI, U.S.A.) and was stored at 4 °C until use.

3.5 DNA Extraction from FFPE Tumor Tissue, Quantification and QC

Six sections of 20 µm thick were cut from the formalin-fixed paraffin-embedded (FFPE) tumor blocks collected during a staging biopsy from LARC patients before treatment initiation. The middle five were subjected to DNA extraction whilst the first section was stained with hematoxylin and eosin and served as references to estimate the tumor cells' content. DNA extraction was performed by means of the GeneRead DNA FFPE Kit (Qiagen, Hilden, Germany), according to the manufacturer's instructions. Briefly, after paraffine removal by means of serial washes with xylol and ethanol, the sample was incubated at 56 °C with proteinase-K to promote the proteins' digestion. Then, DNA was incubated for 1 hour at 90 °C to remove possible cross-links between formalin and DNA that had arisen during the tissue's fixation process. Next, DNA was treated with the enzyme Uracil-N-Glycosilase (UNG), which specifically removes the artificially induced uracil residues from the DNA strand, then it was put into a filter-containing spin column. Remaining contaminants were washed away by means of buffers and ethanol and DNA was eventually eluted in 25 µL of nuclease-free water. Eluted DNA was spectrophotometrically quantified by means of Nanodrop 2000c (Thermo Fisher Scientific, Wilmington, DE, U.S.A.) to check the purity of extracted material. For a more accurate estimation of the quality of DNA, the fraction of amplifiable DNA was assessed by means of QIaSeq DNA QuantiMIZE Assay (Qiagen, Hilden, Germany), according to manufacturer's instructions. This system exploits a qPCR-based protocol to amplify selected regions of 100 bp and 200 bp homogenously spread across the genome to assess the fraction of amplifiable DNA for NGS downstream applications by using a standard DNA as reference control. DNA quality was quantified as the difference between the Ct (cycle threshold) value of the FFPE-derived DNA against the Ct value of the reference control DNA. The fragments' size distribution and the DNA integrity index (DIN) were assessed by using the Agilent 4200 TapeStation (Agilent Technologies, Santa Clara, CA, U.S.A.) with the D1000 genomic DNA ScreenTape and the D1000 genomic DNA Reagent kit.

3.6 Gene Selection and Customized Panel Design

To investigate and monitor the presence of ctDNA in GIST patients, a list of 13 genes have been selected to be analyzed by means of targeted deep sequencing. Genes have been selected to include the most frequently mutated genes in GIST, genes associated with development of resistance to imatinib and genes closely related to the KIT/PDGFRA pathway. (Table 2)

Targeted regions included all exons and exon-flanking sites of selected genes. The amplicon based custom panel was designed by Qiagen (Qiagen, Hilden, Germany), which synthetized PCR primers specific for the regions of interest. The final primer design was manually checked by means of the Integrative Genomics Viewer (IGV) software version 2.4.[130]

Table 2. List of genes selected for the targeted deep sequencing of codifying regions in the cfDNA of GIST patients. The gene name, the genomic coordinates, the transcript IS and the sequence ID (RefSeq) are displayed for each gene.

Gene	Genome Position	Transcript ID	RefSeq
KIT	Chr4: 54,657,918-54,740,715	ENST00000288135.6	NM_000222.3
PDGFRα	Chr4: 54,229,280-54,298,245	ENST00000257290.10	NM_006206.6
MTOR	Chr1: 11,106,535-11,262,551	ENST00000361445.9	NM_004958.4
BRAF	Chr7: 140,719,327-140,924,929	ENST00000644969.2	NM_001374258.1
PIK3CA	Chr3: 179,148,114-179,240,093	ENST00000263967.4	NM_006218.4
KRAS	Chr12: 25,205,246-25,250,936	ENST00000256078.10	NM_033360.4
PTEN	Chr10: 87,863,625-87,971,930	ENST00000371953.8	NM_000314.8
SRC	Chr20: 37,344,685-37,406,050	ENST00000373578.7	NM_198291.3
STAT3	Chr17: 42,313,324-42,388,482	ENST00000264657.10	NM_139276.3
FIP1L1	Chr4: 53,377,641-53,460,862	ENST00000337488.11	NM_030917.4
MAX	Chr14: 65,006,174-65,102,695	ENST00000358664.9	NM_002382.5
FGFR1	Chr8: 38,400,215-38,468,834	ENST00000447712.7	NM_023110.3
TP53	Chr17: 7,661,779-7,687,538	ENST00000269305.9	NM_000546.6

3.7 Next Generation Sequencing

3.7.1 Fragmentation of FFPE DNA of LARC Patients

FFPE DNA samples of different concentrations (23-100 ng) were diluted in water to a final volume of 50 µl in Covaris microTUBE AFA Fiber Screw-Cap 6x16mm tubes (Covaris, Woburn, MA, U.S.A.) and fragmented to an average size distribution of 180-200 bp with Covaris M220 Focused Ultrasonicator with Adaptive Focused Acoustics technology. The following parameters were used for shearing: Peak Incident Power: 50 W; Duty Factor: 20%; Cycles per Burst: 200; Temperature: 20 °C with the fragmentation time of 600 s.

3.7.2 Libraries Preparation for sWGS

Sequencing libraries for sWGS were prepared starting from 8.0 to 22.0 ng of cfDNA and from 23.0 to 100.0 ng of FFPE DNA using the KAPA Hyper Prep Kit with KAPA Dual-Indexed Adapters for Illumina platforms (Roche). sWGS libraries were prepared as follow: after sequencing adapter ligation for 15 hours at 20 °C, DNA libraries were purified by double-sided size selection to selectively capture DNA fragment size comprised between 150 and 350 bp. Adapter ligated libraries were amplified in 11 PCR cycles, for cfDNA, and in 8 PCR cycles for FFPE DNA. The clean-up of amplified libraries was performed according to the manufacturer's instructions and amplified DNA was eluted in 50 µL of nuclease-free water and fluorometrically quantified with the Quantus Fluorometer (Promega, Madison, WI, U.S.A.) with the QuantiFluor dsDNA Dye (Promega, Madison, WI, U.S.A.). The fragment size analysis for the assessment of the median molecular weight and of the presence of primers dimers was done with the Agilent 4200 TapeStation (Agilent Technologies, Santa Clara, CA, U.S.A.) with the High Sensitivity D1000 ScreenTape. Libraries were diluted to a final concentration of 10 nM and samples were pooled together in equimolar amount.

3.7.3 Targeted Sequencing of FFPE DNA from LARC Biopsies

Targeted DNA libraries for genetic characterization of primary LARC tissue biopsies were prepared by means of the commercially available QIaSeq Colorectal Cancer Panel DNA kit (cat. DHS-002Z) (Qiagen, Hilden, Germany) targeting the hotspot regions of 71 genes that are clinically relevant in CRC and covering 215,328 bp. The detailed gene list is reported in *Appendix S1*. Targeted libraries were prepared staring from 40 to 100 ng of FFPE DNA according to the QIaSeq Targeted Panel Handbook. After the enzymatic fragmentation at 32 °C for 14 minutes, the FFPE DNA fragments were ligated at their 5' ends with Illumina-specific adapters containing UMIs and sample index. The UMIs are made of a 12-base fully random sequence that statistically provides 4^{12} possible indices per adapter, thus ensuring that each DNA molecule in the sample receives a unique UMI sequence. Adapter ligated libraries were amplified in the regions of interest by means of six cycles of PCR by using region-specific primers and universal primers complementary to the adapter regions. Next, enriched libraries were amplified in 25 PCR cycles. The clean-up of amplified libraries was performed according to the manufacturer's instructions and amplified DNA was eluted in 30 µL of nuclease-free water. The library preparation workflow is depicted in Figure 5. Final libraries were quantified by means of Quantus Fluorometer (Promega, Madison, WI, U.S.A.) with the QuantiFluor dsDNA Dye (Promega, Madison, WI, U.S.A.) and the fragment size analysis was done with the Agilent 4200 TapeStation (Agilent Technologies, Santa Clara, CA, U.S.A.) with the High Sensitivity D1000 ScreenTape. Libraries were diluted to a final concentration of 10 nM and samples were pooled together in equimolar amount. At the time of sequencing, pooled libraries were diluted at 4 nM, denatured with freshly prepared NaOH 0.1 M and diluted at a final concentration of 10 pM.

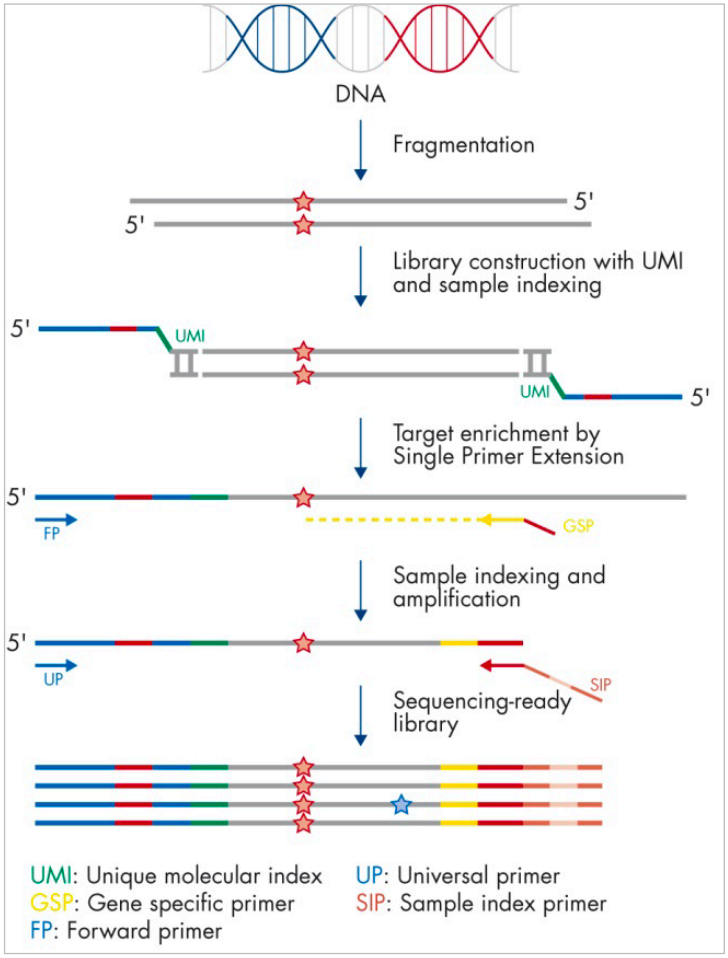

Figure 5. QIaSeq Targeted DNA Panel workflow for libraries preparation (adapted from QIaSeq Targeted DNA Panel Handbook ed. February 2020)

3.7.4 Targeted Sequencing of cfDNA and FFPE DNA from GIST Patients

Targeted DNA libraries for cfDNA and FFPE DNA sequencing of GIST patients were prepared by means of the commercially available QIaSeq Actionable Solid Tumor Panel DNA kit (cat. DHS-101Z) (Qiagen, Hilden, Germany), to set up the NGS workflow, and by means of the Custom Panel described in the section *Materials and Methods 3.6.* The Actionable Solid Tumor Panel comprised the whole exons of 6 genes and the hotspot regions of 13 genes with actionable mutations in human solid tumors, spanning 15.160 bp. The detailed gene list is reported in *Appendix S2*. Targeted libraries were prepared starting from 5 to 80 ng of cfDNA, with the following adaptation to cfDNA: adapter ligated libraries were enriched in the regions of interest by means of eight PCR cycles and amplified with 23 PCR cycles. Libraries were diluted to a final concentration of 10 nM and samples were pooled together in equimolar amount. At the time of sequencing, pooled libraries were diluted at 4 nM, denatured with freshly prepared NaOH 0.1 M and diluted at a final concentration of 6 – 8 pM.

3.7.5 Targeted Sequencing of Genomic DNA from GIST Patients

The genomic DNA extracted from PBMC of GIST patients was used for the characterization of genomic variants affecting drug's metabolizing enzymes and transporters. While the majority of genes were analyzed by means of a targeted allele discrimination assay based on PCR, the imatinib transporters *ABCB1* and *ABCG2* and the cytochrome *CYP2C8* were analyzed by means of NGS. Sequencing libraries were prepared starting from 100 ng of genomic DNA using a customized hybridization based NimbleGen SeqCap EZ Choice Library (Roche, Inc., Madison, WI, USA) targeting the UTRs and the coding sequence of 60 cancer related genes, according to the NimbleGen SeqCap EZ Library SR User's Guide v3.0 (Roche, Inc. Madison, WI, USA). Briefly, genomic DNA was enzymatically fragmented for 15 minutes at 37 °C, end repaired, A-tailed and ligated with Illumina indexed adapters. Ligated libraries were size selected by means of Agencourt AMPure XP Beads (Beckman Coulter, Brea, CA, USA) to retain fragments ranging between 300 and 350 bp and amplified in 12 PCR cycles. Final libraries were quantified by means of Quantus Fluorometer (Promega, Madison, WI, U.S.A.) with the QuantiFluor dsDNA Dye (Promega, Madison, WI, U.S.A.) and the fragment size analysis was performed using the Agilent 4200 TapeStation (Agilent Technologies, Santa Clara, CA, U.S.A.) with the High Sensitivity D1000 ScreenTape. Pooled libraries were obtained by putting together 45 ng of each sample that were amplified in the regions of interest by using the SeqCap EZ Choice Library (Roche, Inc., Madison, WI, USA) followed by 7 PCR cycles. At the time of sequencing, libraries were denatured with fresh NaOH 0.2 M and diluted to a final concentration of 10 pM.

3.8 Sequencing Platforms

For targeted sequencing, pooled libraries of 8 to 12 cfDNA samples and pooled libraries of 10 FFPE DNA samples (LARC patients) were sequenced on an Illumina MiSeq (Illumina, San Diego, CA, USA) using the V2 kit (300 cycles) by using a custom sequencing primer for Read 1 (QIaSeq A Read1 Primer I) and 151 bp paired end reads. Pooled libraries of 16 genomic DNA samples were sequenced on an Illumina MiSeq using the V2 Nano kit (300 cycles) with 151 bp paired end reads. Pooled libraries of 2 to 4 FFPE DNA samples from GIST patients were sequenced on an Illumina MiSeq using the V2 Micro kit (300 cycles) by using a custom sequencing primer for Read 1 (QIaSeq A Read1 Primer I) and 151 bp paired end reads. For sWGS, pooled libraries of 33 FFPE DNA samples and of 44 to 56 cfDNA samples sequenced per lane on an Illumina HiSeq4000 (Illumina, San Diego, CA, USA) with 100 bp paired-end reads.

3.9 Bioinformatics Analysis

For targeted DNA sequencing with the QIaSeq Actionable and Custom Tumor Panel DNA (Qiagen, Hilden, Germany), generated FASTQ files were automatically processed and analyzed by means of the

QIaSeq Targeted DNA Panel Analysis software (Qiagen). Variants were called using smCounter v 2 with default parameters,[131] and identified variants were manual verified using Integrative Genomics Viewer.[130] For targeted DNA sequencing with the NimbleGen SeqCap EZ Choice Library (Roche) generated FASTQ files were processed by using the Variant Studio software (Illumina), for variants' annotation. For sWGS, raw sequencing reads were processed and aligned using the automated pipeline OTP.[132]

3.10 Variants' Calling and CNAs' Detection

Genome-wide copy number profiles and tumor fractions (TFx) were estimated from low coverage sWGS data of cfDNA using the ichorCNA pipeline with default parameters.[133] ichorCNA is an R tool for estimation of tumor fractions in shallow whole genome sequencing (sWGS) and prediction of large-scale CNAs. The ichorCNA algorithm uses a hidden Markov model (HMM) for the probabilistic modeling and works in sequencing coverages down to 0.1X.

3.11 Droplet Digital PCR

Droplet digital PCR (ddPCR) was used to validate NGS results obtained from deep sequencing of cfDNA. All reactions were performed in triplicates and the workflow was as follow: ddPCR reaction mix was prepared at a final volume of 20 µL by using 2X ddPCR SuperMix for probes (No dUTP) (Bio-Rad Inc., Hercules, CA), 1–20 ng of cfDNA quantified using the Quantus Fluorometer high sensitivity assay kit (Promega, Madison, WI, U.S.A.) and 200X ddPCR specific assay containing the forward and reverse primers and the FAM and HEX-labeled probes. Droplets were then generated in the QX200 droplet generator (Bio-Rad) by loading 20 µL of the reaction mixture and 70 µL of droplet generation oil for probes (Bio-Rad) onto matched wells of a DG8 cartridge (Bio-Rad). Approximately 85 µL of the droplet/oil mixture (containing 12,000 – 20,000 droplets) were transferred to a semi-skirted 96-well plate (Bio-Rad), which was sealed with a pierceable foil heat seal using a PX1 PCR plate sealer (Bio-Rad). Generated droplets were processed using the following amplification protocol: 95°C for 10 min, followed by 45 cycles: denaturation at 94°C for 30 seconds; annealing at 60°C for 1 minute; extension at 65°C for 30 seconds. Upon completion of the PCR protocol, the plate was read using the QX200 droplet reader (Bio-Rad) with the following settings: channel 1 = FAM (mutated template) and channel 2 = HEX (wild type template). Droplet counts and amplitudes were then exported to and analyzed with QuantaSoft™ software (Bio-Rad). Positive droplet concentrations were determined using manually assigned fluorescence thresholds. Wild type and mutated copies were automatically calculated after manually removal of false-positive calls (i.e. droplets containing both templates) and was expressed as number of copies per µl loaded. Mutated allele frequency was manually calculated by dividing the number of droplets containing mutated copies for the number of positive droplets.

3.12 Computational Prediction of Splicing Defects

Six publicly available *in silico* tools were used to predict the impact of the splice-site mutation in *TP53* gene on pre-mRNA splicing. The backbone of all software relies on algorithms which predict the likely position of exon-intron boundaries, based on the target sequence uploaded. According to the mathematical algorithm used, each software provides a score rating the strength of the splice signal identified, where a high score corresponds to a splice site that is easily recognized from the splicing machinery. The software used are:

i) SpliceView (available at: http://bioinfo.itb.cnr.it/~webgene/wwwspliceview.html) is based on the basic Position Weight Matrix (PMW) model proposed by Shapiro and Senapathy with the advantage of considering mutual dependency between nucleotides in different positions.[134]

ii) GENSCAN (available at: http://hollywood.mit.edu/GENSCAN.html) exploits the Maximal Dependence Decomposition (MDD) model and provides a probability score describing the likelihood of identifying an exon-intron junction in the sequence provided by the user.[135]

iii) NetGene2: is based on an artificial Neural Network (NN) which is aimed at distinguishing true splice sites from blunders.[136,137] This algorithm assigns a confidence score for each splice site position.

iv) NNSplice 0.9 (available at: https://www.fruitfly.org/seq_tools/splice.html) is based on an artificial Neural Network (NN) as well, generates a score to rank each splice site position.[138]

v) MaxEntScan (available at: http://hollywood.mit.edu/burgelab/maxent/Xmaxentscan_scoreseq.html) is based on the Maximum Entropy Distribution (MED) model and provides a log-odd ratio to the 5' and the 3' splice site.[139] As recommended by Houdayer *et al.*, the score of the mutant splice site should be at least 20% lower than the score of the corresponding wild-type splice site to be considered deleterious on splicing process.[140]

vi) Human Splicing Finder (HSF, available at: http://www.umd.be/HSF/HSF.shtml) incorporates both the PMW and the MED models to identify canonical splice sites, as well ESEs and ESSs.[141]

3.13 GIST Patients Genotyping and Phenotype Assignment

Enzymes and transporters with a role in imatinib metabolism were selected according to the PharmGKB information available at https://www.pharmgkb.org/pathway/PA164713427.[142] Nine CYPs and two transporters were selected and the presence of genetic variants with a documented or suspected impact on their metabolic phenotype was investigated. Selected genes were: *CYP2B6, CYP3A4, CYP3A5, CYP2D6, CYP2C9, CYP2C19, CYP1A2, CYP2C8, ABCB1* and *ABCG2.* Genetic variants affecting the DNA coding sequence and the 3' and 5'UTRs were analyzed by means of NGS in *CYP2C8, ABCB1* and *ABCG2*, as described in the section *Materials and Methods 3.7.5.*

Table 3. List of genes selected for the assessment of functional variants. For each CYP the presence of specific SNPs with documented functional impact on the enzymatic activity was investigated. The allele ID (star), the variant position along the coding sequence and the corresponding ID (rs) are displayed.

Gene	Allele	Variant ID	Corresponding rs
CYP2B6	*6/*9	c.516G>T	rs3745274
CYP2B6	*4/*16	c.785A>G	rs2279343
CYP2B6	*18	c.983T>C	rs28399499
CYP2C9	*2	c.430C>T	rs1799853
CYP2C9	*3	c.1075A>C	rs1057910
CYP2C9	*5	c.1080C>G	rs28371686
CYP2C9	*11	c.1003C>T	rs28371685
CYP2C19	*2	c.681G>A	rs4244285
CYP2C19	*3	c.636G>A	rs4986893
CYP2C19	*4A/B	c.1A>G	rs28399504
CYP2C19	*5	c.1297C>T	rs56337013
CYP2C19	*6	c.395G>A	rs72552267
CYP2C19	*8	c.358T>C	rs41291556
CYP2C19	*9	c.431G>A	rs17884712
CYP2C19	*10	c.680C>T	rs6413438
CYP2C19	*17	c.-806C>T	rs12248560
CYP2D6	*xN	Gene duplication or multiplication	X
CYP2D6	*3	c.2549delA	rs35742686
CYP2D6	*4	c.1846G>A	rs3892097
CYP2D6	*5	Gene deletion	X
CYP2D6	*6	c.1707delT	rs5030655
CYP2D6	*8	c.1758G>T	rs5030865
CYP2D6	*9	c.2615delAAG	rs5030656
CYP2D6	*10	c.100C>T	rs1065852
CYP2D6	*14A/B	c.1758G>A	rs5030865
CYP2D6	*17	c.1023C>T	rs28371706
CYP2D6	*41	c.2988G>A	rs28371725
CYP3A5	*3	c.6986A>G	rs776746
CYP3A5	*6	c.14690G>A	rs10264272
CYP3A5	*7	c.27131_27132insT	rs41303343
CYP3A4	*1B	c.392A>G	rs2740574
CYP3A4	*22	c.522-191C>T	rs35599367
CYP3A4	*1G	c.1023+12G>A	rs2242480
CYP1A2	*1F	c.-164A>C	rs762551
CYP1A2	*1C	c.-3860G>A	rs2069514
CYP1A2	*1K	c.-729C>T	rs12720461

The presence of a panel of thirty-six functional variants in the remaining seven imatinib-related CYPs was investigated by means of allele specific probes, using validated KASP genotyping assays (LGC

Genomics, Novato, CA, U.S.A.) in the semi-automated SNPline PCR Genotyping System (LGC Genomics) and in the Applied Biosystems™ 7500 Real-Time PCR system (Applied Biosystem, Foster City, CA, U.S.A.). The list of the thirty-six target variants is reported in Table 3. To each CYPs' allele an activity score was assigned, in order to provide a quantitative measure of its metabolic capacity, in line with the CPIC recommendations.[143–147] Accordingly, a score of 1 was assigned for each normal activity allele, 0.5 for each decreased activity allele, and 0 for no activity allele. Then, the predicted metabolic phenotype was assigned to each CYPs based on the sum of the single alleles' scores: 0, poor metabolizer (PM); 0.5 – 1, intermediate metabolizer (IM); 1.5 – 2 normal metabolizer (NM) and >2 ultrarapid metabolizer (UM). For CYP2D6 the genotyping assay detected allele duplication, but not which allele was duplicated or the number of allele copies. Therefore, ranged phenotypes were possible (e.g. NM to UM). The detailed assignment of likely phenotypes based on genotypes is reported in *Appendix S3-S7*. To provide a comprehensive measure of the individual metabolic capacity of imatinib, a cumulative activity score comprising the activity score of each CYP was calculated and named pharmacogenetics activity score (PGx-AS). The PGx-AS was calculated for each patient by summing the activity score of single CYPs.

3.14 Acquisition of Data on Concomitant Administered Drugs

The detailed list of drugs, herbal products and food supplements taken by GIST patients during follow-up was retrieved by patients' clinical records. Moreover, at the time of periodical blood sampling, patients were asked to fill a document to provide the following information:

i) smoking habits (nonsmoker, moderate smoker, heavy smoker);
ii) coffee intake over the last 24 hours;
iii) chronic drugs' intake for morbidities aside of GIST;
iv) intake of other drugs beside of imatinib, herbal products or food supplements over the last seven days;
v) intake of grapefruit juice.

3.15 Evaluation and Rating of Imatinib Interacting Drugs

A potential DDI with imatinib was defined by superimposing a period of exposure to imatinib with a period of exposure to drugs that could interact with imatinib. Only drugs administered within the timeframe of a week from the blood sampling were considered for the analysis of potential interaction. The drugs that were administered in case of need (e.g. NSAIDs for pain relief) were considered as potentially interacting. The mechanisms of DDI with imatinib were acquired from the drugs' labels and from five different databanks that were systematically interrogated to assess: i) the impact of drugs on

CYPs and transporters activity and ii) the evidence of documented interaction between drugs and imatinib reported by *in vitro*, *in vivo* and clinical evidences. Screened databanks were:

i) DrugBank. This is an online comprehensive, open source, database containing information on drugs and drug targets, displaying 2649 approved small molecules.[148] Although not primarily developed for clinical use, DrugBank provides a set of 12,128 drug-drug interactions (DDIs), asserted at the ingredient level, along with a brief textual description of the interaction, and information about the possible molecular basis of the interaction (target-based, enzyme-based, transporter-based). In the present thesis, the possible molecular basis of the interaction is reported to be enzyme-based or transporter-based and the version used was the 5.0.

ii) Medscape. This is an online, open source software that provide information upon possible drug interactions by means of the "Drug Interaction Checker" tool. Drug interactions are categorized based on severity as minor (current medications can be continued), significant (close monitoring is required), and serious (suggested for alternative medication). The mechanism of drug interaction is classified as pharmacodynamic and/or pharmacokinetic. [149]

iii) Flockhart Interaction Table. This is one of the most commonly employed data sources for identifying drug interactions via CYPs and their clinical relevance and is curated by the Department of Clinical Pharmacology of the Indiana University (IN, U.S.A.). In Flockhart Interaction Table where all CYP450-relevant drugs in are classified into inhibitors, inducers or substrates of specific isoenzymes. The level of drugs' interaction with CYPs is reported as strong, moderate or weak.[150]

iv) FDA. The FDA website provides information on substrates, inhibitors and inducers of drugs' metabolizing enzymes and transporters, also providing the level of evidence of reported interactions, from *in vitro* to clinical reports.[151]

v) Lexicomp. Lexicomp is a subscription-based pharmacological database app that reports comprehensive drugs' monographs. It is a drug decision support system that is aimed at providing clinicians, pharmacists, nurses and healthcare professionals with a point of care tool to optimize the safety prescription of therapeutics. In the drugs' monographs are reported the likely DDIs based on clinical evidences.[152]

For each drug, information upon the mechanism of possible interaction with imatinib's metabolism were reported into a dataset together with the level of evidence (clinical, *in vivo*, *in vitro*). An example of the dataset for drug interaction data collection is reported in Figure 6. In case of lack of agreement among different databanks, the interactions were considered significant only if supported by clinical evidences, whilst they were discarded in case of evidences supported by *in vitro*/*in vivo* studies.

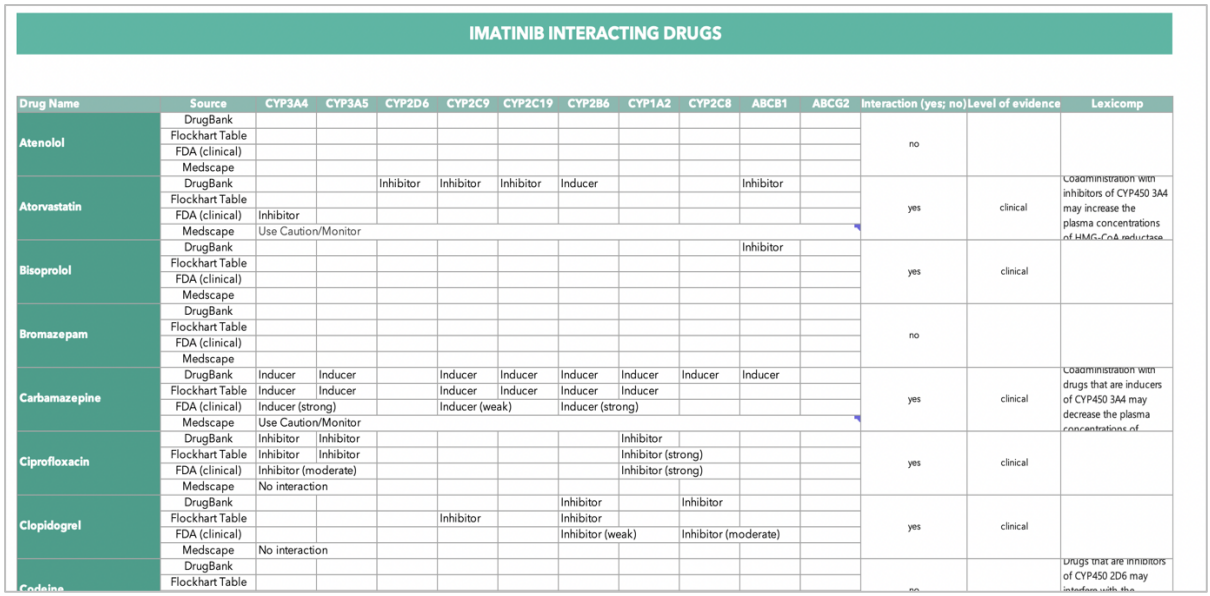

IMATINIB INTERACTING DRUGS

Drug Name	Source	CYP3A4	CYP3A5	CYP2D6	CYP2C9	CYP2C19	CYP2B6	CYP1A2	CYP2C8	ABCB1	ABCG2	Interaction (yes; no)	Level of evidence	Lexicomp
Atenolol	DrugBank											no		
	Flockhart Table													
	FDA (clinical)													
	Medscape													
Atorvastatin	DrugBank			Inhibitor	Inhibitor	Inhibitor	Inducer			Inhibitor		yes	clinical	Coadministration with inhibitors of CYP450 3A4 may increase the plasma concentrations of HMG-CoA reductase
	Flockhart Table													
	FDA (clinical)	Inhibitor												
	Medscape	Use Caution/Monitor												
Bisoprolol	DrugBank									Inhibitor		yes	clinical	
	Flockhart Table													
	FDA (clinical)													
	Medscape													
Bromazepam	DrugBank											no		
	Flockhart Table													
	FDA (clinical)													
	Medscape													
Carbamazepine	DrugBank	Inducer	Inducer		Inducer	Inducer	Inducer	Inducer	Inducer	Inducer		yes	clinical	Coadministration with drugs that are inducers of CYP450 3A4 may decrease the plasma concentrations of
	Flockhart Table	Inducer	Inducer		Inducer	Inducer	Inducer	Inducer						
	FDA (clinical)	Inducer (strong)			Inducer (weak)		Inducer (strong)							
	Medscape	Use Caution/Monitor												
Ciprofloxacin	DrugBank	Inhibitor	Inhibitor					Inhibitor				yes	clinical	
	Flockhart Table	Inhibitor	Inhibitor					Inhibitor (strong)						
	FDA (clinical)	Inhibitor (moderate)						Inhibitor (strong)						
	Medscape	No interaction												
Clopidogrel	DrugBank						Inhibitor		Inhibitor			yes	clinical	
	Flockhart Table				Inhibitor		Inhibitor							
	FDA (clinical)						Inhibitor (weak)		Inhibitor (moderate)					
	Medscape	No interaction												
Codeine	DrugBank											no		Drugs that are inhibitors of CYP450 2D6 may interfere with the
	Flockhart Table													

Figure 6. Exemplary classification of interaction between co-administered drugs and imatinib metabolizing enzymes and transporters. For each drug, the level of inhibition or induction of CYPs and transporters were collected according to five different publicly available databank. The level of evidence of the interaction was then rated into three levels (*in vitro*, *in vivo* and clinical) and the possible interaction with imatinib pharmacokinetic was postulated according to the agreement of different databank used.

3.16 Calculation of the Drug's Impact on CYP's and Transporters' Activity

A drug-interacting score (DIs) was assigned to each drug to rank their level of interaction with CYPs and transporters. A DIs of 1.0 was assigned to each non interacting drug, 0.5 for each weak to moderate inhibitor, 0 for each strong inhibitor, 1.5 to each weak to moderate inducer, and 2.0 to each strong inducer. The DIs was used to refine the genotype predicted activity score of CYPs and transporters, by multiplying the gene activity score and the DIs. For instance, the antipsychotic drug carbamazepine is a strong inducer of the activity of CYP3A4 and CYP2B6, with documented clinical evidences, and a DIs of 2.0 was assigned to carbamazepine to refine the gene activity score of CYP3A4 and CYP2D6. Carbamazepine is also a weak to moderate inducer of CYP2C9 activity, thus its DIs on that enzyme was scored 1.5.

3.17 Assessment of the Pathological Response to Treatment

The pathological response to nCRT was assessed on surgical specimens by evaluating residual tumor size, differentiation grade, presence of necrotic and fibrotic content, lymph nodes status and the development of metastatic lesions. The Mandard's tumor regression grade (TRG) scoring system, which evaluates the residual tumor content over fibrosis, was used to rank the response to nCRT into five categories as follow: TRG1, complete pathological response with absence of residual cancer cells; TRG2, presence of a few residual cancer cells; TRG3, increasing number of discernible cancer cells

with predominant fibrosis; TRG4, predominance of cancer cells over fibrosis; TRG5, no regression (Table 4).[153]

Table 4. Tumor regression grade (TRG) system according to Mandard.

Tumor Regression Grade	Definition
TRG 1	Complete response with absence of residual cancer and fibrosis extending through the tumor margin
TRG 2	Presence of residual isolated cells scattered through the fibrosis
TRG 3	Increase in the number of residual cancer cells, but fibrosis still predominant
TRG 4	Residual cancer outgrowing fibrosis
TRG 5	Absence of regressive changes

3.18 Assessment of Therapeutic Response to Imatinib

Computed tomography (CT) scans were routinely performed and used to assess GIST tumor's dimension and metabolic activity during pharmacological treatment with imatinib. The response to therapy was evaluated through CT imaging based on changes in tumor volume and tumor density, as well as on the appearance of new lesions. The response to imatinib was evaluated using the Response Evaluation Criteria in Solid Tumors (RECIST) v.1.1, which assess single lesions' dimensions based on measurements of the longest axial diameter.[154] Table 5 summarizes the criteria used to assess the tumors' response to imatinib.

Table 5. Summary of RECIST criteria (v. 1.1) for treatment response evaluation in GIST.

Response	Definition
Complete Response (CR)	Disappearance of all lesions Reduction to <10 mm in short axis of any pathological lymph nodes (whether target or non-target) No new lesions
Partial Response (PR)	At least a 30% decrease in SLD of target lesions, taking as reference the baseline SLD No new lesions
Stable Disease (ST)	Does not meet the criteria for CR, PR, or PD
Progression Disease (PD)	At least a 20% increase in SLD of target lesions, taking as reference the smallest sum on study and at least 5 mm absolute increase in SLD New lesions

3.19 Immunohistochemical Analysis and Biomarkers' Expression in LARC Biopsies

The immunohistochemical analysis was performed on 95 FFPE tumor biopsies collected during staging colonoscopy from LARC patients. Three μm-thick sections were cut, and one slide was hematoxylin and eosin (H&E) stained to be reviewed by a trained pathologist. The remaining slides were used for the evaluation of immunohistochemical expression of selected biomarkers, which was independently

reviewed by two trained pathologists. Primary antibodies used for the tumor content assessment were: MLH1, GLUT1, Ki67, CA-IX, CXCR4, COX2, CXCL12, HIF1α, VEGF, CD44 and RAD51. Immunostaining was evaluated at the nuclear level for MLH1, Ki67 and RAD51, at the membrane level for CA-IX, CXCR4 and CD44 and at the cytoplasmatic level for GLUT1, COX2, CXCL12, HIF1α and VEGF. Proteins' expression was assessed by evaluating the intensity of staining (0, absent; 1, weak; 3, moderate and 4, strong) and the proportion of cells presenting nuclear, cytoplasmic or membrane staining positivity (ranging from 0 to 100%). The comprehensive immunoreactivity score (H-score) was calculated using a widely accepted semi-quantitative method.[155] Briefly, the percentage of positive cells was ranked into five categories (0, 0% of positive cells; 1, 1 to 24% of positive cells; 2, 25 to 49% of positive cells; 3, 50 to 74% of positive cells and 4, 75 to 100% of positive cells) according to the fraction of cells exhibiting staining positivity, then the H-score was derived by multiplying the ranked percentage of cells presenting immunostaining positivity by the staining intensity. H-score values ranged from 0 to 12.

3.20 LC/MS-MS Quantification of Imatinib Plasma Concentrations

Data on imatinib plasma concentrations were kindly provided by the Bioanalytical research group of the Experimental and Clinical Pharmacology Unit of IRCCS CRO Aviano (Italy). The quantification of imatinib was obtained using a LC-MS/MS apparatus consisting in a Prominence UFLC XR (Shimadzu) coupled with an API 4000 QTrap mass spectrometer (SCIEX). Imatinib was quantified after a simple protein precipitation with methanol as extraction method. The analyte was separated on a Synergi Fusion RP C18 chromatographic column 4 μm, 50 x 2.0 mm coupled with a C18 precolumn (Phenomenex). Elution chromatography was carried out in gradient mode. The mass spectrometer was equipped with an electrospray ionization interface and operated in positive ion mode. The biological samples were analyzed in Selected Reaction Monitoring mode following three different transitions. The quantifications were performed using the 494.4 > 394.2 imatinib transition and employing imatinib-D8 as internal standard. The developed method was validated according to the FDA and EMA guidelines on bioanalytical method validation assessing linearity, recovery, limit of detection, limit of quantification, matrix effect, inter- and intra-day precision and accuracy, selectivity, stability and reproducibility.

3.21 Estimation of Imatinib Trough Levels

Imatinib plasma levels were quantified in samples taken preferentially after 24 hours from the last imatinib administration, in order to ensure the homogeneous quantification of drug's trough levels. When imatinib was not precisely administered 24 hours before blood collection, a conversion algorithm was used to extrapolate the imatinib trough concentration. The algorithm used was kindly provided by

the Department of Clinical Pharmacy and Toxicology of Leiden Medical Center (NL) and allowed to extrapolate the real imatinib trough concentration based on the imatinib average half-life, the quantified plasma imatinib concentration and the time after the last dose administration. Samples collected up to five hours or after thirty-five hours from the last imatinib dose were excluded from the analysis as they were outside the algorithm's range of linearity.

3.22 Statistical Methods

Differences of cfDNA levels between two groups were evaluated through the non-parametric Mann-Whitney test, while differences of cfDNA levels within more than three groups were assessed through the Kruskal-Wallis test, with Dunn's correction for multiple comparison. The sensitivity and specificity of ctDNA and CEA to predict the local and distant relapse in LARC patients were evaluated by means of Chi-squared test. The pathological tumor response to nCRT in LARC patients was defined according to TRG score. For the assessment of protein biomarkers' expression in pre-treatment LARC biopsies, the complete responders (TRG1) were compared to non-complete responders (TRG2-4) and the biomarkers' expression level was considered as a continuous variable. Differences between TRG1 and TRG2-4 patients were evaluated through the Mann-Whitney test. For each biomarker, a receiver operating characteristic (ROC) analysis was performed to select the optimal cut-off level for response prediction. The risk of complete response (odds ratio - OR) and corresponding 95% confidence intervals (CI) were estimated by applying a multivariable logistic regression model., adjusting for cN stage at the diagnosis, distance from anal verge (<7cm), and neoadjuvant chemotherapy scheme (5-FU-based alone, 5-FU-based in combination and none). To evaluate the potential interaction between biomarkers, a classification and regression tree (CART) analysis was used to predict TRG1. Since a multiparameter scoring system was used to rate the markers' expression, the semiquantitative approach (H-score) was used to perform the CART. A linear regression model was used to test the correlation between the concentration of cfDNA and the DNA integrity index (DIN) and between the input DNA for NGS libraries' preparation and the depth of coverage. To assess the impact of genotype-predicted metabolic phenotype of GIST patients on imatinib trough levels, the average of imatinib trough concentrations for each patient was considered to minimize the discrepancies of the non-homogeneous number of samples collected per patient and the PGx-AS was analyzed as a dichotomic or as a discrete variable for the association with the imatinib trough level. To this end, the non-parametric Mann-Whitney test or the Kruskal-Wallis test were used to compare the differences of imatinib through levels between two or more groups, respectively. The PGx-AS corrected for DDIs was analyzed as a continuous variable and all the individual imatinib trough quantifications were considered to assess the correlation between the gene activity score corrected and the imatinib trough levels by means of a linear regression model. The Student's t-test was used to evaluate the association between single genetic variants in the imatinib transporters *ABCB1* and *ABCG2* and the imatinib plasma trough levels. All statistical analyses and data

visualization were performed using GraphPad Prism version 6 (GraphPad Software, Inc. La Jolla California USA, www.graphpad.com) and R software.[156] Values of $p < 0.05$ (two-sided) were considered statistically significant.

CHAPTER 4. RESULTS

4.1 Locally Advanced Rectal Cancer: Patients' Characteristics and Study Design

Between January 2017 and June 2019, 97 consenting LARC patients, attending the Radiotherapy Unit at IRCCS Centro di Riferimento Oncologico of Aviano (PN) were recruited in a blood acquisition protocol. Thereof, 40 cases were retrospectively selected according to the inclusion criteria for the longitudinal analysis of cfDNA. Clinical and pathological features of the 40 LARC patients are displayed in Table 6.

Table 6. Characteristics of the 40 LARC patients selected for the cfDNA analysis.

Characteristic	**Patients (n)**	**%**
Age at diagnosis, median (range)	66 (44 – 85)	
Gender		
male	17	42.5
female	23	57.5
cT stage at diagnosis		
T2	2	5.0
T3	33	82.5
T4	5	12.5
cN stage at diagnosis		
N0	10	25.0
N+	30	75.0
Chemotherapy		
Capecitabine, monotherapy	29	72.5
Capecitabine + oxaliplatin	11	27.5
Capecitabine daily dose (mg)		
2500	15	37.5
3000	13	32.5
other*	10	25.0
Radiotherapy cumulative dose (cGy)		
5400 (45/54 Gy/fraction)	40	100
Surgery		
yes	34	85.0
no**	6	15.0
Tumor Regression Grade (TRG)		
1	14	35.0
2 - 3	17	42.5
4 - 5	7	17.5
N.A.	2	5.0

* Other capecitabine daily doses include: 1500 mg (n = 1), 2000 mg (n = 2), 3300 mg (n = 1), 3500 mg (n = 2), 3800 mg (n = 1), 4000 mg (n = 2). ** 5 patients had a complete clinical response to nCRT and were selected for surgery-spearing follow-up and 1 patient discontinued the treatment due to poor performance status.

Patients were equally gender distributed, with a slight prevalence of female over male (23 vs 17) and the median age of diagnosis was 66 years. Patients were homogeneously treated with a radiotherapy scheme entailing a cumulative dose of 5400 cGy, divided in 25 fractions over a period of five weeks. 29 (72.5%) patients received oral capecitabine in monotherapy, while 11 (27.5%) patients were concomitantly administered with oxaliplatin as they were considered at higher risk to develop local and distance recurrence, according to clinical and pathological tumors' features that were assessed at the time of diagnosis. Total mesorectal excision (TME) was delivered to 34 (85.0%) patients, while 5 (12.5%) patients, who presented an excellent tumor regression with no clinical evidence of residual tumor cells after nCRT, were selected for a watch and wait surveillance protocol. One patient (#19939) did not received surgery due to the scarce performance status developed as a consequence of fast disease progression while on treatment. After completing nCRT, 14 (35.0%) patients achieved a TRG1 (pCR, ypT0N0), while 24 (60.0%) patients reported a partial or null tumor response. Thereof, 2/40 (5.0%) got a TRG2, 13/40 (32.5%) a TRG3, 4/40 (10.0%) a TRG4 and 3 a TRG5 (7.5%). For statistical purposes, in the present thesis the 5 patients who achieved a clinical complete response were included in the TRG1 group, while the patient who developed PD while on treatment was included in the TRG5 group. With a median follow-up of 27.9 months (range: 6.6 – 42.9), the local or distant 2-years recurrence rate was 34.6%, whereas the 2-years OS rate was 95.7%.

In Figure 7 is illustrated the time frame of the blood collection for LARC patients. Overall, 84 blood samples were obtained from the 40 LARC patients, with a median of 2 samples per patient (range: 1 – 4).

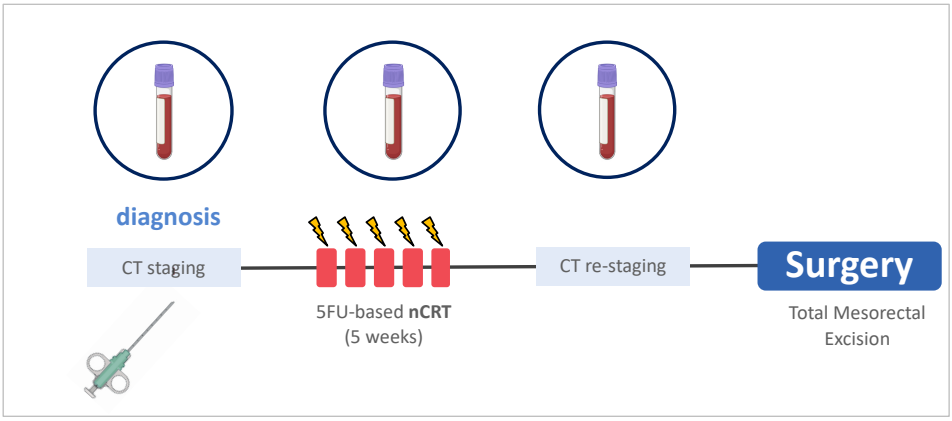

Figure 7. Time frame of the blood acquisition protocol from LARC patients. A baseline blood sample was collected before nCRT (T_1), a second sample was collected during nCRT (T_2), and a third sample was collected in between the end of nCRT and the surgery (T_3). Patients received 5-FU based nCRT for five weeks and thereafter they underwent surgery. (Created with BioRender.com).

A first blood sample was collected for all patients before nCRT initiation (T_1, n = 40), a second sample was taken in course of nCRT from 24 patients (T_2) and a third sample was collected in between the end of nCRT and the surgery from 15 patients (T_3). Moreover, a treatment naïve tissue sample, acquired from a diagnostic staging colonoscopy by means of biopsy, was retrieved from 15 patients.

4.2 Molecular Characterization of Plasma cfDNA of LARC Patients

4.2.1 Plasma cfDNA Levels in LARC Patients: Analysis and Clinical Considerations

cfDNA was successfully extracted from all 84 blood samples collected from the 40 patients included in the study population. The cfDNA concentration in plasma, as well as its fragmentation pattern, were assessed by means of fluorimetric quantification and capillary electrophoresis, as described in the section *Materials and Methods 3.3*. The median cfDNA concentration in the T_1 plasma samples from LARC patients (n = 40; median, 30.98 ng/mL) was significantly higher than that recorded in the cfDNA of the healthy donors (n = 16; median, 14.22 ng/mL) who volunteered their blood for research (Figure 8-A). Moreover, patients who were classified as low-risk (n = 29; median, 26.11 ng/mL) had lower cfDNA plasma levels than patients classified as high-risk (n = 11; median, 34.91 ng/mL; $p = 0.0031$, Mann-Whitney U-test) (Figure 8-B). However, after correcting the results for multiple comparisons, the difference between the two patients' groups lost their significance. The cfDNA concentrations in the healthy donors' group were slightly superior to that reported in previous studies.[157,158]

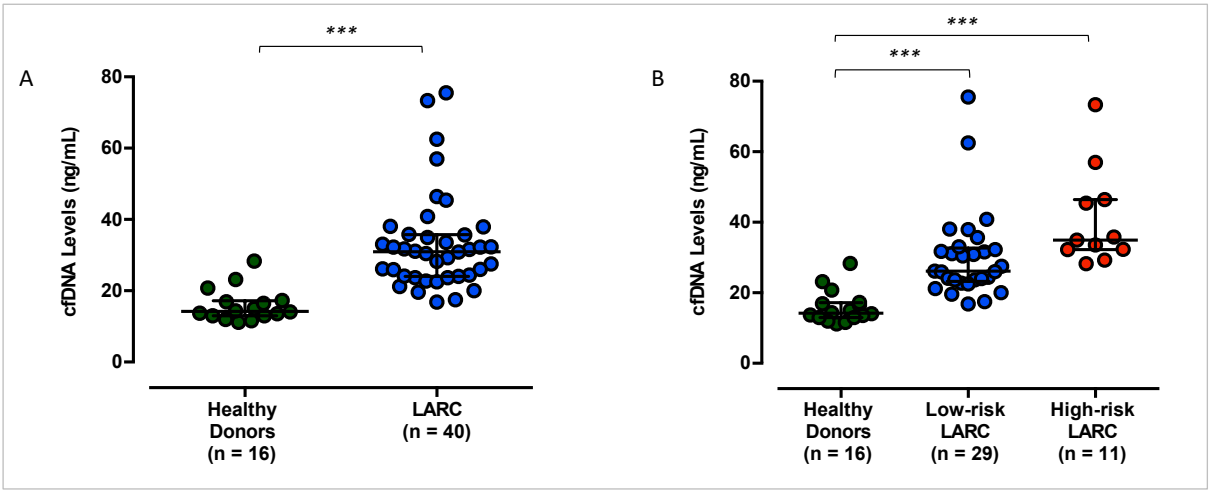

Figure 8. A) Comparison of total plasma cfDNA levels in the T_1 samples of healthy donors (n = 16) and in the LARC patients (n = 40). The median cfDNA levels were 30.98 ng/mL (IQR range: 24.07 – 35.75 ng/mL) for the patients' group and 14.22 ng/mL (IQR range: 12.96 – 17.19 ng/mL) for the controls' group ($p < 0.0001$, two-tailed Mann-Whitney U-test); B) Comparison of total plasma cfDNA levels in the T_1 samples of healthy donors (n = 16) and in the LARC patients stratified into low-risk (n = 29) and high-risk (n = 11). The median cfDNA levels were 26.11 ng/mL (IQR range: 23.21 – 32.67 ng/mL) for the low-risk group and 34.91 ng/mL (IQR range: 32.27 – 46.42 ng/mL) for the high-risk group. Significant difference was observed between the control group and the low-risk and between the control group and the high-risk group ($p < 0.0001$, Kruskal-Wallis test with Dunn's correction for multiple comparisons). Each dot represents one sample. Horizontal bars represent the median (± interquartile range).

An optimal cfDNA threshold of 17.39 ng/mL was identified to accurately discriminate LARC patients from healthy donors with a sensitivity of 81.25% and a specificity of 97.5% by means of ROC analysis ($p < 0.0001$). No differences were observed between the total cfDNA levels at T_1 and clinical or pathological characteristics, such as cTN stage at diagnosis or TRG (data not shown). Moreover, the fluctuation of cfDNA levels throughout the treatment were not associated with clinical or pathological features.

4.2.2 CNAs Profiling of Plasma cfDNA of LARC Patients

In order to evaluate the copy number profile of cfDNA in LARC patients before and throughout the treatments, low-coverage whole genome sequencing was performed on the 84 cfDNA samples from the 40 LARC patients, as well as on the 16 cfDNA samples from the 16 healthy donors. A median of 12.3 x 10^6 (range 8.0 x 10^6 – 17.0 x 10^6) sequencing reads per sample, corresponding to a median read depth of 0.34 X (range 0.20 – 0.50) were obtained. Three healthy controls (#4, #5, #13) were excluded from the analysis of CNAs as they had poor sequencing quality. The ichorCNA pipeline was applied to detect the presence of CNAs through the genome and to estimate the tumor fraction (TFx) at the genome wide scale. A positive TFx, *i.e.* TFx > 1%, was detected in 17 out 84 (20.2%) cfDNA samples. No CNAs were detected in the cfDNA of healthy donors. The analysis of CNAs revealed alterations characteristics of CRC and rectal adenocarcinoma, including gains of chromosomes 20q and 20p, 13q, 8q and 7, and losses at chromosomes 4, 8p, 17p, 18p and 18q (Rectal Cancer MSK; n = 300 patients).[159,160]

4.2.3 Distribution of CNAs in Pre-treatment cfDNA (T_1)

A positive TFx, *i.e.* TFx > 1%, was detected in the cfDNA of 6 out 40 (15.0%) patients at T_1, with a median estimated TFx of 10.41% (range 5.89% – 27.34%). Notably, the presence of CNAs was exclusively evident in patients showing a cT stage of 3 to 4, with concomitant lymph nodes involvement at the time of diagnosis. Moreover, the detected TFx in cfDNA was enriched and quantitatively higher in the group of 11 patients who were classified at higher risk of disease recurrence than in the remaining 29 patients. In fact, a positive TFx was detected in 3 out 11 (27.3%) high-risk LARC, who exhibited an average TFx of 18.03%, while it emerged in 3 out 29 (10.3%) low-risk LARC, who displayed an average TFx of 9.06% (Table 7).

Table 7. Detection rate of CNAs and estimated TFx in the cfDNA T_1 samples of LARC patients (n = 40), well as in the cfDNA of healthy donors (n = 13). LARC patients were stratified according to their clinical risk-category into high-risk (n = 11) and low-risk (n = 29).

Group	Patients (n)	Positive TFx n (%)	TFx Average
Low-risk LARC	29	3 (10.3)	9.06
High-risk LARC	11	3 (27.3)	18.03
Healthy Donors	13	0 (0.0)	0

Next, the prognostic role of CNAs detection in plasma T_1 cfDNA was investigated as a possible early marker of treatment outcome. Notably, in the group of patients with a positive TFx at T_1, the incidence of pCR was the 16.7% (1 out 6 patients), against the 59.1% (13 out 22 patients) in the group without detectable TFx. Moreover, 4 out 6 (66.7%) patients with positive TFx developed local or distant relapse within two years from the diagnosis. Conversely, the diagnosis of relapse in the group without TFx was reported in 5 out 17 (29.4%) patients. Despite the lower and higher rates of pCR and of relapse, respectively, detected in the group with positive TFx in the cfDNA T_1 with respect to the other group, the differences lacked to be significant due to the low sample size. However, when looking at the concurrent presence of CNAs and of high baseline CEA levels (CEA > 5.0 ng/mL), the combination of the two markers allowed the identification of recurrent patients with a sensitivity of 85.7% and a specificity of 90.0% (Fisher's exact test, $p = 0.0006$) (Table 8).

Table 8. Estimated TFx in the cfDNA of LARC patients at the baseline (T_1) and CEA level at the diagnosis in patients who developed distant or local recurrence within two years from the diagnosis (n = 9). In the last column is indicated which marker (ctDNA or CEA) could be suitable to predict the tumor relapse.

Patient	Positive TFx T_1	CEA (ng/mL)	Prediction of relapse
#2020-01	yes	4.3	ctDNA
#19834	no	n.a.	n.a.
#19871	yes	4.4.	ctDNA
#19948	no	n.a.	n.a.
#19947	no	2.0	None
#19946	no	68.0	CEA
#105-0019	yes	32.6	ctDNA + CEA
#19914	no	21.4	CEA
#19918	yes	22.5	ctDNA + CEA

4.2.4 Distribution of CNAs in cfDNA During nCRT (T_2)

With the aim of assessing the ctDNA content in course of nCRT and its performance as a marker of treatment outcome, the 24 cfDNA samples collected at T_2 were analyzed to check the presence of CNAs and their trend with respect to the matched T_1 sample, when evaluable. T_2 samples were obtained at a median time of 21 days from nCRT initiation (range: 13 – 28 days). The presence of CNAs was detected in 8 out 24 (33.3%) T_2 samples, with a median identified TFx of 7.96% (range: 5.60% – 19.10%). Specifically, the presence of positive TFx was detected in 5 out 9 (55.6%) patients who achieved a pCR and in 3 out 14 (21.4%) patients without pCR. Moreover, 2 out 8 (25.0%) patients presented a reduction of the detected TFx with respect to the T_1, while the remaining 6 (75.0%) showed an increased TFx with respect to the T_1. Notably, an increase of the TFx detected during nCRT (T_2) was positively associated with a higher likelihood of achieving a pCR with respect to the absence or the decrease of TFx (RR: 3.75; 95% CI 1.47 – 9.56; $p = 0.0147$) (Table 9). Only 1 out 6 (16.7%) patients who showed an increased TFx in the plasma cfDNA T_2 had a poor treatment's response (TRG5).

Table 9. LARC patients achieving a pCR in the group with increased TFx (n = 6) or reduced or absent TFx (n = 18) in the cfDNA collected during nCRT (T_2).

Group	Patients (n)	pCR n (%)	No pCR n (%)
Total	24	9 (37.5)	15 (62.5)
Increased TFx at T_2	6	5 (83.3)	1 (16.7)
Reduced or absent TFx at T_2	18	4 (22.2)	14 (77.8)

4.2.5 Distribution of CNAs in Post-treatment cfDNA (T_3)

Next, the presence of ctDNA the 15 patients with available cfDNA collected between the end of nCRT and surgery (T_3) was evaluated to test the presence of CNAs as a possible marker of incomplete response to nCRT. A positive TFx was detected in 3 out 15 (20.0%) patients at T_3 and none of them achieved a pCR (Table 10). However, no significant correlation between the CNAs status after nCRT and the TRG was underscored, due to the small fraction of patients with positive TFx.

Table 10. LARC patients achieving a pCR in the group with detectable CNAs (n = 3) or non-detectable CNAs (n = 12) in the cfDNA collected after nCRT (T_3).

Group	Patients (n)	pCR n (%)	No pCR n (%)
Total	15	5 (33.3)	10 (66.7)
Presence of TFx at T_3	3	0 (0.0)	3 (100)
Absence of TFx at T_3	12	5 (41.7)	7 (58.3)

LARC patient #19939 showed the presence of detectable TFx in the three serial plasma samples collected during treatment. The patient was diagnosed at the age of 69 with a cT4N2M0 rectal adenocarcinoma and was classified as at high risk of tumor relapse. Accordingly, he was treated with capecitabine with concomitant oxaliplatin and radiotherapy in the neoadjuvant setting. The sWGS of cfDNA sample T_1 revealed the presence of CNAs affecting the chromosomes 9p and 7p with an estimated TFx of 7.3%. The T_2 sample, collected in course of nCRT, revealed a steep increase of the TFx (14.1%) with a concurrent evident augment of the CNAs detectable at the genome scale. Notably, after completing nCRT, the detected TFx in cfDNA sample T_3 underscored the permanence of detectable TFx, which rose to 15.7% (Figure 9). The patient displayed a very poor outcome and developed DP during treatment, which led to the discontinuation of further therapeutic strategies, e.g. surgery. The patient died one month after the end of nCRT with disease spread to the liver and the lungs.

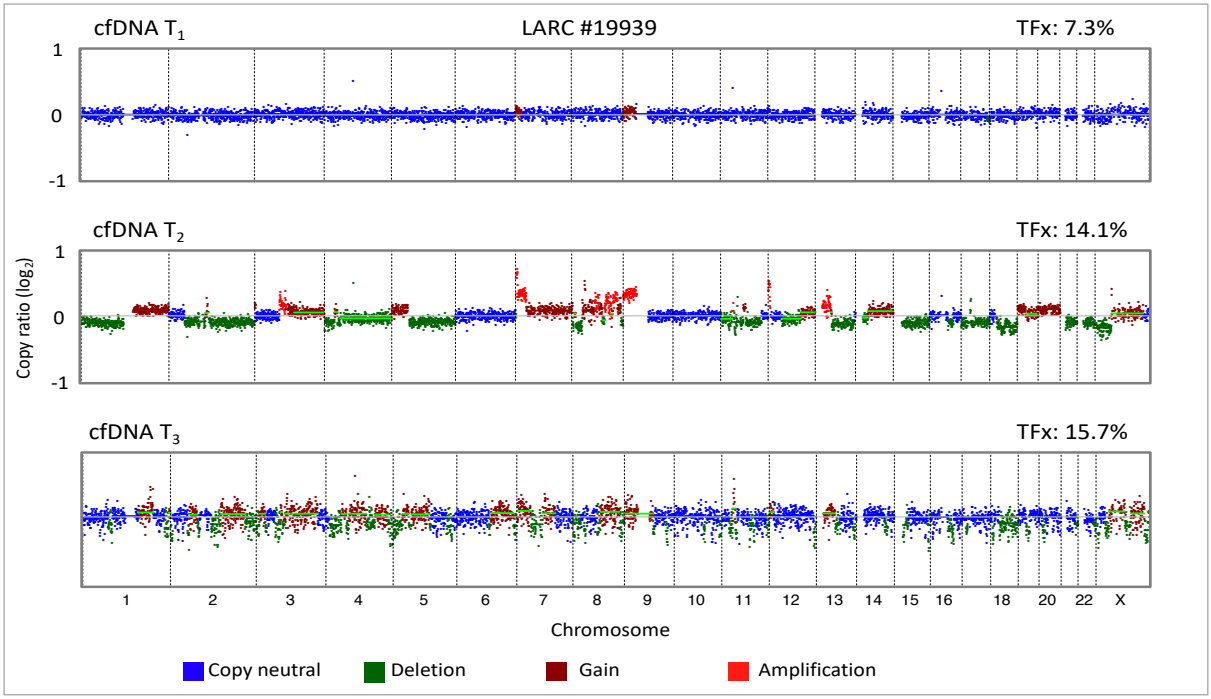

Figure 9. Exemplary genome-wide copy number profiles inferred from sWGS of plasma cfDNA. Profiles of patient #19939 illustrated detectable CNAs at baseline sampling (T_1), during treatment (T_2) and at the end of treatment (T_3), with concurrent increase of the estimated TFx.

4.3 Molecular Characterization of Primary tumor tissue of LARC

The FFPE primary tumor tissue was retrieved from 36 LARC patients who underwent a diagnostic staging colonoscopy at IRCCS CRO Avaino (PN). Thereof, 15 samples derived from the 40 LARC patients included in the cfDNA surveillance study. All FFPE samples were kindly provided by the Pathology Division of CRO Aviano, directed by Prof. Dr. Vincenzo Canzonieri, and were analyzed by an experienced pathologist to estimate the fraction of tumor content present in the sample. The 15 samples with matched plasma cfDNA were analyzed by means of sWGS, to test the specificity of CNAs detection in the cfDNA of LARC. Moreover, they were also analyzed by means of targeted deep sequencing to characterize the presence of tumor specific SNVs. Tumor DNA was extracted from the 36 FFPE tissues and its amount was assessed spectrophotometrically by means of NanoDrop (Thermo Fisher Scientific, Wilmington, DE, U.S.A.) (n = 33) as well as fluorometrically by means of Quantus Fluorometer (Promega, Madison, WI, U.S.A.) (n = 36). The DNA showed a highly heterogeneous yield in term of amount, showing a median concentration of 7.6 ng/µL (range: 1.2 – 98.0 ng/µL) with the Quantus and of 67.2 ng/µL (range: 10.9 – 588.5 ng/µL) with the NanoDrop. The two means of DNA quantification showed a huge disagreement, with the Nanodrop overrating the DNA amount over the Quantus. However, a linear correlation between the two measures was observed (Figure 10-A) The DNA quality was assessed by analyzing the fragmentation's degree of the DNA by means of capillary electrophoresis with High Sensitivity TapeStation (Agilent Technologies, Santa Clara, CA, U.S.A.) with the Genomic DNA kit. For each sample, the DNA integrity index (DIN) was recorded as a

quantitative measure of the level of the DNA fragmentation. The DNA resulted to be moderately to highly fragmented (median DIN, 2.3; range, 1.7 - 3.3), consistently with the quality of DNA commonly recovered from FFPE tissues. The DIN showed a positive linear correlation with the DNA concentration ($p < 0.0001$) (Figure 10-B).

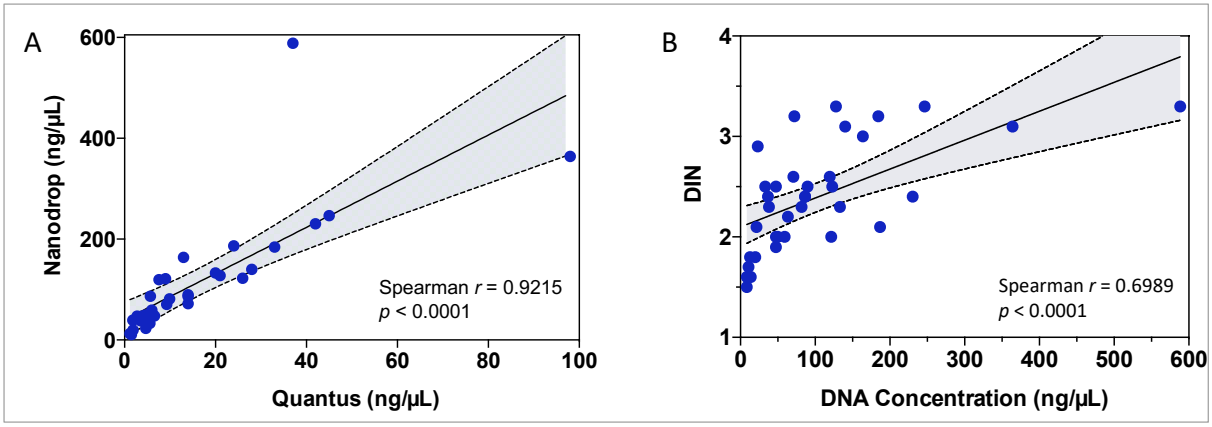

Figure 10. A) Correlation between DNA concentrations measured with fluorometric assay (Quantus, Promega) and spectrophotometrically (NanoDrop, Thermo Fisher Scientific) in 36 DNA samples extracted from FFPE tumor tissue of 36 LARC patients. x-axis indicates the DNA concentration measured with the Quantus (ng/µL) and the y-axis indicates the DNA concentration measured with Nanodrop (ng/µL). B) Correlation between the DNA integrity index (DIN) and the DNA concentration according to the spectrophotometric quantification. Each dot represents a single DNA sample. The black lines represent the linear regression curve and the dashed black lines indicate the 95% confidence interval.

4.3.1 CNAs Profiling of Primary Tumor DNA and Comparison with cfDNA in LARC

First, the 15 tissue DNA with available matched plasma cfDNA were analyzed by means of sWGS. A median of 15.8 x 10^6 (range 4.3 x 10^6 – 20.1 x 10^6) sequencing reads per sample, corresponding to a median read depth of 0.51 X (range 0.47 – 0.56) were obtained. The ichorCNA pipeline was applied to detect the presence of CNAs through the genome and to estimate the tumor fraction (TFx) at the genome wide scale, using the same parameters of the cfDNA. As expected, all 15 tumor samples presented a positive TFx, spanning between 19.0% to 59.0%. The most frequently genomic regions affected by the presence of CNAs comprised gains of chromosomes 20q and 20p, 13q and 13p, 7p, which contains the genetic locus of EGFR and was amplified in 9 out 15 (60.0%) samples, 8q and 17q, as well as losses of 8p, 18p and 18q. The overall scenario of CNAs identified in the primary tissue was in agreement with the most common CNAs reported in LARC.[47]

Moreover, the majority of identified CNAs in the cfDNA samples with matched primary tumor DNA available (n = 8) recapitulated the aberrations identified in the primary tumor, proving the specificity of the analysis also in the clinical context of a non-metastatic disease. Figure 11 shows a graphical representation of the genome wide copy number profile of the plasma cfDNA sample collected at T_1 and its matched tissue DNA of a patient (#19871) with LARC diagnosis cT3N0. In both samples it can be observed the presence of chr20 and chr13 gain, as well as the loss of 1p, 8p, 17p and 18. Moreover,

in the primary tumor, other significantly amplified and deleted regions were recorded, such as the gain of chromosome 1q, 5q, 7, 11q, 12 and 17 and the deletion of 10p.

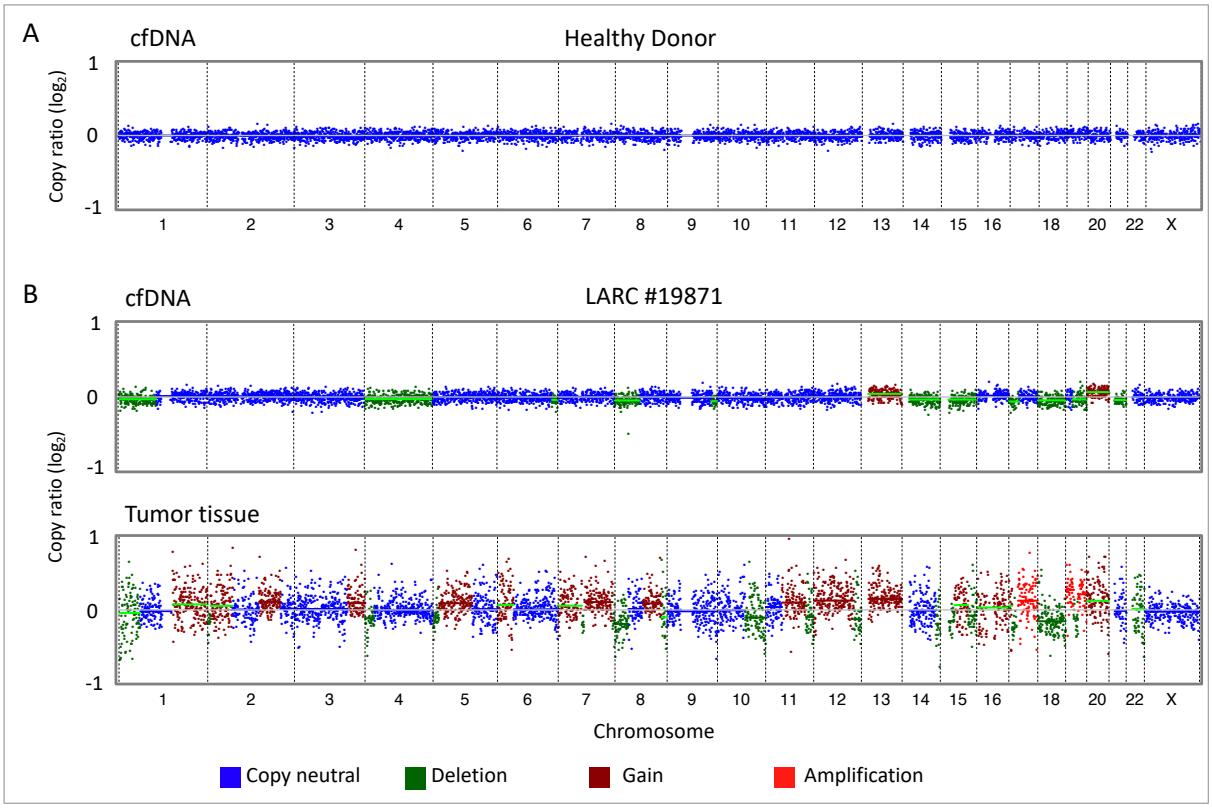

Figure 11. Copy number and tumor fraction from sWGS. A) Genome wide copy number from 0.4X sWGS of cfDNA from a healthy donor. B) Genome wide copy number from 0.4X sWGS of T_1 cfDNA from a LARC patient (#19871) and 0.4X sWGS of the matched tumor tissue from the same patient.

4.3.2 Genetic Variants in Primary Tumor DNA of LARC

The molecular genetic background of the primary tumors was profiled to characterize point mutations and small indels by means of targeted deep sequencing, using the QIaSeq Colorectal Cancer Panel DNA kit (Qiagen, Hilden, Germany). 19 primary tumor samples from LARC patients were analyzed, including the 15 samples derived from the study population here described (n = 40). The median output per sample on MiSeq Illumina platform was 1,874,386 sequence reads (range 1,169,761 – 4,191,498) and 952 x depth of coverage (range 58 – 7,106). A total of 129 COSMIC mutations were identified in the 19 patients, 53 of which were excluded as suspected germline variants that will be reconsidered after the sequencing of matched PBMC isolated genomic DNA. Other 28 mutations were also excluded as they were predicted as non-pathogenic according to ClinVar, Polyphen2 and FATHMM prediction tools.[161–163] A panel of 59 COSMIC mutations were finally selected in the 19 patients. Thereof, 38 mutations were private for a single tumor sample and 11 were shared among two or more tumor samples. The 59 COSMIC mutations included 23 mutations of APC, 11 of TP53, 10 of KRAS, 6 of PIK3CA, 4 of *FBWX7*, 3 of BRAF and 2 of EGFR (Figure 12). The most frequently mutated gene was *APC*, whose mutations emerged in 16 out 19 (84.2%) patients, followed by *TP53*, which was mutated in 11 (57.9%)

patients and *KRAS*, detected in 10 (52.6%) patients. Both *PIK3CA* and *FBWX7* presented mutations in 4/19 (21.1%) patients, while other identified mutated genes were *BRAF* and *EGFR*, detected in 3/19 (15.8%) and in 2/19 (10.5%) patients, respectively. The median number of significant mutations per patient was 3 (range 2 – 7)

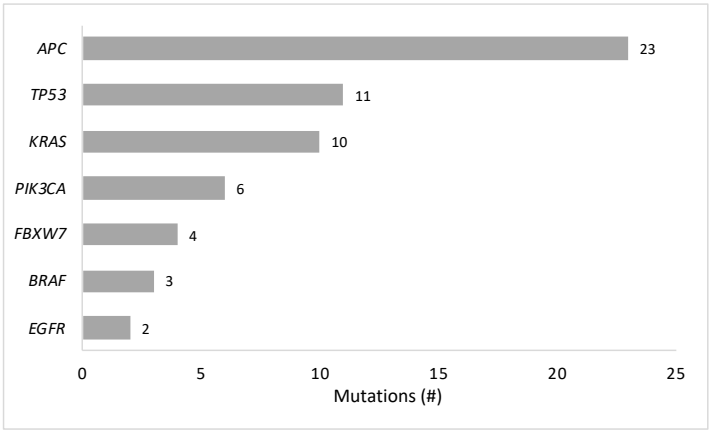

Figure 12. Number of significant mutations per gene identified in 19 screened LARC patients. A total of different 45 mutations were identified in the genes of interest by means of QIaSeq Colorectal Cancer Panel DNA kit (Qiagen, Hilden, Germany).

Detailed data for each gene is reported in Figure 13. Comparison with samples annotated as *rectum* in the TCGA Rectum Adenocarcinoma (READ) cohort (n = 91), showed similar frequencies of mutations in known CRC-related genes to our cohort, with *APC* and *TP53* being the most frequently mutated genes (TCGA, *APC* 91.1% and *TP53* 84.8%). Notably, in our cohort we observed a higher incidence of KRAS and BRAF mutations, with respect to TCGA cohort (our cohort, *KRAS* 52.6% and *BRAF* 15.8%; TCGA, *KRAS* 41.8% and *BRAF* 2.9%).

Next, the presence of specific mutational patterns affecting the primary tumor was investigated as a possible marker of response to treatment. In Table 11, the distribution of mutated genes in patients presenting pCR and incomplete response is reported. Specifically, the achievement of the pCR was considered in this regard. Among the 19 tumors characterized, the pCR was achieved by 7 (36.8%) patients. Notably, patients presenting *KRAS/BRAF* mutations showed a lower incidence of pCR with respect to patients with *KRAS/BRAF* wild type tumors (mutant, pCR 23.1% vs wild type, pCR 66.7%). In fact, among the 13 out 19 (68.4%) patients with *KRAS/BRAF* activating mutations, 3/13 (23.1%) achieved a pCR, while 4 out 6 (66.7%) patients without *KRAS/BRAF* mutations achieved a pCR. Results were not significant due to the small sample size.

Table 11. Distribution of mutated genes identified in the 19 LARC tumor biopsies. For each gene, the number of patients with detected variants is reported, as well as the distribution of mutated genes in patients with pCR (n = 7) and in patients with incomplete response (n = 12).

Gene	Patients (n)	pCR (n= 7) n (%)	No pCR (n = 12) n (%)
KRAS	10	2 (28.6)	8 (66.7)
BRAF	3	1 (14.3)	2 (16.7)
APC	18	6 (85.7)	12 (100)
TP53	7	3 (42.9)	4 (33.3)
PIK3CA	4	2 (28.6)	2 (16.7)
EGFR	2	2 (28.6)	0
FBWX7	4	1 (14.3)	3 (25.0)

Gene	HGVS.c	HGVS.p	COSM	T1-19784	T1-19914	T1-19917	T1-19845	T1-19843	T1-19853	T1-2020-01	T1-19912	T1-19947	T1-19810	T1-19852	T1-19838	T1-19871	T1-19886	T1-19738	T1-19842	T1-19932	T1-2020-03	T1-19744
KRAS	c.35G>A	p.Gly12Asp	521	■	■	■																
	c.35G>T	p.Gly12Val	520				■	■														
	c.38G>A	p.Gly13Asp	532						■	■												
	c.34G>T	p.Gly12Cys	516												■							
	c.34G>A	p.Gly12Ser	517									■										
	c.182A>C	p.Gln61Pro	551								■											
BRAF	c.1799T>A	p.Val600Glu	476										■	■								
	c.1406G>T	p.Gly469Val	459													■						
APC	c.3340C>T	p.Arg1114*	13125																	■		■
	c.4348C>T	p.Arg1450*	13127		■		■															
	c.637C>T	p.Arg213*	13134																■			
	c.1660C>T	p.Arg554*	19040	■																		
	c.2626C>T	p.Arg876*	18852							■			■									
	c.3520G>A	p.Asp1174Asn	87547															■				
	c.4099C>T	p.Gln1367*	13121					■														
	c.4132C>T	p.Gln1378*	18862																■			
	c.3916G>T	p.Glu1306*	18760												■							
	c.3925_3926delGA	p.Glu1309fs	19672			■																
	c.3845C>A	p.Ser1282*	235663									■										
	c.3980C>G	p.Ser1327*	18858																		■	
	c.4393_4394delAG	p.Ser1465fs	18873	■																		
	c.4460delC	p.Thr1487fs	19598						■													
	c.2054G>A	p.Trp685*	1432191			■																
	c.2805C>A	p.Tyr935*	19031		■																	
	c.2804dupA	p.Tyr935fs	19657								■						■					
	c.4240delG	p.Val1414fs	18887								■					■						
FBXW7	c.1393C>T	p.Arg465Cys	22932				■															
	c.1394G>A	p.Arg465His	22965					■														
	c.1513C>T	p.Arg505Cys	74637						■													
	c.1972C>T	p.Arg658*	22967	■																		
TP53	c.542G>A	p.Arg181His	10738					■														
	c.716A>G	p.Asn239Ser	1649401																			■
	c.801delG	p.Asn268fs	44362																	■		
	c.749C>T	p.Pro250Leu	10771		■																	
	c.497C>A	p.Ser166*	11508															■				
	c.707A>G	p.Tyr236Cys	10731										■									
	c.376-4_376-2delCAA	p.Asn131del	44589															■				
	c.584T>C	p.Ile195Thr	11089													■						
	c.725G>A	p.Cys242Tyr	10646						■													
	c.742C>T	p.Arg248Trp	10656			■																
	c.412G>A	p.Ala138Thr	44821									■										
PIK3CA	c.3197C>T	p.Ala1066Val	13477	■																		
	c.3068G>A	p.Arg1023Gln	13594	■																		
	c.1624G>A	p.Glu542Lys	760														■	■	■			
	c.1634A>G	p.Glu545Gly	764	■																		
EGFR	c.2563G>A	p.D855N	29577																		■	
	c.2515G>A	p.Ala839Thr	13430				■															

Figure 13. Details of 59 significant mutations associated with rectal cancer for each patient. 47 types of mutations were detected in 19 screened patients. Black boxes indicate mutations identified in tumor samples by means of QIaSeq Colorectal Cancer Panel DNA kit (Qiagen, Hilden, Germany).

4.3.3 Immunohistochemical Analysis of Pre-treatment Tumor Tissue of LARC

Moreover, an ancillary analysis, which involved a retrospective population of 95 LARC patients with a pretreatment tumor biopsy available, was performed in order to identify protein markers that are differentially expressed in responder (pCR) and in non-responder patients. To this end, a panel of 11 tumor related markers (MLH1, GLUT1, Ki67, CA-IX, CXCR4, COX2, CXCL12, HIF1α, VEGF, CD44, and RAD51) with a potential role in the response to nCRT was investigated by immunohistochemistry (IHC) in the pretreatment biopsies of the 95 LARC patients and the biomarkers' level of expression was evaluated to identify the best cut-off value of expression to accurately predict the response to nCRT. Moreover, the potential interaction among the investigated biomarkers and the patients clinical-pathological features in defining the tumor response phenotype was assessed by a classification and regression tree (CART) analysis. All patients were homogeneously treated with 5-FU based nCRT for five weeks. After completing nCRT, 25/95 (26.3%) patients achieved a pCR (ypT0N0) (responders), while 70/95 (23.7%) patients reported a partial or null tumor response (non-responders). No patient reported a TRG5. The markers' expression was assessed by means of cellularity (% of positive cells), intensity of immunostaining and by their combination (H-score), as described in the section *Materials and Methods 3.19*. Table 12 reports the optimal cut-off values according to ROC analysis, to discriminate between responders and non-responders. The multivariate odds ratio to get a pCR to nCRT were calculated for each marker based on those cut-off values. A successful discrimination based on the H-score cut-off values was achieved for five markers, *i.e.* Ki67, CXCR4, COX2, HIF1α and RAD51. Specifically, Ki67, HIF1α and RAD51 were overexpressed in non-responders, while CXCR4 and COX2 were overexpressed in responder patients. Among the 34/95 patients showing low expression of Ki67 (H-score < 7), 14/34 (41.1%) were responders, while among 61/95 showing high expression of Ki67 (H-score ≥ 7), only 11/61 (18.0%) patients were responders. Similarly, low levels of HIF1α expression (H-score < 5) were more favorable of pCR than high levels (35.4% vs 17.0%), and patients expressing low levels of RAD51 (H-score < 2) also exhibited a greater incidence of pCR (50.0% vs 19.4%). By contrast, the high expression of CXCR4 (H-score ≥ 2) was more favorable of pCR than low expression (34.0% vs 9.7%), as well as the high expression of COX2 (H-score ≥ 6), with patients reporting COX2 levels above the optimal cut-off were more likely to be responders (37.2% vs 17.3%). H-score summarizes IHC cellularity and immunostaining intensity parameters. However, when looking at the association of these single parameters, it can be observed that the association between the H-score parameter and tumor response for Ki67 is exclusively driven by its cellularity, which allowed discriminating responders from non-responders with a greater specificity than the H-score (81.4% vs 71.4%) but with a lower sensitivity (48.0% vs 56.0%). Ki67 staining intensity did not change between responders and non-responders. Conversely, for CXCR4 the staining intensity alone allowed the discrimination of responders with a higher specificity (75.4% vs 45.9%) but a lower sensitivity (60.0% vs 85.0%) with respect to H-score, while for COX2 the stain

intensity underlined a lower specificity (58.6% vs 61.4%) and a higher sensitivity (68.0% vs 64.0%) than the H-score.

A CART analysis, including all the protein H-scores and clinical and demographic variables, was performed on the 95 patients study cohort for the prediction of pCR. A classification and regression tree was generated (Figure 14). It identified Ki67 H-score as the major factor associated to pCR and CXCR4 H-score as the secondary significant discriminating marker. A cut-off H-score value for Ki67 and a cut-off for CXCR4 identified three distinct subgroups presenting a different probability of reporting a TRG2-4. Patients ranked with Ki67 ≥ 8 represent the terminal node with the lowest chance of pCR (18% of patients got a pCR) and were chosen as reference group. The terminal node containing the intermediate risk group is composed by patients presenting Ki67 < 8 with concomitant CXCR4 < 4, with the 29% of included patients reporting a pCR (OR 1.85; 95% CI 0.57 – 5.97). On the other hand, the terminal node comprising patients with Ki67 < 8 and concomitantly CXCR4 ≥ 4 represents the group with the highest percentage of complete responders (70%) (OR 13.49; 95% CI 2.64 – 68.99).

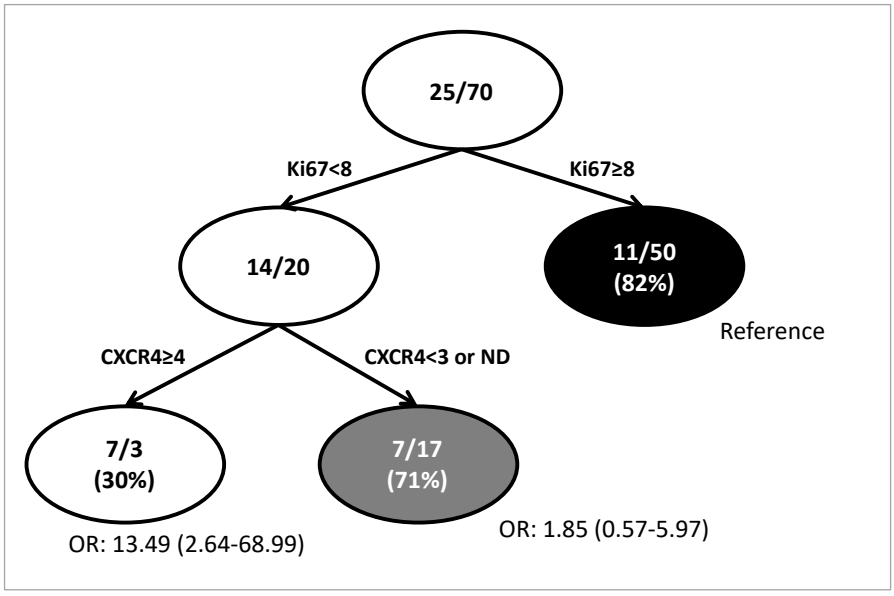

Figure 14. CART representation of the biomarkers' expression combination significantly predictive of pCR (TRG1) in LARC patients. Fractions indicate the number of patients reporting a pCR vs patients reporting an incomplete pathological response (TRG2-4). Black circles represent terminal nodes with high probability to have TRG2-4 (ratio ≥ 80%); gray circles represent terminal nodes with intermediate probability to have TRG2-4 (20% ≤ ratio < 70%); while white circles represent terminal nodes with low probability to report a TRG2-4 (ratio ≤ 30%). Odds ratio and 95% CI were calculated for each group with respect to the reference group (high probability) through logistic regression model.

Table 12. Odds ratio (OR) and 95% confidence interval (CI)[a] for TRG 1 in 95 patients with non-metastatic rectal cancer.

	H-score (Huang F)				Cellularity (%)				Staining Intensity			
	Cut-off	**TRG1**	**TRG2-4**	**OR (95% CI)**	**Cut-off**	**TRG1**	**TRG2-4**	**OR (95% CI)**	**Cut-off**	**TRG1**	**TRG2-4**	**OR (95% CI)**
MLH1	<5	48.0%	27.4%	2.62 (0.93-7.39)	≤50	48.0%	258%	2.79 (0.98-7.92)	M/S	64.0%	77.4%	0.52 (0.17-1.60)
GLUT 1	<3	16.0%	7.1%	1.84 (0.37-9.27)	≤50	60.0%	45.7%	1.74 (0.64-4.76)	M/S	84.0%	82.9%	1.26 (0.35-4.62)
Ki67	<7	56.0%	28.6%	3.30 (1.19-9.13)	≤30	48.0%	18.6%	4.27 (1.47-12.5)	M/S	100%	100%	---
CA IX	≥1	84.0%	74.3%	2.23 (0.62-7.98)	≤5	56.0%	48.6%	1.22 (0.46-3.29)	M/S	52.0%	48.6%	1.33 (0.49-3.63)
CXCR4	≥2	85.0%	54.1%	4.67 (1.15-17.4)	≥20	81.8%	59.0%	3.08 (0.89-10.6)	M/S	59.1%	24.6%	6.08 (1.98-18.7)
COX2	≥6	64.0%	38.6%	3.21 (1.14-9.09)	≤80	92.0%	82.9%	2.00 (0.38-10.5)	M/S	68.0%	41.4%	3.29 (1.15-9.43)
CXCL12	<3	60.0%	48.6%	1.80 (0.67-4.85)	≤30	68.0%	52.9%	2.35 (0.81-6.78)	M/S	64.0%	55.7%	1.20 (0.45-3.23)
HIF1α	<5	68.0%	44.3%	2.91 (1.01-8.40)	≤40	32.0%	27.1%	1.07 (0.36-3.18)	M/S	36.0%	55.7%	0.43 (0.15-1.21)
VEGF	<7	96.0%	80.0%	4.60 (0.55-38.7)	≤60	84.0%	58.6%	2.86 (0.84-9.73)	M/S	16.0%	28.6%	0.63 (0.18-2.19)
CD44	<7	68.0%	64.3%	1.42 (0.49-4.06)	≤60	52.0%	44.3%	1.60 (0.58-4.39)	M/S	92.0%	84.3%	2.19 (0.41-11.6)
RAD51	<2	27.3%	10.3%	3.87 (1.05-14.2)	≤60	95.5%	75.0%	7.18 (0.82-63.2)	M/S	59.1%	74.6%	0.60 (0.20-1.78)

[a]Adjusted for cN (0, 1+), distance from anal margin<7cm, and neoadjuvant chemotherapy (none, 5-FU, 5-FU+other). [b]Estimated through ROC analysis based on TRG1.

4.4 Gastrointestinal Stromal Tumor: Patients' Characteristics

Between March 2015 and May 2020, 39 consenting imatinib-receiving GIST patients, attending the Medical Oncology Unit at IRCCS Centro di Riferimento Oncologico of Aviano (PN) and Ospedale Ca'Foncello of Treviso (TV), were prospectively enrolled in a blood acquisition protocol. Clinical and pathological features of the 39 GIST patients enrolled into the clinical protocol are displayed in Table 13. At recruitment, the median age was 61 years (range: 32 – 82), 19 patients were male and 20 were female, thus showing an equal gender distribution. Primary tumor was located in the stomach in the majority of cases (59.0%), followed by the small bowel (30.8%). Other primary tumor sites were pelvic region (n = 1), abdomen (n = 1) and peritoneum (n = 2).

Table 13. Characteristics of the 39 GIST patients enrolled in the study.

Characteristic	**Patients (n)**	**%**
Age at enrollment, median (range)	61 (32 – 82)	
Gender		
male	19	48.7
female	20	51.3
Primary tumor site		
stomach	23	59.0
small bowel	12	30.8
other*	4	10.3
Primary tumor genotype		
KIT exon 11	16	41.0
KIT exon 13	1	2.6
KIT exon 9	1	2.6
N.A.	21	53.8
Tumor dissemination at enrollment		
localized	6	15.4
metastatic	16	41.0
no evidence of disease (NED)	17	43.6
Imatinib setting at enrollment		
adjuvant	9	23.1
first line (400 mg/die)	28	71.8
first line (800 mg/die)	2	5.1
Disease progression/relapse during follow-up		
yes	11	28.2
no	28	71.8

* Other primary tumor sites were pelvic region (n = 1), abdomen (n = 1) and peritoneum (n = 2)

Despite the recommendations by the international guidelines, the primary tumor genotyping was performed only on a small fraction of cases (46.2%) and all tested patients presented activating mutations on *KIT*. Thereof, 16 patients had *KIT* exon 11 mutated, one patient had *KIT* exon 13 mutated and one patient had *KIT* exon 9 mutated. The precise location of *KIT* activating mutations was available only in a small proportion of patients. At the time of enrollment, 6 patients (15.4%) had localized active disease, 16 (41.0%) had proven metastatic disease, and the remaining 17 patients (43.6%) had no evidence of residual disease as a consequence of either surgical tumor removal or complete response to imatinib. The main metastatic sites were liver (n = 10), peritoneum (n = 3), pelvic region (n = 1), pancreas (n = 1) and lung (n = 1). In all cases, plasma samples were obtained while on imatinib treatment, which was administered either in the adjuvant or in the first line setting. No patients were recruited as treatment naïve. The median length of follow-up was 22 months (range 2 – 61). Four patients were lost at follow-up soon after the enrollment and for them only one blood sample was collected. During the course of monitoring, 11 patients developed clinical diagnosis of disease's progression (n = 9) or tumor relapse (n = 2).

Imatinib treatment was interrupted by six patients during follow-up, with a median length of imatinib suspension of 3.8 months (range: 10 days to 12 months). The causes of treatment interruption were toxicity (n = 3), pregnancy (n = 1) and end of the three years of adjuvant treatment (n = 2). Eleven patients discontinued imatinib during follow up as a consequence of toxicity (n = 3), switch to the second line treatment with sunitinib (n = 5) and end of the three years of adjuvant treatment (n = 3).

4.5 Plasma cfDNA Levels in GIST Patients: Analysis and Clinical Considerations

During follow-up, 194 serial plasma samples were collected from the 39 GIST patients, with a median of 4 samples per patient (range 1– 11). The cfDNA from 188 plasma samples was successfully extracted from 1 – 4 mL of plasma and quantified fluorometrically. The median cfDNA concentration in the population was 9.33 ng/mL of plasma (range: 0.82 – 70.20 ng/mL). The distribution of cfDNA plasma level was investigated as a possible marker related to the presence of active DNA-shedding disease. Therefore, patients were stratified according to the presence or the absence of active measurable disease, assessed by means of computed tomography (CT) scan, during follow-up. Twenty patients presented active disease, *i.e.* metastatic spread disease or localized disease, and contributed 103 plasma samples, while seventeen patients did not show the presence of measurable GIST as a consequence of complete response (CR) to imatinib or of complete surgical tumor's eradication and contributed 79 plasma samples. Two patients were excluded from the analysis as their tumors' dimensions were not available (#11 and #40). The cfDNA extracted from sixteen healthy donors was used as a negative control. Results of cfDNA quantifications in the three groups are summarized in Table 14.

Table 14. cfDNA levels measured in GIST patients with active measurable disease (n = 20), with no evidence of residual disease (n = 17) as well as in healthy plasma donors (n = 16). Median cfDNA levels and interquartile range in the three groups are reported.

Group	Patients (n)	cfDNA levels, median (ng/mL)	cfDNA levels, interquartile range (ng/mL)
Active Disease	20	9.46	6.36 – 17.06
No Evidence of Disease	17	9.02	7.36 – 12.34
Healthy Donors	16	14.22	12.96 – 17.01

GIST patients with active disease did not show a significant difference in cfDNA plasma levels with respect to patients with no imaging-based evidence of disease. Moreover, although not significant, the median cfDNA levels in healthy donors were higher than in GIST patients, suggesting that the quantification of total cfDNA is not a reliable marker to replace or refine the imaging-based detection of residual GIST tumor cells (Figure 15). Some patients exhibited higher cfDNA levels in multiple repeated samples than most of other patients, both in the group with active disease and in the group with no evidence of disease. Specifically, in the last group, two patients (#2 and #20) reported cfDNA levels above 35.0 ng/mL, thus standing out in the plot. Patient #2, who was under imatinib since 2002 with good tolerance and CR, presented extremely high cfDNA concentrations in the two first plasma samples, *i.e* 70.47 ng/mL in #2.1 and 74.90 ng/mL in #2.2, that dropped thereafter and ranged between 2.22 and 9.35 ng/mL in the following seven samples. Notably, the sample #2.1 was collected in course of concomitant prostate cancer, which might partially explain the detection of such a high cfDNA amount at that time point. Patient #20 was receiving first-line imatinib treatment since 2015 with CR and reported cfDNA levels of 37.50 ng/mL (sample #20.1), 66.84 ng/mL (#20.2) and 82.40 (#20.4), with an average of 32.64 ng/mL in the seven samples collected. Notably, he reported PD in concomitance of imatinib interruption, when the cfDNA detected amount was 8.01 ng/mL. In the group of patients with measurable disease, 4 patients reported cfDNA levels during treatment above 35.0 ng/mL. Patient #22 presented a cfDNA amount of 70.70 ng/mL in the first plasma sample (#22.1), while showing a SD (lesions' dimensions are not available at that time point) and of 79.20 ng/mL in the fifth sample (#22.5) in concomitance of PD. Other three samples collected in course of SD had cfDNA levels ranging between 1.21 and 6.98 ng/mL. Patient #27 showed an increase of cfDNA levels (60.00 ng/mL) in concomitance to the clinical diagnosis of DP (sample #27.2) with respect to other available samples collected in course of SD or PR. Similarly, patient #31 showed high cfDNA amount in two out three samples taken in course of DP (sample #31.2, 64.68 ng/mL and sample 31.4, 55.20 ng/mL). Conversely, patient #32 reported high cfDNA levels (61.68 ng/mL) in course of PR to imatinib (sample #32.2), while no cfDNA increase was identified during PD developed in course of follow-up (sample #32.7).

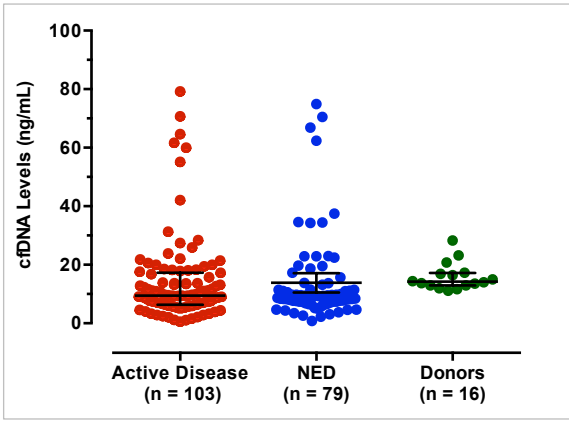

Figure 15. cfDNA levels measured in 103 plasma samples from GIST patients with active measurable disease (n = 20), in 79 plasma samples from GIST patients with no evidence of residual disease (n = 17) as well as in 16 plasma samples from healthy plasma donors (n = 16). The non-parametric Kruskal-Wallis test with Dunn's correction for multiple comparisons was used to analyze the tree groups (p = n.s.)

In the GIST study cohort, it emerged that the total cfDNA levels were not associated with clinical or pathological characteristics and that only in selected cases their increase actually reflect the development of PD. Specifically, the lack of differences in cfDNA plasma concentrations between patients with active measurable disease and patients with no evidence of disease hamper the possibility to exploit the amount of total cfDNA as a surrogate of tumor volume. Moreover, the fluctuation of cfDNA levels, which were recorded in course of follow-up, did not reflect the response or the lack of sensitivity to imatinib, showing a trend that was independent on the tumors' shrinkage or progression in most cases. However, the tumors' volume of patients bearing measurable disease were hugely heterogenous and comprised patients with localized GIST and patients with metastatic disease involving different anatomical districts. The tumors' dimensions at the time of blood collection for patients with measurable disease was retrieved from patients' clinical records and the sum of the longest diameters of lesions was calculated and used as a surrogate of tumor size. The calculated tumor size ranged from a minimum of 9 mm to a maximum of 662 mm, with a median of 55 mm. Patients were stratified based on their tumor size by applying a cut-off of 50 mm. Accordingly, 11 patients presented a tumor size greater than 50 mm and 6 patients had a tumor size below 50 mm. Six patients with active disease were excluded from the analysis as their tumors' dimensions were not available. The eleven patients belonging to the first group provided 27 plasma samples during follow-up, which showed a median cfDNA concentration of 12.36 ng/mL (range: 9.29 – 21.8), while patients from the second group provided 24 plasma samples having a median cfDNA concentration of 7.89 ng/mL (range: 5.33 – 12.16) (Figure 16). All plasma samples from the seventeen analyzed patients were considered as single variables for statistical purposes as the tumor dimensions have changed in course of follow-up.

Notably, patients exhibiting a greater tumor burden (above 50 mm) reported significantly higher cfDNA levels with respect to patients with smaller disease, suggesting a possible contribution of the tumor to the total amount of the cfDNA shed in the circulation.

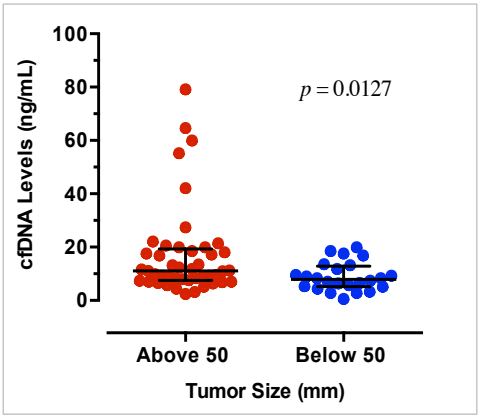

Figure 16. Distributions of cfDNA levels in plasma samples taken from patient with tumor size greater than 50 mm (n = 27) and smaller than 50 mm (n = 24). Dots represent single cfDNA values and the horizontal bars indicate the median and the interquartile ranges. Two-tailed Mann Whitney test was used to compare the two groups (p = 0.0127).

Also, the five patients presenting cfDNA levels above 25.0 ng/mL, who stand out in the plot, were all presenting metastatic spread disease at the time of sampling with peritoneum involvement in all but one cases and liver metastasis in two cases. The difference between the two groups remained significant after the removal of the top five high-cfDNA samples.

4.6 Dynamic Monitoring of ctDNA in GIST Patients

cfDNA was extracted from 188 plasma samples and the targeted deep sequencing was performed on 168 cfDNA samples that met the quantity and quality requirements for NGS. cfDNA samples were analyzed by means of amplicon-based targeted deep sequencing with UMIs to underscore the presence of ctDNA. cfDNA samples derived from five patients (#3, #4, #7, #21, #22) were firstly analyzed by using the commercially available QIaSeq Actionable Solid Tumor Panel DNA kit (Qiagen, Hilden, Germany) to test the workflow's feasibility and the analytical sensitivity. The remaining samples were sequenced by using a QIaSeq Custom Panel DNA kit (Qiagen, Hilden, Germany), comprising the most relevant genes playing a role in GIST onset and response to TKIs. Details on panel design are reported in the section *Materials and Methods 3.6*.

An average of 18.8 ng of cfDNA (median: 16.2 ng, range: 2.5 to 50 ng) was used to prepare amplicon-based libraries. The median output per sample on MiSeq Illumina platform was 1,874,386 sequence reads (range 1,169,761 – 4,191,498) and an average depth of coverage of 14,509 X was achieved before duplicated reads removal (Figure 17-A). After duplicates removal, an average depth of UMI-based coverage of 4,409 X (median: 3751 X, range: 518 to 12,467 X). A linear direct correlation was observed between the input of cfDNA used for library preparation and the UMI depth of coverage (p<0.0001; Spearman r = 0.68; Figure 17-B).

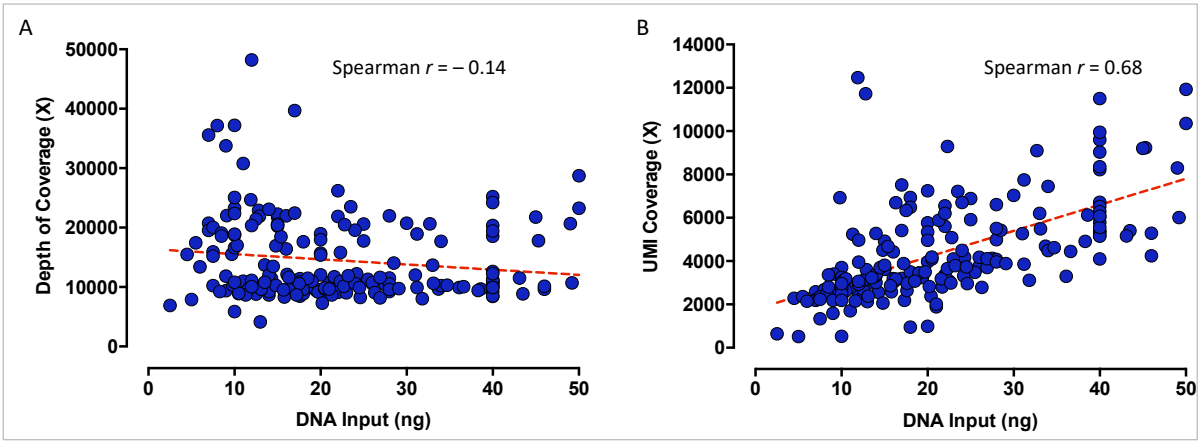

Figure 17. Correlation between cfDNA amount used for library preparation and depth of coverage (A) and UMI-based coverage obtained after duplicate reads' removal (B). Amplicon-based libraries from cfDNA were prepared with the QIaSeq Actionable and the QIaSeq Custom panels. Each dot represents a single cfDNA sample and the dashed red line is the linear regression curve.

The presence of ctDNA was detected in three plasma samples obtained from two patients in course of disease progression (#16 and #21). The panel failed to detect ctDNA in the 17 patients with no evidence of residual disease at the time of diagnosis. Thereof, two patients (#7 and #20) developed PD in course of follow-up. Patient #7 were receiving imatinib in the adjuvant setting and after three years of relapse-free survival (RFS) she discontinued imatinib, according to the standard of care. Eighteen months after treatment interruption she developed GIST hepatic relapse and imatinib first line was started at the standard dose of 400 mg/die, promptly leading to excellent tumor regression and CR at the time of the following imaging check-up, three months after imatinib reintroduction. No plasma samples were taken for patient #7 at the time of PD, which might have elucidated the underling mechanisms of recurrence, while no ctDNA was detected in the other samples collected. Patient #20, after two years of CR while on first line imatinib treatment, reported hepatic relapse as a presumed consequence of poor compliance in drug's intake. In this case also, no ctDNA was detected in concomitance of tumor relapse. The six patients with localized disease did not reported PD during follow-up and no ctDNA was detected in their plasma. Conversely, among the seventeen patients presenting metastatic disease, the presence of ctDNA was detected in two of them in course of PD. The ctDNA detection rate in the present study cohort was pretty low, as it was detected only in 2 out 39 patients (5.1%). However, when considering patients with metastatic and PD, the ctDNA detection rose to the 22.2% as it was found in 2 out 9 patients. Moreover, in the two positive cases, the ctDNA identified was informative upon the mechanism leading the progression of the disease. The identified mutations were a *KIT* exon 13 resistance mutation (#16, *KIT* c.1971T>C), known to drive an imatinib-resistant phenotype, and a *TP53* splice-site indel that had never been described before (#21, *TP53* c.560-7_560-2delCTCTTAinsT).[164] Single patients' cases are described below.

4.6.1 Case Report #16

The patient #16 is a 39 years-old woman, who was diagnosed with metastatic GIST in February 2005 in another hospital. The primary tumor was localized in the duodenum along with metastatic sites affecting liver and bones. Due to the metastatic disease, the patient underwent surgery and the first line imatinib treatment was initiated at the standard dose of 400 mg/die. The mutational status of *KIT*/*PDGFRA* was not assessed on the primary tumor tissue at the time of diagnosis. The pharmacological treatment was well tolerated and allowed an excellent disease control and the stabilization of residual disease. The patient was enrolled in the cfDNA monitoring protocol in July 2015, when the first blood sample was collected. In November 2017, PET imaging revealed liver disease progression and the imatinib dosage was increased to 800 mg/die. In January 2018, in light of the further liver and bones progression, the patient was switched to sunitinb, which allowed the stabilization of the active disease till the last follow-up in March 2019.

For patient #16, three serial blood samples were collected while on imatinib (#16.1, #16.2 and #16.3) and one additional sample was drawn during sunitinb (#16.4). From all samples the cfDNA was extracted and fluorometrically quantified. Sequencing libraries were prepared using the QIaSeq Custom Panel DNA (Qiagen, Hilden, Germany) and sequenced on MiSeq platform (Illumina, La Jolla, CA, USA). Details upon samples and sequencing output are summarized in Table 15. The NGS output underscored the presence of a somatic variant in the cfDNA sample #16.3 (*KIT* c.1961T>C) with an allele frequency of 0.9%. NGS did not to reveal the presence of further tumor derived mutations in the other analyzed cfDNA samples.

Table 15. Date of sampling of available blood samples for patient #16, response to treatment according to RECIST criteria and cfDNA concentration in plasma are shown. For each sample the mean read coverage and the mean Unique Molecular Index (UMI) depth are reported. The identified somatic *KIT* mutation in sample #16.3 and the relative allele fraction is shown.

Sample ID	Sampling Date	Response (RECIST)	cfDNA (ng/mL)	Mean Read Depth	Mean UMI Depth	Tumor Mutations	MAF (%)
#16.1	17/07/2015	SD	11.23	10,383	882	===	
#16.2	11/08/2017	PD	17.64	11,635	721	===	
#16.3	20/11/2017	PD	5.18	11,519	746	*KIT* c.1961T>C	0.9
#16.4	14/03/2019	SD	19.99	11,797	1,393	===	

The identified *KIT* c.1961T>C (COSM12706) is a missense variant located in *KIT* exon 13 that leads to the amino acid substitution in KIT protein's position 654 (p.V654A). This specific mutation had already been described in GIST and has been associated with the development of an imatinib-resistant phenotype. Notably, this mutation was detected while the patient was receiving imatinib double daily dose (800 mg/die) as a consequence of the clinical diagnosis of disease progression and its presence in the cfDNA is consistent with the lack of clinical response to imatinib dose implementation. The clinical and molecular history of patient #16 is graphically summarized in Figure 18.

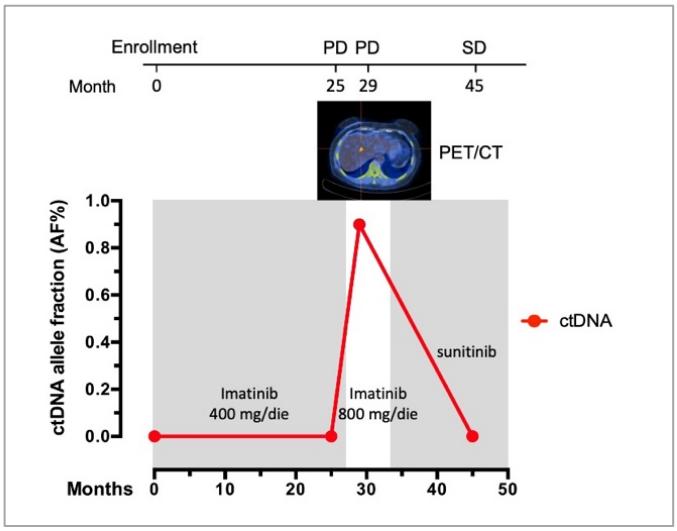

Figure 18. Clinical and molecular summary of the case report of patient #16. In the upper part of the figure the treatment outcome (RECIST criteria) and the time from enrollment are shown. At the bottom, the plot represents the allele frequency of the *KIT* c.1961T>C mutation tracked in the cfDNA (red line), as well as the pharmacological treatments.

The NGS results were validated by using a commercially available ddPCR specific assay targeting the mutation *KIT* c.1961T>C, developed and validated by BioRad (Hercules, CA, U.S.A.). As a wild type control, the genomic DNA derived from a GIST patient previously sequenced to rule out the presence of the same mutation was used, while a synthetic oligonucleotide bearing the *KIT* c.1961T>C was used as a mutated control. The ddPCR analysis recapitulated the NGS output, revealing the presence of *KIT* c.1961T>C only in the sample #16.3 with an allele frequency of 0.8% (Figure 19).

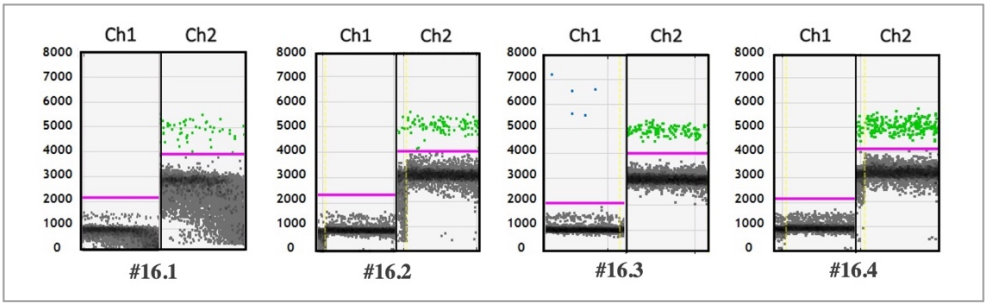

Figure 19. ddPCR plots reporting the signals registered from the two channels (Ch1 and Ch2) that are generated from the wild-type (green dots) and the mutated (blue dots) DNA are shown. The four cfDNA samples from patient #16 are reported in chronological order.

The analysis of the primary tumor tissue was not feasible as the patient underwent surgery long before the enrollment into the clinical study at another hospital. The biological origin of the *KIT* resistance mutation remains therefore to be clarified. However, it is reasonable to assume that it could be arose spontaneously during the twelve years of imatinib first line treatment, while its presence in the primary tumor tissue and its clonal selection under imatinib is less conceivable given the very long period of disease control.

4.6.2 Case Report #21

The patient #21 was a 53 years-old male diagnosed with gastric GIST in May 2015 at another hospital for which he underwent a total gastrectomy with no evidences of residual disease. The tumor tissue examination revealed the characteristic spindle cells morphology of GIST and displayed a low mitotic index (<1/50 HPF). Immunohistochemical stain revealed positivity for Ki67 and CD117 (c-KIT) antigens, confirming the diagnosis of GIST, whereas stains for smooth muscle alpha-actin, desmin, CD34 and S-100 were negative. The mutational status of *KIT*/*PDGFRA* was not assessed and, according to the risk classification criteria of GISTs, the patient was classified as a low risk of recurrence and the wait and see approach was preferred to adjuvant treatment with imatinib. In November 2015 magnetic resonance showed the presence of six hepatic nodules with maximum diameter of 2.5 cm consistent with metastatic GIST lesions, so imatinib first-line therapy was started at the standard dosage of 400 mg/die. In March 2016 the patient accessed medical care at IRCCS Centro di Riferimento Oncologico of Aviano (PN), where a magnetic resonance showed hepatic disease progression. The GIST derivation of hepatic lesions was confirmed through the IHC examination of tissue biopsy (Figure 20), therefore imatinib dosage was increased to 800 mg/die. In October 2017 PET imaging revealed further hepatic disease progression in addiction to bone and intra-abdominal metastatic spread. The patient was therefore switched to sunitinib, but the treatment was interrupted soon due to the scarce performance status. The patient died for disease progression in March 2018.

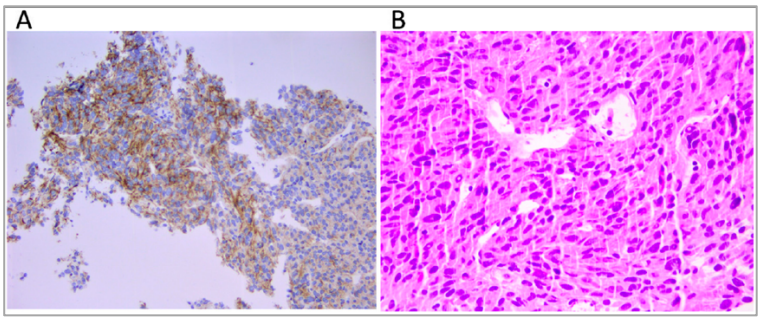

Figure 20. A) Immunohistochemical staining for CD117 (c-KIT) and B) tumor composition of spindle cells and eosinophilic cytoplasm (hematoxylin and eosin) on the metastatic hepatic lesion.

The patient was enrolled into the cfDNA monitoring protocol while on imatinib 800 mg/die, in course of active disease progression. Two serial blood samples (#21.1 and #21.2) were collected six months apart from each other and the total cfDNA was extracted from plasma. The two cfDNA samples were fluorometrically quantified showing a concentration of 2.48 ng/mL (#21.1) and of 27.48 ng/mL (#21.2). Sequencing libraries were prepared using the QIaSeq Actionable Solid Tumor Panel DNA (Qiagen, Hilden, Germany) and sequenced on MiSeq platform (Illumina, La Jolla, CA, USA). The NGS output revealed the presence of a somatic *TP53* indel (c.560-7_560-2delCTCTTAinsT), affecting the exon 6 flanking site of *TP53* gene at nucleotide position c.560-2 – c.560-7, with a growing allele frequency in

the two serial samples (MAF: 2.7%, #21.1; 9.7%, #21.2) (Table 16). The presence of the identified variant was manually checked on the bam files by means of IGV software (Figure 21-B).[130]

Table 16. TP53 somatic mutation identified by NGS. Genomic coordinates of the mutation and the read depth are reported. The total number of reads bearing the same Unique Molecular Index (UMI) and those reporting the mutation (Variant Mutational Fraction, VMF) was used to calculate the mutation frequency in each sample.

Sample ID	Genomic Coordinates	Read Depth	UMI	VMF	MAF (%)	cDNA change	Type of mutation
#21.1	17:7,578,291	6672	1023	28	2.7	c.560-7_560-2delCTCTTAinsT	Indel
#21.2	17:7,578,291	5868	876	85	9.7	c.560-7_560-2delCTCTTAinsT	Indel

To confirm the somatic nature of the *TP53* indel, the genomic DNA extracted from lymphocytes and the DNA extracted from the primary tumor tissue were analyzed with the same gene panel. The tumor tissue was kindly provided by the Pathology Unit of Ulss 17 Monselice-Este, Padova (Italy), where the patient underwent gastric surgery. As expected, the NGS output revealed the absence of the *TP53* indel in the genomic DNA, proving its somatic nature, as well as its presence in the tumor DNA, with an allele frequency of the 0.1%. These analyses confirmed that the indel detected in the cfDNA were actually shed from the tumor' cells and allowed the quantification of the ctDNA over time. Notably, no other clinically relevant mutations were identified in the primary tumor DNA, whose genotype for *KIT*/*PDGFRA* was wild type. However, the tumor tissue analyzed, although having a high tumor content, might not represent the whole mutational status of the tumor itself as a consequence of the spatial limitation provided by the sampling and might introduce a bias when assessing the presence of imatinib sensitizer mutations.

Since the ctDNA was detected in course of active disease progression, which were mainly localized in the liver, the DNA extracted from the metastatic hepatic lesion was also interrogated to assess the i) the presence of the *TP53* indel and ii) the genotype of the relapsed tumor, with specific interest to the presence of druggable mutations that might have guided the therapeutic decisions. NGS output revealed the almost exclusive presence of the *TP53* indel in the metastatic lesion, which exhibited an allele frequency of > 99.0%. Consistently with the genotype of the primary tumor, also the metastatic tissue was proven to be *KIT*/*PDGFRA* wild type. Moreover, no actionable mutations were identified in the relapsed tumor DNA. The clinical and molecular history of patient #21 is graphically summarized in Figure 21-A.

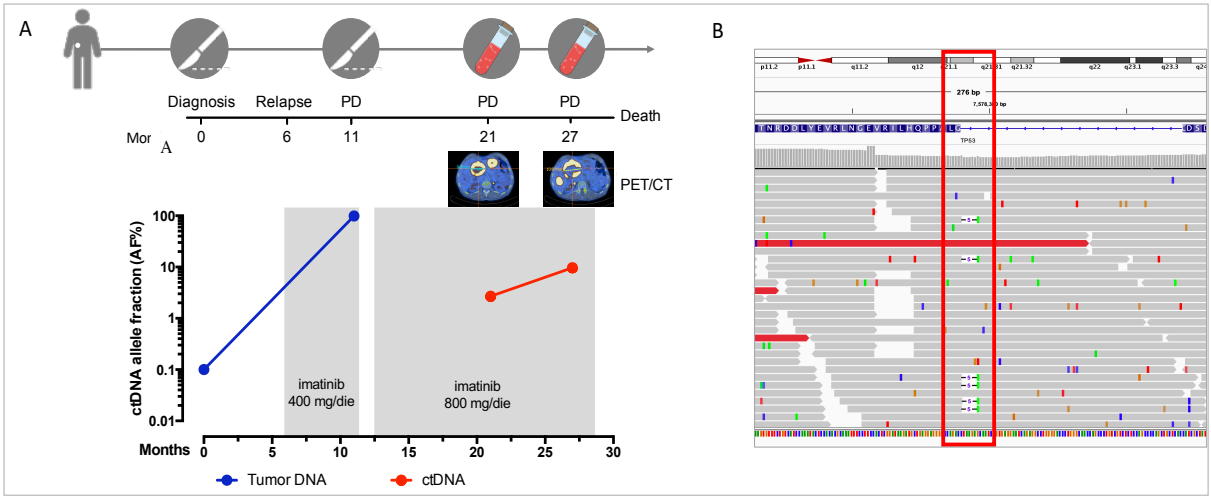

Figure 21. A) Clinical and molecular summary of the case report of patient #21. In the upper part of the figure the biological samples taken and examined by targeted NGS are represented. Below are reported the treatment outcome, according to RECIST criteria and the time from diagnosis. At the bottom, the plot represents the allele frequency of the *TP53* indel (c.560-7_560-2delCTCTTAinsT) tracked in the tumor DNA (blue line) and in the cfDNA (red line) and the imatinib dosage (adapted from Dalle Fratte *et al.* 2020). B) *TP53* c.560-7_560-2delCTCTTAinsT visualization of IGV in the cfDNA sample #21.2.

The NGS results were validated by using a custom ddPCR assay, developed by BioRad (Hercules, CA, U.S.A.) and targeting the *TP53* indel. As a wild type control, the genomic DNA derived from a GIST patient previously sequenced to rule out the presence of the same mutation was used, while a synthetic oligonucleotide bearing the *TP53* c.560-7_560-2delCTCTTAinsT was used as mutated control. The analysis was performed on metastatic tumor DNA, on primary tumor DNA and on the cfDNA sample #21.2, while the cfDNA sample #21.1 had been used for NGS and no residual DNA was available for further analysis. ddPCR assay confirmed the presence of the TP53 indel in the cfDNA #21.2, revealing the presence of 16 mutated DNA copies/µL of sample, corresponding to 277 mutated DNA copies/mL of plasma. Therefore, the estimated ddPCR MAF was 17%, superior to that reported by NGS (MAF, 9.7%). The allele frequencies of the *TP53* indel detected by ddPCR in the primary tumor and in the metastatic tumor were comparable to that obtained by NGS (Figure 22).

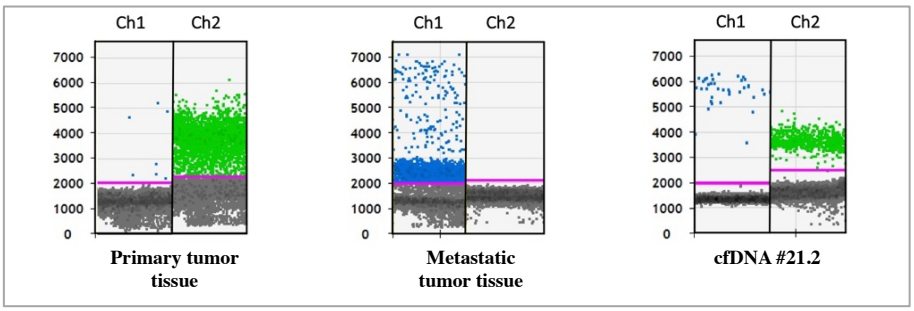

Figure 22. ddPCR plots reporting the signals registered from the two channels (Ch1 and Ch2) that are generated from the wild-type (green dots) and the mutated (blue dots) DNA are shown. In chronological order the primary tumor DNA, the metastatic DNA and the #21.2 cfDNA are reported.

The identified *TP53* indel had never been reported in literature before and was not included in the latest release of the International Agency for Research on Cancer (IARC) TP53 Mutation Database (Database R19, released on August 2018).[165] The functional impact of the *TP53* indel was unknown, although it was supposed to be deleterious given its localization in a splice acceptor site. Molecular biology analyses to confirm the indel's impact on TP53 mRNA splicing were attempted on the cDNA derived from the metastatic tumor tissue, but not feasible due to the very poor quality of FFPE RNA (data not shown). Therefore, an *in-silico* prediction model was exploited to predict the effect of the *TP53* indel at mRNA level by using publicly available bioinformatic tools (Table 17). The six different predictive tools used were specifically developed to assess the functional impact of mutations on mRNA splicing by scoring and comparing the presence of splice acceptor or donor site in the wild-type and in the mutated DNA sequence. All but one tools agree in identifying the canonical splice site in the wild-type *TP53* sequence and all of them predicted the splice site destruction in the mutated sequence. NetGene2 failed to detect the wild-type *TP53* splice site.

Table 17. Computational prediction of the effect of the mutation on the *TP53* splice site by the use of six different bioinformatic tools. The wild-type DNA sequence was compared with the mutated one and the effect was predicted by comparing the two generated scores.

Tool	Output	Wild-type Score	Mutated Score	Predicted Effect	Ref.
SpliceView	Score (0-100)	83	Not detected	Deleterious	134
Genscan	Probability Score (0-1)	0.120	Not detected	Deleterious	135
NetGene2	Confidence Score	0.00	Not detected	Not Evaluable	136, 137
NNSplice 0.9	Score (0-1)	0.94	Not detected	Deleterious	138
HSF	Score (0-100)	80.49	Not detected	Deleterious	141
MaxEntScan	Maximum Entropy Score	1.08	–2.91	Deleterious	139

Moreover, the activation of an alternative splice site was predicted by HSF that identified a likely new splicing acceptor site located thirty nucleotides downstream from the canonical site. The new splice site was scored 50.40 by HSF, and it is weaker than the canonical ones, which was scored 80.49. The activation of the new cryptic splice site would lead to an in-frame deletion of ten amino acids from the mature protein. The description of the *TP53* indel and its predicted effect on mRNA strand are depicted in Figure 23. The *in-silico* prediction of the functional impact of *TP53* indel might partially explain the highly aggressive phenotype of the GIST here described, whose lack of sensitivity to imatinib at any time point is consistent with the *KIT*/*PDGFRA* wild type genotype.

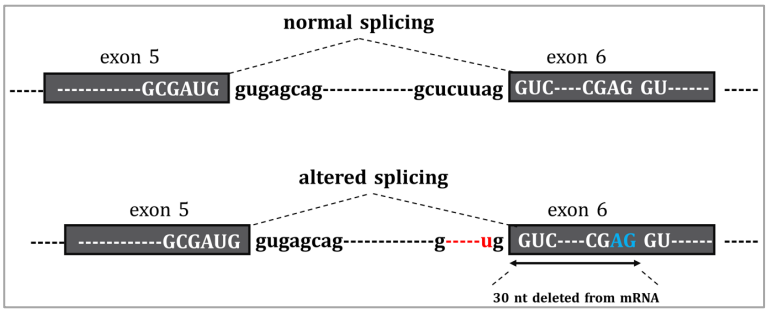

Figure 23. (A) The normal sequence and exon splicing of TP53 pre-mRNA (exon 5–6) and (B) aberrant splicing caused by the c.560-7_560-2delCTCTTAinsT (red) likely to generate an in-frame deletion of thirty nucleotides from mRNA due to the activation of a cryptic splice site (blu).

4.7 Imatinib Pharmacogenetics

4.7.1 Genotyping of CYPs and Transporters in GIST Patients

33 GIST patients were selected to study the impact of the genotype of CYPs and transporters and of the potential DDIs on imatinib plasma exposure. Non-Caucasian patients (n = 1) and patients administered with imatinib daily dose different from 400 mg (n = 5) were excluded from the analysis to minimize the number of covariates and to improve the uniformity of raw data for statistical analyses.

Genotyping of imatinib metabolizer CYPs (*CYP3A4*, *CYP3A5*, *CYP2C8*, *CYP2B6*, *CYP1A2*, *CYP2C9*, *CYP2C19* and *CYP2D6*) and transporters (*ABCB1* and *ABCG2*) was successfully performed in all the 33 genomic DNA samples analyzed. For each protein, the genotype was translated into the predicted gene AS and thereafter into the metabolic phenotype, in accordance to the PGx information provided by the CPIC and the Dutch Pharmacogenetic Working Group (DPWG) of the Royal Dutch Pharmacists Association, as described in the section *Materials and Methods 3.13*). For *CYP3A4*, *CYP1A2*, *CYP2C8*, *ABCB1* and *ABCG2*, since no genotype-predicted phenotype has been proposed from PGx working groups so far, the functional interpretation of detected genetic variants was based on literature evidences that had previously investigated the effect of PGx variants on these CYPs and transporters' activity. In the present work, the impact that CYPs and transporters might have on imatinib pharmacokinetic has been analyzed separately owing to the functional heterogeneity of CYPs and transporters in drug's metabolism, where the firsts are devoted to the bio-inactivation (*i.e.* catabolism) of the substrate drug, while the latter are in charge to regulate the drug's intake and extrusion from the blood stream, thus affecting the bioavailability.

4.7.2 Assessment of the Metabolic Phenotype of CYPs

The predicted metabolic phenotypes of CYPs is reported in Table 18. Notably, the vast majority of patients were extensive metabolizers (EM) for the CYPs analyzed, thus showing a proficiency capacity of imatinib bio-inactivation. The *CYP2D6* has emerged as the most polymorphic gene, with 14 out 33 (42.4%) patients classified as intermediate metabolizers (IM) and 3 (9.1%) classified as poor

metabolizers (PM). On the other side, *CYP3A4* and *CYP3A5* were the less frequently polymorphic genes, with 2 (6.1%) patients scored as IM (CYP3A4) and 2 (6.1%) classified as ultrarapid metabolizers (UM).

Table 18. Number of GIST patients (n = 33) with different metabolic phenotypes of cytochromes. For each gene is reported the number and, in brackets, the fraction of patients being scored poor metabolizers (PM), intermediate metabolizers (IM), extensive metabolizers (EM) or ultrarapid metabolizers (UM).

	Cytochromes' Genotype							
Phenotype	**3A4**	**3A5**	**2D6**	**2C9**	**2C19**	**2B6**	**1A2**	**2C8**
PM			3 (9.1)	2 (6.1)		1 (3.0)		
IM	2 (6.1)		14 (42.4)	9 (27.3)	9 (27.3)	14 (42.4)	15 (45.5)	
EM	31 (93.9)	31 (93.9)	16 (48.5)	22 (66.7)	22 (66.7)	18 (54.5)	18 (54.5)	25 (75.8)
UM		2 (6.1)			2 (6.1)			8 (24.2)

The phenotype of CYP3A4, CYP1A2 and CYP2C8 was assigned according to literature evidences due to the lack of a universal agreement upon PGx alleles' nomenclature for these genes. To this end, two heterozygous carriers of the *CYP3A4**22 allele, which is characterized by the functional SNP CYP3A4 c.522-191 C>T in intron 6 (rs35599367), were classified as intermediate metabolizers (IM) as the *22 allele has been associated with a reduced CYP3A4 protein expression.[166,167] Fifteen patients were heterozygous carriers of the *CYP1A2* rs762551 variant, which had been previously associated with the need for imatinib dose reduction in GIST patients,[107] and were classified as IM. Targeted NGS analysis on *CYP2C8* revealed that 8 patients were heterozygous carriers of the *CYP2C8**3 allele, which is composed by two missense variants that are in *linkage disequilibrium* (c.1196A>G and c.416G>A) and leads to an increased enzymatic activity of CYP2C8. Consistently, the presence of *CYP2C8**3 allele in imatinib-receiving patients had been previously associated with a faster imatinib metabolism and to a higher imatinib/nor-imatinib ratio.[168] Accordingly, carriers of the *3 allele were classified as ultrarapid metabolizers (UM) (Table 19).

Table 19. Prediction of the functional impact of identified genetic variants on genes *CYP3A4*, *CYP1A2* and *CYP2C8*. For each evaluated variant, its position on the coding sequence (CDS) and its rs ID are reported.

Gene	**CDS Position**	**Allele ID**	**rs**	**Functional Impact**	**Ref.**
CYP3A4	c.522-191 C>T	*22	rs35599367	Loss-of-function	166,167
CYP3A4	c.1026+12G>A	*1G	rs2242480	Neutral	166
CYP1A2	c.-163C>A	*1F	rs762551	Loss-of-function	107
CYP2C8	c.1196A>G c.416G>A	*3	rs10509681 rs11572080	Gain-of-function	168
CYP2C8	c.*24C>T	---	---	Neutral	

4.7.3 Assessment of the Metabolic Phenotype of Transporters

The predicted metabolic phenotypes of transporters are reported in Table 20. As for CYPs, the majority of patients were classified as EM. With respect to *ABCB1*, 2 out 33 (6.1%) of patients were considered

UM and 9 (27.3%) were classified as IM. For ABCG2, 1 out 33 (3.0%) patient was classified as PM and 10 (27.3%) were classified as IM. The remaining patients were wild types for the genetic variants that were considered for the phenotype assignment.

Table 20. Number of GIST patients (n = 33) with different metabolic phenotypes of the transporters ABCB1 and ABCG2. For each gene is reported the number and, in brackets, the fraction of patients being scored poor metabolizers (PM), intermediate metabolizers (IM), extensive metabolizers (EM) or ultrarapid metabolizers (UM).

	Transporters Genotype	
Phenotype	**ABCB1**	**ABCG2**
PM	0	1 (3.0%)
IM	9 (27.3)	10 (27.3)
EM	22 (66.7)	22 (66.7)
UM	2 (6.1)	0

The interpretation of ABCB1 and ABCG2 metabolic activity has required a careful appraisal of the functional impact of identified variants. The functional effect of *ABCB1* variants has been largely investigated as a determinant of drugs' efficacy and toxicity both in patients' study cohorts and in cell lines. However, since the activity of ABCB1 as a transporter is highly dependent on the drug substrate, the assessment of its AS has been deduced according to evidences reported in the framework of imatinib and TKIs. A few studies have investigated the impact of ABCB1 variants on imatinib exposure.[169–171] Specifically, major attention has been devoted to the role of the three most common variants in the *ABCB1* coding region, *i.e.* rs1128503 (c.1236C > T, Gly412Gly), rs2032582 (c.2677G > T/A, Ala893Ser/Thr) and rs1045642 (c.3435C > T, Ile1145Ile). These variants present a minor allele frequency (MAF) in the Caucasian population of approximatively 50% and are in *linkage disequilibrium*. A general consensus has been achieved upon the evidence that carriers of 1236C-2677G-3435C wild-type haplotype shows a lower sensitivity to imatinib, which was assessed by evaluating the major molecular response to the drug, the imatinib plasma concentrations,[170] and the cellular resistance to imatinib.[171] Consistently with those evidences, in our study cohort the presence of *ABCB1* haplotype has been associated to a reduced ABCB1 activity and homozygous carriers of rs1045642 variant allele were classified as IM. Further evidences support the role of the *ABCB1* rs2229109 (c.1199G>A, Ser400Asn) as a gain-of-function variant, allowing a more efficient imatinib transport by the ABCB1 variant carriers (Asn400) compared with the wild-type carriers (Ser400).[172] In our study cohort, patients carrying the ABCB1 c.1199G>A variant were considered as UM. Other identified genetic variants on *ABCB1* were not considered for the phenotype's prediction due to the paucity of literature data but were independently considered as single variables in the formal statistical analysis.

The sequencing of *ABCG2* coding regions has revealed the presence in the study cohort of two common missense variants with a previously documented functional impact on ABCG2 protein. The *ABCG2*

rs2231142 (c.421C>A, Gln141Lys) was reported in heterozygosity in 9 out 33 (27.3%) patients and in homozygosity in 1 (3.0%) patient, showing a MAF of 16.7%. This is a loss-of-function variant located in the ATP binding domain and it is the most extensively investigated ABCG2 variant because of its high allele frequency in the Caucasian population (MAF 12.1%). The presence of the A allele in imatinib receiving patients have been associated with an increase of imatinib plasma levels, whereas the wild type genotype (CC) has been associated with lower plasmatic exposure of rosuvastatin when compared to CA or AA genotypes.[173–179] The variant *ABCG2* rs2231137 (c.34G>A, Val12Met) was reported in heterozygosity in 4 out 33 (12.1%) patients, showing a MAF of 6.06% in the study population. This variant, which has been reported in the Caucasian population with a MAF of 11.0% has been associated with a reduced transporter's activity and to a reduction in the resistance to TKIs.[180] In the present thesis, the *ABCG2* variants rs2231142 and rs2231137 were considered as affecting the ABCG2 protein activity and the gene AS were calculated accordingly (Table 21).

Table 21. Prediction of the functional impact of identified genetic variants on genes *ABCB1* and *ABCG2*. For each evaluated variant, its position on the coding sequence (CDS) and its rs ID are reported.

Gene	CDS Position	rs	Functional Impact	Ref.
ABCB1	c.1236C>T	rs1128503	Neutral	169
ABCB1	c.3435C>T	rs1045642	Loss-of-function	169
ABCB1	c.2677G>T	rs2032582	Neutral	169
ABCB1	c.1199G>A	rs2229109	Gain-of-function	172,181
ABCG2	c.421C>A	rs2231142	Loss-of-function	173–179
ABCG2	c.34G>A	rs2231137	Loss-of-function	180

Other identified genetic variants affecting *ABCB1* and *ABCG2* were not considered for the estimation of transporters' phenotypes due to the paucity of literature data available but were independently considered as single variables in the formal statistical analysis.

4.7.4 Description of Imatinib Interacting Drugs in the Study Population

Among the 33 patients exposed to imatinib and selected for the pharmacogenetic analysis, 23 (69.7%) had at least one drug co-prescription during follow-up that could interact with imatinib. Overall, 33 drugs with proven or suspected imatinib interaction were recorded. Table 22 shows the distribution of patients according to drugs that could interact with imatinib. The most frequent was pantoprazole (15.2%) and its interaction with imatinib might result in an increased imatinib exposure. The mechanism of TKIs interaction with proton pump inhibitors (PPIs) is a matter of open debate among pharmacologists since the increase of gastric pH from the PPIs intake dramatically reduces the solubility, and thus the absorption, of many TKIs (e.g. sunitinib, dasatinib). At the same time, most PPIs also act as inhibitors of the drugs' transporters ABCB1 and ABCG2 and may reduce the fraction of substrate drugs that are transported outside the systemic circulation.[125] Since imatinib absorption is

independent on the intragastric pH, PPIs were exclusively considered as transporters' inhibitors. Four patients also had potential DDIs with paracetamol (12.1%) that may increase the imatinib exposure by inhibiting CYP3A4 and ABCB1 activity.

Table 22. Number of patients who had received at least one of the potentially imatinib interacting drugs. The 33 GIST patients administered with imatinib 400 mg/die were considered. Single drugs, the therapeutic class and the effect on imatinib pharmacokinetics are reported.

Drugs that could interact with imatinib	Class	Patients N = 33 n (%)	Predicted Effect on Imatinib exposure
Pantoprazole	PPIs	5 (15.2)	↑ imatinib
Paracetamol	NSAIDs	4 (12.1)	↑ imatinib
Levothyroxine	Thyroid Hormones	3 (9.1)	↑ imatinib
Bisoprolol	Beta blockers	3 (9.1)	↑ imatinib
Colecalciferol	Vitamin D3	2 (6.1)	↑ imatinib
Aspirin	NSAIDs	2 (6.1)	↓ imatinib
Allopurinol	Antigout Agents	2 (6.1)	↑ imatinib
Amlodipine	Calcium channel Blockers	2 (6.1)	↑ imatinib
Lansoprazole	PPIs	2 (6.1)	↑ imatinib
Omeprazole	PPIs	2 (6.1)	↑ imatinib
Ciprofloxacine	Fluoroquinolones	2 (6.1)	↑ imatinib
Insulin	Glucose Lowering Agents	2 (6.1)	↓ imatinib
Ranitidine	H2 receptor blockers	1 (3.0)	↑ imatinib
Carbamazepine	Antiepileptics	1 (3.0)	↓ imatinib
Esomeprazole	PPIs	1 (3.0)	↑ imatinib
Enalapril	ACE Inhibitors	1 (3.0)	↑ imatinib
Telmisartan	Sartans	1 (3.0)	↑ imatinib
Simvastatin	Statins	1 (3.0)	↑ imatinib
Atorvastatin	Statins	1 (3.0)	↑ imatinib
Flecainide	Antiarrhythmics	1 (3.0)	↑ imatinib
Edoxaban	Anticoagulants	1 (3.0)	↑ imatinib
Doxazosin	Alpha blockers	1 (3.0)	↑ imatinib
Venlafaxin	SNRIs	1 (3.0)	↑ imatinib
Ketoprofen	NSAIDs	1 (3.0)	↑ imatinib
Losartan	Sartans	1 (3.0)	↑ imatinib
Warfarin	Vitamin K Antagonists	1 (3.0)	↓ imatinib

PPI = proton pump inhibitors; NSAIDs = non-steroidal anti-inflammatory drugs; SNRIs = serotonin noradrenaline reuptake inhibitors

In addition to the recorded drugs, tobacco smoke was classified as an inducer of CYP1A2 activity, potentially leading to a reduced imatinib exposure. Three patients (9.1%) were moderate smokers and were considered for the interaction.

4.7.5 Assessment of Imatinib Trough Levels

Imatinib was successfully quantified in 127 plasma samples of the 33 imatinib receiving patients by means of a LC-MS/MS validated method. Data on imatinib plasma concentrations were kindly provided by the Therapeutic Drug Monitoring group of the Experimental and Clinical Pharmacology Unit of IRCCS CRO Aviano (Italy) headed by Dr. Bianca Posocco.

Imatinib and nor-imatinib trough levels (ng/mL) at the steady state were calculated from the raw concentration data by extrapolating the imatinib trough levels from the imatinib concentration-time algorithm, as described in the section *Materials and Methods 3.21*. The imatinib trough levels (ng/mL) quantified in the 127 plasma samples are reported in Figure 24.

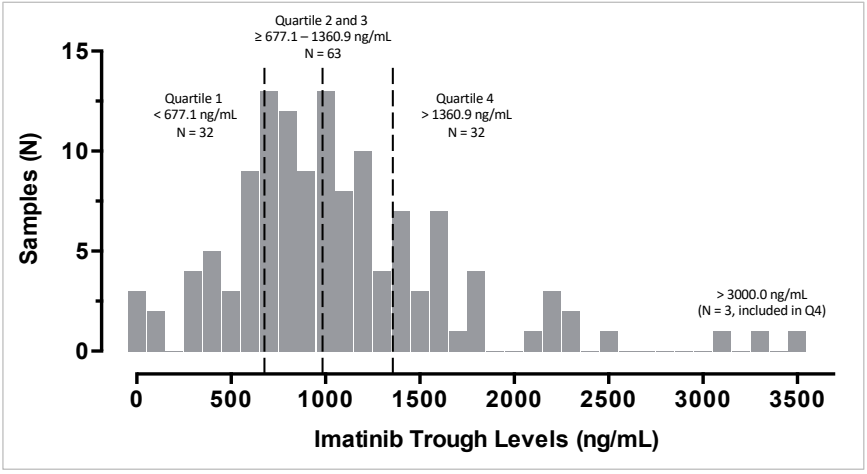

Figure 24. Distribution of imatinib trough levels (ng/mL) at 400 mg/die at steady state in 127 serial plasma samples from the 33 GIST patients. X-axis represents the imatinib trough level and y-axis indicates the number of samples. The black dashed lines indicate the first, the second (median) and the third quartile of imatinib trough levels in the study population.

The calculated imatinib trough levels ranged between a minimum of 0.0 ng/mL to a maximum of 3494.6 ng/mL, with a median value of 980.0 ng/mL, highlighting a huge interpatient variability in imatinib exposure at the same administered dose. One patient (#27) showed imatinib trough levels above 3000 mg/mL in three distinct blood samples (individual values: 3082.1, 3494.6 and 3294.6 ng/mL), while another patient (#20) exhibited extremely low imatinib trough levels in six different blood samples (maximum value: 383.2 ng/mL). Overall, the 38.8% of analyzed samples (47 out 121) were above the threshold level of 1100 ng/mL, which is the recommended trough level of imatinib in GIST patients to guarantee a clinically effective drug exposure as a precondition for good clinical response.[182] By contrary, the majority of analyzed samples were below the optimal threshold level of 1100 ng/mL, confirming the huge variability of imatinib plasma concentration at the standard dose of 400 mg/die.

To better investigate the interpatient variability of imatinib trough levels and to minimize the effect of multiple sampling over time, which was not homogeneous for all patients, the average imatinib trough concentration for the 33 patients while on imatinib 400 mg/die was calculated and plotted in Figure 25. The imatinib trough levels in the population ranged between a minimum of 89.1 ng/mL in patient #20

and a maximum of 2452.8 ng/mL in patient #27, with a median concentration of 991.5 ng/mL. It emerged that 13 (39.4%) patients exhibited an average imatinib trough level above the recommended threshold of 1100 ng/mL, while the majority of patients analyzed (60.6%) had an average imatinib trough concentration during follow-up below the optimal cut-off.

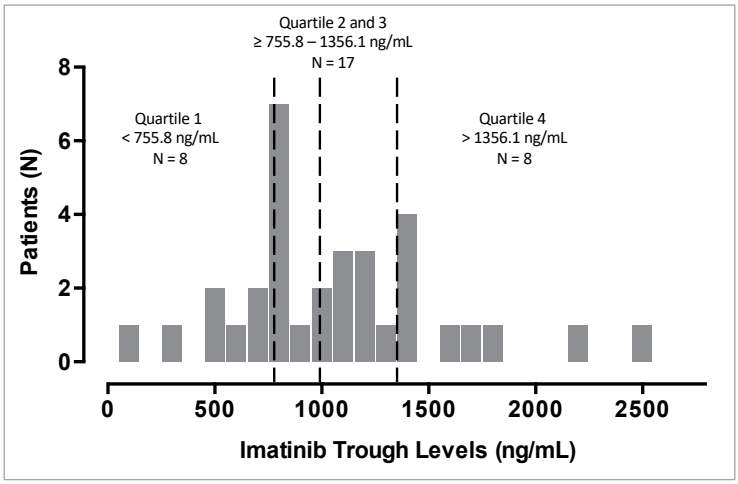

Figure 25. Distribution of average imatinib trough levels (ng/mL) at 400 mg/die at the steady state in 127 plasma samples from 33 GIST patients. X-axis represents the average imatinib trough level and y-axis indicates the number of patients. The black dashed lines indicate the first, the second (median) and the third quartile of imatinib trough levels in the study population.

4.7.6 Impact of Pharmacokinetic Variability on the Disease Progression

The impact of imatinib plasma exposure on treatment efficacy have been investigated to assess the probability of having PD in patients with imatinib trough levels below or above the recommended threshold level of 1100 ng/mL while on 400 mg/die. To this end, the 33 GIST patients were divided in two groups: group A, including the 13 patients with average imatinib trough levels above 1100 ng/mL, and group B, comprising the 20 patients with average imatinib trough levels below 1100 ng/mL. In group A, a clinical diagnosis of PD during follow-up was reported in four patients (#22, #31, #32, #34). #22 is a female patient who was receiving imatinib 400 mg/die from April 2016, for the management of metastatic disease affecting liver, peritoneum and bones. In October 2018 a radiological progression of liver metastases was observed and the imatinib daily dose was increased at 800 mg. No clinical benefit was gained from the dose's doubling, as in January 2019 the NMR underlined a further PD and the patient was switched to sunitinib. Afterwards, the follow-up was discontinued. Four plasma samples were collected while on imatinib surveillance, with individual imatinib trough levels of 2473.1 ng/mL (sample 1), 945.7 ng/mL (sample 2), 849.9 ng/mL (sample 3) and 1155.6 ng/mL (sample 4), corresponding to an average (± sd) concentration of 1356.1 (± 755.4) ng/mL (Figure 26-A). #31 was a female patient who was receiving imatinib 400 mg/die from May 2018 for the treatment of liver metastatic disease. In December 2018 the clinical diagnosis of hepatic PD led to the doubling imatinib daily dose (800 mg/die), which was soon reduced at 600 mg/die due to severe grade 3 cutaneous toxicity

and diffuse lymphoedema. In April 2019, in light of the further PD and the weak tolerance to imatinib higher dose, the treatment with sunitinib was started but it was soon interrupted due to scarce performance status and liver impairment. The patient died for PD in June 2019. For patient #31, two serial plasma samples were collected while on imatinib 400 mg/die, with individual plasma trough levels of 1397.6 ng/mL (sample 1) and 1335.3 ng/mL (sample 2), and an average of 1366.5 ng/mL. Only one sample was obtained on 800 mg/die, corresponding to a plasma trough concentration of 2756.0 ng/mL (Figure 26-B). #32 is a female patient treated with imatinib 400 mg/die from April 2018 for the metastatic liver disease. In August 2019 hepatic PD was diagnosed and in October 2019 the patient underwent debulking surgery for liver metastases removal. Afterwards, the first line treatment with imatinib 400 mg/die was re-started from January 2020. For patient #32, six serial plasma samples collected while on imatinib before and concomitantly to the diagnosis of PD were collected, with nominal values of trough plasma concentrations of 1443.3 ng/mL (sample 1), 1559.1 ng/mL (sample 2), 1480.8 ng/mL (sample 3), 1200.8 ng/mL (sample 4), 1393.7 ng/mL (sample 5) and 1147.8 ng/mL (sample 6). The average plasma trough level (± sd) was 1370.9 (± 162.5) ng/mL (Figure 26-C). #34 is a female patient in treatment with imatinib from August 2018 for the metastatic spread disease affecting liver, peritoneum and abdominal lymph nodes. After showing a remarkable clinical benefit from imatinib therapy at the beginning of treatment, with clinical reduction of tumor's metabolic activity, the patient experienced a dramatic PD with abdominal rupture of the major abdominal lesion that required urgent surgery in March 2019. The molecular analysis was carried out by means of NGS panels QIaSeq Actionable and QIaSeq Custom Panel DNA kits on two tumor entities obtained from surgery, comprising a fresh tissue slice from the major abdominal mass and a fresh tissue slice from a lymph node. The analysis revealed the absence of clinically relevant mutations affecting *KIT*, *PDGFRA* and *BRAF* genes, thus partially explaining the lack of sensitivity to imatinib. Given the absence of imatinib sensitizer mutations in tumor tissue, the second line sunitinib treatment was started from April 2019, showing good tolerance and disease control. The patient was lost at follow-up a few months later as she moved to another place. For patient #34, three serial plasma samples were collected while on imatinib 400 mg/die, which showed imatinib trough levels of 1204.7 ng/mL (sample 1), 1439.0 ng/mL (sample 2) and 973.0 ng/mL (sample 3), and an average (± sd) concentration of 1205.6 (± 233.0) ng/mL (Figure 26-D).

In group B, the clinical diagnosis of PD during follow-up was reported in four patients (#4, #10, #16, #20). #4 is a male patient in treatment with imatinib 400 mg/die from June 2011 for metastatic liver disease. In February 2017 he developed PD of hepatic lesions and imatinib daily dose was increased to 800 mg, but soon reduced at 600 mg due to gastrointestinal toxicity. PET/CT revealed further PD in April 2017 and in January 2018. Afterwards, the patient was lost at follow-up. The two plasma samples collected while on imatinib 400 mg/die exhibited a trough imatinib concentration of 1005.3 ng/mL (sample 1) and of 849.2 ng/mL (sample 2), with an average of 927.3 ng/mL (Figure 26-E). #10 is a male patient in treatment with imatinib 400 mg/die from September 2013 for the management of not operable

metastatic disease, with primary tumor site in the abdomen and metastatic involvement of liver. After showing stable disease (SD) for almost six years, he developed liver progression in March 2019, for which he was treated with imatinib 800 mg/die. After the imatinib dose was increased, diagnostic imaging showed disease's stabilization and partial tumor regression till the date of last follow-up (February 2020). Six plasma samples were collected from patient #10 in course of imatinib 400 mg/die. The imatinib trough levels were extremely low and showed nominal values of 146.3 ng/mL (sample 1), 124.9 ng/mL (sample 2), 264.1 ng/mL (sample 3), 326.8 ng/mL (sample 4), 289.5 ng/mL (sample 5) and 383.2 ng/mL (sample 6), with an average (± sd) trough concentration of 255.8 (± 101.6) ng/mL (Figure 26-F). #16 is a female patient whose clinical history has been described in the section *Results 4.6.1*. For patient #16, two serial plasma samples were available while on 400 mg/die, yielding an imatinib trough concentration of 1266.8 ng/mL (sample 1) and 843.1 ng/mL (sample 2), with an average of 1055 ng/mL, while the sample taken during imatinib 800 mg/die showed that the drug's trough concentration was 3053.2 ng/mL (Figure 26-G). #20 is a male patient in treatment with imatinib 400 mg/die from September 2014 for the management of metastatic spread disease involving gastric region and abdomen, exhibiting a clinical response to treatment. In November 2019 the NMR revealed the presence of multiple relapsed regions affecting liver, pancreas and abdomen and the imatinib dose was increased to 800 mg/die with disease's stabilization till the date of last follow-up in April 2020. For patient #20, four serial plasma samples were taken while on imatinib 400 mg/die and individual imatinib trough levels were 350.7 ng/mL (sample 1), 3.5 ng/mL (sample 2), "below detection limit" (sample 3) and 2.0 ng/mL (sample 4) (Figure 26-H).

Notably, in the group of patients with higher imatinib trough levels (group A), the clinical diagnosis of PD was reported in 4 out 13 (30.7%). Conversely, in the group B, 4 out 20 (20.0%) patients developed PD. Although the onset of PD did not show a remarkable prevalence in one of the two groups, it might be observed that the mechanism by which the PD was promoted could be ascribable for some extent to an extremely deficient imatinib bioavailability at the steady state. Indeed, if the development of PD cannot be ruled out from a proficient imatinib exposure, at the same time the patients' exposure to sub therapeutic imatinib levels represents a risk factor for a poor treatment outcome.

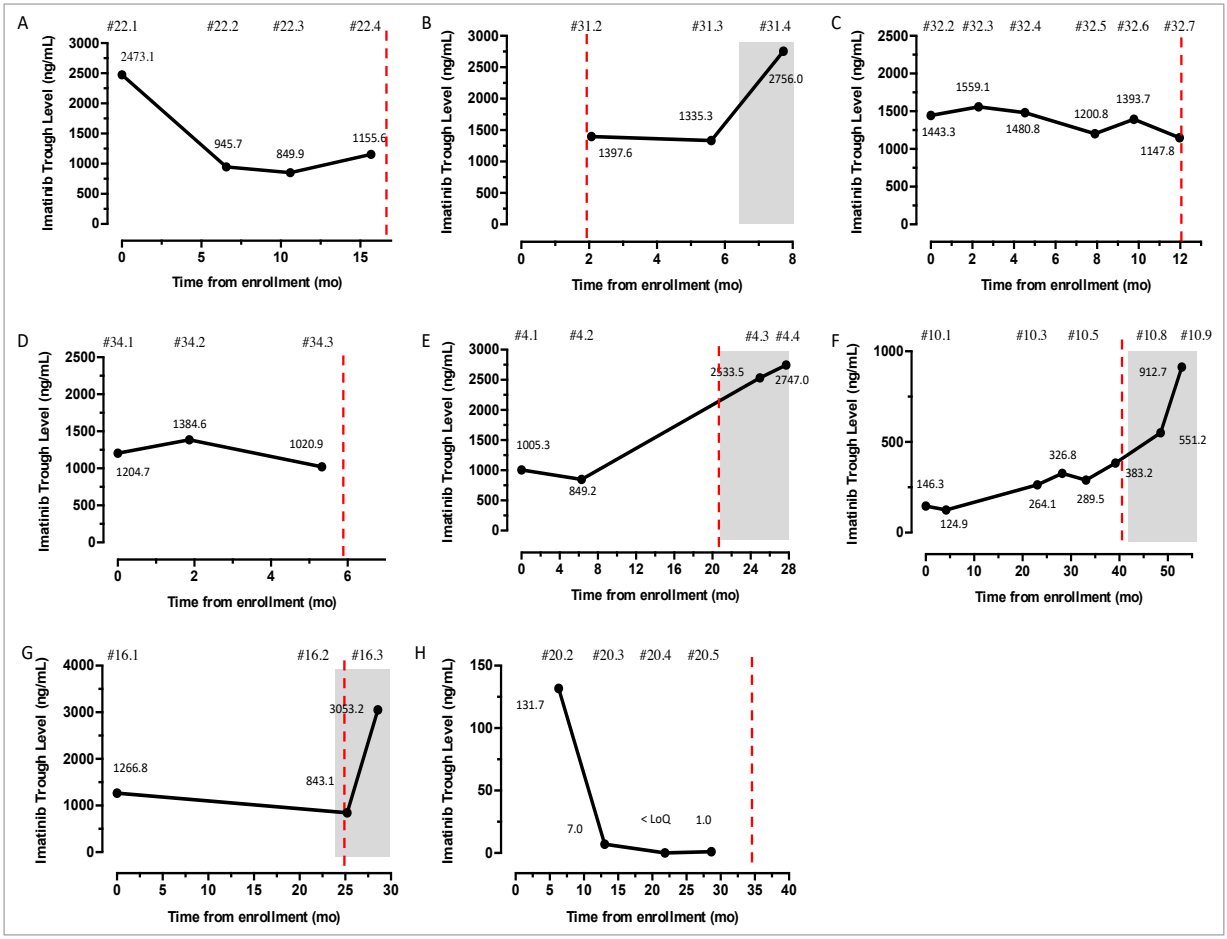

Figure 26. Trend of imatinib through levels (ng/mL) in the 8 patients who reported PD in course of follow up. The black line represents the single imatinib measures while the dashed red line indicates the clinical diagnosis of PD. The gray background represents the treatment with imatinib 800 mg/die, while the white background refers to the treatment with imatinib standard dose (400 mg/die).

4.7.7 Impact of the Metabolic Phenotype of CYPs on Imatinib Pharmacokinetics

4.7.7.1 The Pharmacogenetics Activity Score (PGx-AS) approach

First, the impact of the metabolic phenotype of CYPs was investigated as a possible decisive factor in determining the pharmacokinetic of imatinib and, thus, the drug's plasma exposure. Ideally, patients presenting a slow metabolic phenotype of CYPs were supposed to have a reduced imatinib clearance that results in higher drug's plasma concentration when compared to patients with a proficient metabolic activity. In the first place, the impact of the global phenotype of CYPs was considered to test whether the overall activity of CYPs involved in imatinib metabolism could explain for some extent the interindividual variability in imatinib trough concentrations. To this end, the PGx-AS of CYPs was calculated as described in the section *Materials and Methods 3.13*. Briefly, the metabolic phenotype of every single CYP, quantified by means of the gene activity score system, was summed up to generate a comprehensive activity score of CYPs that was aimed at recapitulating the grade of proficiency of the imatinib catabolism for each patient and that was called PGx-AS. The PGx-AS of CYPs ranged between the 11 of the patients with a reduced metabolic function, and the 16 of patients with a higher metabolic

activity. Owing to the small sample size, which hampered the possibility of multiple stratifications, to statistical purposes the patients were divided into two groups according to their PGx- AS. Therefore, patients presenting a PGx-AS of 11 to 13 were classified as intermediate metabolizers (IM), while those with PGx-AS of 14 to 16 were classified as extensive metabolizers (EM). Imatinib trough levels in the two groups are reported in Table 23.

Table 23. Imatinib trough levels (median and interquartile range) in the 33 GIST patients according to their PGx-AS. The PGx-AS was translated into a metabolic phenotype (IM and EM) that summarizes the overall patients' proficiency in imatinib catabolism.

PGx-AS	Metabolic Phenotype	Patients (n)	Imatinib Trough Level, median (ng/mL)	Interquartile range (ng/mL)
11 – 13	IM	9	1292.0	946.9 – 1972.0
14 – 16	EM	24	886.0	750.7 – 1220.0

Notably, the IM group presented a median imatinib trough level that was significantly higher than that reported in the EM group (IM, 1292.0 ng/mL; EM, 886.0 ng/mL; $p < 0.05$) (Figure 27), suggesting that the genetic makeup of cytochromes actually contributes in determining the average plasma exposure to imatinib at the steady state.

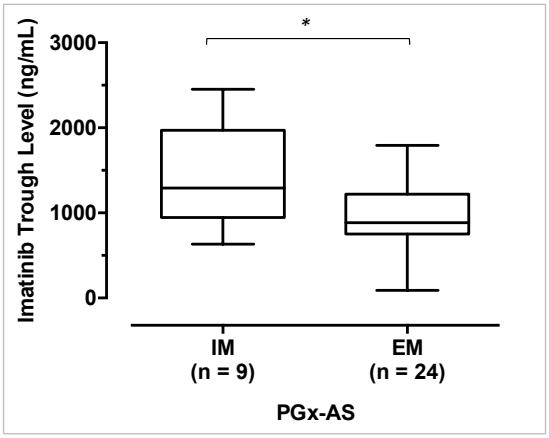

Figure 27. Imatinib trough levels (ng/mL) in intermediate metabolizers (IM, n = 9) and in extensive metabolizers (EM, n = 24) predicted according to the PGx-AS model for CYPs. The average trough concentration of imatinib during follow-up was considered for the 33 GIST patients. Boxes represent the data distribution within the first and the second quartile, while the whiskers represent the highest and the lowest values. The non-parametric Mann-Whitney test was used to compare the two groups.

4.7.7.2 The Single Gene Approach

Despite the observation that the CYPs' genotype plays actually a substantial role in defining different pharmacokinetic phenotypes in patients who receive imatinib, the extent to which every single CYP takes part to the imatinib's catabolism is not equally shared between CYPs. Therefore, to ponder the individual contribution of every CYP in imatinib pharmacokinetic, the impact of the metabolic phenotype in imatinib trough levels was independently analyzed for each CYPs to identify the most

relevant determiners of the interindividual pharmacokinetics' variability. To this end, a multilevel regression model was exploited to precisely infer the impact of each CYP on exposure (Table 24).

Table 24. Association between gene activity score (AS) of CYPs and Imatinib trough level in 33 patients undergoing treatment with imatinib 400 mg/die. Associations are estimated on 127 plasma samples from 33 patients using multilevel regression model. The β value indicates the slope of the linear regression curve and quantifies the increase ($\beta > 0$) or the decrease ($\beta < 0$) of imatinib trough levels for each unit of gene AS gained.

Gene	β	p
CYP3A4	85.4	0.8096
CYP3A5	-103.8	0.7542
CYP2D6	**-331.2**	**0.0128**
CYP2C9	88.7	0.5516
CYP2C19	-134.1	0.4063
CYP2B6	-210.3	0.1815
CYP1A2	56.1	0.6522
CYP2C8	-220.2	0.2925

Remarkably, an inverse association between the CYP2D6 metabolic phenotype and the plasma exposure to imatinib has emerged, suggesting that patients expressing a reduced CYP2D6 metabolic activity are more likely to present higher imatinib plasma concentrations, with respect to patients with proficiency CYP2D6 activity. Specifically, the calculated β score suggested that each point of CYP2D6 activity score gained resulted in a decrease of imatinib level of 331.2 ng/mL. Among the 33 analyzed patients, 3 (9.1%) presented a CYP2D6 activity score of 0.0 (PM), thus having an almost completely ineffective enzymatic activity, 14 (42.4%) had a CYP2D6 activity score of 1.0 (IM), as a consequence of only one functional allele, and the remaining 16 had an activity score of 2.0, being therefore extensive metabolizers for the CYP2D6 substrates. Consistently with the regression model, patients who showed a CYP2D6 reduced activity (AS = 0 – 1) presented a median imatinib Ctrough of 1292 ng/mL (IQR range: 991.5 – 1568.0 ng/mL) with respect to those with CYP2D6 proficiency activity (AS = 2) who had a median Ctrough of 771.9 (IQR range: 682.3 – 998.4 ng/mL) ($p < 0.005$) (Figure 28-A). No other significant associations between imatinib Ctrough and the other CYPs were underscored. However, the concomitant presence of CYP2D6 and CYP2B6 loss of function alleles seemed to identify a subgroup of patients bearing an extremely high imatinib Ctrough. In fact, the 9 out 33 (27.3%) patients with concomitant CYP2D6 and CYP2B6 reduced activity (AS = 0 – 1) showed a higher imatinib Ctrough (median: 1359.0 ng/mL) when compared with those with CYP2D6 reduced activity (AS = 0 – 1) and concurrent CYP2B6 proficiency (AS = 2) (median: 1023 ng/mL) (Figure 28-B). Although this difference was not statistically significant, the selection of concomitantly poor metabolizers for CYP2D6 and CYP2B6 allowed the identification of the three patients presenting the highest imatinib trough levels (#15, #27 and #29). Moreover, among the 5 patients with the highest imatinib trough levels, *i.e.* those showing a mean concentration during follow-up greater than 1568.0 ng/mL, all of them

(100%) displayed a low activity of CYP2D6 and 4 (80.0%) had concurrent low activity of CYP2D6 and CYP2B6.

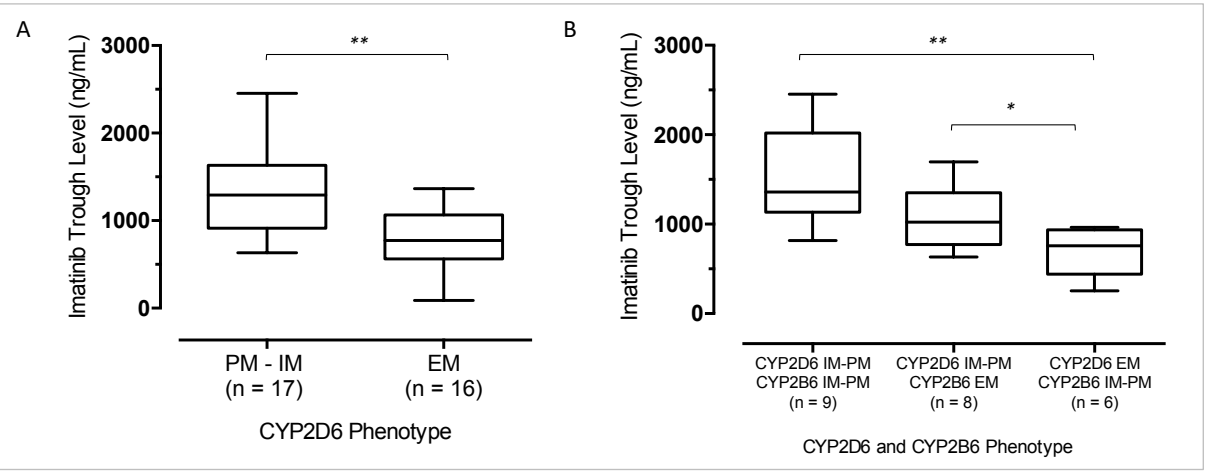

Figure 28. A) Imatinib trough levels (ng/mL) in GIST patients with proficient CYP2D6 metabolic activity (n = 16) and in patients with reduced to null CYP2D6 metabolic activity (n =17). The gene activity score was used to quantify the impact of genetic variants on CYP2D6 metabolic phenotype. The Mann-Whitney non-parametric test was used to compare the two groups. B) Imatinib trough levels (ng/mL) in GIST patients with concurrent decreased function of CYP2D6 and CYP2B6 (n = 9), as well as in patients with reduced activity of only CYP2D6 (n = 8) and with reduced activity of only CYP2B6 (n = 6). The average trough concentration of imatinib during follow-up was considered. Boxes represent the data distribution within the first and the second quartile, while the whiskers represent the highest and the lowest values. The non-parametric Kruskal-Wallis test with Dunn's correction for multiple comparison was used to compare the three groups.

4.7.8 Impact of the Metabolic Phenotype of Transporters on Imatinib Pharmacokinetics

Next, the metabolic phenotype of the imatinib transporters ABCB1 and ABCG2 was considered as a possible determiner of drug's exposure. The application of a PGx-AS for imatinib transporters failed to underscore a correlation between the predicted metabolic phenotype of ABCB1 and ABCG2 and imatinib trough level (data not shown). Consistently, also the single-gene approach aimed at evaluating the association of every single transporter with the imatinib trough level by means of a multilinear regression model, did not highlight a correlation between the transporters' predicted phenotype and the imatinib C trough (Table 25).

Next, since the sequencing of transporters reported many genetic variants in addition to those considered for the metabolic phenotype assessment, the impact of single SNPs affecting the drug transporters *ABCB1* and *ABCG2* on imatinib trough levels was analyzed.

Table 25. Association between gene activity score (AS) of transporters and Imatinib trough level in 33 patients undergoing treatment with 400 mg/die. Associations are estimated on 127 plasma samples from 33 patients using multilevel regression model. The β value indicates the slope of the linear regression curve and quantifies the increase ($\beta > 0$) or the decrease ($\beta < 0$) of imatinib trough levels for each unit of gene AS gained.

Gene	β	p
ABCB1	99.6	0.5860
ABCG2	-207.1	0.5236

The results of the associations are reported in Table 26. Notably, a SNP located in the 3'UTR of the *ABCB1* gene (c.*89T>A, rs17064) was found significantly associated with a decreased imatinib trough level in the study population. The variant rs17064 was identified in heterozygosity in 4 out 33 patients (12.1%), showing a MAF of 6.1% in the study population (European MAF, 8.5%). Patients bearing the identified *ABCB1* variant presented an average imatinib plasma trough level of 580.7 ng/mL, with individual values of 89.1 ng/mL (#20), 502.9 ng/mL (#24), 634.2 ng/mL (#11) and 1096.6 ng/mL (#26). The functional impact of rs17064 has not been elucidate yet, albeit previous reports has underscored an association between rs17064 and the plasma exposure to vitamin D3 in 39 healthy subjects.[183] In our study cohort, the presence of rs17064 was detected in 3 out the 5 patients who showed the lowest imatinib plasma levels, thus allowing the identification of a high-risk category for treatment inefficacy.

Table 26. List of the SNPs in *ABCB1* and in *ABCG2* whose association with imatinib trough levels was tested in the 33 GIST patients. The position along the coding sequence (CDS) of identified variants in *ABCB1* and *ABCG2* was reported, as well as the SNPs' ID and the minor allele frequency (MAF) in the European population. Student t-test was used to assess the association between identified variants and the imatinib trough levels.

Gene	CDS Position	SNP ID	European MAF (%) GenomeAD	p-value
ABCB1	c.1236C>T	rs1128503	54.5	0.2778
ABCB1	c.3435C>T	rs1045642	51.1	0.9264
ABCB1	c.2677G>T	rs2032582	54.9	0.2778
ABCB1	c.61A>G	rs9282564	7.5	0.1613
ABCB1	c.1199G>A	rs2229109	2.7	0.6313
ABCB1	c.287-25G>T	rs2235015	18.2	0.3146
ABCB1	c.-1T>A	rs2214102	94.5	0.5463
ABCB1	c.-129T>C	rs3213619	5.3	0.5434
ABCB1	c.*193T>C	rs3842	15.4	0.1346
ABCB1	**c.*89T>A**	**rs17064**	**8.5**	**0.0406**
ABCG2	c.421C>A	rs2231142	12.1	0.3385
ABCG2	c.34G>A	rs2231137	11.0	0.7126
ABCG2	c.77A>G	rs373683219	0.003	0.5657
ABCG2	c.263+10A>G	rs2231138	7.5	0.6760
ABCG2	c.*530T>G	rs778502653	0.04	0.5348
ABCG2	c.-476T>C	rs2231135	5.1	0.1338
ABCG2	c.-29A>G	rs45630471	0.2	---
ABCG2	c.-273A>G	---	---	0.6106

4.7.9 Concurrent Impact of DDI and Genotype on Imatinib Pharmacokinetics

Next, the impact of imatinib-drugs interactions was investigated in the study population of 33 GIST patients as a possible element to refine the prediction of patients' metabolic phenotype based on genetics. To this end, the impact of concurrently administered drugs in course of imatinib on the function of single CYPs and transporters was calculated as described in the section *Materials and Methods 3.15*. According to the coadministration of enzymes' inducers or inhibitors, the activity score of CYPs and transporters was refined to take into account at the same time the contribution of genetics and of DDIs. In Figure 29 is reported a graphical representation of the electronic worksheet used to calculate the DDIs-corrected activity score for each gene. The two red boxes are aimed at drawing the attention to two specific cases in which the gene activity score was modulated by DDIs that had an impact on that specific enzyme. Patient #8 was a full metabolizer for *CYP3A5* (gene AS = 2.0). At the time of second blood sampling (#8.2) he was taking an inhibitor of CYP3A5, the antimicrobial drug ciprofloxacin, whose correction factor was scored 0.5 and that yielded a *CYP3A5* corrected AS of 1.0. At the time of the third blood sampling (#8.3), no DDIs affecting CYP3A5 activity were recorded and the correction factor was scored 1.0, yielding a neutral effect on the *CYP3A5* corrected AS (= 2.0). Patient #10 was a full metabolizer for CYP3A4 (AS = 2.0), but at the time of the third blood sampling (#10.3) he was concomitantly treated with a strong CYP3A4 inducer, the antiepileptic drug carbamazepine, which contributed a correction factor of 2.0 and increased the AS of *CYP3A4* to 4.0. At the time of fourth sampling (#10.4) the patient was taking, together with the carbamazepine, also a weak CYP3A4 inhibitor, *i.e.* pantoprazole, whose effect modified the correction factor to 1.5, thus making the corrected *CYP3A4* AS equal to 3.0.

	A	B	C	D	E	F	G	H	I	J	K	L	M	N	O	P
1	Patient_ID	Gender	Age at diagnosis	Age at sampling date	Sample_ID	Sampling Date	Number of Concomitant Drugs	CYP3A4 Gene Activity Score	CYP3A4 Correction Factor	Corrected CYP3A4 Gene Activity Score	CYP3A5 Gene Activity Score	CYP3A5 Correction Factor	Corrected CYP3A5 Gene Activity Score	CYP2D6 Gene Activity Score	CYP2D6 Correction Factor	Corrected CYP2D6 Gene Activity Score
2	IM_8	M	61	67	IM_8.2	16/09/2015	1	2.00	0.50	1.00	2.00	0.50	1.00	2.00	1.00	2.00
3	IM_8	M	61	69	IM_8.3	12/09/2017	2	2.00	0.50	1.00	2.00	1.00	2.00	2.00	0.50	1.00
4	IM_8	M	61	70	IM_8.4	29/03/2018	2	2.00	0.50	1.00	2.00	1.00	2.00	2.00	0.50	1.00
5	IM_8	M	61	70	IM_8.5	14/09/2018	2	2.00	0.50	1.00	2.00	1.00	2.00	2.00	0.50	1.00
6	IM_8	M	61	71	IM_8.6	20/03/2019	2	2.00	0.50	1.00	2.00	1.00	2.00	2.00	0.50	1.00
7	IM_8	M	61	71	IM_8.7	27/09/2019	2	2.00	0.50	1.00	2.00	1.00	2.00	2.00	0.50	1.00
8	IM_9	F	72	73	IM_9.1	12/05/2015	1	2.00	1.00	2.00	2.00	1.00	2.00	2.00	1.00	2.00
9	IM_10	M	58	59	IM_10.1	20/05/2015	2	2.00	2.00	4.00	2.00	1.50	3.00	2.00	1.00	2.00
10	IM_10	M	58	60	IM_10.2	23/09/2015	2	2.00	2.00	4.00	2.00	1.50	3.00	2.00	1.00	2.00
11	IM_10	M	58	61	IM_10.3	11/04/2017	2	2.00	2.00	4.00	2.00	1.50	3.00	2.00	1.00	2.00
12	IM_10	M	58	62	IM_10.4	12/09/2017	5	2.00	1.50	3.00	2.00	1.50	3.00	2.00	1.00	2.00
13	IM_10	M	58	62	IM_10.5	06/02/2018	3	2.00	1.50	3.00	2.00	1.50	3.00	2.00	1.00	2.00
14	IM_10	M	58	63	IM_10.6	08/08/2018	3	2.00	1.50	3.00	2.00	1.50	3.00	2.00	1.00	2.00
15	IM_10	M	58	63	IM_10.7	15/05/2019	6	2.00	1.00	2.00	2.00	0.50	1.00	2.00	0.50	1.00
16	IM_10	M	58	64	IM_10.8	23/09/2019	6	2.00	1.00	2.00	2.00	0.50	1.00	2.00	0.50	1.00
17	IM_10	M	58	64	IM_10.9	24/02/2020	7	2.00	1.00	2.00	2.00	0.50	1.00	2.00	0.50	1.00
18	IM_11	M	68	68	IM_11.1	25/05/2015	4	2.00	1.00	2.00	2.00	1.00	2.00	1.00	1.00	1.00
19	IM_12	M	62	75	IM_12.3	24/11/2017	1	2.00	1.00	2.00	2.00	1.00	2.00	1.00	1.00	1.00
20	IM_12	M	62	76	IM_12.4	24/05/2018	1	2.00	1.00	2.00	2.00	1.00	2.00	1.00	1.00	1.00
21	IM_13	F	32	35	IM_13.1	25/06/2015	0	2.00	1.00	2.00	2.00	1.00	2.00	2.00	1.00	2.00
22	IM_13	F	32	35	IM_13.2	19/11/2015	0	2.00	1.00	2.00	2.00	1.00	2.00	2.00	1.00	2.00
23	IM_13	F	32	39	IM_13.3	09/12/2019	0	2.00	1.00	2.00	2.00	1.00	2.00	2.00	1.00	2.00
24	IM_14	F	71	76	IM_14.1	13/07/2015	2	2.00	1.00	2.00	2.00	1.00	2.00	2.00	1.00	2.00
25	IM_14	F	71	77	IM_14.2	08/05/2017	2	2.00	1.00	2.00	2.00	1.00	2.00	2.00	1.00	2.00
26	IM_14	F	71	78	IM_14.3	06/11/2017	2	2.00	1.00	2.00	2.00	1.00	2.00	2.00	1.00	2.00
27	IM_14	F	71	78	IM_14.4	07/05/2018	2	2.00	1.00	2.00	2.00	1.00	2.00	2.00	1.00	2.00
28	IM_14	F	71	79	IM_14.5	12/11/2018	2	2.00	1.00	2.00	2.00	1.00	2.00	2.00	1.00	2.00
29	IM_14	F	71	79	IM_14.6	13/05/2019	5	2.00	0.50	1.00	2.00	0.50	1.00	2.00	1.00	2.00
30	IM_14	F	71	80	IM_14.7	11/11/2019	5	2.00	0.50	1.00	2.00	0.50	1.00	2.00	1.00	2.00

Figure 29. Exemplary corrected gene activity score calculation model. For the 33 patients, the impact of DDI on every CYPs (*i.e.* correction factor) was used to refine the genotype guided gene activity score by using a multiplicative model. Red boxes indicate that the corrected gene activity score may vary within the same patient as a consequence of the administration of different interacting or non-interacting drugs during follow-up.

For each patient, the PGx-AS corrected per DDIs was calculated at each time point. The transporters were not considered for the DDI analysis due to the paucity of drugs' transporters inhibitors and inducers recorded in the study population. To statistical purposes, the PGx-AS corrected per DDIs was analyzed as a continuous variable, as it ranged from a minimum of 7.5 to a maximum of 21.5. Moreover, all 127 plasma samples were considered as independent variables since the administration of interacting drugs was varying within individual patients during imatinib treatment. An inverse linear correlation between the PGx-AS and the imatinib trough levels ($p = 0.0002$; Spearman $r = -0.35$) highlighted that patients with a lower metabolic activity driven by both the genotype and the DDIs were more likely to have high imatinib trough concentrations than patients with a higher metabolic activity (Figure 30-A). Then, patients were stratified within three groups according to their PGx-AS corrected to identify a possible association between the metabolic phenotype and the exposure to imatinib. Stratification criteria and imatinib trough levels in the three groups are reported in Table 27. Notably, intermediate metabolizers showed significantly higher imatinib trough levels (median, 1296.0 ng/mL; IQR range, 846.6 – 1630.0 ng/mL) when compared with extensive metabolizers (median, 943.4 ng/mL; IQR range, 666.6 – 1205.0 ng/mL; $p < 0.05$) and with ultrarapid metabolizers (median, 559.8 ng/mL; IQR range, 276.8 – 913.8 ng/mL; $p < 0.0001$) as indicated in Figure 30-B.

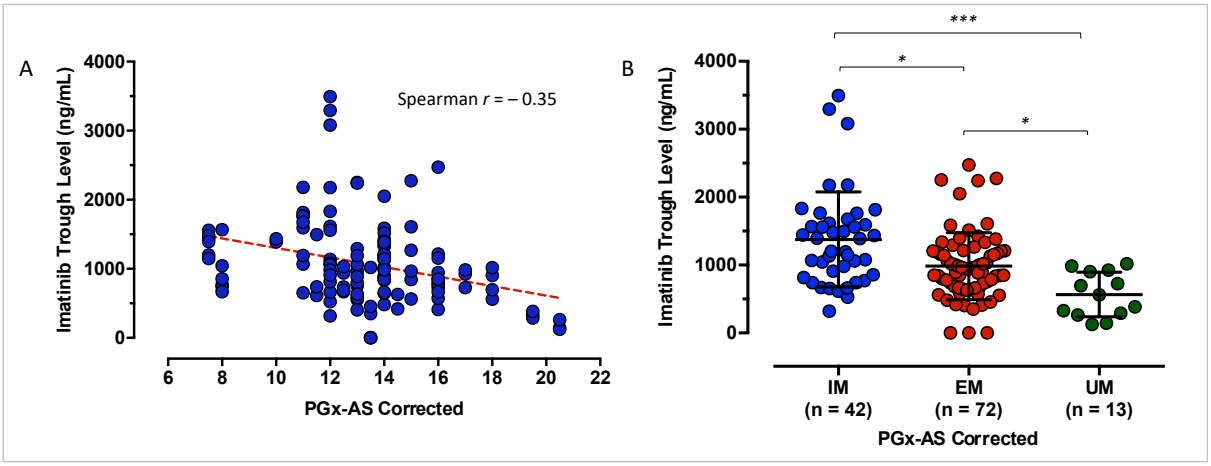

Figure 30. A) Distribution of imatinib trough levels (ng/mL) in accordance to the PGx-AS corrected for DDIs in 127 plasma samples from 33 GIST patients. In x-axis the PGx-AS corrected is reported. In y-axis, imatinib plasma trough levels (ng/mL) are reported. Dashed red line indicates the regression line curve and dots indicates the individual imatinib trough quantifications. B) Distribution of imatinib trough levels (ng/mL) in accordance to the metabolic phenotype of CYPs corrected for DDIs. 42 plasma samples were attributed to IM patients, 72 to EM patients and 13 to UM metabolizer patients. Dots represent the individual imatinib trough levels and the horizontal bars indicate the median and the interquartile rage. The non-parametric Kruskal-Wallis test with Dunn's correction for multiple comparison was used to compare the three groups.

Table 27. Imatinib trough levels and interquartile range in the 127 plasma samples from the 33 GIST patients according to their PGx-AS corrected for DDIs. The PGx-AS was ranked and translated into the metabolic phenotype (IM, EM and UM) that summarizes the overall patients' proficiency in imatinib catabolism.

PGx-AS Corrected	Metabolic Phenotype	Samples (n)	Imatinib Trough Level, median (ng/mL)	Interquartile range (ng/mL)
7.5 – 12.0	IM	42	1296.0	846.6 – 1630.0
12.5 – 16.0	EM	72	943.4	666.6 – 1205.0
17.0 – 21.5	UM	13	559.8	276.8 – 913.8

Next, the association between the DDIs-corrected gene AS of every CYP and the imatinib trough levels was investigated to better clarify the impact that DDIs might have in modulating the metabolic phenotype of CYPs and, thus, in describing the pharmacokinetic variability of imatinib. As previously described for CYPs and transporters, a multilinear regression model to the DDIs-corrected CYPs AS was used to infer a possible association between the two variables. However, the model failed to refine the previously described association between the activity of CYPs and the imatinib exposure, partially due to the narrow variability of different DDIs affecting the activity of CYPs (Table 28).

Table 28. Association between corrected gene activity score (AS) of CYPs and Imatinib trough level in 33 patients undergoing treatment with 400 mg/die. Associations are estimated on 127 plasma samples from 33 patients using multilevel regression model. The β value indicates the slope of the linear regression curve and quantifies the increase ($\beta > 0$) or the decrease ($\beta < 0$) of imatinib trough levels for each unit of gene AS gained.

Gene	β	p
CYP3A4	-205.7	0.3626
CYP3A5	-214.8	0.3626
CYP2D6	-327.2	0.0091
CYP2C9	93.8	0.5007
CYP2C19	-72.6	0.5877
CYP2B6	-229.4	0.1475
CYP1A2	-59.5	0.6060
CYP2C8	-102.3	0.5553

Only the CYP2D6 corrected genotype remained significantly associated with imatinib exposure, but the observed trend was exclusively driven by the genotype over the DDIs.

4.7.10 Impact of Carbamazepine on Imatinib Pharmacokinetics: the Role of CYP3A4

A clear example of DDI with a clinically relevant impact on imatinib exposure was observed in patient #10. Patient #10, whose clinical history was described in the section *Results 4.7.6,* presented extremely low imatinib trough levels throughout multiple sampling and was concurrently treated with imatinib and the antiepileptic drug carbamazepine. Carbamazepine is known to be a strong inducer of CYP3A4 and CYP2B6 enzymatic function. By a genetic point of view, the patient resulted wild type for all but two CYPs, the *CYP2B6* and *CYP1A2*, which presented a loss-of-function allele (AS = 1.0). The

induction of CYP2B6 from carbamazepine determines a *CYP2B6* metabolic phenotype that is equal to a CYP2B6 wild type carrier (AS = 2.0), in light of the contrasting effect between genotype and carbamazepine. Therefore, the dramatically low imatinib plasma trough levels could be mainly attributable to the induction of CYP3A4, which is the main enzyme involved in the metabolism of imatinib. In Figure 31 are reported the imatinib trough levels registered for patient #10 in course of imatinib and carbamazepine treatment. The patient developed PD after 40 months from enrollment as a suspected consequence of the very fast imatinib clearance triggered by carbamazepine activity on CYPs. Imatinib trough levels have risen after dose implementation to 800 mg/die with clinical benefit (SD). However, at the time of last follow-up the administration of carbamazepine had not been discontinued.

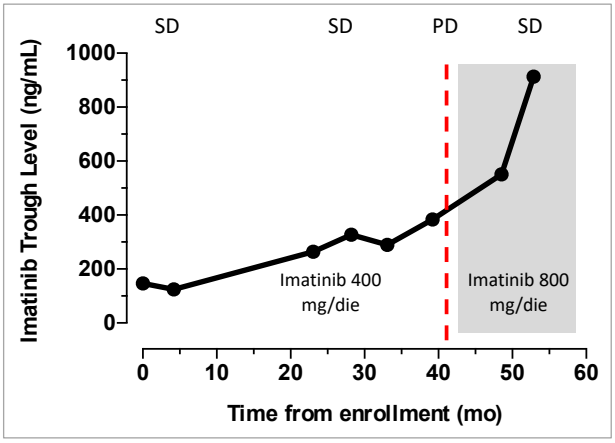

Figure 31. Changes of imatinib plasma trough levels of patient #10. In x-axis is reported the time from enrollment (months). In y-axis is reported the imatinib plasma trough level (ng/mL). Dashed vertical line indicates the diagnosis of PD. On the top of the plot the clinical disease status is indicated in accordance to RECIST criteria. White background indicates the administration of imatinib daily dose of 400 mg, grey background indicates imatinib daily dose of 800 mg.

In the summary of imatinib product characteristics, it is clearly reported that the concomitant use of imatinib and products that induce CYP3A4 (e.g. dexamethasone, phenytoin, carbamazepine, rifampicin, phenobarbital or *Hypericum perforatum*) may significantly reduce exposure to imatinib, potentially increasing the risk of therapeutic failure. Therefore, concomitant use of strong CYP3A4 inducers and imatinib should be avoided. In the study population here described, no other strong CYP3A4 inducers besides carbamazepine were recorded.

4.7.11 Impact of the Tobacco Smoke on Imatinib Pharmacokinetics: the Role of CYP1A2

A noteworthy association was found between the consumption of tobacco smoke and the imatinib exposure. Tobacco is classified as a strong inducer of CYP1A2, potentially hampering the pharmacokinetic of CYP1A2 substrates. The association between the tobacco smoke and imatinib exposure or efficacy has never been described so far, partially because CYP1A2 plays a minor role in imatinib catabolism. In Figure 32-A is reported the impact that CYP1A2 genotype had on imatinib

exposure. Notably, no difference has emerged between patients having a CYP1A2 proficient metabolic activity (EM) and those classified as IM (median EM, 1039.0 ng/mL; median IM, 957.0 ng/mL, p = n.s.), proving again that the genetic makeup of CYP1A2 is not a major determiner in imatinib pharmacokinetic. Conversely, when stratifying patients' according to the refined CYP1A2 phenotype in presence of regular tobacco consumption, a significant difference in imatinib exposure was observed between imatinib plasma levels in smokers and in non-smokers (Figure 32-B). The regular smoke habit was registered in 3 patients (#7, #24, #28) who contributed 17 serial plasma samples. As a reference control group, 15 patients with CYP1A2 proficiency activity who were not administered with concurrent CYP1A2 inducers or inhibitors were considered. Smoker patients presented lower imatinib trough levels when compared with the other group (smokers, median: 696.3 ng/mL, IQR range: 556.3 – 930.7 ng/mL; non-smokers, median: 984.5 ng/mL, IQR range: 742.4 – 1210.0 ng/mL; p = 0.0008), suggesting a likely involvement of the tobacco smoke in fasting the catabolism of imatinib throughout a *CYP1A2*-mediated mechanism.

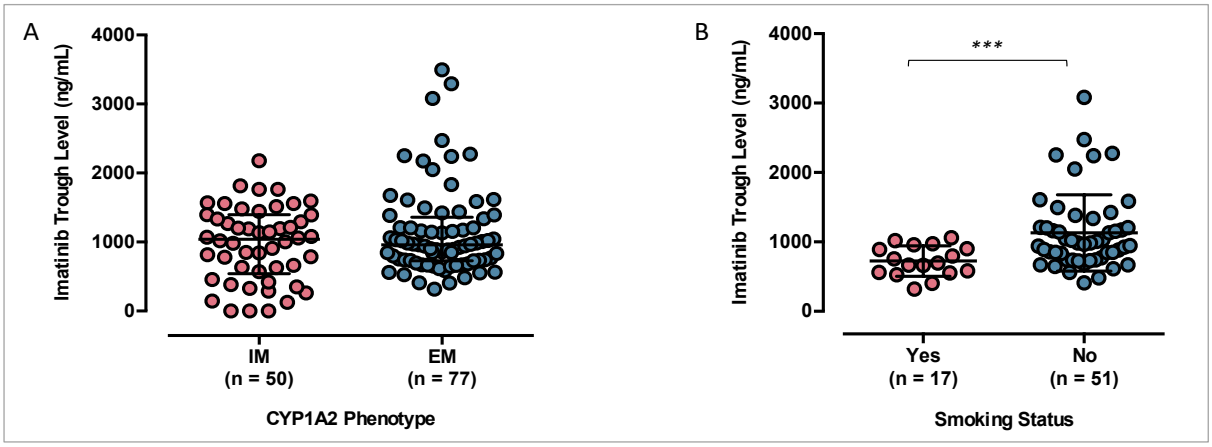

Figure 32. A) Impact of the metabolic phenotype of CYP1A2 predicted by the *CYP1A2* genotype on imatinib plasma trough levels. Individual imatinib plasma trough levels are displayed for 15 IM patients (n = 50 samples) as well as for 18 EM patients (n = 77 samples). B) Impact of the CYP1A2 corrected phenotype according to the concomitant tobacco habit on imatinib plasma trough levels. Individual imatinib plasma trough levels are displayed for 3 smokers (n = 17 samples) and for 15 non-smokers patients who were wild type for CYP1A2 and did not intake CYP1A2 inducers/inhibitors (n = 51 samples). Dots represent individual imatinib levels and the horizontal bars represent the median and the interquartile range. The Mann-Whitney non-parametric test was used to compare the two groups.

CHAPTER 5. DISCUSSION

The clinical application of highly sensitive and specific technologies able to describe and monitor the genetic landscape of tumors offers new opportunities for the early treatment intervention and therapy personalization. The possibility to apply customized therapeutic strategies based on the molecular characteristics of tumors and to stratify patients according to their genetic background represents a valuable and precious tool to implement the efficacy and safety profile of oncological treatments. For LARC patients, the use of multimodal therapeutic approaches based on clinical and pathological tumors' features has significantly improved the prognosis of patients.[49] However, the improvement of long-term survival outcomes is still limited to selected subgroup of patients and the occurrence of local and distant relapse remains the first cause of death for LARC patients. Therefore, the identification of early biomarkers to predict patients' prognosis is urgently needed. Pioneering studies provided initial evidences for the possibility of interrogating ctDNA as a liquid biopsy to predict the outcome of nCRT.[40] Despite the detection of ctDNA after surgery was clearly associated with poor clinical outcomes, its validity as an early molecular marker to refine the patients' stratification remains questionable. For GIST patients, inhibitors targeting KIT and PDGFRA receptors are approved and ensure excellent disease control and good tolerance. However, the secondary tumor resistance during the first line imatinib treatment occurs in a half of patients with active disease and represents the leading cause of disease progression within two years from treatment initiation.[74] Moreover, the interpatient variability in imatinib plasma exposure represents a major challenge for the implementation of personalized imatinib dosage and can significantly reduce the clinical prognosis of patients.[184] The aim of the present doctoral thesis is devoted to identifying early prognostic markers for LARC patients by means of ctDNA analysis and primary tumor characterization. Moreover, the possibility of exploiting the ctDNA detection as a low-invasive marker to identify imatinib-resistant subclones in GIST patients was investigated as a possible tool to optimize the clinical decision making for treatment selection. Then, the issue related to the pharmacokinetic variability of imatinib was analyzed to test whether the host genetic variability and specific environmental factors (i.e. co-administered drugs and tobacco smoke) might represent concurrent elements in driving the pharmacokinetics imatinib phenotype.

5.1 ctDNA Monitoring in LARC Patients to Predict nCRT Outcome and Prognosis

In LARC, the pathological complete response to nCRT is commonly observed in a minority of patients and has been associated with improved OS and RFS.[49,185] The necessity to predict the outcome of nCRT at the very beginning of nCRT treatment is of pivotal relevance to select and optimize the downstream therapeutic strategies. In fact, the early stratification of patients according to the risk categories would allow the implementation of multimodal treatment strategies that entail the delivery of intensified treatment schemes for the high-risk groups or the application of organ preserving approaches for the

low-risk groups. With the aim of identifying early markers that could refine the selection of good and poor responder patients, the clinical prognostic role of ctDNA has been investigated in a study cohort of 40 LARC patients receiving nCRT. As a complementary approach, a panel of genetics and protein markers was investigated in baseline LARC biopsies to identify possible candidate to implement the currently available risk-stratification algorithms.

We observed that the total plasma levels of cfDNA in newly diagnosed LARC patients allowed the effective discrimination of patients with confirmed diagnosis of rectal cancer from healthy subjects with a sensitivity of 81.25% and a specificity of 97.5% ($p < 0.0001$). Moreover, the presence of higher cfDNA levels in patients classified at high-risk with respect to the low-risk was observed, even though the association was lost after conditional analyses for multiple groups. In the context of LARC, a high cfDNA level at the time of patients' diagnosis was significantly associated with a shorter time to progression and with a worst DFS.[186] In our study cohort, the total cfDNA levels were not associated with prognostic outcomes, such as the response to nCRT or the survival, but provide first evidence upon a possible application to implement the currently available risk stratification algorithms. The evidence that cancer patients present significantly increased cfDNA plasma concentration than non-cancer subjects has been known for a long time and hold the promise to serve as a potential complementary diagnostic biomarker.[187] Although significantly related to the presence of disease, the clinical validity of total cfDNA quantification in plasma to diagnose cancer remains questionable for two main reasons. First, the total cfDNA levels do not represent a cancer specific biomarker, thus hampering its clinical application in oncology.[188] Then, the sensitivity of the total cfDNA quantification to accurately discriminate cancer from non-cancer patients is deeply affected by analytical and pre-analytical factors, from the blood collection to the techniques used for cfDNA measurement.[189] The difficulty in making reproducible the workflow cfDNA analysis at the inter- and intra-laboratory level dramatically demolishes the identification of universally recognized clinically actionable cut-off levels of total cfDNA both for diagnostic and for patients' stratification. Furthermore, the identification of a validated control group (*i.e.* healthy subjects, patients with non-malignant diseases) is always required to test the analytical specificity of total cfDNA quantification. Therefore, the detection of tumor-associated molecular markers in the cfDNA represents an extremely specific approach to interrogate the tumor's genome in a minimally invasive fashion. Moreover, it allows following the dynamics of the tumors in course of treatment. The greatest advantage of whole genome analysis over targeted approaches is the fact that no prior knowledge of tumor-specific alterations is required. Moreover, since somatic CNAs affect a greater fraction of the genome than SNVs, this method might better recapitulate the overall circulating tumor fraction than a limited number of target mutations. Furthermore, since CNAs are a relevant component of genetic alterations in almost all tumors and are deeply connected to the genomic instability, this un-targeted approach can be applied to almost all tumor entities. The application of sWGS to depict the presence of CNAs in cfDNA of LARC patients had never been investigated so far and remains mainly devoted to metastatic tumors entities. The CNA analysis of cfDNA samples

revealed alteration characteristic of colorectal cancer and rectal cancer.[47] Specifically, it was observed that chromosome 20 and 13 underwent gains most frequently and chromosome 18 and 8p underwent number losses. The specificity of the analysis found a further confirmation in the analysis of matched primary tumor DNA, suggesting that the cfDNA might actually represent a suitable candidate for the identification of somatic CNAs in a tumor-agnostic way. Notably, the copy number analysis of pre-nCRT cfDNA samples of LARC patients revealed a tight association with the disease stage at the time of diagnosis, highlighting the presence of CNAs only in patients with cT stage of 3 to 4, with concomitant lymph nodes involvement. Even though this association might be hampered by the limited number of patients without lymph node involvement in the study population, it is consistent with the evidence that tumors of higher stages are more prone to release detectable quantities of ctDNA.[190] Moreover, an increase of the detectable TFx in course of nCRT, with respect to the baseline cfDNA, was positively associated with a higher probability to have a pCR after nCRT, whereas the persistence of the TFx after nCRT was identified only in the non-responders (RR: 3.75; 95% CI 1.47 – 9.56; p = 0.0147). These results are consistent with previous evidences reporting that the presence of ctDNA after nCRT in LARC is an independent prognostic marker of incomplete pathological response,[36] and with the observation that an increased ctDNA release in course of treatment might indicate a massive DNA release from dying cancer cells, and that might represent a reliable marker of tumor sensitivity to chemotherapy.[191,192] However, whether or not the midterm ctDNA detection might serve as early estimator of pCR needs to be further sustained by focused analyses. In fact, the precise time point for cfDNA collection after treatment initiation for the early assessment of prognosis remains to be clarified and further studies entailing a closer cfDNA monitoring at the very beginning of the treatment are warranted to clarify the biological meaning of the ctDNA release from cancer cells. In the present study, the time point of cfDNA collection from nCRT initiation showed a median of 21 days, but it was not strictly uniform for all patients (range: 13 – 28 days), thus representing a limitation for the results' reproducibility. On the contrary, the identification of TFx in pre-nCRT cfDNA was not predictive of nCRT outcome, but it was positively associated with the risk to develop disease recurrence within two years from the diagnosis. Furthermore, a combined analysis of pre-nCRT TFx and pre-nCRT CEA serum levels revealed that the number of risk factors (only TFx, only CEA or both) has a cumulative effect on predicting the risk of local and distance recurrence and that patients presenting positive TFx or high CEA levels had higher risk to develop tumor relapse within two years from diagnosis (p = 0.0006). These findings add further evidence to that reported by Murahashi *et al.*, who showed how the presence of postoperative ctDNA and CEA in a cohort of 85 LARC patients were independent prognostic markers for risk of recurrence after surgery and showed a cumulative effect on the prediction of recurrence free survival.[193] The possibility to identify patients who are at higher risk to develop a poor outcome in term of RFS at the time of diagnosis is of much interest for the application of intensified therapeutic protocols or to schedule a closer monitoring during postoperative patients' follow-up. The results of a study involving 47 patients with LARC with 243 available plasma samples collected

pretreatment, in course of nCRT, after completing nCRT and after surgery suggest that recurrence-free survival is shorter in patients with detectable ctDNA after completion of chemoradiotherapy (HR 7.1, 95% CI 2.4 – 21.5; P < 0.001) and even shorter in patients exhibiting permanence of ctDNA pre-, during and after nCRT (HR 11.5, 95% CI 3.3 – 40.4; P < 0.001).[194] In line with this finding, we observed that patient #19939, who reported a positive TFx throughout the whole follow-up exhibited a very poor sensitivity to nCRT and experienced a fast disease progression to distant organs.

Several parameters have been reported as possible early predictors of pCR and recurrence status in patients with LARC, including CEA levels, the distance of the tumor from the anal verge, presence of ctDNA and biomarkers' level in tumor cells.[195–197] Some studies have identified an association between the concurrence of *KRAS/BRAF* and *TP53* mutations in primary tumors and the lower sensitivity no nCRT in LARC patients. The development of *KRAS*/*BRAF* mutations, which are mutually exclusive, are reported to occur in a very early phase of tumor development and their role in the response to nCRT in rectal cancer is conflicting.[198,199] On the contrary, *TP53* mutations occur later in rectal and colorectal cancer development and have been reported to lead to a reduced sensitivity to radiotherapy.[200] In our study cohort, the targeted analysis of the primary tumor tissue revealed mutation frequencies that were in line with those determined in the TCGA rectal cohort.[47] The most frequently mutated gene was *APC*, a key oncogenic driver mutated in most CRC and that mediates the activation of the Wnt signaling pathway.[201] It was reported that the *in vitro* activation of the Wnt signaling pathway mediates chemoradiotherapy resistance in CRC cell lines.[202] However, our results did not demonstrate any significant alteration in the frequency of *APC* mutations between responders and non-responders. On the contrary, patients presenting activating mutations of *KRAS/BRAF* genes showed a lower incidence of pCR with respect to patients with *KRAS/BRAF* wild type tumors (mutant, pCR 23.1% vs wild type, pCR 66.7%). Despite a trend has emerged, the results were not statistically significant ($p > 0.05$) and our data did not identify substantial difference in response to nCRT between patients with *KRAS/BRAF* wild-type and mutant tumors, nor did our data validate the enrichment of concurrent *KRAS*/*BRAF* and *TP53* mutations in non-responders *vs* responders.

To identify potential predictive markers of pCR, we also evaluated the IHC expression of twelve candidate proteins with relevant biological implication in LARC. For five markers (Ki67, CXCR4, COX-2, HIF1α, RAD51) we identified a cut-off value of protein expression that could successfully discriminate patients achieving a pCR from non-responder patients. In our study cohort, a high Ki67 was associated with a bad tumor response after nCRT (OR 3.30; 95% CI: 1.19-9.13). Ki67 is a well-known proliferation marker, which overexpression is commonly recognized as a marker of highly malignant phenotypes in several type of tumors.[203,204] The prognostic role of Ki67 in LARC has not been clarified yet. A similar trend was previously reported by Jacob *et al.*, who compared the Ki67 protein levels in pre- and post-treatment LARC biopsies and demonstrated that its overexpression at any time point is an early marker of poor tumor regression.[205] On the other hand, other studies showed

that a higher rate of Ki67 positive cells in treatment naïve LARC biopsies was associated with a greater incidence of pCR.[206,207]

Moreover, we observed that the tumor expression of the chemokine receptor CXCR4 was increased in patients with pCR (OR 4.67; 95% CI: 1.15-17.4). Despite some data are available on CXCR4 prognostic effect,[208] it was poorly investigated for its role in contributing the sensitivity toward nCRT in LARC. It is reasonable to assume that the high proliferation rate of cells overexpressing CXCR4 might increase the local effectiveness of chemo-radiation treatments. A recent study, which investigated the predictive role of CXCR4 expression in 85 LARC patients before nCRT, highlighted that, beside its expression level, an important role is played by its cellular localization, with the nuclear, or combined cytoplasmic and nuclear localization, related to the greater chance of tumor response.[209] Unfortunately, this information is not available in our study and further investigations are probably needed to shed light upon the biological interplay between CXCR4-mediated pathways and tumor response to nCRT and its predictive role. Moreover, we observed that Ki67 significantly interact with CXCR4, that notably characterize highly proliferating tumor cells, to discriminate responders from non-responders by CART analysis.

Our results support also a predictive potential for COX2 that appears to be associated with a higher chance of pCR when expressed above the herein defined cut-off value (OR=3.21; 95% CI: 1.14-9.09). Despite the well accepted role of COX2 in supporting tumor's growth and development,[210] literature data are conflicting regarding its predictive significance in LARC, with some studies sustaining,[211–213] and others disproving, [214,215] a COX2 involvement in predicting the nCRT efficacy. These discrepancies might be partially attributable to the heterogeneities of study cohorts and/or therapeutic schemes as well as to the huge methodological heterogeneity in the scoring system used to classify COX2 expression. Consistently with other investigators,[216] we classified tumors as COX2-overexpressing when the immunostaining intensity was defined by the pathologists as 'strong' to 'moderate'. However, when looking at the rate of COX2 positive cells, we noticed that tumors with an extremely high percentage of expressing cells (> 80%) were more likely to get a bad tumor response to treatment (data not shown). While the research on the mechanism by which COX2 modulates the sensitivity to nCRT in LARC remains a matter of open investigation, our data lead to reconsider its predictive significance as an early biomarker of treatment outcome.

In our cohort, HIF1α as well as RAD51 overexpression, assessed by means of the H-score and based on specific cut-off values, were associated to a bad tumor response. Consistently with the biological connection between RAD51 and HIF1α, our results sustain their matched clinical value as early predictors of poor treatment outcome. Specifically, RAD51 plays an essential role in DNA repair via homologous recombination and many studies have suggested that the RAD51 expression increased cellular resistance to chemotherapy and radiotherapy.[217] HIF1α plays a key role in the cellular adaptation to hypoxia. A few studies reported conflicting findings upon the predictive role of HIF1α in pre-treatment LARC biopsies. In a cohort of 86 LARC patients, Havelung *et al.* showed that the HIF1α

expression has no predictive impact on the response to chemoradiotherapy.[218] Similarly, Shioya *et al.*, who quantified the percentage of HIF1α positive cells in 50 LARC patients, did not find significant associations with the pathological grading or pCR.[61] The semi-quantitative scoring system (H-score) we applied in our study, which couples the fraction of positive cells with their staining intensity, possibly allows a more comprehensive assessment of HIF1α expression and could have helped to highlight previously overlooked associations.

In the framework of complex phenotypic traits, it is of crucial importance to define the mutual interaction between the different players in driving the clinical phenotype. As mentioned above, we exploited a CART analysis to put together clinical variables and biomarkers expression and found that the combination of Ki67 and CXCR4 expression assessment enabled the stratification of LARC patients into three distinct categories according to response to treatment. A correlation between the level of CXCR4 and Ki67 mutual expression was reported in other cancers,[219,220] supporting their cross-interaction in defining the proliferative and metastatic cells phenotype. However, despite the reported biological interplay between Ki67 and CXCR4, their expression levels were proven to change considerably depending on the location of the primary tumor,[221] rising the need for devoted investigations focused on LARC.

5.2 Clinical Application of ctDNA Monitoring in GIST Patients

GIST represents a paradigmatic model to study the oncogenic addiction to targeted therapies, and the possibility to interrogate ctDNA for the early identification of imatinib-resistant tumor's subclones would ideally represent a promising strategy to improve the efficacy of available treatments.[222] Despite these premises, the clinical utility of ctDNA monitoring in GIST is facing many hurdles that hamper the clinical translation of ctDNA-based liquid biopsy into the routine clinical practice. Beside the great specificity of ctDNA in recapitulating the mutations of the primary tumor, the molecular approaches attempted so far for the ctDNA tracking and monitoring in GIST exhibited a limited sensitivity with respect to the ctDNA detection.[223] Specifically, the application of high-sensitivity techniques, such as the barcode-aware deep sequencing and the ddPCR, revealed that the ctDNA detection rate was deeply dependent on the tumor's dimension, with tumors greater than 10 cm were more likely to shed detectable quantities of ctDNA.[223,224] This evidence, accompanied by the higher sensitivity of ddPCR over NGS,[87,89] reduces the clinical validity of ctDNA for the detection of MRD or for the monitoring of advanced disease in a tumor-agnostic scenario. The primary aim of this work was to test the feasibility of ctDNA detection in a cohort of 39 GIST patients as a tool to early identify the occurrence of disease progression to imatinib within different setting of treatment.

In the global GIST population (n = 39), the overall ctDNA detection rate was 5.1%. However, the detection rate rose to 22.2% (2 out 9 patients) when considering patients with metastatic and PD. These results are consistent with previously reported evidences that described the lack of detectable ctDNA in

GIST patients suffering from localized or small disease. Conversely, the ctDNA detection rate in patients with advanced GIST was reported to be 45.0%. and 56.3% in two independent study cohorts comprising 243 and 32 advanced GISTs, respectively.[223,224] Our analysis showed a lower sensitivity in ctDNA detection with respect to previous reports, partially due to the lack of knowledge on primary tumor's mutations in our study cohort and the impossibility to perform a cross-platform comparison (e.g. NGS and ddPCR) for ctDNA detection in selected point regions. However, the results of cfDNA analysis of our GIST cohort draws the attention upon some molecular mechanism governing the imatinib failure. Accordingly, the two cases herein reported illustrate i) a case of primary resistance to imatinib (case #21) and ii) an example of secondary acquired resistance to imatinib (case #16). In the first scenario, the lack of activating mutations in imatinib related genes (*KIT*, *PDGFRA*, *BRAF*) in the primary tumor might explain the lack of sensitivity toward imatinib, as well as the fast onset of a dramatic disease progression that culminated in a fatal outcome for the patient. This evidence urges the need for the routinely genotyping of primary tumor DNA in newly diagnosed GIST patients for the characterization of tumor's mutational status and for the identification of actionable mutations capable of ensuring the sensitivity to imatinib. Despite widely recommended from the good clinical practice guidelines, the genotyping of primary GIST is performed only in referral centers for GIST management, partially owing to the rarity of the disease. Furthermore, the administration of imatinib in *KIT/PDGFRA* wild type GISTs is a matter of heated debate as most of the patients, who are classified as wild type, tend to display an indolent tumor's behavior and might benefit for some extent from imatinib intake. Although only few studies have investigated the role of TP53 somatic mutations as a possible risk factor in GIST, a general consensus upon their association with imatinib resistance has been achieved.[68] The first evidence demonstrating the correlation between TP53 mutations and imatinib insensitivity was described by Wendel *et al.* in BCR-ABL positive leukemic cells, where they observed that the mechanism of imatinib resistance was independent of the chemical inhibition of BCR-ABL kinase by imatinib, suggesting a downstream involvement of TP53 mutations in leading the resistance phenotype.[225] Further studies confirmed the loss of TP53 in chronic myeloid leukemia as a molecular marker, which is likely associated with imatinib resistance.[226] Furthermore, in a study aimed at identifying genes involved in imatinib resistance in GIST-T1 cells through a CRISP-Cas9 knockout genome-wide screening, Cao *et al.* identified *TP53* as one of the main genes associated to imatinib resistance.[227] These evidences suggest that genomic alterations in genes related to the apoptosis pathway might represent an escape route exploited by tumor cells to evade imatinib therapy. In *KIT*/*PDGFRA* mutant GISTs there is no doubt upon the origin of the oncogenic signaling and the development of imatinib resistance is mainly restricted to the acquisition of secondary *KIT*/*PDGFRA* mutant clones bearing novel mutations. In these groups of GISTs, the overall *TP53* mutation rate was reported as low, emphasizing the oncogenic reliance on kinase-mediated signaling. However, a straightforward association between presence of *TP53* aberrations and GIST malignancy has been observed, with a significant increase of *TP53* aberrations in high-risk rather than in low-risk tumors.[228–230] On the other

hand, *TP53* has emerged as one of the main mutated genes in wild-type GISTs, supporting its possible role not only as a determiner of malignant behavior, but also in the pathogenesis of wild-type GISTs.[231] In this case, the rapid metastatic evolution is consistent with the *TP53* mutant clonal selection from the primary to the relapsed tumor. The homozygous presence of *TP53* indel (c.560-7_560-2delCTCTTAinsT) in fundamentally all hepatic relapsed cells suggests once again the association between *TP53* deleterious mutations in GIST and the establishment of an aggressive phenotype insensitive to imatinib. Moreover, the observation of no clinically actionable mutations, which might represent a molecular target for currently available therapeutic options, corroborates the lack of sensitivity toward imatinib reported here and implies the impossibility of prescribing further targeted drugs. Indeed, the administration of targeted therapies is limited to the presence of specific overexpressed or mutated molecular targets in tumor cells, thus making the management of wild-type tumors a challenging task. In this case, the clinical tumor progression was well recapitulated by the longitudinal sequencing of ctDNA, which revealed the presence of *TP53* c.560-7_560-2delCTCTTAinsT at increasing allele frequency over six months. This finding is significant, since it sustains the feasibility of relying on information obtained by liquid rather than tissue biopsies for the assessment of genetic features in metastatic GISTs. A good concordance between mutated cfDNA and tumor tissue in GIST patients was reported by previous studies that observed a higher detection rate of ctDNA in patients with active disease and high tumor burden, rather than in patients with complete response or localized disease.[223,232] In this framework, the allele frequency of ctDNA was shown to increase according to disease progression, allowing the dynamic monitoring of tumor changes in advanced GIST. On the contrary, the case of patient #16 brilliantly recapitulates the development of secondary resistance to imatinib as a consequence of the proliferation of a tumor resistant subclone. Although the primary tumor genotype was unknown, it is reasonable to assume that the patient should have presented a sensitizer mutation in imatinib targeted genes, given the excellent disease control she has displayed for more than ten years. The detection of *KIT* c.1961T>C mutation, affecting the imatinib binding domain of KIT receptor, in concomitance to disease progression shed light upon the mechanism of GIST escape from the imatinib's control. This observation is consistent with the lack of sensitivity to imatinib daily dose doubling as a first clinical strategy to postpone imatinib interruption and with the disease stability observed after the switch to the second therapy line with sunitinib, in line with other recent report.[89] Overall, the ctDNA detection did not anticipate the clinical diagnosis of disease progression but represented instead an excellent marker capable to recapitulate the clinical progression, in case of increased VAF, or response, in case of decreased VAF.

5.3 Pharmacogenetics and DDIs

The efficacy of drugs is deeply influenced by both pharmacodynamics and pharmacokinetics parameters.[92] Accordingly, the pharmacodynamics of imatinib is affected by the genetic makeup of its

molecular targets, *i.e.* TKI receptors *KIT* and *PDGFRA*, with the development or the selection of resistance subclones being the leading cause of treatment failure as a consequence of a pharmacodynamic imbalance between the drug and its target.[233] As a counterpart, the pharmacokinetic of imatinib plays an equally important role in ensuring the exposure of tumor cells to adequate drugs concentrations capable to guarantee the clinical efficacy, while at the same time preventing toxic effects as a consequence of over-dosage. Imatinib presents an unpredictable interpatient pharmacokinetic variability, which might expose patients to the risk of treatment inefficacy or, more rarely, toxicity.[234] With the aim of identifying potential factor that might contribute to the huge heterogeneity of imatinib exposure, two specific aspects were investigated in the present work. First, the impact of the host's genetic variants affecting imatinib metabolizing enzymes (CYPs) and transporters was considered as a possible genetic factor capable to determine the fluctuation of imatinib levels in the study population. Then, the co-administration of drugs, which are known to modulate the activity of specific CYPs and transporters, was considered as a possible non-genetic factor that might concur the variability of imatinib exposure. Consistently with previous findings,[184] the study population selected for the pharmacokinetic analysis (n = 33) exhibited a huge variability in term of imatinib exposure (range 89.1 to 2452.8 ng/mL) in presence of the same imatinib daily dose (400 mg) and this was reported to partially explain the development disease progression in patients with sub-therapeutic imatinib trough levels.

Notably, the development and the application of a PGx-AS to rank the CYPs metabolic proficiency level, revealed a correlation between the activity of CYPs and the imatinib trough levels. Specifically, patients presenting a higher PGx-AS were shown to have lower imatinib trough levels when compared with patients with a lower PGx-AS ($p < 0.05$), suggesting that the presence of genetic variants affecting the activity of imatinib metabolizing enzymes could actually have some clinically relevant implications on imatinib clearance. More specifically, the metabolic phenotype of *CYP2D6* has emerged as the major genetic determiner of the interindividual variability of imatinib exposure, with patients presenting a decreased number of *CYP2D6* functional alleles showing higher imatinib concentrations when compared with the *CYP2D6* extensive metabolizers (1292 ng/mL vs 771.9 ng/mL; $p < 0.005$). This is the second time that the *CYP2D6* genotype was found significantly associated with the interpatient variability of imatinib pharmacokinetic at the clinical level, as a previous study including 82 GIST patients identified how the presence of at least one *CYP2D6**4 allele might potentially reduce the apparent oral clearance of imatinib.[123] In line with these findings, the *CYP2D6**4 allele, which yields a non-functional truncated protein due to an aberrant spicing defect, was identified in our study cohort with a minor allele frequency of 21.2%, thus representing the most frequently detected loss-of-function *CYP2D6* allele. Furthermore, a restricted subgroup of patients (n = 9), who were simultaneously carrier of decreased metabolic activity of CYP2D6 and CYP2B6, exhibited extremely high imatinib trough levels (median: 1359.0 ng/mL), allowing the identification of four out the five patients with the highest imatinib plasma trough concentrations in the entire patients' cohort. Although the investigation of imatinib's safety profile is beyond the aims of the present work, the preemptive identification of

patients, who are more likely to exhibit an extremely remarkable imatinib overexposure, might help to early select the subject that are at higher risk to develop dosage-related side effects. Imatinib shows an excellent safety profile with respect to other cytostatic agents, with the most frequently reported toxicities being oedema, asthenia and gastrointestinal toxicity that rarely reach the CTCTAE grade 3,[235] and whose symptoms can be usually managed without resorting to the patient's hospitalization.[236] However, the onset of non-hematological low-grade chronic toxicities throughout a lifelong imatinib administration might lead to the frequent treatment's interruption, as well as to a reduction of the patient's quality of life.[104] This might negatively impact not only on the personal and social lives of patients, but could also ultimately result into a poor patient's compliance in the routinely imatinib intake. Although *CYP2D6* plays a minor role on the metabolism of imatinib, it might be reasonable to assume that the inhibition of *CYP3A4* by imatinib itself could actually gather to a central role of the other enzymes in the catabolism of imatinib and that the presence of non-functional alleles in *CYP2D6*, and optionally in *CYP2B6*, could become of pivotal relevance in influencing the imatinib clearance.[119] An association with low imatinib levels and A-allele in rs17064 *ABCB1* was found in patients who showed the A-variant allele having a lower imatinib exposure when compared with the wild type carriers (580.7 ng/mL vs 980.0 ng/mL; $p = 0.0406$). The ATP-binding cassette sub-family B member 1 is encoded by the ABCB1 gene and it functions as a cellular transmembrane transporter able to excrete xenobiotic molecules,[105] and imatinib is known to be transported through this molecule in the intestinal epithelium.[106] Association between rs17064 and imatinib pharmacokinetics parameters had never been described before, partially owing to the centralized efforts paid towards the role of pharmacogenetic variants that affect the gene codifying sequence or that were already reported as clinically relevant.[107] However, the reduced plasma exposure to vitamin D3 in 39 healthy subjects bearing the A-allele rs17064 had been previously described,[183] but the mechanism by which this SNP may lead to altered plasma levels of xenobiotics is still uncertain. The 3'UTRs of mRNA transcripts are known to exhibit important sequences regulating the fate of mRNA and thus, proteosynthesis. A previous *in vitro* study showed that rs17064 did not alter ABCB1 mRNA stability,[237] but further research is needed to evaluate whether this variant can influence ABCB1 protein function or expression levels through other mechanisms, e.g., microRNA-mediated gene regulation. Based on these findings, we can speculate that rs17064 might have an implication on ABCB1 expression, which may lead to a faster imatinib transport and, thus, extrusion from the blood stream. Other single SNPs in transporters previously reported to be associated with imatinib trough levels in GIST patients were not associated to the pharmacokinetic endpoint here considered.[110,170,238]

In the context of a complex phenotypic trait, such as the systemic exposure to an oral cytostatic agent, multiple genetic and non-genetic factors may concurrently contribute and interact with each other to define a clinical outcome. In the present work, the impact of drugs on imatinib metabolism was analyzed throughout an imatinib-independent approach, by evaluating the impact of single drugs as inducer or inhibitor of the activity of each enzyme and transporter involved in the imatinib metabolism, regardless

to the previous knowledge of clinical interactions between imatinib and the other drugs. Notably, after adjusting the PGx-AS of CYPs for DDIs, an inverse linear correlation between the corrected PGx-AS and the imatinib exposure was observed, suggesting that considering the genotype together with concurrent DDIs might help to comprehensively describe the overall imatinib exposure. A similar approach has shown excellent results with respect to the CYP2D6 and the exposure to the analgesic drugs codeine and tramadol. In fact, the adjustment of *CYP2D6* activity score per DDIs in patients receiving codeine or tramadol, which are CYP2D6 substrate, significantly improved the identification of patients at risk of poor treatment efficacy when compared to the only *CYP2D6* genotyping.[239] However, it is difficult to precisely identify any one factor of small to modest effect and the clinical validity of every single factor to predict the clinical endpoint might be little, especially in a small sample size. Therefore, the identification of an association between specific DDIs and imatinib exposure has been possible only in specific cases, and further investigations involving wider study cohorts will be needed to clarify and quantify the impact of single drugs and their combination on the imatinib exposure. Imatinib is mainly metabolized by CYP3A4, into its main metabolite desmethyilimatinib. It is well documented that the concomitant administration of CYP3A4 strong inducers could lead to clinically significant interactions, resulting in lower plasma concentrations of imatinib. In the case here presented, the patient #10 was concomitantly taking imatinib and the strong CYP3A4 inducer, carbamazepine. Consistently, the trough concentrations of imatinib in the plasma of patients were much lower than the concentrations measured in the whole population

It is reasonable to assume that the extreme phenotype observed could be for large extent mediated by the CYP3A4 activation by carbamazepine, in agreement with previous case reports.[240] Notably, the imatinib dose implementation to 800 mg/die, gathered to a clinical benefit and to the disease stabilization, suggesting that the suspension of carbamazepine administration might not be the only viable solution to restore the clinically effective imatinib plasma levels. Even though the summary of product characteristics of imatinib recommend to avoid the concomitant administration of imatinib and strong inducer of CYP3A4, a careful appraisal of the pharmacokinetic parameters of the single co-treated patients might be considered, and the imatinib dose adjustment could represent a valuable therapeutic strategy in spite of the switch to sunitinib or to another medicament to treat the concurrent morbidity. Tobacco smoke is a potent inducer of the CYP1A2 and may therefore affect the pharmacokinetics of drugs metabolized by that isoform. In the present work, current smokers were shown to present lower imatinib plasma trough concentrations when compared to the control group (696.3 ng/mL vs 984.5 ng/mL, $p = 0.0008$) sustaining a possible mechanism of imatinib increased clearance throughout a CYP1A2-mediated mechanism. A few studies have investigated the impact of tobacco smoke on the disposition of TKIs, but results were not conclusive. Consistently with our observation, Hamilton *et al.* have shown a major increase of erlotinib clearance in smokers versus non-smokers. Notably, erlotinib is metabolized by CYP3A4 and, for a minor extent, by CYP1A2, thus showing an overlap with the catabolic pathway of imatinib.[241] On the contrary, Van Erp *et al.*

investigated the impact of smoking habit on imatinib pharmacokinetic parameters (*i.e.* oral clearance, AUC, distribution volume and elimination half-life) in 45 GIST patients administered with imatinib, without finding any association between the smoke habit and imatinib exposure.[242] A possible explanation for the lack of association in the study of Van Erp *et al.* could be that the imatinib exposure was measured after a single oral dose administration and not at the steady state. Consequently, it might be assumed that at the beginning of the treatment with imatinib a major role with respect to its elimination is played by CYP3A4, whose inhibition from imatinib is time and dose dependent.[119] Therefore, the contribution of CYP1A2 to imatinib metabolism might be neglectable in presence of a fully functional CYP3A4 activity, and the impact of tobacco smoke could be therefore irrelevant.

5.4 Conclusions and Outlooks

This thesis aimed at investigating the clinical validity of ctDNA analysis as an early prognostic marker in LARC patients receiving nCRT and as a possible biomarker to early identify the development of disease progression in GIST patients administered with imatinib in different setting of treatment. Moreover, the secondary aim was to assess the impact on imatinib pharmacokinetics of (i) pharmacogenetic variants affecting the activity of CYPs and transporters involved in imatinib catabolism and distribution and of (ii) drugs that can potentially interact with the clinical pharmacokinetics of imatinib. The main findings of the present work suggest that the detection of ctDNA by means of sWGS is feasible in LARC and provides information upon the detectable fraction of ctDNA present in the blood at the time of diagnosis, during and after treatment. Specifically, the detection of ctDNA at the time of diagnosis was associated with the tumor burden and with the risk to develop disease recurrence within two years from the diagnosis, showing also an additive prognostic value with the CEA. This finding shed light upon a possible application of the CNAs quantification in newly diagnosed LARC patients into the clinical decision support algorithms for risk stratification at the aim of tailoring the following therapeutic strategies. Moreover, the presence of an increasing TFx in course of nCRT was associated with a greater sensitivity to the chemoradiation treatment. Even though this observation requires further investigation upon the kinetic of ctDNA release in radiated tumor cells, it might suggest that the monitoring of CNAs in LARC patients while on nCRT could provide early evidences on the patients' sensitivity to chemoradiation, which might complement the imaging-based follow-up. The presence of detectable CNAs after nCRT was associated with a partial tumor response to treatment and indicates the permanence of residual tumor cells after nCRT. Even though the sensitivity of ctDNA detection after nCRT is narrow, it might be useful to exclude the achievement of pCR and represent a decisive factor for planning the delivery of surgery. Further studies are needed to clarify the prognostic role ctDNA detection in LARC, and future plans include the application of targeted deep sequencing approaches for the joint identification of CNAs and SNVs in the cfDNA, as well as the plasma profiling of a larger study population.

In the context of GIST, the application of liquid biopsy for the ctDNA monitoring in course of imatinib has revealed that the ctDNA detection can serve as a tumor-specific marker to monitor the tumor's progression in a subset of metastatic patients, also providing information upon the mechanism governing the imatinib resistance phenotype. However, use of ctDNA as an early marker to anticipate the clinical diagnosis of disease progression seems to be limited, as in the present work it was detected after the clinical diagnosis of disease progression. However, the precise time frame for cfDNA collection to anticipate the imaging-based identification of progression has not been defined, and a closer cfDNA monitoring in high-risk patients might represent a valuable strategy to implement the clinical translation of liquid biopsy into the routine clinical practice. The pharmacokinetic analysis of imatinib in patients administered with imatinib standard dose has revealed a major contribution of the patients' genotype, and specifically of *CYP2D6*, in determining the interpatient variability of imatinib clearance. This evidence suggests that the personalised imatinib dosing might improve treatment outcomes when compared to a "one-dose-fits-all" approach, with a potential additional role for pharmacogenetics. Moreover, dedicated attention should be devoted to the concomitant administration of imatinib and strong CYPs' inhibitors or inducers, which might expose the patients to a high risk of imatinib under-dosage. Specifically, in the study population here described, the concomitant administration of carbamazepine and the smoke habit were shown to have a clinically relevant interaction with the imatinib pharmacokinetics. These evidences lead to reconsider the straightforward association between genotype and predicted phenotype and shed light upon the relevance of a drug-induced phenoconversion into the routine clinical practice.

References

(1) U.S. Food and Drug Administration: Paving the Way for Personalized Medicine.(Http://Www.Fda.Gov/Downloads/Scienceresearch/Specialtopics/Personalizedmedicine/Ucm372421.Pdf. 2013) [Accessed on; 23.03.2020].

(2) Métais P, M. P. Les Acides Nucléiques Du Plasma Sanguin Chez l'Homme. *Comptes Rendus des Seances de la Societe de Biologie et de ses Filiales* **1948**, *142*, 241–243.

(3) Leon, S. A.; Shapiro, B.; Sklaroff, D. M.; Yaros, M. J. Free DNA in the Serum of Cancer Patients and the Effect of Therapy. **1977**, *36*, 646 - 650.

(4) Vasioukhin, V.; Anker, P.; Maurice, P.; Lyautey, J.; Lederrey, C.; Stroun, M. Point Mutations of the N-Ras Gene in the Blood Plasma DNA of Patients with Myelodysplastic Syndrome or Acute Myelogenous Leukaemia. *British Journal of Haematology* **1994**, *86* (4), 774–779. https://doi.org/10.1111/j.1365-2141.1994.tb04828.x.

(5) Diaz, L. A.; Bardelli, A. Liquid Biopsies: Genotyping Circulating Tumor DNA. *Journal of Clinical Oncology* **2014**, *32* (6), 579–586. https://doi.org/10.1200/JCO.2012.45.2011.

(6) Snyder, M. W.; Kircher, M.; Hill, A. J.; Daza, R. M.; Shendure, J. Cell-Free DNA Comprises an In Vivo Nucleosome Footprint That Informs Its Tissues-Of-Origin. *Cell* **2016**, *164* (1–2), 57–68. https://doi.org/10.1016/j.cell.2015.11.050.

(7) Sanchez, C.; Snyder, M. W.; Tanos, R.; Shendure, J.; Thierry, A. R. New Insights into Structural Features and Optimal Detection of Circulating Tumor DNA Determined by Single-Strand DNA Analysis. *npj Genomic Medicine* **2018**, *3* (1). https://doi.org/10.1038/s41525-018-0069-0.

(8) Schwarzenbach, H.; Hoon, D. S. B.; Pantel, K. Cell-Free Nucleic Acids as Biomarkers in Cancer Patients. *Nature Reviews Cancer* **2011**, *11* (6), 426–437. https://doi.org/10.1038/nrc3066.

(9) Duvvuri, B.; Lood, C. Cell-Free DNA as a Biomarker in Autoimmune Rheumatic Diseases. *Frontiers in Immunology* **2019**, *10*. https://doi.org/10.3389/fimmu.2019.00502.

(10) Shen, J.; Zhou, Y.; Chen, Y.; Li, X.; Lei, W.; Ge, J.; Peng, W.; Wu, J.; Liu, G.; Yang, G.; Shi, H.; Chen, J.; Jiang, T.; Wang, R. Dynamics of Early Post-Operative Plasma DdcfDNA Levels in Kidney Transplantation: A Single-Center Pilot Study. *Transplant International* **2019**, *32* (2), 184–192. https://doi.org/10.1111/tri.13341.

(11) Yan, L.; Chen, Y.; Zhou, J.; Zhao, H.; Zhang, H.; Wang, G. Diagnostic Value of Circulating Cell-Free DNA Levels for Hepatocellular Carcinoma. *International Journal of Infectious Diseases* **2018**, *67*, 92–97. https://doi.org/10.1016/j.ijid.2017.12.002.

(12) Meddeb, R.; Pisareva, E.; Thierry, A. R. Guidelines for the Preanalytical Conditions for Analyzing Circulating Cell-Free DNA. *Clinical Chemistry* **2019**, *65* (5), 623–633. https://doi.org/10.1373/clinchem.2018.298323.

(13) Bettegowda, C.; Sausen, M.; Leary, R. J.; Kinde, I.; Wang, Y.; Agrawal, N.; Bartlett, B. R.; Wang, H.; Luber, B.; Alani, R. M.; Antonarakis, E. S.; Azad, N. S.; Bardelli, A.; Brem, H.; Cameron,

J. L.; Lee, C. C.; Fecher, L. A.; Gallia, G. L.; Gibbs, P.; Le, D.; Giuntoli, R. L.; Goggins, M.; Hogarty, M. D.; Holdhoff, M.; Hong, S.-M.; Jiao, Y.; Juhl, H. H.; Kim, J. J.; Siravegna, G.; Laheru, D. A.; Lauricella, C.; Lim, M.; Lipson, E. J.; Marie, S. K. N.; Netto, G. J.; Oliner, K. S.; Olivi, A.; Olsson, L.; Riggins, G. J.; Sartore-Bianchi, A.; Schmidt, K. Detection of Circulating Tumor DNA in Early- and Late-Stage Human Malignancies. *Science Translational Medicine* **2014**, *6* (224), 224ra24. https://doi.org/10.1126/scitranslmed.3007094.

(14) Lee, J.-S.; Kim, M.; Seong, M.-W.; Kim, H.-S.; Lee, Y. K.; Kang, H. J. Plasma vs. Serum in Circulating Tumor DNA Measurement: Characterization by DNA Fragment Sizing and Digital Droplet Polymerase Chain Reaction. *Clinical Chemistry and Laboratory Medicine (CCLM)* **2020**, *58* (4), 527–532. https://doi.org/10.1515/cclm-2019-0896.

(15) Medina Diaz, I.; Nocon, A.; Mehnert, D. H.; Fredebohm, J.; Diehl, F.; Holtrup, F. Performance of Streck CfDNA Blood Collection Tubes for Liquid Biopsy Testing. *PLOS ONE* **2016**, *11* (11), e0166354. https://doi.org/10.1371/journal.pone.0166354.

(16) Haselmann, V.; Ahmad-Nejad, P.; Geilenkeuser, W. J.; Duda, A.; Gabor, M.; Eichner, R.; Patton, S.; Neumaier, M. Results of the First External Quality Assessment Scheme (EQA) for Isolation and Analysis of Circulating Tumour DNA (CtDNA). *Clinical Chemistry and Laboratory Medicine (CCLM)* **2018**, *56* (2), 220–228. https://doi.org/10.1515/cclm-2017-0283.

(17) Elazezy, M.; Joosse, S. A. Techniques of Using Circulating Tumor DNA as a Liquid Biopsy Component in Cancer Management. *Computational and Structural Biotechnology Journal* **2018**, *16*, 370–378. https://doi.org/10.1016/j.csbj.2018.10.002.

(18) Zhou, Q.; Moser, T.; Perakis, S.; Heitzer, E. Untargeted Profiling of Cell-Free Circulating DNA. *Translational Cancer Research* **2018**, *7* (S2), S140–S152. https://doi.org/10.21037/tcr.2017.10.11.

(19) Yoon, S.; Xuan, Z.; Makarov, V.; Ye, K.; Sebat, J. Sensitive and Accurate Detection of Copy Number Variants Using Read Depth of Coverage. *Genome Research* **2009**, *19* (9), 1586–1592. https://doi.org/10.1101/gr.092981.109.

(20) Magi, A.; Tattini, L.; Pippucci, T.; Torricelli, F.; Benelli, M. Read Count Approach for DNA Copy Number Variants Detection. *Bioinformatics* **2012**, *28* (4), 470–478. https://doi.org/10.1093/bioinformatics/btr707.

(21) Bray, F.; Ferlay, J.; Soerjomataram, I.; Siegel, R. L.; Torre, L. A.; Jemal, A. Global Cancer Statistics 2018: GLOBOCAN Estimates of Incidence and Mortality Worldwide for 36 Cancers in 185 Countries. *CA: A Cancer Journal for Clinicians* **2018**, *68* (6), 394–424. https://doi.org/10.3322/caac.21492.

(22) Cobas EGFR Mutation Test v2. 2016. (Available Online: Http://Www.Fda.Gov/Drugs/InformationOnDrugs/ApprovedDrugs/Ucm504540.Htm).

(23) Cescon, D. W.; Bratman, S. V.; Chan, S. M.; Siu, L. L. Circulating Tumor DNA and Liquid Biopsy in Oncology. *Nature Cancer* **2020**, *1* (3), 276–290. https://doi.org/10.1038/s43018-020-0043-5.

(24) Siravegna, G.; Mussolin, B.; Venesio, T.; Marsoni, S.; Seoane, J.; Dive, C.; Papadopoulos, N.; Kopetz, S.; Corcoran, R. B.; Siu, L. L.; Bardelli, A. How Liquid Biopsies Can Change Clinical Practice in Oncology. *Annals of Oncology* **2019**, *30* (10), 1580–1590. https://doi.org/10.1093/annonc/mdz227.

(25) Beaver, J. A.; Jelovac, D.; Balukrishna, S.; Cochran, R. L.; Croessmann, S.; Zabransky, D. J.; Wong, H. Y.; Valda Toro, P.; Cidado, J.; Blair, B. G.; Chu, D.; Burns, T.; Higgins, M. J.; Stearns, V.; Jacobs, L.; Habibi, M.; Lange, J.; Hurley, P. J.; Lauring, J.; VanDenBerg, D. A.; Kessler, J.; Jeter, S.; Samuels, M. L.; Maar, D.; Cope, L.; Cimino-Mathews, A.; Argani, P.; Wolff, A. C.; Park, B. H. Detection of Cancer DNA in Plasma of Patients with Early-Stage Breast Cancer. *Clinical Cancer Research* **2014**, *20* (10), 2643–2650. https://doi.org/10.1158/1078-0432.CCR-13-2933.

(26) Osumi, H.; Shinozaki, E.; Takeda, Y.; Wakatsuki, T.; Ichimura, T.; Saiura, A.; Yamaguchi, K.; Takahashi, S.; Noda, T.; Zembutsu, H. Clinical Relevance of Circulating Tumor DNA Assessed through Deep Sequencing in Patients with Metastatic Colorectal Cancer. *Cancer Medicine* **2019**, *8* (1), 408–417. https://doi.org/10.1002/cam4.1913.

(27) Murray, D. H.; Symonds, E. L.; Young, G. P.; Byrne, S.; Rabbitt, P.; Roy, A.; Cornthwaite, K.; Karapetis, C. S.; Pedersen, S. K. Relationship between Post-Surgery Detection of Methylated Circulating Tumor DNA with Risk of Residual Disease and Recurrence-Free Survival. *Journal of Cancer Research and Clinical Oncology* **2018**, *144* (9), 1741–1750. https://doi.org/10.1007/s00432-018-2701-x.

(28) Flamini, E.; Mercatali, L.; Nanni, O.; Calistri, D.; Nunziatini, R.; Zoli, W.; Rosetti, P.; Gardini, N.; Lattuneddu, A.; Verdecchia, G. M.; Amadori, D. Free DNA and Carcinoembryonic Antigen Serum Levels: An Important Combination for Diagnosis of Colorectal Cancer. *Clinical Cancer Research* **2006**, *12* (23), 6985–6988. https://doi.org/10.1158/1078-0432.CCR-06-1931.

(29) Johnson, C. M.; Wei, C.; Ensor, J. E.; Smolenski, D. J.; Amos, C. I.; Levin, B.; Berry, D. A. Meta-Analyses of Colorectal Cancer Risk Factors. *Cancer Causes & Control* **2013**, *24* (6), 1207–1222. https://doi.org/10.1007/s10552-013-0201-5.

(30) Russano, M.; Napolitano, A.; Ribelli, G.; Iuliani, M.; Simonetti, S.; Citarella, F.; Pantano, F.; Dell'Aquila, E.; Anesi, C.; Silvestris, N.; Argentiero, A.; Solimando, A. G.; Vincenzi, B.; Tonini, G.; Santini, D. Liquid Biopsy and Tumor Heterogeneity in Metastatic Solid Tumors: The Potentiality of Blood Samples. *Journal of Experimental & Clinical Cancer Research* **2020**, *39* (1). https://doi.org/10.1186/s13046-020-01601-2.

(31) Thierry, A. R.; Mouliere, F.; El Messaoudi, S.; Mollevi, C.; Lopez-Crapez, E.; Rolet, F.; Gillet, B.; Gongora, C.; Dechelotte, P.; Robert, B.; Del Rio, M.; Lamy, P.-J.; Bibeau, F.; Nouaille, M.; Loriot, V.; Jarrousse, A.-S.; Molina, F.; Mathonnet, M.; Pezet, D.; Ychou, M. Clinical Validation of the Detection of KRAS and BRAF Mutations from Circulating Tumor DNA. *Nature Medicine* **2014**, *20* (4), 430–435. https://doi.org/10.1038/nm.3511.

(32) Zill, O. A.; Banks, K. C.; Fairclough, S. R.; Mortimer, S. A.; Vowles, J. V.; Mokhtari, R.; Gandara, D. R.; Mack, P. C.; Odegaard, J. I.; Nagy, R. J.; Baca, A. M.; Eltoukhy, H.; Chudova, D. I.; Lanman, R. B.; Talasaz, A. The Landscape of Actionable Genomic Alterations in Cell-Free Circulating Tumor DNA from 21,807 Advanced Cancer Patients. *Clinical Cancer Research* **2018**, *24* (15), 3528–3538. https://doi.org/10.1158/1078-0432.CCR-17-3837.

(33) Kurtz, D. M.; Scherer, F.; Jin, M. C.; Soo, J.; Craig, A. F. M.; Esfahani, M. S.; Chabon, J. J.; Stehr, H.; Liu, C. L.; Tibshirani, R.; Maeda, L. S.; Gupta, N. K.; Khodadoust, M. S.; Advani, R. H.; Levy, R.; Newman, A. M.; Dührsen, U.; Hüttmann, A.; Meignan, M.; Casasnovas, R.-O.; Westin, J. R.; Roschewski, M.; Wilson, W. H.; Gaidano, G.; Rossi, D.; Diehn, M.; Alizadeh, A. A. Circulating Tumor

DNA Measurements As Early Outcome Predictors in Diffuse Large B-Cell Lymphoma. *Journal of Clinical Oncology* **2018**, *36* (28), 2845–2853. https://doi.org/10.1200/JCO.2018.78.5246.

(34) Saluja, H.; Karapetis, C. S.; Pedersen, S. K.; Young, G. P.; Symonds, E. L. The Use of Circulating Tumor DNA for Prognosis of Gastrointestinal Cancers. *Frontiers in Oncology* **2018**, *8*. https://doi.org/10.3389/fonc.2018.00275.

(35) Lee, J. H.; Saw, R. P.; Thompson, J. F.; Lo, S.; Spillane, A. J.; Shannon, K. F.; Stretch, J. R.; Howle, J.; Menzies, A. M.; Carlino, M. S.; Kefford, R. F.; Long, G. V.; Scolyer, R. A.; Rizos, H. Pre-Operative CtDNA Predicts Survival in High-Risk Stage III Cutaneous Melanoma Patients. *Annals of Oncology* **2019**, *30* (5), 815–822. https://doi.org/10.1093/annonc/mdz075.

(36) Tie, J.; Cohen, J. D.; Wang, Y.; Li, L.; Christie, M.; Simons, K.; Elsaleh, H.; Kosmider, S.; Wong, R.; Yip, D.; Lee, M.; Tran, B.; Rangiah, D.; Burge, M.; Goldstein, D.; Singh, M.; Skinner, I.; Faragher, I.; Croxford, M.; Bampton, C.; Haydon, A.; Jones, I. T.; Karapetis, C. S.; Price, T.; Schaefer, M. J.; Ptak, J.; Dobbyn, L.; Silliman, N.; Kinde, I.; Tomasetti, C.; Papadopoulos, N.; Kinzler, K.; Volgestein, B.; Gibbs, P. Serial Circulating Tumour DNA Analysis during Multimodality Treatment of Locally Advanced Rectal Cancer: A Prospective Biomarker Study. *Gut* **2019**, *68* (4), 663–671. https://doi.org/10.1136/gutjnl-2017-315852.

(37) Abbosh, C.; Birkbak, N. J.; Swanton, C. Early Stage NSCLC — Challenges to Implementing CtDNA-Based Screening and MRD Detection. *Nature Reviews Clinical Oncology* **2018**, *15* (9), 577–586. https://doi.org/10.1038/s41571-018-0058-3.

(38) Tie, J.; Wang, Y.; Tomasetti, C.; Li, L.; Springer, S.; Kinde, I.; Silliman, N.; Tacey, M.; Wong, H.-L.; Christie, M.; Kosmider, S.; Skinner, I.; Wong, R.; Steel, M.; Tran, B.; Desai, J.; Jones, I.; Haydon, A.; Hayes, T.; Price, T. J.; Strausberg, R. L.; Diaz, L. A.; Papadopoulos, N.; Kinzler, K. W.; Vogelstein, B.; Gibbs, P. Circulating Tumor DNA Analysis Detects Minimal Residual Disease and Predicts Recurrence in Patients with Stage II Colon Cancer. *Sci Transl Med* **2016**, *8* (346), 346ra92. https://doi.org/10.1126/scitranslmed.aaf6219.

(39) Coakley, M.; Garcia-Murillas, I.; Turner, N. C. Molecular Residual Disease and Adjuvant Trial Design in Solid Tumors. *Clinical Cancer Research* **2019**, *25* (20), 6026–6034. https://doi.org/10.1158/1078-0432.CCR-19-0152.

(40) Tie, J.; Cohen, J. D.; Wang, Y.; Li, L.; Christie, M.; Simons, K.; Elsaleh, H.; Kosmider, S.; Wong, R.; Yip, D.; Lee, M.; Tran, B.; Rangiah, D.; Burge, M.; Goldstein, D.; Singh, M.; Skinner, I.; Faragher, I.; Croxford, M.; Bampton, C.; Haydon, A.; Jones, I. T.; S Karapetis, C.; Price, T.; Schaefer, M. J.; Ptak, J.; Dobbyn, L.; Silliman, N.; Kinde, I.; Tomasetti, C.; Papadopoulos, N.; Kinzler, K.; Volgestein, B.; Gibbs, P. Serial Circulating Tumour DNA Analysis during Multimodality Treatment of Locally Advanced Rectal Cancer: A Prospective Biomarker Study. *Gut* **2019**, *68* (4), 663–671. https://doi.org/10.1136/gutjnl-2017-315852.

(41) Spano, J.-P.; Lagorce, C.; Atlan, D.; Milano, G.; Domont, J.; Benamouzig, R.; Attar, A.; Benichou, J.; Martin, A.; Morere, J.-F.; Raphael, M.; Penault-Llorca, F.; Breau, J.-L.; Fagard, R.; Khayat, D.; Wind, P. Impact of EGFR Expression on Colorectal Cancer Patient Prognosis and Survival. *Annals of Oncology* **2005**, *16* (1), 102–108. https://doi.org/10.1093/annonc/mdi006.

(42) Dahabreh, I. J.; Terasawa, T.; Castaldi, P. J.; Trikalinos, T. A. Systematic Review: Anti–Epidermal Growth Factor Receptor Treatment Effect Modification by *KRAS* Mutations in Advanced

Colorectal Cancer. *Annals of Internal Medicine* **2011**, *154* (1), 37. https://doi.org/10.7326/0003-4819-154-1-201101040-00006.

(43) Diaz Jr, L. A.; Williams, R. T.; Wu, J.; Kinde, I.; Hecht, J. R.; Berlin, J.; Allen, B.; Bozic, I.; Reiter, J. G.; Nowak, M. A.; Kinzler, K. W.; Oliner, K. S.; Vogelstein, B. The Molecular Evolution of Acquired Resistance to Targeted EGFR Blockade in Colorectal Cancers. *Nature* **2012**, *486* (7404), 537–540. https://doi.org/10.1038/nature11219.

(44) Siravegna, G.; Mussolin, B.; Buscarino, M.; Corti, G.; Cassingena, A.; Crisafulli, G.; Ponzetti, A.; Cremolini, C.; Amatu, A.; Lauricella, C.; Lamba, S.; Hobor, S.; Avallone, A.; Valtorta, E.; Rospo, G.; Medico, E.; Motta, V.; Antoniotti, C.; Tatangelo, F.; Bellosillo, B.; Veronese, S.; Budillon, A.; Montagut, C.; Racca, P.; Marsoni, S.; Falcone, A.; Corcoran, R. B.; Di Nicolantonio, F.; Loupakis, F.; Siena, S.; Sartore-Bianchi, A.; Bardelli, A. Clonal Evolution and Resistance to EGFR Blockade in the Blood of Colorectal Cancer Patients. *Nature Medicine* **2015**, *21* (7), 795–801. https://doi.org/10.1038/nm.3870.

(45) Bardelli, A.; Corso, S.; Bertotti, A.; Hobor, S.; Valtorta, E.; Siravegna, G.; Sartore-Bianchi, A.; Scala, E.; Cassingena, A.; Zecchin, D.; Apicella, M.; Migliardi, G.; Galimi, F.; Lauricella, C.; Zanon, C.; Perera, T.; Veronese, S.; Corti, G.; Amatu, A.; Gambacorta, M.; Diaz, L. A.; Sausen, M.; Velculescu, V. E.; Comoglio, P.; Trusolino, L.; Di Nicolantonio, F.; Giordano, S.; Siena, S. Amplification of the *MET* Receptor Drives Resistance to Anti-EGFR Therapies in Colorectal Cancer. *Cancer Discovery* **2013**, *3* (6), 658–673. https://doi.org/10.1158/2159-8290.CD-12-0558.

(46) Ferlay, J.; Soerjomataram, I.; Dikshit, R.; Eser, S.; Mathers, C.; Rebelo, M.; Parkin, D. M.; Forman, D.; Bray, F. Cancer Incidence and Mortality Worldwide: Sources, Methods and Major Patterns in GLOBOCAN 2012: Globocan 2012. *International Journal of Cancer* **2015**, *136* (5), E359–E386. https://doi.org/10.1002/ijc.29210.

(47) The Cancer Genome Atlas Network. Comprehensive Molecular Characterization of Human Colon and Rectal Cancer. *Nature* **2012**, *487* (7407), 330–337. https://doi.org/10.1038/nature11252.

(48) Bosset, J.-F.; Collette, L.; Calais, G.; Mineur, L.; Maingon, P.; Radosevic-Jelic, L.; Daban, A.; Bardet, E.; Beny, A.; Ollier, J.-C. Chemotherapy with Preoperative Radiotherapy in Rectal Cancer. *N Engl J Med* **2006**, *355* (11), 1114–1123. https://doi.org/10.1056/NEJMoa060829.

(49) van Gijn, W.; Marijnen, C. A.; Nagtegaal, I. D.; Kranenbarg, E. M.-K.; Putter, H.; Wiggers, T.; Rutten, H. J.; Påhlman, L.; Glimelius, B.; van de Velde, C. J. Preoperative Radiotherapy Combined with Total Mesorectal Excision for Resectable Rectal Cancer: 12-Year Follow-up of the Multicentre, Randomised Controlled TME Trial. *The Lancet Oncology* **2011**, *12* (6), 575–582. https://doi.org/10.1016/S1470-2045(11)70097-3.

(50) Engelen, S. M. E.; Maas, M.; Lahaye, M. J.; Leijtens, J. W. A.; van Berlo, C. L. H.; Jansen, R. L. H.; Breukink, S. O.; Dejong, C. H. C.; van de Velde, C. J. H.; Beets-Tan, R. G. H.; Beets, G. L. Modern Multidisciplinary Treatment of Rectal Cancer Based on Staging with Magnetic Resonance Imaging Leads to Excellent Local Control, but Distant Control Remains a Challenge. *European Journal of Cancer* **2013**, *49* (10), 2311–2320. https://doi.org/10.1016/j.ejca.2013.03.006.

(51) Bujko, K.; Glynne-Jones, R.; Bujko, M. Does Adjuvant Fluoropyrimidine-Based Chemotherapy Provide a Benefit for Patients with Resected Rectal Cancer Who Have Already Received

Neoadjuvant Radiochemotherapy? A Systematic Review of Randomised Trials. *Annals of Oncology* **2010**, *21* (9), 1743–1750. https://doi.org/10.1093/annonc/mdq054.

(52) Breugom, A. J.; Swets, M.; Bosset, J.-F.; Collette, L.; Sainato, A.; Cionini, L.; Glynne-Jones, R.; Counsell, N.; Bastiaannet, E.; van den Broek, C. B. M.; Liefers, G.-J.; Putter, H.; van de Velde, C. J. H. Adjuvant Chemotherapy after Preoperative (Chemo)Radiotherapy and Surgery for Patients with Rectal Cancer: A Systematic Review and Meta-Analysis of Individual Patient Data. *The Lancet Oncology* **2015**, *16* (2), 200–207. https://doi.org/10.1016/S1470-2045(14)71199-4.

(53) Sanghera, P.; Wong, D. W. Y.; McConkey, C. C.; Geh, J. I.; Hartley, A. Chemoradiotherapy for Rectal Cancer: An Updated Analysis of Factors Affecting Pathological Response. *Clinical Oncology* **2008**, *20* (2), 176–183. https://doi.org/10.1016/j.clon.2007.11.013.

(54) Maas, M.; Nelemans, P. J.; Valentini, V.; Das, P.; Rödel, C.; Kuo, L.-J.; Calvo, F. A.; García-Aguilar, J.; Glynne-Jones, R.; Haustermans, K.; Mohiuddin, M.; Pucciarelli, S.; Small, W.; Suárez, J.; Theodoropoulos, G.; Biondo, S.; Beets-Tan, R. G.; Beets, G. L. Long-Term Outcome in Patients with a Pathological Complete Response after Chemoradiation for Rectal Cancer: A Pooled Analysis of Individual Patient Data. *The Lancet Oncology* **2010**, *11* (9), 835–844. https://doi.org/10.1016/S1470-2045(10)70172-8.

(55) Zorcolo, L.; Rosman, A. S.; Restivo, A.; Pisano, M.; Nigri, G. R.; Fancellu, A.; Melis, M. Complete Pathologic Response after Combined Modality Treatment for Rectal Cancer and Long-Term Survival: A Meta-Analysis. *Annals of Surgical Oncology* **2012**, *19* (9), 2822–2832. https://doi.org/10.1245/s10434-011-2209-y.

(56) Pang, K.; Rao, Q.; Qin, S.; Jin, L.; Yao, H.; Zhang, Z. Prognosis Comparison between Wait and Watch and Surgical Strategy on Rectal Cancer Patients after Treatment with Neoadjuvant Chemoradiotherapy: A Meta-Analysis. *Therapeutic Advances in Gastroenterology* **2019**, *12*, 175628481989247. https://doi.org/10.1177/1756284819892477.

(57) Renehan, A. G.; Malcomson, L.; Emsley, R.; Gollins, S.; Maw, A.; Myint, A. S.; Rooney, P. S.; Susnerwala, S.; Blower, A.; Saunders, M. P.; Wilson, M. S.; Scott, N.; O'Dwyer, S. T. Watch-and-Wait Approach versus Surgical Resection after Chemoradiotherapy for Patients with Rectal Cancer (the OnCoRe Project): A Propensity-Score Matched Cohort Analysis. *The Lancet Oncology* **2016**, *17* (2), 174–183. https://doi.org/10.1016/S1470-2045(15)00467-2.

(58) Massihnia, D.; Pizzutilo, E. G.; Amatu, A.; Tosi, F.; Ghezzi, S.; Bencardino, K.; Di Masi, P.; Righetti, E.; Patelli, G.; Scaglione, F.; Vanzulli, A.; Siena, S.; Sartore-Bianchi, A. Liquid Biopsy for Rectal Cancer: A Systematic Review. *Cancer Treatment Reviews* **2019**, *79*, 101893. https://doi.org/10.1016/j.ctrv.2019.101893.

(59) Pazdirek, F.; Minarik, M.; Benesova, L.; Halkova, T.; Belsanova, B.; Macek, M.; Stepanek, L.; Hoch, J. Monitoring of Early Changes of Circulating Tumor DNA in the Plasma of Rectal Cancer Patients Receiving Neoadjuvant Concomitant Chemoradiotherapy: Evaluation for Prognosis and Prediction of Therapeutic Response. *Frontiers in Oncology* **2020**, *10*. https://doi.org/10.3389/fonc.2020.01028.

(60) Do Canto, L. M. do; Larsen, S. J.; Catin Kupper, B. E.; Begnami, M. D. F. de S.; Scapulatempo-Neto, C.; Petersen, A. H.; Aagaard, M. M.; Baumbach, J.; Aguiar, S.; Rogatto, S. R. Increased Levels

of Genomic Instability and Mutations in Homologous Recombination Genes in Locally Advanced Rectal Carcinomas. *Frontiers in Oncology* **2019**, *9*. https://doi.org/10.3389/fonc.2019.00395.

(61) Shioya, M.; Takahashi, T.; Ishikawa, H.; Sakurai, H.; Ebara, T.; Suzuki, Y.; Saitoh, J.; Ohno, T.; Asao, T.; Kuwano, H.; Nakano, T. Expression of Hypoxia-Inducible Factor 1α Predicts Clinical Outcome after Preoperative Hyperthermo-Chemoradiotherapy for Locally Advanced Rectal Cancer. *Journal of Radiation Research* **2011**, *52* (6), 821–827. https://doi.org/10.1269/jrr.11117.

(62) Vanderstichele, A.; Busschaert, P.; Smeets, D.; Landolfo, C.; Van Nieuwenhuysen, E.; Leunen, K.; Neven, P.; Amant, F.; Mahner, S.; Braicu, E. I.; Zeilinger, R.; Coosemans, A.; Timmerman, D.; Lambrechts, D.; Vergote, I. Chromosomal Instability in Cell-Free DNA as a Highly Specific Biomarker for Detection of Ovarian Cancer in Women with Adnexal Masses. *Clinical Cancer Research* **2017**, *23* (9), 2223–2231. https://doi.org/10.1158/1078-0432.CCR-16-1078.

(63) Rubin, B. P.; Heinrich, M. C.; Corless, C. L. Gastrointestinal Stromal Tumour. *The Lancet* **2007**, *369* (9574), 1731–1741. https://doi.org/10.1016/S0140-6736(07)60780-6.

(64) Søreide, K.; Sandvik, O. M.; Søreide, J. A.; Giljaca, V.; Jureckova, A.; Bulusu, V. R. Global Epidemiology of Gastrointestinal Stromal Tumours (GIST): A Systematic Review of Population-Based Cohort Studies. *Cancer Epidemiology* **2016**, *40*, 39–46. https://doi.org/10.1016/j.canep.2015.10.031.

(65) Corless, C. L.; Barnett, C. M.; Heinrich, M. C. Gastrointestinal Stromal Tumours: Origin and Molecular Oncology. *Nature Reviews Cancer* **2011**, *11* (12), 865–878. https://doi.org/10.1038/nrc3143.

(66) Corless, C. L.; Fletcher, J. A.; Heinrich, M. C. Biology of Gastrointestinal Stromal Tumors. *JCO* **2004**, *22* (18), 3813–3825. https://doi.org/10.1200/JCO.2004.05.140.

(67) Liang, J.; Wu, Y.-L.; Chen, B.-J.; Zhang, W.; Tanaka, Y.; Sugiyama, H. The C-Kit Receptor-Mediated Signal Transduction and Tumor-Related Diseases. *International Journal of Biological Sciences* **2013**, *9* (5), 435–443. https://doi.org/10.7150/ijbs.6087.

(68) Kays, J. K.; Sohn, J. D.; Kim, B. J.; Goze, K.; Koniaris, L. G. Approach to Wild-Type Gastrointestinal Stromal Tumors. *Translational Gastroenterology and Hepatology* **2018**, *3*, 92–92. https://doi.org/10.21037/tgh.2018.10.13.

(69) Flavahan, W. A.; Drier, Y.; Johnstone, S. E.; Hemming, M. L.; Tarjan, D. R.; Hegazi, E.; Shareef, S. J.; Javed, N. M.; Raut, C. P.; Eschle, B. K.; Gokhale, P. C.; Hornick, J. L.; Sicinska, E. T.; Demetri, G. D.; Bernstein, B. E. Altered Chromosomal Topology Drives Oncogenic Programs in SDH-Deficient GISTs. *Nature* **2019**, *575* (7781), 229–233. https://doi.org/10.1038/s41586-019-1668-3.

(70) Schaefer, I.-M.; Wang, Y.; Liang, C.; Bahri, N.; Quattrone, A.; Doyle, L.; Mariño-Enríquez, A.; Lauria, A.; Zhu, M.; Debiec-Rychter, M.; Grunewald, S.; Hechtman, J. F.; Dufresne, A.; Antonescu, C. R.; Beadling, C.; Sicinska, E. T.; van de Rijn, M.; Demetri, G. D.; Ladanyi, M.; Corless, C. L.; Heinrich, M. C.; Raut, C. P.; Bauer, S.; Fletcher, J. A. MAX Inactivation Is an Early Event in GIST Development That Regulates P16 and Cell Proliferation. *Nature Communications* **2017**, *8* (1). https://doi.org/10.1038/ncomms14674.

(71) Schneider-Stock, R.; Boltze, C.; Lasota, J.; Peters, B.; Corless, C. L.; Ruemmele, P.; Terracciano, L.; Pross, M.; Insabato, L.; Vizio, D. D.; Iesalnieks, I.; Dirnhofer, S.; Hartmann, A.; Heinrich, M.; Miettinen, M.; Roessner, A.; Tornillo, L. Loss of P16 Protein Defines High-Risk Patients with Gastrointestinal Stromal Tumors: A Tissue Microarray Study. 9.

(72) Heinrich, M. C. PDGFRA Activating Mutations in Gastrointestinal Stromal Tumors. *Science* **2003**, *299* (5607), 708–710. https://doi.org/10.1126/science.1079666.

(73) Hirota, S. Gain-of-Function Mutations of c-Kit in Human Gastrointestinal Stromal Tumors. *Science* **1998**, *279* (5350), 577–580. https://doi.org/10.1126/science.279.5350.577.

(74) Demetri, G. D.; von Mehren, M.; Blanke, C. D.; Van den Abbeele, A. D.; Eisenberg, B.; Roberts, P. J.; Heinrich, M. C.; Tuveson, D. A.; Singer, S.; Janicek, M.; Fletcher, J. A.; Silverman, S. G.; Silberman, S. L.; Capdeville, R.; Kiese, B.; Peng, B.; Dimitrijevic, S.; Druker, B. J.; Corless, C.; Fletcher, C. D. M.; Joensuu, H. Efficacy and Safety of Imatinib Mesylate in Advanced Gastrointestinal Stromal Tumors. *New England Journal of Medicine* **2002**, *347* (7), 472–480. https://doi.org/10.1056/NEJMoa020461.

(75) Andersson, J.; Bümming, P.; Meis–Kindblom, J. M.; Sihto, H.; Nupponen, N.; Joensuu, H.; Odén, A.; Gustavsson, B.; Kindblom, L.; Nilsson, B. Gastrointestinal Stromal Tumors With KIT Exon 11 Deletions Are Associated With Poor Prognosis. *Gastroenterology* **2006**, *130* (6), 1573–1581. https://doi.org/10.1053/j.gastro.2006.01.043.

(76) Liu, X.-H. Prognostic Value of KIT Mutation in Gastrointestinal Stromal Tumors. *World Journal of Gastroenterology* **2005**, *11* (25), 3948. https://doi.org/10.3748/wjg.v11.i25.3948.

(77) Corless, C. L.; Schroeder, A.; Griffith, D.; Town, A.; McGreevey, L.; Harrell, P.; Shiraga, S.; Bainbridge, T.; Morich, J.; Heinrich, M. C. *PDGFRA* Mutations in Gastrointestinal Stromal Tumors: Frequency, Spectrum and In Vitro Sensitivity to Imatinib. *Journal of Clinical Oncology* **2005**, *23* (23), 5357–5364. https://doi.org/10.1200/JCO.2005.14.068.

(78) Heinrich, M. C.; Corless, C. L.; Demetri, G. D.; Blanke, C. D.; von Mehren, M.; Joensuu, H.; McGreevey, L. S.; Chen, C.-J.; Van den Abbeele, A. D.; Druker, B. J.; Kiese, B.; Eisenberg, B.; Roberts, P. J.; Singer, S.; Fletcher, C. D. M.; Silberman, S.; Dimitrijevic, S.; Fletcher, J. A. Kinase Mutations and Imatinib Response in Patients With Metastatic Gastrointestinal Stromal Tumor. *JCO* **2003**, *21* (23), 4342–4349. https://doi.org/10.1200/JCO.2003.04.190.

(79) Patrikidou, A.; Chabaud, S.; Ray-Coquard, I.; Bui, B. N.; Adenis, A.; Rios, M.; Bertucci, F.; Duffaud, F.; Chevreau, C.; Cupissol, D.; Domont, J.; Pérol, D.; Blay, J. Y.; Le Cesne, A. Influence of Imatinib Interruption and Rechallenge on the Residual Disease in Patients with Advanced GIST: Results of the BFR14 Prospective French Sarcoma Group Randomised, Phase III Trial. *Annals of Oncology* **2013**, *24* (4), 1087–1093. https://doi.org/10.1093/annonc/mds587.

(80) Liegl, B.; Kepten, I.; Le, C.; Zhu, M.; Demetri, G.; Heinrich, M.; Fletcher, C.; Corless, C.; Fletcher, J. Heterogeneity of Kinase Inhibitor Resistance Mechanisms in GIST. *The Journal of Pathology* **2008**, *216* (1), 64–74. https://doi.org/10.1002/path.2382.

(81) Serrano, C.; George, S. Gastrointestinal Stromal Tumor: Challenges and Opportunities for a New Decade. *Clinical Cancer Research* **2020**, *26* (19), 5078–5085. https://doi.org/10.1158/1078-0432.CCR-20-1706.

(82) Blay, J.-Y.; Serrano, C.; Heinrich, M. C.; Zalcberg, J.; Bauer, S.; Gelderblom, H.; Schöffski, P.; Jones, R. L.; Attia, S.; D'Amato, G.; Chi, P.; Reichardt, P.; Meade, J.; Shi, K.; Ruiz-Soto, R.; George, S.; von Mehren, M. Ripretinib in Patients with Advanced Gastrointestinal Stromal Tumours (INVICTUS): A Double-Blind, Randomised, Placebo-Controlled, Phase 3 Trial. *The Lancet Oncology* **2020**, *21* (7), 923–934. https://doi.org/10.1016/S1470-2045(20)30168-6.

(83) Serrano, C.; Mariño-Enríquez, A.; Tao, D. L.; Ketzer, J.; Eilers, G.; Zhu, M.; Yu, C.; Mannan, A. M.; Rubin, B. P.; Demetri, G. D.; Raut, C. P.; Presnell, A.; McKinley, A.; Heinrich, M. C.; Czaplinski, J. T.; Sicinska, E.; Bauer, S.; George, S.; Fletcher, J. A. Complementary Activity of Tyrosine Kinase Inhibitors against Secondary Kit Mutations in Imatinib-Resistant Gastrointestinal Stromal Tumours. *British Journal of Cancer* **2019**, *120* (6), 612–620. https://doi.org/10.1038/s41416-019-0389-6.

(84) von Mehren, M.; Randall, R. L.; Benjamin, R. S.; Boles, S.; Bui, M. M.; Ganjoo, K. N.; George, S.; Gonzalez, R. J.; Heslin, M. J.; Kane, J. M.; Keedy, V.; Kim, E.; Koon, H.; Mayerson, J.; McCarter, M.; McGarry, S. V.; Meyer, C.; Morris, Z. S.; O'Donnell, R. J.; Pappo, A. S.; Paz, I. B.; Petersen, I. A.; Pfeifer, J. D.; Riedel, R. F.; Ruo, B.; Schuetze, S.; Tap, W. D.; Wayne, J. D.; Bergman, M. A.; Scavone, J. L. Soft Tissue Sarcoma, Version 2.2018, NCCN Clinical Practice Guidelines in Oncology. *Journal of the National Comprehensive Cancer Network* **2018**, *16* (5), 536–563. https://doi.org/10.6004/jnccn.2018.0025.

(85) Demetri, G. D.; Reichardt, P.; Kang, Y.-K.; Blay, J.-Y.; Rutkowski, P.; Gelderblom, H.; Hohenberger, P.; Leahy, M.; von Mehren, M.; Joensuu, H.; Badalamenti, G.; Blackstein, M.; Le Cesne, A.; Schöffski, P.; Maki, R. G.; Bauer, S.; Nguyen, B. B.; Xu, J.; Nishida, T.; Chung, J.; Kappeler, C.; Kuss, I.; Laurent, D.; Casali, P. G. Efficacy and Safety of Regorafenib for Advanced Gastrointestinal Stromal Tumours after Failure of Imatinib and Sunitinib (GRID): An International, Multicentre, Randomised, Placebo-Controlled, Phase 3 Trial. *The Lancet* **2013**, *381* (9863), 295–302. https://doi.org/10.1016/S0140-6736(12)61857-1.

(86) Kang, G.; Sohn, B. S.; Pyo, J.-S.; Kim, J. Y.; Lee, B.; Kim, K.-M. Detecting Primary KIT Mutations in Presurgical Plasma of Patients with Gastrointestinal Stromal Tumor. *Molecular Diagnosis & Therapy* **2016**, *20* (4), 347–351. https://doi.org/10.1007/s40291-016-0203-6.

(87) Serrano, C.; Vivancos, A.; López-Pousa, A.; Matito, J.; Mancuso, F. M.; Valverde, C.; Quiroga, S.; Landolfi, S.; Castro, S.; Dopazo, C.; Sebio, A.; Virgili, A. C.; Menso, M. M.; Martín-Broto, J.; Sansó, M.; García-Valverde, A.; Rosell, J.; Fletcher, J. A.; George, S.; Carles, J.; Arribas, J. Clinical Value of next Generation Sequencing of Plasma Cell-Free DNA in Gastrointestinal Stromal Tumors. *BMC Cancer* **2020**, *20* (1). https://doi.org/10.1186/s12885-020-6597-x.

(88) Namløs, H. M.; Boye, K.; Mishkin, S. J.; Barøy, T.; Lorenz, S.; Bjerkehagen, B.; Stratford, E. W.; Munthe, E.; Kudlow, B. A.; Myklebost, O.; Meza-Zepeda, L. A. Noninvasive Detection of CtDNA Reveals Intratumor Heterogeneity and Is Associated with Tumor Burden in Gastrointestinal Stromal Tumor. *Molecular Cancer Therapeutics* **2018**, *17* (11), 2473–2480. https://doi.org/10.1158/1535-7163.MCT-18-0174.

(89) Jilg, S.; Rassner, M.; Maier, J.; Waldeck, S.; Kehl, V.; Follo, M.; Philipp, U.; Sauter, A.; Specht, K.; Mitschke, J.; Lange, T.; Bauer, S.; Jost, P. J.; Peschel, C.; Duyster, J.; Gaiser, T.; Hohenberger, P.; Bubnoff, N. Circulating *CKIT* and *PDGFRA* DNA Indicates Disease Activity in Gastrointestinal Stromal Tumor (GIST). *International Journal of Cancer* **2019**, *145* (8), 2292–2303. https://doi.org/10.1002/ijc.32282.

(90) Peng, B.; Lloyd, P.; Schran, H. Clinical Pharmacokinetics of Imatinib: *Clinical Pharmacokinetics* **2005**, *44* (9), 879–894. https://doi.org/10.2165/00003088-200544090-00001.

(91) European Medicines Agency EPAR Product Information on Imatinib Glivec, Available at:Www.Ema.Europa.Eu/Ema/Index.Jsp?

Curl1⁄4pages/Medicines/Human/Medicines/000406/Human_med_000808.Jsp&mid1⁄4WC0b01ac058001d124.

(92) Peng, B.; Hayes, M.; Resta, D.; Racine-Poon, A.; Druker, B. J.; Talpaz, M.; Sawyers, C. L.; Rosamilia, M.; Ford, J.; Lloyd, P.; Capdeville, R. Pharmacokinetics and Pharmacodynamics of Imatinib in a Phase I Trial With Chronic Myeloid Leukemia Patients. *Journal of Clinical Oncology* **2004**, *22* (5), 935–942. https://doi.org/10.1200/JCO.2004.03.050.

(93) Picard, S.; Titier, K.; Etienne, G.; Teilhet, E.; Ducint, D.; Bernard, M.-A.; Lassalle, R.; Marit, G.; Reiffers, J.; Begaud, B.; Moore, N.; Molimard, M.; Mahon, F.-X. Trough Imatinib Plasma Levels Are Associated with Both Cytogenetic and Molecular Responses to Standard-Dose Imatinib in Chronic Myeloid Leukemia. *Blood* **2007**, *109* (8), 3496–3499. https://doi.org/10.1182/blood-2006-07-036012.

(94) Glabbeke, M. V.; Verweij, J.; Casali, P. G.; Simes, J.; Cesne, A. L.; Reichardt, P.; Issels, R.; Judson, I. R.; van Oosterom, A. T.; Blay, J.-Y. Predicting Toxicities for Patients with Advanced Gastrointestinal Stromal Tumours Treated with Imatinib: A Study of the European Organisation for Research and Treatment of Cancer, the Italian Sarcoma Group, and the Australasian Gastro-Intestinal Trials Group (EORTC–ISG–AGITG). *European Journal of Cancer* **2006**, *42* (14), 2277–2285. https://doi.org/10.1016/j.ejca.2006.03.029.

(95) Evans, W. E.; McLeod, H. L. Pharmacogenomics — Drug Disposition, Drug Targets, and Side Effects. *New England Journal of Medicine* **2003**, *348* (6), 538–549. https://doi.org/10.1056/NEJMra020526.

(96) Relling, M. V.; Klein, T. E. CPIC: Clinical Pharmacogenetics Implementation Consortium of the Pharmacogenomics Research Network. *Clinical Pharmacology & Therapeutics* **2011**, *89* (3), 464–467. https://doi.org/10.1038/clpt.2010.279.

(97) Swen, J. J.; Nijenhuis, M.; de Boer, A.; Grandia, L.; Maitland-van der Zee, A. H.; Mulder, H.; Rongen, G. A. P. J. M.; van Schaik, R. H. N.; Schalekamp, T.; Touw, D. J.; van der Weide, J.; Wilffert, B.; Deneer, V. H. M.; Guchelaar, H.-J. Pharmacogenetics: From Bench to Byte— An Update of Guidelines. *Clinical Pharmacology & Therapeutics* **2011**, *89* (5), 662–673. https://doi.org/10.1038/clpt.2011.34.

(98) van Kuilenburg, A. B. P. Dihydropyrimidine Dehydrogenase and the Efficacy and Toxicity of 5-Fluorouracil. *European Journal of Cancer* **2004**, *40* (7), 939–950. https://doi.org/10.1016/j.ejca.2003.12.004.

(99) Henricks, L. M.; Lunenburg, C. A. T. C.; de Man, F. M.; Meulendijks, D.; Frederix, G. W. J.; Kienhuis, E.; Creemers, G.-J.; Baars, A.; Dezentjé, V. O.; Imholz, A. L. T.; Jeurissen, F. J. F.; Portielje, J. E. A.; Jansen, R. L. H.; Hamberg, P.; ten Tije, A. J.; Droogendijk, H. J.; Koopman, M.; Nieboer, P.; van de Poel, M. H. W.; Mandigers, C. M. P. W.; Rosing, H.; Beijnen, J. H.; Werkhoven, E. van; van Kuilenburg, A. B. P.; van Schaik, R. H. N.; Mathijssen, R. H. J.; Swen, J. J.; Gelderblom, H.; Cats, A.; Guchelaar, H.-J.; Schellens, J. H. M. DPYD Genotype-Guided Dose Individualisation of Fluoropyrimidine Therapy in Patients with Cancer: A Prospective Safety Analysis. *The Lancet Oncology* **2018**, *19* (11), 1459–1467. https://doi.org/10.1016/S1470-2045(18)30686-7.

(100) Henricks, L. M.; Lunenburg, C. A.; Meulendijks, D.; Gelderblom, H.; Cats, A.; Swen, J. J.; Schellens, J. H.; Guchelaar, H.-J. Translating *DPYD* Genotype into DPD Phenotype: Using the *DPYD* Gene Activity Score. *Pharmacogenomics* **2015**, *16* (11), 1275–1284. https://doi.org/10.2217/pgs.15.70.

(101) Amstutz, U.; Henricks, L. M.; Offer, S. M.; Barbarino, J.; Schellens, J. H. M.; Swen, J. J.; Klein, T. E.; McLeod, H. L.; Caudle, K. E.; Diasio, R. B.; Schwab, M. Clinical Pharmacogenetics Implementation Consortium (CPIC) Guideline for Dihydropyrimidine Dehydrogenase Genotype and Fluoropyrimidine Dosing: 2017 Update. *Clinical Pharmacology & Therapeutics* **2018**, *103* (2), 210–216. https://doi.org/10.1002/cpt.911.

(102) Lunenburg, C. A. T. C.; Henricks, L. M.; Guchelaar, H.-J.; Swen, J. J.; Deenen, M. J.; Schellens, J. H. M.; Gelderblom, H. Prospective DPYD Genotyping to Reduce the Risk of Fluoropyrimidine-Induced Severe Toxicity: Ready for Prime Time. *European Journal of Cancer* **2016**, *54*, 40–48. https://doi.org/10.1016/j.ejca.2015.11.008.

(103) Toffoli, G.; Innocenti, F.; Polesel, J.; De Mattia, E.; Sartor, F.; Dalle Fratte, C.; Ecca, F.; Dreussi, E.; Palazzari, E.; Guardascione, M.; Buonadonna, A.; Foltran, L.; Garziera, M.; Bignucolo, A.; Nobili, S.; Mini, E.; Favaretto, A.; Berretta, M.; D'Andrea, M.; De Paoli, A.; Roncato, R.; Cecchin, E. The Genotype for *DPYD* Risk Variants in Patients With Colorectal Cancer and the Related Toxicity Management Costs in Clinical Practice. *Clinical Pharmacology & Therapeutics* **2019**, *105* (4), 994–1002. https://doi.org/10.1002/cpt.1257.

(104) Fragoulakis, V.; Roncato, R.; Dalle Fratte, C.; Ecca, F.; Bartsakoulia, M.; Innocenti, F.; Toffoli, G.; Cecchin, E.; Patrinos, G. P.; Mitropoulou, C. Estimating the Effectiveness of DPYD Genotyping in Italian Individuals Suffering from Cancer Based on the Cost of Chemotherapy-Induced Toxicity. *The American Journal of Human Genetics* **2019**, *104* (6), 1158–1168. https://doi.org/10.1016/j.ajhg.2019.04.017.

(105) Eechoute, K.; Sparreboom, A.; Burger, H.; Franke, R. M.; Schiavon, G.; Verweij, J.; Loos, W. J.; Wiemer, E. A. C.; Mathijssen, R. H. J. Drug Transporters and Imatinib Treatment: Implications for Clinical Practice. *Clinical Cancer Research* **2011**, *17* (3), 406–415. https://doi.org/10.1158/1078-0432.CCR-10-2250.

(106) Burger, H.; van Tol, H.; Boersma, A. W. M.; Brok, M.; Wiemer, E. A. C.; Stoter, G.; Nooter, K. Imatinib Mesylate (STI571) Is a Substrate for the Breast Cancer Resistance Protein (BCRP)/ABCG2 Drug Pump. *Blood* **2004**, *104* (9), 2940–2942. https://doi.org/10.1182/blood-2004-04-1398.

(107) Verboom, M. C.; Kloth, J. S. L.; Swen, J. J.; Sleijfer, S.; Reyners, A. K. L.; Steeghs, N.; Mathijssen, R. H. J.; Gelderblom, H.; Guchelaar, H.-J. Genetic Polymorphisms in ABCG2 and CYP1A2 Are Associated with Imatinib Dose Reduction in Patients Treated for Gastrointestinal Stromal Tumors. *The Pharmacogenomics Journal* **2019**, *19* (5), 473–479. https://doi.org/10.1038/s41397-019-0079-z.

(108) Kim, D. H.; Sriharsha, L.; Xu, W.; Kamel-Reid, S.; Liu, X.; Siminovitch, K.; Messner, H. A.; Lipton, J. H. Clinical Relevance of a Pharmacogenetic Approach Using Multiple Candidate Genes to Predict Response and Resistance to Imatinib Therapy in Chronic Myeloid Leukemia. *Clinical Cancer Research* **2009**, *15* (14), 4750–4758. https://doi.org/10.1158/1078-0432.CCR-09-0145.

(109) Koo, D.-H.; Ryu, M.-H.; Ryoo, B.-Y.; Beck, M. Y.; Na, Y.-S.; Shin, J.-G.; Lee, S. S.; Kim, E.-Y.; Kang, Y.-K. Association of ABCG2 Polymorphism with Clinical Efficacy of Imatinib in Patients with Gastrointestinal Stromal Tumor. *Cancer Chemotherapy and Pharmacology* **2015**, *75* (1), 173–182. https://doi.org/10.1007/s00280-014-2630-6.

(110) Liu, J.; Chen, Z.; Chen, H.; Hou, Y.; Lu, W.; He, J.; Tong, H.; Zhou, Y.; Cai, W. Genetic Polymorphisms Contribute to the Individual Variations of Imatinib Mesylate Plasma Levels and

Adverse Reactions in Chinese GIST Patients. *International Journal of Molecular Sciences* **2017**, *18* (3), 603. https://doi.org/10.3390/ijms18030603.

(111) Von Richter, O.; Burk, O.; Fromm, M.; Thon, K.; Eichelbaum, M.; Kivisto, K. Cytochrome P450 3A4 and P-Glycoprotein Expression in Human Small Intestinal Enterocytes and Hepatocytes: A Comparative Analysis in Paired Tissue Specimens. *Clinical Pharmacology & Therapeutics* **2004**, *75* (3), 172–183. https://doi.org/10.1016/j.clpt.2003.10.008.

(112) Schuetz, E. G.; Schinkel, A. H.; Relling, M. V.; Schuetz, J. D. P-Glycoprotein: A Major Determinant of Rifampicin-Inducible Expression of Cytochrome P4503A in Mice and Humans. *Proceedings of the National Academy of Sciences* **1996**, *93* (9), 4001–4005. https://doi.org/10.1073/pnas.93.9.4001.

(113) Dagenais, C.; Avdeef, A.; Tsinman, O.; Dudley, A.; Beliveau, R. P-Glycoprotein Deficient Mouse in Situ Blood–Brain Barrier Permeability and Its Prediction Using an in Combo PAMPA Model. *European Journal of Pharmaceutical Sciences* **2009**, *38* (2), 121–137. https://doi.org/10.1016/j.ejps.2009.06.009.

(114) Hoffmeyer, S.; Burk, O.; Eichelbaum, M.; Brinkmann, U. Functional Polymorphisms of the Human Multidrug- Resistance Gene: Multiple Sequence Variations and Correlation of One Allele with P-Glycoprotein Expression and Activity in Vivo. *Medical Sciences* **2020**, *97* (7), 3473–3478.

(115) Loeuillet, C.; Weale, M.; Deutsch, S.; Rotger, M.; Soranzo, N.; Wyniger, J.; Lettre, G.; Dupré, Y.; Thuillard, D.; Beckmann, J. S.; Antonarakis, S. E.; Goldstein, D. B.; Telenti, A. Promoter Polymorphisms and Allelic Imbalance in ABCB1 Expression: *Pharmacogenetics and Genomics* **2007**, *17* (11), 951–959. https://doi.org/10.1097/FPC.0b013e3282eff934.

(116) Filppula, A.; Laitila, J.; Neuvonen, P.; Backman, J. Potent Mechanism-Based Inhibition of CYP3A4 by Imatinib Explains Its Liability to Interact with CYP3A4 Substrates: Imatinib Is a Time-Dependent CYP3A4 Inhibitor. *British Journal of Pharmacology* **2012**, *165* (8), 2787–2798. https://doi.org/10.1111/j.1476-5381.2011.01732.x.

(117) Dutreix, C.; Peng, B.; Mehring, G.; Hayes, M.; Capdeville, R.; Pokorny, R.; Seiberling, M. Pharmacokinetic Interaction between Ketoconazole and Imatinib Mesylate (Glivec) in Healthy Subjects. *Cancer Chemotherapy and Pharmacology* **2004**, *54* (4). https://doi.org/10.1007/s00280-004-0832-z.

(118) van Erp, N. P.; Gelderblom, H.; Karlsson, M. O.; Li, J.; Zhao, M.; Ouwerkerk, J.; Nortier, J. W.; Guchelaar, H.-J.; Baker, S. D.; Sparreboom, A. Influence of CYP3A4 Inhibition on the Steady-State Pharmacokinetics of Imatinib. *Clinical Cancer Research* **2007**, *13* (24), 7394–7400. https://doi.org/10.1158/1078-0432.CCR-07-0346.

(119) Filppula, A. M.; Neuvonen, M.; Laitila, J.; Neuvonen, P. J.; Backman, J. T. Autoinhibition of CYP3A4 Leads to Important Role of CYP2C8 in Imatinib Metabolism: Variability in CYP2C8 Activity May Alter Plasma Concentrations and Response. *Drug Metabolism and Disposition* **2013**, *41* (1), 50–59. https://doi.org/10.1124/dmd.112.048017.

(120) Kirchheiner, J.; Thomas, S.; Bauer, S.; Tomalikscharte, D.; Hering, U.; Doroshyenko, O.; Jetter, A.; Stehle, S.; Tsahuridu, M.; Meineke, I. Pharmacokinetics and Pharmacodynamics of Rosiglitazone in Relation to CYP2C8 Genotype. *Clinical Pharmacology & Therapeutics* **2006**, *80* (6), 657–667. https://doi.org/10.1016/j.clpt.2006.09.008.

(121) Tornio, A.; Niemi, M.; Neuvonen, P. J.; Backman, J. T. Trimethoprim and the *CYP2C8 * 3* Allele Have Opposite Effects on the Pharmacokinetics of Pioglitazone. *Drug Metabolism and Disposition* **2008**, *36* (1), 73–80. https://doi.org/10.1124/dmd.107.018010.

(122) Aquilante, C. L.; Kosmiski, L. A.; Bourne, D. W. A.; Bushman, L. R.; Daily, E. B.; Hammond, K. P.; Hopley, C. W.; Kadam, R. S.; Kanack, A. T.; Kompella, U. B.; Le, M.; Predhomme, J. A.; Rower, J. E.; Sidhom, M. S. Impact of the *CYP2C8 * 3* Polymorphism on the Drug-Drug Interaction between Gemfibrozil and Pioglitazone: *CYP2C8 * 3* and the Interaction between Gemfibrozil and Pioglitazone. *British Journal of Clinical Pharmacology* **2013**, *75* (1), 217–226. https://doi.org/10.1111/j.1365-2125.2012.04343.x.

(123) Gardner, E.; Burger, H.; Vanschaik, R.; Vanoosterom, A.; Debruijn, E.; Guetens, G.; Prenen, H.; Dejong, F.; Baker, S.; Bates, S. Association of Enzyme and Transporter Genotypes with the Pharmacokinetics of Imatinib. *Clinical Pharmacology & Therapeutics* **2006**, *80* (2), 192–201. https://doi.org/10.1016/j.clpt.2006.05.003.

(124) Wang, Y.; Zhou, L.; Dutreix, C.; Leroy, E.; Yin, Q.; Sethuraman, V.; Riviere, G.-J.; Yin, O. Q. P.; Schran, H.; Shen, Z.-X. Effects of Imatinib (Glivec) on the Pharmacokinetics of Metoprolol, a CYP2D6 Substrate, in Chinese Patients with Chronic Myelogenous Leukaemia. *British Journal of Clinical Pharmacology* **2008**, *65* (6), 885–892. https://doi.org/10.1111/j.1365-2125.2008.03150.x.

(125) Hussaarts, K. G. A. M.; Veerman, G. D. M.; Jansman, F. G. A.; van Gelder, T.; Mathijssen, R. H. J.; van Leeuwen, R. W. F. Clinically Relevant Drug Interactions with Multikinase Inhibitors: A Review. *Therapeutic Advances in Medical Oncology* **2019**, *11*, 175883591881834. https://doi.org/10.1177/1758835918818347.

(126) Scripture, C. D.; Figg, W. D. Drug Interactions in Cancer Therapy. *Nature Reviews Cancer* **2006**, *6* (7), 546–558. https://doi.org/10.1038/nrc1887.

(127) Shah, R. R.; Smith, R. L. Addressing Phenoconversion: The Achilles' Heel of Personalized Medicine: Impact of Phenoconversion. *British Journal of Clinical Pharmacology* **2015**, *79* (2), 222–240. https://doi.org/10.1111/bcp.12441.

(128) Malki, M. A.; Pearson, E. R. Drug–Drug–Gene Interactions and Adverse Drug Reactions. *The Pharmacogenomics Journal* **2020**, *20* (3), 355–366. https://doi.org/10.1038/s41397-019-0122-0.

(129) Bahar, M. A.; Setiawan, D.; Hak, E.; Wilffert, B. Pharmacogenetics of Drug–Drug Interaction and Drug–Drug–Gene Interaction: A Systematic Review on CYP2C9, CYP2C19 and CYP2D6. *Pharmacogenomics* **2017**, *18* (7), 701–739. https://doi.org/10.2217/pgs-2017-0194.

(130) Robinson, J. T.; Thorvaldsdóttir, H.; Wenger, A. M.; Zehir, A.; Mesirov, J. P. Variant Review with the Integrative Genomics Viewer. *Cancer Research* **2017**, *77* (21), e31–e34. https://doi.org/10.1158/0008-5472.CAN-17-0337.

(131) Xu, C.; Gu, X.; Padmanabhan, R.; Wu, Z.; Peng, Q.; DiCarlo, J.; Wang, Y. SmCounter2: An Accurate Low-Frequency Variant Caller for Targeted Sequencing Data with Unique Molecular Identifiers. *Bioinformatics* **2019**, *35* (8), 1299–1309. https://doi.org/10.1093/bioinformatics/bty790.

(132) Reisinger, E.; Genthner, L.; Kerssemakers, J.; Kensche, P.; Borufka, S.; Jugold, A.; Kling, A.; Prinz, M.; Scholz, I.; Zipprich, G.; Eils, R.; Lawerenz, C.; Eils, J. OTP: An Automatized System for

Managing and Processing NGS Data. *J Biotechnol* **2017**, *261*, 53–62. https://doi.org/10.1016/j.jbiotec.2017.08.006.

(133) Adalsteinsson, V. A.; Ha, G.; Freeman, S. S.; Choudhury, A. D.; Stover, D. G.; Parsons, H. A.; Gydush, G.; Reed, S. C.; Rotem, D.; Rhoades, J.; Loginov, D.; Livitz, D.; Rosebrock, D.; Leshchiner, I.; Kim, J.; Stewart, C.; Rosenberg, M.; Francis, J. M.; Zhang, C.-Z.; Cohen, O.; Oh, C.; Ding, H.; Polak, P.; Lloyd, M.; Mahmud, S.; Helvie, K.; Merrill, M. S.; Santiago, R. A.; O'Connor, E. P.; Jeong, S. H.; Leeson, R.; Barry, R. M.; Kramkowski, J. F.; Zhang, Z.; Polacek, L.; Lohr, J. G.; Schleicher, M.; Lipscomb, E.; Saltzman, A.; Oliver, N. M.; Marini, L.; Waks, A. G.; Harshman, L. C.; Tolaney, S. M.; Van Allen, E. M.; Winer, E. P.; Lin, N. U.; Nakabayashi, M.; Taplin, M.-E.; Johannessen, C. M.; Garraway, L. A.; Golub, T. R.; Boehm, J. S.; Wagle, N.; Getz, G.; Love, J. C.; Meyerson, M. Scalable Whole-Exome Sequencing of Cell-Free DNA Reveals High Concordance with Metastatic Tumors. *Nature Communications* **2017**, *8* (1). https://doi.org/10.1038/s41467-017-00965-y.

(134) Shapiro, M. B.; Senapathy, P. RNA Splice Junctions of Different Classes of Eukaryotes: Sequence Statistics and Functional Implications in Gene Expression. *Nucleic Acids Res* **1987**, *15* (17), 7155–7174. https://doi.org/10.1093/nar/15.17.7155.

(135) Burge, C.; Karlin, S. Prediction of Complete Gene Structures in Human Genomic DNA. *Journal of Molecular Biology* **1997**, *268* (1), 78–94. https://doi.org/10.1006/jmbi.1997.0951.

(136) Hebsgaard, S. M.; Korning, P. G.; Tolstrup, N.; Engelbrecht, J.; Rouzé, P.; Brunak, S. Splice Site Prediction in Arabidopsis Thaliana Pre-MRNA by Combining Local and Global Sequence Information. *Nucleic Acids Res* **1996**, *24* (17), 3439–3452.

(137) Brunak, S.; Engelbrecht, J.; Knudsen, S. Prediction of Human MRNA Donor and Acceptor Sites from the DNA Sequence. *Journal of Molecular Biology* **1991**, *220* (1), 49–65. https://doi.org/10.1016/0022-2836(91)90380-O.

(138) Reese, M. G.; Eeckman, F. H.; Kulp, D.; Haussler, D. Improved Splice Site Detection in Genie. *Journal of Computational Biology* **1997**; *4* (3), 311-23. doi: 10.1089/cmb.1997.4.311.

(139) Yeo, G.; Burge, C. B. Maximum Entropy Modeling of Short Sequence Motifs with Applications to RNA Splicing Signals. *Journal of Computational Biology* **2004**;*11* (2-3), 377-94. doi: 10.1089/1066527041410418

(140) Houdayer, C.; Dehainault, C.; Mattler, C.; Michaux, D.; Caux-Moncoutier, V.; Pagès-Berhouet, S.; d'Enghien, C. D.; Laugé, A.; Castera, L.; Gauthier-Villars, M.; Stoppa-Lyonnet, D. Evaluation of in Silico Splice Tools for Decision-Making in Molecular Diagnosis. *Human Mutation* **2008**, *29* (7), 975–982. https://doi.org/10.1002/humu.20765.

(141) Desmet, F.-O.; Hamroun, D.; Lalande, M.; Collod-Béroud, G.; Claustres, M.; Béroud, C. Human Splicing Finder: An Online Bioinformatics Tool to Predict Splicing Signals. *Nucleic Acids Res* **2009**, *37* (9), e67. https://doi.org/10.1093/nar/gkp215.

(142) Thorn, C. F.; Klein, T. E.; Altman, R. B. PharmGKB: The Pharmacogenomics Knowledge Base. In *Pharmacogenomics*; Innocenti, F., van Schaik, R. H. N., Eds.; Methods in Molecular Biology; Humana Press: Totowa, NJ, **2013**; Vol. 1015, pp 311–320. https://doi.org/10.1007/978-1-62703-435-7_20.

(143) Desta, Z.; Gammal, R. S.; Gong, L.; Whirl-Carrillo, M.; Gaur, A. H.; Sukasem, C.; Hockings, J.; Myers, A.; Swart, M.; Tyndale, R. F.; Masimirembwa, C.; Iwuchukwu, O. F.; Chirwa, S.; Lennox, J.; Gaedigk, A.; Klein, T. E.; Haas, D. W. Clinical Pharmacogenetics Implementation Consortium (CPIC) Guideline for *CYP2B6* and Efavirenz-Containing Antiretroviral Therapy. *Clinical Pharmacology & Therapeutics* **2019**, *106* (4), 726–733. https://doi.org/10.1002/cpt.1477.

(144) Scott, S. A.; Sangkuhl, K.; Stein, C. M.; Hulot, J.-S.; Mega, J. L.; Roden, D. M.; Klein, T. E.; Sabatine, M. S.; Johnson, J. A.; Shuldiner, A. R. Clinical Pharmacogenetics Implementation Consortium Guidelines for CYP2C19 Genotype and Clopidogrel Therapy: 2013 Update. *Clinical Pharmacology & Therapeutics* **2013**, *94* (3), 317–323. https://doi.org/10.1038/clpt.2013.105.

(145) Theken, K. N.; Lee, C. R.; Gong, L.; Caudle, K. E.; Formea, C. M.; Gaedigk, A.; Klein, T. E.; Agúndez, J. A. G.; Grosser, T. Clinical Pharmacogenetics Implementation Consortium Guideline (CPIC) for *CYP2C9* and Nonsteroidal Anti-Inflammatory Drugs. *Clinical Pharmacology & Therapeutics* **2020**, *108* (2), 191–200. https://doi.org/10.1002/cpt.1830.

(146) Crews, K. R.; Gaedigk, A.; Dunnenberger, H. M.; Leeder, J. S.; Klein, T. E.; Caudle, K. E.; Haidar, C. E.; Shen, D. D.; Callaghan, J. T.; Sadhasivam, S.; Prows, C. A.; Kharasch, E. D.; Skaar, T. C. Clinical Pharmacogenetics Implementation Consortium Guidelines for Cytochrome P450 2D6 Genotype and Codeine Therapy: 2014 Update. *Clinical Pharmacology & Therapeutics* **2014**, *95* (4), 376–382. https://doi.org/10.1038/clpt.2013.254.

(147) Birdwell, K.; Decker, B.; Barbarino, J.; Peterson, J.; Stein, C.; Sadee, W.; Wang, D.; Vinks, A.; He, Y.; Swen, J.; Leeder, J.; van Schaik, R.; Thummel, K.; Klein, T.; Caudle, K.; MacPhee, I. Clinical Pharmacogenetics Implementation Consortium (CPIC) Guidelines for *CYP3A5* Genotype and Tacrolimus Dosing. *Clinical Pharmacology & Therapeutics* **2015**, *98* (1), 19–24. https://doi.org/10.1002/cpt.113.

(148) Wishart, D. S.; Feunang, Y. D.; Guo, A. C.; Lo, E. J.; Marcu, A.; Grant, J. R.; Sajed, T.; Johnson, D.; Li, C.; Sayeeda, Z.; Assempour, N.; Iynkkaran, I.; Liu, Y.; Maciejewski, A.; Gale, N.; Wilson, A.; Chin, L.; Cummings, R.; Le, D.; Pon, A.; Knox, C.; Wilson, M. DrugBank 5.0: A Major Update to the DrugBank Database for 2018. *Nucleic Acids Research* **2018**, *46* (D1), D1074–D1082. https://doi.org/10.1093/nar/gkx1037.

(149) Drug Interaction Checker. New York: Medscape; 1994. [Last Accessed on 2020 Oct 10]. Available from: Https://Reference.Medscape.Com/Drug-Interactionchecker.

(150) Flockhart DA. Drug Interactions: Cytochrome P450 Drug Interaction Table. Indiana University School of Medicine (2007). "Https://Drug-Interactions.Medicine.Iu.Edu" Accessed 10 April 2020.

(151) FDA: Https://Www.Fda.Gov/Drugs/Drug-Interactions-Labeling/Drug-Development-and-Drug-Interactions-Table-Substrates-Inhibitors-and-Inducers [Accessed 10 April 2020].

(152) LexiComp: Www.Lexi.Com. [Last Accessed on 2020 Apr 28]

(153) Mandard, A.-M.; Dalibard, F.; Mandard, J.-C.; Marnay, J.; Henry-Amar, M.; Petiot, J.-F.; Roussel, A.; Jacob, J.-H.; Segol, P.; Samama, G.; Ollivier, J.-M.; Bonvalot, S.; Gignoux, M. Pathologic Assessment of Tumor Regression after Preoperative Chemoradiotherapy of Esophageal Carcinoma. Clinicopathologic Correlations. *Cancer* **1994**, *73* (11), 2680–2686. https://doi.org/10.1002/1097-0142(19940601)73:11<2680::AID-CNCR2820731105>3.0.CO;2-C.

(154) Eisenhauer, E. A.; Therasse, P.; Bogaerts, J.; Schwartz, L. H.; Sargent, D.; Ford, R.; Dancey, J.; Arbuck, S.; Gwyther, S.; Mooney, M.; Rubinstein, L.; Shankar, L.; Dodd, L.; Kaplan, R.; Lacombe, D.; Verweij, J. New Response Evaluation Criteria in Solid Tumours: Revised RECIST Guideline (Version 1.1). *European Journal of Cancer* **2009**, *45* (2), 228–247. https://doi.org/10.1016/j.ejca.2008.10.026.

(155) Huang, D.; Sun, W.; Zhou, Y.; Li, P.; Chen, F.; Chen, H.; Xia, D.; Xu, E.; Lai, M.; Wu, Y.; Zhang, H. Mutations of Key Driver Genes in Colorectal Cancer Progression and Metastasis. *Cancer and Metastasis Reviews* **2018**, *37* (1), 173–187. https://doi.org/10.1007/s10555-017-9726-5.

(156) R Core Team (2013). R: A Language and Environment for Statistical Computing. R Foundation for Statistical Computing, Vienna, Austria.

(157) Myint, N. N. M.; Verma, A. M.; Fernandez-Garcia, D.; Sarmah, P.; Tarpey, P. S.; Al-Aqbi, S. S.; Cai, H.; Trigg, R.; West, K.; Howells, L. M.; Thomas, A.; Brown, K.; Guttery, D. S.; Singh, B.; Pringle, H. J.; McDermott, U.; Shaw, J. A.; Rufini, A. Circulating Tumor DNA in Patients with Colorectal Adenomas: Assessment of Detectability and Genetic Heterogeneity. *Cell Death & Disease* **2018**, *9* (9). https://doi.org/10.1038/s41419-018-0934-x.

(158) Mead, R.; Duku, M.; Bhandari, P.; Cree, I. A. Circulating Tumour Markers Can Define Patients with Normal Colons, Benign Polyps, and Cancers. *British Journal of Cancer* **2011**, *105* (2), 239–245. https://doi.org/10.1038/bjc.2011.230.

(159) Cerami, E.; Gao, J.; Dogrusoz, U.; Gross, B. E.; Sumer, S. O.; Aksoy, B. A.; Jacobsen, A.; Byrne, C. J.; Heuer, M. L.; Larsson, E.; Antipin, Y.; Reva, B.; Goldberg, A. P.; Sander, C.; Schultz, N. The CBio Cancer Genomics Portal: An Open Platform for Exploring Multidimensional Cancer Genomics Data: Figure 1. *Cancer Discovery* **2012**, *2* (5), 401–404. https://doi.org/10.1158/2159-8290.CD-12-0095.

(160) Gao, J.; Aksoy, B. A.; Dogrusoz, U.; Dresdner, G.; Gross, B.; Sumer, S. O.; Sun, Y.; Jacobsen, A.; Sinha, R.; Larsson, E.; Cerami, E.; Sander, C.; Schultz, N. Integrative Analysis of Complex Cancer Genomics and Clinical Profiles Using the CBioPortal. *Science Signaling* **2013**, *6* (269), pl1–pl1. https://doi.org/10.1126/scisignal.2004088.

(161) Landrum, M. J.; Lee, J. M.; Riley, G. R.; Jang, W.; Rubinstein, W. S.; Church, D. M.; Maglott, D. R. ClinVar: Public Archive of Relationships among Sequence Variation and Human Phenotype. *Nucleic Acids Research* **2014**, *42* (D1), D980–D985. https://doi.org/10.1093/nar/gkt1113.

(162) Adzhubei, I.; Jordan, D. M.; Sunyaev, S. R. Predicting Functional Effect of Human Missense Mutations Using PolyPhen-2. *Current Protocols in Human Genetics* **2013**, *76* (1), 7.20.1-7.20.41. https://doi.org/10.1002/0471142905.hg0720s76.

(163) Rogers, M. F.; Shihab, H. A.; Mort, M.; Cooper, D. N.; Gaunt, T. R.; Campbell, C. FATHMM-XF: Accurate Prediction of Pathogenic Point Mutations via Extended Features. *Bioinformatics* **2018**, *34* (3), 511–513. https://doi.org/10.1093/bioinformatics/btx536.

(164) Dalle Fratte, C.; Guardascione, M.; De Mattia, E.; Borsatti, E.; Boschetto, R.; Farruggio, A.; Canzonieri, V.; Romanato, L.; Borsatti, R.; Gagno, S.; Marangon, E.; Polano, M.; Buonadonna, A.; Toffoli, G.; Cecchin, E. Clonal Selection of a Novel Deleterious TP53 Somatic Mutation Discovered in CtDNA of a KIT/PDGFRA Wild-Type Gastrointestinal Stromal Tumor Resistant to Imatinib. *Front Pharmacol* **2020**, *11*, 36. https://doi.org/10.3389/fphar.2020.00036.

(165) Bouaoun, L.; Sonkin, D.; Ardin, M.; Hollstein, M.; Byrnes, G.; Zavadil, J.; Olivier, M. TP53 Variations in Human Cancers: New Lessons from the IARC TP53 Database and Genomics Data. *Hum. Mutat.* **2016**, *37* (9), 865–876. https://doi.org/10.1002/humu.23035.

(166) Okubo, M.; Murayama, N.; Shimizu, M.; Shimada, T.; Guengerich, F. P.; Yamazaki, H. The CYP3A4 Intron 6 C>T Polymorphism (CYP3A4*22) Is Associated with Reduced CYP3A4 Protein Level and Function in Human Liver Microsomes. *The Journal of Toxicological Sciences* **2013**, *38* (3), 349–354. https://doi.org/10.2131/jts.38.349.

(167) Elens, L.; van Gelder, T.; Hesselink, D. A.; Haufroid, V.; van Schaik, R. H. N. CYP3A4*22: Promising Newly Identified CYP3A4 Variant Allele for Personalizing Pharmacotherapy. *Pharmacogenomics* **2013**, *14* (1), 47–62. https://doi.org/10.2217/pgs.12.187.

(168) Barratt, D. T.; Cox, H. K.; Menelaou, A.; Yeung, D. T.; White, D. L.; Hughes, T. P.; Somogyi, A. A. CYP2C8 Genotype Significantly Alters Imatinib Metabolism in Chronic Myeloid Leukaemia Patients. *Clin Pharmacokinet* **2017**, *56* (8), 977–985. https://doi.org/10.1007/s40262-016-0494-0.

(169) Dessilly, G.; Panin, N.; Elens, L.; Haufroid, V.; Demoulin, J.-B. Impact of ABCB1 1236C > T-2677G > T-3435C > T Polymorphisms on the Anti-Proliferative Activity of Imatinib, Nilotinib, Dasatinib and Ponatinib. *Scientific Reports* **2016**, *6* (1). https://doi.org/10.1038/srep29559.

(170) Dulucq, S.; Bouchet, S.; Turcq, B.; Lippert, E.; Etienne, G.; Reiffers, J.; Molimard, M.; Krajinovic, M.; Mahon, F.-X. Multidrug Resistance Gene (MDR1) Polymorphisms Are Associated with Major Molecular Responses to Standard-Dose Imatinib in Chronic Myeloid Leukemia. *Blood* **2008**, *112* (5), 2024–2027. https://doi.org/10.1182/blood-2008-03-147744.

(171) Au, A.; Aziz Baba, A.; Goh, A. S.; Wahid Fadilah, S. A.; Teh, A.; Rosline, H.; Ankathil, R. Association of Genotypes and Haplotypes of Multi-Drug Transporter Genes ABCB1 and ABCG2 with Clinical Response to Imatinib Mesylate in Chronic Myeloid Leukemia Patients. *Biomedicine & Pharmacotherapy* **2014**, *68* (3), 343–349. https://doi.org/10.1016/j.biopha.2014.01.009.

(172) Dessilly, G.; Elens, L.; Panin, N.; Karmani, L.; Demoulin, J.-B.; Haufroid, V. *ABCB1* 1199G>A Polymorphism (Rs2229109) Affects the Transport of Imatinib, Nilotinib and Dasatinib. *Pharmacogenomics* **2016**, *17* (8), 883–890. https://doi.org/10.2217/pgs-2016-0012.

(173) Tomlinson, B.; Hu, M.; Lee, V. W. Y.; Lui, S. S. H.; Chu, T. T. W.; Poon, E. W. M.; Ko, G. T. C.; Baum, L.; Tam, L. S.; Li, E. K. ABCG2 Polymorphism Is Associated with the Low-Density Lipoprotein Cholesterol Response to Rosuvastatin. *Clin Pharmacol Ther* **2010**, *87* (5), 558–562. https://doi.org/10.1038/clpt.2009.232.

(174) Hu, M.; Lui, S. S. H.; Mak, V. W. L.; Chu, T. T. W.; Lee, V. W. Y.; Poon, E. W. M.; Tsui, T. K. C.; Ko, G. T. C.; Baum, L.; Tam, L.-S.; Li, E. K.; Tomlinson, B. Pharmacogenetic Analysis of Lipid Responses to Rosuvastatin in Chinese Patients. *Pharmacogenet Genomics* **2010**, *20* (10), 634–637. https://doi.org/10.1097/FPC.0b013e32833de489.

(175) Zhang, W.; Yu, B.-N.; He, Y.-J.; Fan, L.; Li, Q.; Liu, Z.-Q.; Wang, A.; Liu, Y.-L.; Tan, Z.-R.; Fen-Jiang, null; Huang, Y.-F.; Zhou, H.-H. Role of BCRP 421C>A Polymorphism on Rosuvastatin Pharmacokinetics in Healthy Chinese Males. *Clin Chim Acta* **2006**, *373* (1–2), 99–103. https://doi.org/10.1016/j.cca.2006.05.010.

(176) Keskitalo, J. E.; Zolk, O.; Fromm, M. F.; Kurkinen, K. J.; Neuvonen, P. J.; Niemi, M. ABCG2 Polymorphism Markedly Affects the Pharmacokinetics of Atorvastatin and Rosuvastatin. *Clin Pharmacol Ther* **2009**, *86* (2), 197–203. https://doi.org/10.1038/clpt.2009.79.

(177) Lee, H.-K.; Hu, M.; Lui, S. S.; Ho, C.-S.; Wong, C.-K.; Tomlinson, B. Effects of Polymorphisms in ABCG2, SLCO1B1, SLC10A1 and CYP2C9/19 on Plasma Concentrations of Rosuvastatin and Lipid Response in Chinese Patients. *Pharmacogenomics* **2013**, *14* (11), 1283–1294. https://doi.org/10.2217/pgs.13.115.

(178) Birmingham, B. K.; Bujac, S. R.; Elsby, R.; Azumaya, C. T.; Zalikowski, J.; Chen, Y.; Kim, K.; Ambrose, H. J. Rosuvastatin Pharmacokinetics and Pharmacogenetics in Caucasian and Asian Subjects Residing in the United States. *Eur J Clin Pharmacol* **2015**, *71* (3), 329–340. https://doi.org/10.1007/s00228-014-1800-0.

(179) Jiang, Z.-P.; Zhao, X.-L.; Takahashi, N.; Angelini, S.; Dubashi, B.; Sun, L.; Xu, P. Trough Concentration and ABCG2 Polymorphism Are Better to Predict Imatinib Response in Chronic Myeloid Leukemia: A Meta-Analysis. *Pharmacogenomics* **2017**, *18* (1), 35–56. https://doi.org/10.2217/pgs-2016-0103.

(180) Fohner, A. E.; Brackman, D. J.; Giacomini, K. M.; Altman, R. B.; Klein, T. E. PharmGKB Summary: Very Important Pharmacogene Information for ABCG2. *Pharmacogenet Genomics* **2017**, *27* (11), 420–427. https://doi.org/10.1097/FPC.0000000000000305.

(181) Leschziner, G. D.; Andrew, T.; Pirmohamed, M.; Johnson, M. R. ABCB1 Genotype and PGP Expression, Function and Therapeutic Drug Response: A Critical Review and Recommendations for Future Research. *Pharmacogenomics J* **2007**, *7* (3), 154–179. https://doi.org/10.1038/sj.tpj.6500413.

(182) Joensuu, H.; Trent, J. C.; Reichardt, P. Practical Management of Tyrosine Kinase Inhibitor-Associated Side Effects in GIST. *Cancer Treatment Reviews* **2011**, *37* (1), 75–88. https://doi.org/10.1016/j.ctrv.2010.04.008.

(183) Margier, M.; Collet, X.; May, C.; Desmarchelier, C.; André, F.; Lebrun, C.; Defoort, C.; Bluteau, A.; Borel, P.; Lespine, A.; Reboul, E. ABCB1 (P-glycoprotein) Regulates Vitamin D Absorption and Contributes to Its Transintestinal Efflux. *The FASEB Journal* **2019**, *33* (2), 2084–2094. https://doi.org/10.1096/fj.201800956R.

(184) Demetri, G. D.; Wang, Y.; Wehrle, E.; Racine, A.; Nikolova, Z.; Blanke, C. D.; Joensuu, H.; von Mehren, M. Imatinib Plasma Levels Are Correlated With Clinical Benefit in Patients With Unresectable/Metastatic Gastrointestinal Stromal Tumors. *Journal of Clinical Oncology* **2009**, *27* (19), 3141–3147. https://doi.org/10.1200/JCO.2008.20.4818.

(185) Sauer, R.; Liersch, T.; Merkel, S.; Fietkau, R.; Hohenberger, W.; Hess, C.; Becker, H.; Raab, H.-R.; Villanueva, M.-T.; Witzigmann, H.; Wittekind, C.; Beissbarth, T.; Rödel, C. Preoperative Versus Postoperative Chemoradiotherapy for Locally Advanced Rectal Cancer: Results of the German CAO/ARO/AIO-94 Randomized Phase III Trial After a Median Follow-Up of 11 Years. *Journal of Clinical Oncology* **2012**, *30* (16), 1926–1933. https://doi.org/10.1200/JCO.2011.40.1836.

(186) Schou, J. V.; Larsen, F. O.; Sørensen, B. S.; Abrantes, R.; Boysen, A. K.; Johansen, J. S.; Jensen, B. V.; Nielsen, D. L.; Spindler, K. L. Circulating Cell-Free DNA as Predictor of Treatment Failure after Neoadjuvant Chemo-Radiotherapy before Surgery in Patients with Locally Advanced Rectal Cancer. *Annals of Oncology* **2018**, *29* (3), 610–615. https://doi.org/10.1093/annonc/mdx778.

(187) Szpechcinski, A.; Chorostowska-Wynimko, J.; Struniawski, R.; Kupis, W.; Rudzinski, P.; Langfort, R.; Puscinska, E.; Bielen, P.; Sliwinski, P.; Orlowski, T. Cell-Free DNA Levels in Plasma of Patients with Non-Small-Cell Lung Cancer and Inflammatory Lung Disease. *British Journal of Cancer* **2015**, *113* (3), 476–483. https://doi.org/10.1038/bjc.2015.225.

(188) Fernandez-Garcia, D.; Hills, A.; Page, K.; Hastings, R. K.; Toghill, B.; Goddard, K. S.; Ion, C.; Ogle, O.; Boydell, A. R.; Gleason, K.; Rutherford, M.; Lim, A.; Guttery, D. S.; Coombes, R. C.; Shaw, J. A. Plasma Cell-Free DNA (CfDNA) as a Predictive and Prognostic Marker in Patients with Metastatic Breast Cancer. *Breast Cancer Research* **2019**, *21* (1). https://doi.org/10.1186/s13058-019-1235-8.

(189) Fleischhacker, M.; Schmidt, B. Pre-Analytical Issues in Liquid Biopsy – Where Do We Stand? *Journal of Laboratory Medicine* **2020**, *0* (0). https://doi.org/10.1515/labmed-2019-0167.

(190) For the UK Early Cancer Detection Consortium; Cree, I. A.; Uttley, L.; Buckley Woods, H.; Kikuchi, H.; Reiman, A.; Harnan, S.; Whiteman, B. L.; Philips, S. T.; Messenger, M.; Cox, A.; Teare, D.; Sheils, O.; Shaw, J. The Evidence Base for Circulating Tumour DNA Blood-Based Biomarkers for the Early Detection of Cancer: A Systematic Mapping Review. *BMC Cancer* **2017**, *17* (1). https://doi.org/10.1186/s12885-017-3693-7.

(191) Butler, T. M.; Boniface, C. T.; Johnson-Camacho, K.; Tabatabaei, S.; Melendez, D.; Kelley, T.; Gray, J.; Corless, C. L.; Spellman, P. T. Circulating Tumor DNA Dynamics Using Patient-Customized Assays Are Associated with Outcome in Neoadjuvantly Treated Breast Cancer. *Molecular Case Studies* **2019**, *5* (2), a003772. https://doi.org/10.1101/mcs.a003772.

(192) Riediger, A. L.; Dietz, S.; Schirmer, U.; Meister, M.; Heinzmann-Groth, I.; Schneider, M.; Muley, T.; Thomas, M.; Sültmann, H. Mutation Analysis of Circulating Plasma DNA to Determine Response to EGFR Tyrosine Kinase Inhibitor Therapy of Lung Adenocarcinoma Patients. *Scientific Reports* **2016**, *6* (1). https://doi.org/10.1038/srep33505.

(193) Murahashi, S.; Akiyoshi, T.; Sano, T.; Fukunaga, Y.; Noda, T.; Ueno, M.; Zembutsu, H. Serial Circulating Tumour DNA Analysis for Locally Advanced Rectal Cancer Treated with Preoperative Therapy: Prediction of Pathological Response and Postoperative Recurrence. *British Journal of Cancer* **2020**, *123* (5), 803–810. https://doi.org/10.1038/s41416-020-0941-4.

(194) Khakoo, S.; Carter, P. D.; Brown, G.; Valeri, N.; Picchia, S.; Bali, M. A.; Shaikh, R.; Jones, T.; Begum, R.; Rana, I.; Wotherspoon, A.; Terlizzo, M.; von Loga, K.; Kalaitzaki, E.; Saffery, C.; Watkins, D.; Tait, D.; Chau, I.; Starling, N.; Hubank, M.; Cunningham, D. MRI Tumor Regression Grade and Circulating Tumor DNA as Complementary Tools to Assess Response and Guide Therapy Adaptation in Rectal Cancer. *Clinical Cancer Research* **2020**, *26* (1), 183–192. https://doi.org/10.1158/1078-0432.CCR-19-1996.

(195) Das, S.; Raj, L.; Zhao, B.; Kimura, Y.; Bernstein, A.; Aaronson, S. A.; Lee, S. W. Hzf Determines Cell Survival upon Genotoxic Stress by Modulating P53 Transactivation. *Cell* **2007**, *130* (4), 624–637. https://doi.org/10.1016/j.cell.2007.06.013.

(196) Restivo, A.; Zorcolo, L.; Cocco, I. M. F.; Manunza, R.; Margiani, C.; Marongiu, L.; Casula, G. Elevated CEA Levels and Low Distance of the Tumor from the Anal Verge Are Predictors of Incomplete Response to Chemoradiation in Patients with Rectal Cancer. *Annals of Surgical Oncology* **2013**, *20* (3), 864–871. https://doi.org/10.1245/s10434-012-2669-8.

(197) Russo, A. L.; Ryan, D. P.; Borger, D. R.; Wo, J. Y.; Szymonifka, J.; Liang, W.-Y.; Kwak, E. L.; Blaszkowsky, L. S.; Clark, J. W.; Allen, J. N.; Zhu, A. X.; Berger, D. L.; Cusack, J. C.; Mamon, H. J.; Haigis, K. M.; Hong, T. S. Mutational and Clinical Predictors of Pathologic Complete Response in the Treatment of Locally Advanced Rectal Cancer. *Journal of Gastrointestinal Cancer* **2014**, *45* (1), 34–39. https://doi.org/10.1007/s12029-013-9546-y.

(198) Chow, O. S.; Kuk, D.; Keskin, M.; Smith, J. J.; Camacho, N.; Pelossof, R.; Chen, C.-T.; Chen, Z.; Avila, K.; Weiser, M. R.; Berger, M. F.; Patil, S.; Bergsland, E.; Garcia-Aguilar, J. KRAS and Combined KRAS/TP53 Mutations in Locally Advanced Rectal Cancer Are Independently Associated with Decreased Response to Neoadjuvant Therapy. *Annals of Surgical Oncology* **2016**, *23* (8), 2548–2555. https://doi.org/10.1245/s10434-016-5205-4.

(199) Toomey, S.; Gunther, J.; Carr, A.; Weksberg, D. C.; Thomas, V.; Salvucci, M.; Bacon, O.; Sherif, E.-M.; Fay, J.; Kay, E. W.; Sheehan, K. M.; McNamara, D. A.; Sanders, K. L.; Mathew, G.; Breathnach, O. S.; Grogan, L.; Morris, P. G.; Foo, W. C.; You, Y.-Q. N.; Prehn, J. H.; O'Neill, B.; Krishnan, S.; Hennessy, B. T.; Furney, S. J. Genomic and Transcriptomic Characterisation of Response to Neoadjuvant Chemoradiotherapy in Locally Advanced Rectal Cancer. *Cancers* **2020**, *12* (7), 1808. https://doi.org/10.3390/cancers12071808.

(200) Chen, M.-B.; Wu, X.-Y.; Yu, R.; Li, C.; Wang, L.-Q.; Shen, W.; Lu, P.-H. P53 Status as a Predictive Biomarker for Patients Receiving Neoadjuvant Radiation-Based Treatment: A Meta-Analysis in Rectal Cancer. *PLoS ONE* **2012**, *7* (9), e45388. https://doi.org/10.1371/journal.pone.0045388.

(201) Sadanandam, A.; Lyssiotis, C. A.; Homicsko, K.; Collisson, E. A.; Gibb, W. J.; Wullschleger, S.; Ostos, L. C. G.; Lannon, W. A.; Grotzinger, C.; Del Rio, M.; Lhermitte, B.; Olshen, A. B.; Wiedenmann, B.; Cantley, L. C.; Gray, J. W.; Hanahan, D. A Colorectal Cancer Classification System That Associates Cellular Phenotype and Responses to Therapy. *Nature Medicine* **2013**, *19* (5), 619–625. https://doi.org/10.1038/nm.3175.

(202) Emons, G.; Spitzner, M.; Reineke, S.; Möller, J.; Auslander, N.; Kramer, F.; Hu, Y.; Beissbarth, T.; Wolff, H. A.; Rave-Fränk, M.; Heßmann, E.; Gaedcke, J.; Ghadimi, B. M.; Johnsen, S. A.; Ried, T.; Grade, M. Chemoradiotherapy Resistance in Colorectal Cancer Cells Is Mediated by Wnt/β-Catenin Signaling. *Molecular Cancer Research* **2017**, *15* (11), 1481–1490. https://doi.org/10.1158/1541-7786.MCR-17-0205.

(203) Yerushalmi, R.; Woods, R.; Ravdin, P. M.; Hayes, M. M.; Gelmon, K. A. Ki67 in Breast Cancer: Prognostic and Predictive Potential. *The Lancet Oncology* **2010**, *11* (2), 174–183. https://doi.org/10.1016/S1470-2045(09)70262-1.

(204) Zhou, Y.; Hu, W.; Chen, P.; Abe, M.; Shi, L.; Tan, S.; Li, Y.; Zong, L. Ki67 Is a Biological Marker of Malignant Risk of Gastrointestinal Stromal Tumors: A Systematic Review and Meta-Analysis. *Medicine* **2017**, *96* (34), e7911. https://doi.org/10.1097/MD.0000000000007911.

(205) Jakob, C.; Liersch, T.; Meyer, W.; Becker, H.; Baretton, G. B.; Aust, D. E. Neuro-Regulation of Lower Esophageal Sphincter Predictive Value of Ki67 and P53 in Locally Advanced Rectal Cancer: Correlation with Thymidylate Synthase and Histopathological Tumor Regression after Neoadjuvant 5-FU-Based Chemoradiotherapy. *World Journal of Gastroenterology* **2008**, *14* (7), 1060. https://doi.org/10.3748/wjg.14.1060.

(206) Kim, N. K.; Park, J. K.; Lee, K. Y.; Yang, W. I.; Yun, S. H.; Sung, J.; Min, J. S. P53, BCL-2, and Ki-67 Expression According to Tumor Response After Concurrent Chemoradiotherapy for Advanced Rectal Cancer. *Ann Surg Oncol* **2001**, *8* (5), 7.

(207) Hur, H.; Kim, N. K.; Min, B. S.; Baik, S. H.; Lee, K. Y.; Koom, W. S.; Ahn, J. B.; Kim, H. Can a Biomarker-Based Scoring System Predict Pathologic Complete Response After Preoperative Chemoradiotherapy for Rectal Cancer?: *Diseases of the Colon & Rectum* **2014**, *57* (5), 592–601. https://doi.org/10.1097/DCR.0000000000000109.

(208) Furusato, B.; Mohamed, A.; Uhlén, M.; Rhim, J. S. CXCR4 and Cancer: CXCR4 and Cancer. *Pathology International* **2010**, *60* (7), 497–505. https://doi.org/10.1111/j.1440-1827.2010.02548.x.

(209) González, I.; Bauer, P. S.; Chapman, W. C.; Alipour, Z.; Rais, R.; Liu, J.; Chatterjee, D. Clinicopathologic Determinants of Pathologic Treatment Response in Neoadjuvant Treated Rectal Adenocarcinoma. *Annals of Diagnostic Pathology* **2020**, *45*, 151452. https://doi.org/10.1016/j.anndiagpath.2019.151452.

(210) Brown, J. R.; DiGiovanna, M. P.; Killelea, B.; Lannin, D. R.; Rimm, D. L. Quantitative Assessment Ki-67 Score for Prediction of Response to Neoadjuvant Chemotherapy in Breast Cancer. *Laboratory Investigation* **2014**, *94* (1), 98–106. https://doi.org/10.1038/labinvest.2013.128.

(211) Edden, Y.; Wexner, S. D.; Berho, M. The Use of Molecular Markers as a Method to Predict the Response to Neoadjuvant Therapy for Advanced Stage Rectal Adenocarcinoma: Molecular Markers in Rectal Cancers. *Colorectal Disease* **2012**, *14* (5), 555–561. https://doi.org/10.1111/j.1463-1318.2011.02697.x.

(212) Min, B. S. Cyclooxygenase-2 Expression in Pretreatment Biopsy as a Predictor of Tumor Responses After Preoperative Chemoradiation in Rectal Cancer. *Archives of Surgery* **2008**, *143* (11), 1091. https://doi.org/10.1001/archsurg.143.11.1091.

(213) Smith, F. M.; Reynolds, J. V.; Kay, E. W.; Crotty, P.; Murphy, J. O.; Hollywood, D.; Gaffney, E. F.; Stephens, R. B.; Kennedy, M. J. COX-2 Overexpression in Pretreatment Biopsies Predicts Response of Rectal Cancers to Neoadjuvant Radiochemotherapy. *International Journal of Radiation Oncology*Biology*Physics* **2006**, *64* (2), 466–472. https://doi.org/10.1016/j.ijrobp.2005.07.961.

(214) Pauzas, H.; Gyvyte, U.; Latkauskas, T.; Kairevice, L.; Lizdenis, P.; Svagzdys, S.; Birgiolaite, E.; Kuliaviene, I.; Kupcinskas, J.; Tamelis, A. The Role of VEGFA, COX2, HUR and CUGBP2 in Predicting the Response to Neoadjuvant Therapy in Rectal Cancer Patients. *Medicina* **2020**, *56* (4), 192. https://doi.org/10.3390/medicina56040192.

(215) Giralt, J.; Navalpotro, B.; Hermosilla, E.; de Torres, I.; Espin, E.; Reyes, V.; Cerezo, L.; de las Heras, M.; Ramon y Cajal, S.; Armengol, M.; Benavente, S. Prognostic Significance of Vascular Endothelial Growth Factor and Cyclooxygenase-2 in Patients with Rectal Cancer Treated with Preoperative Radiotherapy. *Oncology* **2006**, *71* (5–6), 312–319. https://doi.org/10.1159/000107105.

(216) Ogino, S.; Kirkner, G. J.; Nosho, K.; Irahara, N.; Kure, S.; Shima, K.; Hazra, A.; Chan, A. T.; Dehari, R.; Giovannucci, E. L.; Fuchs, C. S. Cyclooxygenase-2 Expression Is an Independent Predictor of Poor Prognosis in Colon Cancer. *Clinical Cancer Research* **2008**, *14* (24), 8221–8227. https://doi.org/10.1158/1078-0432.CCR-08-1841.

(217) Vispe, S.; Cazaux, C.; Lesca, C.; Defais, M. Overexpression of Rad51 Protein Stimulates Homologous Recombination and Increases Resistance of Mammalian Cells to Ionizing Radiation. *Nucleic Acids Research* **1998**, *26* (12), 2859–2864. https://doi.org/10.1093/nar/26.12.2859.

(218) Havelund, B. M.; Sørensen, F. B.; Lindebjerg, J.; Spindler, K.-L. G.; Jakobsen, A. Pretreatment HIF-1α and GLUT-1 Expressions Do Not Correlate with Outcome after Preoperative Chemoradiotherapy in Rectal Cancer. *Anticancer Research* **2011**, *31*(5), 1559-65.

(219) Kaemmerer, D.; Träger, T.; Hoffmeister, M.; Sipos, B.; Hommann, M.; Sänger, J.; Schulz, S.; Lupp, A. Inverse Expression of Somatostatin and CXCR4 Chemokine Receptors in Gastroenteropancreatic Neuroendocrine Neoplasms of Different Malignancy. *Oncotarget* **2015**, *6* (29), 27566–27579. https://doi.org/10.18632/oncotarget.4491.

(220) Zhang, J.; Liu, C.; Mo, X.; Shi, H.; Li, S. Mechanisms by Which CXCR4/CXCL12 Cause Metastatic Behavior in Pancreatic Cancer. *Oncology Letters* **2017**. https://doi.org/10.3892/ol.2017.7512.

(221) Mai, R.; Kaemmerer, D.; Träger, T.; Neubauer, E.; Sänger, J.; Baum, R. P.; Schulz, S.; Lupp, A. Different Somatostatin and CXCR4 Chemokine Receptor Expression in Gastroenteropancreatic Neuroendocrine Neoplasms Depending on Their Origin. *Scientific Reports* **2019**, *9* (1). https://doi.org/10.1038/s41598-019-39607-2.

(222) Nannini, M.; Astolfi, A.; Urbini, M.; Biasco, G.; Pantaleo, M. A. Liquid Biopsy in Gastrointestinal Stromal Tumors: A Novel Approach. *Journal of Translational Medicine* **2014**, *12* (1), 210. https://doi.org/10.1186/1479-5876-12-210.

(223) Xu, H.; Chen, L.; Shao, Y.; Zhu, D.; Zhi, X.; Zhang, Q.; Li, F.; Xu, J.; Liu, X.; Xu, Z. Clinical Application of Circulating Tumor DNA in the Genetic Analysis of Patients with Advanced GIST. *Molecular Cancer Therapeutics* **2018**, *17* (1), 290–296. https://doi.org/10.1158/1535-7163.MCT-17-0436.

(224) Arshad, J.; Roberts, A.; Ahmed, J.; Cotta, J.; Pico, B. A.; Kwon, D.; Trent, J. C. Utility of Circulating Tumor DNA in the Management of Patients With GI Stromal Tumor: Analysis of 243 Patients. *JCO Precision Oncology* **2020**, No. 4, 66–73. https://doi.org/10.1200/PO.19.00253.

(225) Wendel, H.-G.; de Stanchina, E.; Cepero, E.; Ray, S.; Emig, M.; Fridman, J. S.; Veach, D. R.; Bornmann, W. G.; Clarkson, B.; McCombie, W. R.; Kogan, S. C.; Hochhaus, A.; Lowe, S. W. Loss of P53 Impedes the Antileukemic Response to BCR-ABL Inhibition. *Proc Natl Acad Sci U S A* **2006**, *103* (19), 7444–7449. https://doi.org/10.1073/pnas.0602402103.

(226) Al-achkar, W.; Wafa, A.; Moassass, F.; Othman, M. A. K. A Novel Dic (17;18) (P13.1;Q11.2) with Loss of TP53 and BCR/ABL Rearrangement in an Imatinib Resistant Chronic Myeloid Leukemia. *Mol Cytogenet* **2012**, *5*, 36. https://doi.org/10.1186/1755-8166-5-36.

(227) Cao, J.; Wei, J.; Yang, P.; Zhang, T.; Chen, Z.; He, F.; Wei, F.; Chen, H.; Hu, H.; Zhong, J.; Yang, Z.; Cai, W.; Li, W.; Wang, Q. Genome-Scale CRISPR-Cas9 Knockout Screening in Gastrointestinal Stromal Tumor with Imatinib Resistance. *Mol. Cancer* **2018**, *17* (1), 121. https://doi.org/10.1186/s12943-018-0865-2.

(228) Ihle, M. A.; Huss, S.; Jeske, W.; Hartmann, W.; Merkelbach-Bruse, S.; Schildhaus, H.-U.; Büttner, R.; Sihto, H.; Sundby Hall, K.; Eriksson, M.; Reichardt, P.; Joensuu, H.; Wardelmann, E.

Expression of Cell Cycle Regulators and Frequency of TP53 Mutations in High Risk Gastrointestinal Stromal Tumors Prior to Adjuvant Imatinib Treatment. *PLoS ONE* **2018**, *13* (2), e0193048. https://doi.org/10.1371/journal.pone.0193048.

(229) Merten, L.; Agaimy, A.; Moskalev, E. A.; Giedl, J.; Kayser, C.; Geddert, H.; Schaefer, I.-M.; Cameron, S.; Werner, M.; Ströbel, P.; Hartmann, A.; Haller, F. Inactivating Mutations of RB1 and TP53 Correlate With Sarcomatous Histomorphology and Metastasis/Recurrence in Gastrointestinal Stromal Tumors. *Am. J. Clin. Pathol.* **2016**, *146* (6), 718–726. https://doi.org/10.1093/ajcp/aqw193.

(230) Heinrich, M. C.; Patterson, J.; Beadling, C.; Wang, Y.; Debiec-Rychter, M.; Dewaele, B.; Corless, C. L.; Duensing, A.; Raut, C. P.; Rubin, B.; Ordog, T.; van de Rijn, M.; Call, J.; Mühlenberg, T.; Fletcher, J. A.; Bauer, S. Genomic Aberrations in Cell Cycle Genes Predict Progression of KIT-Mutant Gastrointestinal Stromal Tumors (GISTs). *Clin Sarcoma Res* **2019**, *9*, 3. https://doi.org/10.1186/s13569-019-0112-7.

(231) Pantaleo, M. A.; Urbini, M.; Indio, V.; Ravegnini, G.; Nannini, M.; De Luca, M.; Tarantino, G.; Angelini, S.; Gronchi, A.; Vincenzi, B.; Grignani, G.; Colombo, C.; Fumagalli, E.; Gatto, L.; Saponara, M.; Ianni, M.; Paterini, P.; Santini, D.; Pirini, M. G.; Ceccarelli, C.; Altimari, A.; Gruppioni, E.; Renne, S. L.; Collini, P.; Stacchiotti, S.; Brandi, G.; Casali, P. G.; Pinna, A. D.; Astolfi, A.; Biasco, G. Genome-Wide Analysis Identifies MEN1 and MAX Mutations and a Neuroendocrine-Like Molecular Heterogeneity in Quadruple WT GIST. *Mol. Cancer Res.* **2017**, *15* (5), 553–562. https://doi.org/10.1158/1541-7786.MCR-16-0376.

(232) Maier, J.; Lange, T.; Kerle, I.; Specht, K.; Bruegel, M.; Wickenhauser, C.; Jost, P.; Niederwieser, D.; Peschel, C.; Duyster, J.; von Bubnoff, N. Detection of Mutant Free Circulating Tumor DNA in the Plasma of Patients with Gastrointestinal Stromal Tumor Harboring Activating Mutations of CKIT or PDGFRA. *Clinical Cancer Research* **2013**, *19* (17), 4854–4867. https://doi.org/10.1158/1078-0432.CCR-13-0765.

(233) Antonescu, C. R. Acquired Resistance to Imatinib in Gastrointestinal Stromal Tumor Occurs Through Secondary Gene Mutation. *Clinical Cancer Research* **2005**, *11* (11), 4182–4190. https://doi.org/10.1158/1078-0432.CCR-04-2245.

(234) Mughal, T. Principal Long-Term Adverse Effects of Imatinib in Patients with Chronic Myeloid Leukemia in Chronic Phase. *Biologics: Targets & Therapy* **2010**, 315. https://doi.org/10.2147/BTT.S5775.

(235) Common Terminology Criteria for Adverse Events (CTCAE). **2017**, 147.

(236) Francis, J.; Dubashi, B.; Sundaram, R.; Pradhan, S. C.; Chandrasekaran, A. A Study to Explore the Correlation of ABCB1, ABCG2, OCT1 Genetic Polymorphisms and Trough Level Concentration with Imatinib Mesylate-Induced Thrombocytopenia in Chronic Myeloid Leukemia Patients. *Cancer Chemotherapy and Pharmacology* **2015**, *76* (6), 1185–1189. https://doi.org/10.1007/s00280-015-2905-6.

(237) Gow, J. M.; Chinn, L. W.; Kroetz, D. L. The Effects of *ABCB1* 3′-Untranslated Region Variants on MRNA Stability. *Drug Metabolism and Disposition* **2008**, *36* (1), 10–15. https://doi.org/10.1124/dmd.107.017087.

(238) Takahashi, N.; Miura, M.; Scott, S. A.; Kagaya, H.; Kameoka, Y.; Tagawa, H.; Saitoh, H.; Fujishima, N.; Yoshioka, T.; Hirokawa, M.; Sawada, K. Influence of CYP3A5 and Drug Transporter

Polymorphisms on Imatinib Trough Concentration and Clinical Response among Patients with Chronic Phase Chronic Myeloid Leukemia. *Journal of Human Genetics* **2010**, *55* (11), 731–737. https://doi.org/10.1038/jhg.2010.98.

(239) Fulton, C. R.; Zang, Y.; Desta, Z.; Rosenman, M. B.; Holmes, A. M.; Decker, B. S.; Zhang, Y.; T Callaghan, J.; Pratt, V. M.; Levy, K. D.; Gufford, B. T.; Dexter, P. R.; Skaar, T. C.; Eadon, M. T. Drug–Gene and Drug–Drug Interactions Associated with Tramadol and Codeine Therapy in the INGENIOUS Trial. *Pharmacogenomics* **2019**, *20* (6), 397–408. https://doi.org/10.2217/pgs-2018-0205.

(240) Taguchi, K.; Kouroki, M.; Ohmura, T.; Jono, H.; Endo, F.; Saito, H. Carbamazepine-Imatinib Interaction in a Child with Chronic Myeloid Leukemia: EIAED Alter Imatinib Pharmacokinetics. *Pediatrics International* **2014**, *56* (4), e33–e36. https://doi.org/10.1111/ped.12382.

(241) Hamilton, M. Effects of Smoking on the Pharmacokinetics of Erlotinib. *Clinical Cancer Research* **2006**, *12* (7), 2166–2171. https://doi.org/10.1158/1078-0432.CCR-05-2235.

(242) van Erp, N.; Gelderblom, H.; van Glabbeke, M.; Van Oosterom, A.; Verweij, J.; Guchelaar, H.-J.; Debiec-Rychter, M.; Peng, B.; Blay, J.-Y.; Judson, I. Effect of Cigarette Smoking on Imatinib in Patients in the Soft Tissue and Bone Sarcoma Group of the EORTC. *Clinical Cancer Research* **2008**, *14* (24), 8308–8313. https://doi.org/10.1158/1078-0432.CCR-08-1303.

Appendix

Table S1. Gene List QIaSeq Colorectal Cancer Panel DNA kit (cat. DHS-002Z) (Qiagen, Hilden, Germany)

Colorectal Cancer Panel					
BRAF	ACVR1B	CDC27	FGFR3	MLH3	PTEN
FBXW7	AKT1	CDH1	FLCN	MSH2	PTPN12
KRAS	ATM	CDK4	FZD3	MSH3	RET
CTNNB1	ATP6V0D2	CDKN2A	GALNT12	MSH6	RPS20
NRAS	AXIN2	CHEK2	GPC6	MUTYH	SLC9A9
PIK3CA	BAX	CTNNA1	GREM1	MYO1B	SMAD2
APC	BLM	DCC	KIT	PALB2	SRC
DMD	BMPR1A	EGFR	MAP2K4	PIK3R1	TCERG1
SMAD4	BRCA1	ENG	MAP7	PMS1	TGFBR2
STK11	BRCA2	EP300	MET	PMS2	WBSCR17
TCF7L2	BUB1B	EPCAM	MIER3	POLD1	SCG5
TP53	CASP8	ERBB2	MLH1	POLE	

Table S2. Gene List QIaSeq Actionable Solid Tumor Panel DNA kit (cat. DHS-101Z) (Qiagen, Hilden, Germany)

Actionable Solid Tumor Panel			
BRAF	AKT1	GNA11	RET
PDGFRA	ALK	GNAQ	ERBB2
EGFR	CTNNB1	IDH1	PIK3CA
KRAS	ERBB3	IDH2	TP53
NRAS	ESR1	MET	
KIT	FOXL2	RAF1	

Table S3. Assignment of likely CYP2C9 phenotypes based on genotypes [145]

Likely phenotype	**Genotypes**	**Examples of *CYP2C9* diplotypes**
Normal metabolizer	An individual carrying two normal function alleles	**1/*1*
Intermediate metabolizer	An individual carrying one normal function allele plus one decreased function allele; OR one normal function allele plus one no function allele OR two decreased function alleles	**1/*2 *1/*3, *2/*2*
Poor metabolizer	An individual carrying one no function allele plus one decreased function allele; OR two no function alleles	**2/*3 *3/*3*
Indeterminate metabolizer	An individual carrying allele combinations with uncertain and/or unknown function alleles	**1/*7, *1/*10, *7/*10, *1/*57*

Table S4. Assignment of likely CYP2D6 phenotypes based on genotypes [146]

Likely phenotype	**Genotypes**	**Examples of CYP2D6 diplotypes**
Ultrarapid metabolizer	An individual carrying more than two copies of functional alleles	**1/*1xN*, **1/*2xN*
Extensive metabolizer	An individual carrying two alleles encoding full or reduced function; or one full- function allele together with either one nonfunctional or one reduced-function allele	**1/*1*, **1/*2*, **2/*2*, **1/*41*, **1/*4*, **2/*5*, **1/*10*
Intermediate metabolizer	An individual carrying one reduced-function and one nonfunctional allele	**4/*10*, **5/*41*
Poor metabolizer	An individual carrying no functional alleles	**4/*4*, **4/*5*, **5/*5*, **4/*6*

Table S5. Assignment of likely CYP2C19 phenotypes based on genotypes[144]

Likely phenotype	Genotypes	Examples of *CYPC19* diplotypes
Ultrarapid metabolizer: normal or increased activity (~5–30% of patients)	An individual carrying two increased activity alleles (*17) or one functional allele (*1) plus one increased-activity allele (*17)	*1/*17, *17/*17
Extensive metabolizer: homozygous wild-type or normal activity (~35–50% of patients)	An individual carrying two functional (*1) alleles	*1/*1
Intermediate metabolizer: heterozygote or intermediate activity (~18–45% of patients)	An individual carrying one functional allele (*1) plus one loss-of-function allele (*2–*8) or one loss-of-function allele (*2–*8) plus one increased-activity allele (*17)	*1/*2, *1/*3, *2/*17
Poor metabolizer: homozygous variant, mutant, low, or deficient activity (~2–15% of patients)	An individual carrying two loss-of-function alleles (*2–*8)	*2/*2, *2/*3, *3/*3

Table S6. Assignment of likely CYP2B6 phenotypes based on genotypes [143]

Likely phenotype	Genotypes	Examples of *CYP2B6* diplotypes
Ultrarapid metabolizer	An individual carrying two increased function alleles	*4/*4, *22/*22, *4/*22
Rapid metabolizer	An individual carrying one normal function allele and one increased function allele	**1/*4*, **1/*22*
Normal metabolizer	An individual carrying two normal function alleles	*1/*1
Intermediate metabolizer	An individual carrying one normal function allele and one decreased function allele OR one normal function allele and one no-function allele OR one increased function allele and one decreased function allele OR one increased function allele and one no-function allelea	**1/*6*, **1/*18*, **4/*6*, **4/*18*, **6/*22*, **18/*22*
Poor metabolizer	An individual carrying two decreased function alleles OR two no-function alleles OR one decreased function allele and one no-function allele	**6/*6*, **18/*18*, **6/*18*

Table S7. Assignment of likely CYP3A5 phenotypes based on genotypes[147]

Likely phenotype	Genotypes	Examples of CYP3A5 diplotypes
Extensive metabolizer (CYP3A5 expresser)	An individual carrying two functional alleles	*1/*1
Intermediate metabolizer (CYP3A5 expresser)	An individual carrying one functional allele and one nonfunctional allele	*1/*3, *1/*6, *1/*7
Poor metabolizer (CYP3A5 nonexpresser)	An individual carrying two nonfunctional alleles	*3/*3, *6/*6, *7/*7, *3/*6, *3/*7, *6/*7

Publications

1. Dietz S, Christopoulos P, Yuan Z, Gu L, Volckmar AL, Ogrodnik SJ, Angeles AK, **Dalle Fratte C**, Zemojtel T, Schneider MA, Kazdal D, Endris V, Meister M, Muley T, Cecchin E, Reck M, Schlesner M, Thomas M, Stenzinger A, and Sültmann H "Longitudinal therapy monitoring of ALK-positive lung cancer by combined copy number and targeted mutation profiling of cell-free DNA" *EBioMedicine* **2020**; 62 : 103103
2. **Dalle Fratte C**, Guardascione M, De Mattia E, Borsatti E, Boschetto R, Farruggio A, Canzonieri V, Romanato L, Borsatti R, Gagno S, Marangon E, Polano M, Buonadonna A, Toffoli G and E Cecchin "Clonal selection of a novel deleterious *TP53* somatic mutation discovered in ctDNA of a *KIT/PDGFRA* wild type Gastrointestinal Stromal Tumor resistant to imatinib" *Front Pharmacol.* **2020**; 11: 36
3. Mezzalira S, De Mattia E, Guardascione M, **Dalle Fratte C**, Cecchin E, Toffoli G. "Circulating-Free DNA Analysis in Hepatocellular Carcinoma: A Promising Strategy to Improve Patients' Management and Therapy Outcomes" Review. *Int. J. Mol. Sci.* **2019**; 20(21): 5498
4. Fragoulakis V, Roncato R, **Dalle Fratte C**, Ecca F, Bartsakoulia M, Innocenti F, Toffoli G, Cecchin E, Patrinos GP, Mitropoulou C "Estimating the Effectiveness of *DPYD* Genotyping in Italian Individuals Suffering from Cancer Based on the Cost of Chemotherapy-Induced Toxicity" *Am J Hum Genet.* **2019**; 104(6): 1158-1168.
5. De Mattia E, Roncato R, **Dalle Fratte C**, Ecca F, Toffoli G, Cecchin E. "The use of pharmacogenetics to increase the safety of colorectal cancer patients treated with fluoropyrimidines" *Cancer Drug Resist.* **2019**; 2: 116-130
6. **Dalle Fratte C**, Polesel J, Roncato R, De Mattia E, Ecca F, Bignucolo A, Garziera M, Dreussi E, Palazzari E, Buonadonna A, Guardascione M, Berretta M, Foltran L, Sartor F, D'Andrea M, Favaretto A, Mini E, Nobili S, De Paoli A, Toffoli G and Cecchin E "*DPYD* gene activity score predicts dose-limiting toxicity in fluoropyrimidine-treated colorectal cancer patients" *J. Cell. Mol. Med.* **2018**; 1(3): 143-150
7. Toffoli G, Innocenti F, Polesel J, De Mattia E, Sartor F, **Dalle Fratte C**, Ecca F, Dreussi E, Palazzari E, Guardascione M, Buonadonna A, Foltran L, Garziera M, Bignucolo A, Nobili S, Mini E, Favaretto A, Berretta M, D'Andrea M, De Paoli A, Roncato R, Cecchin E. "The genotype for *DPYD* risk variants in patients with colorectal cancer and the related toxicity management costs in clinical practice" *Clin. Pharmacol. Ther*. **2018**; 105(4): 994-1002.

Publications in Preparation

1. **Dalle Fratte C**, Mezzalira S, Polesel J, De Mattia E, Palumbo A, Palazzari E, De Paoli A, Belluco C, Canzonieri V, Toffoli G and Cecchin E "A panel of tumor biomarkers to predict complete pathological response to neo-adjuvant treatment in Locally Advanced Rectal Cancer" (submitted)

Acknowledgments

First and foremost, I would like to thank my PhD supervisor, Dr. Erika Cecchin, for giving me the opportunity to work in her research group. I am very thankful for her continuous support and encouragement throughout my studies. I also would like to acknowledge Dr. Giuseppe Toffoli for hosting me in the Clinical and Experimental Pharmacology Unit of CRO Aviano and for granting financial support.

Furthermore, I would like to express my gratitude to Prof. Dr. Holger Sültmann for giving me the opportunity to spend a part of my work on liquid biopsy in his research group as well as for his scientific support and guidance.

This thesis work would have not been possible without all the fruitful collaborations that I would like to acknowledge: many thanks to Dr. Elisa Palazzari and Dr. Antonino De Paoli, not only for providing us patients' samples for liquid biopsy analyses and detailed clinical information, but also for the interesting and useful discussions we had. I am also very thankful to Prof. Dr. Vincenzo Canzonieri and Dr. Antonio Palumbo for providing us the precious tissue samples from rectal cancer patients, for the histopathological analyses and for the very productive discussions.

I also would like to acknowledge the Therapeutic Drug Monitoring group, headed by Dr. Bianca Posocco, for their excellent work on Imatinib project as well as for providing us the quantification data.

I would like to thank Prof. Dr. Alessio Squassina for being my PhD thesis co-supervisor and for sharing his advices and suggestions on my project during the annual meetings.

Very special thanks go to Dr. Elena De Mattia, for her time and support during my PhD studies, and to Dr. Jerry Polesel, for his valuable support on biostatistical analyses.

I am also very grateful to have worked with Rachele Borsatti on her thesis. It has been a pleasure to share thoughts and ideas during her work.

A big thank goes to all current and former members of the Division of Clinical and Experimental Pharmacology Unit of CRO Aviano for their help and support throughout these years. I would especially like to thank my brother in arm, Dr. Fabrizio Ecca, and a very precious friend, Ariana Soledad Poetto, for their never-ending support and for all the scientific and non-scientific conversations we had inside and outside the lab. A warm thank goes also to Viola Donadello and Ottavia Bellotto for the great time we had together and for have encouraged me to pursuit my goals. Special thanks also to Antonella Moro, Franca Sartor, Loredana Romanato and Monica D'Andrea for their experimental support and help in administrative affairs.

I also would like to thank all the members of the Division of Cancer Genome Research of the DKFZ of Heidelberg for welcoming me and for the very pleasant time we had together. I would especially like to thank Dr. Steffen Dietz, for his time and support during my first months in the group, as well as the other passionate scientists I had the pleasure to come across with: Dr. Sabine Klauck, Dr. Arlou Kristina

Angeles, Simone Bauer, Ann-Kathrin Daum, Florian Janke, Simon Ogrodnik, Sabrina Gerhardt, Niclas Flosdorf, Saskia Müller, Alessa Klär, Philipp Hecht and Louise Appenheimer.

I miei ringraziamenti personali vanno prima di tutto alla mia famiglia. Ai miei genitori, per aver supportato i miei studi, a mia sorella, per aver sopportato le mie cartacce e le mie crisi e a Federico, per non aver mai smesso di incoraggiarmi e di credere nelle mie capacità. Un caro pensiero va alle amiche di sempre, Elena, Eleonora, Sara e Veronica, per tutto il supporto e l'affetto dimostrato nei momenti di gioia e di disperazione.